U.PORTO

DOUTORAMENTO EM PATOLOGIA E GENÉTICA MOLECULAR

Translational applications in emerging viruses: understanding the disease mechanisms to improve diagnosis and treatment

Ana Cristina Magalhães

D
2022

U.PORTO

Ana Cristina Magalhães. Translational applications in emerging viruses: understanding the disease mechanisms to improve diagnosis and treatment

Translational applications in emerging viruses: understanding the disease mechanisms to improve diagnosis and treatment
Ana Cristina Magalhães

SEDE ADMINISTRATIVA

INSTITUTO DE CIÊNCIAS BIOMÉDICAS ABEL SALAZAR
FACULDADE DE MEDICINA

D.ICBAS **2022**

ANA CRISTINA FREITAS MAGALHÃES

TRANSLATIONAL APPLICATIONS IN EMERGING VIRUSES: UNDERSTANDING THE DISEASE MECHANISMS TO IMPROVE DIAGNOSIS AND TREATMENT

Tese de Candidatura ao grau de Doutor em Patologia e Genética Molecular, submetida ao Instituto de Ciências Biomédicas Abel Salazar da Universidade do Porto e Faculdade de Medicina da Universidade do Porto

Orientador – Doutora Luísa Pereira

Categoria – Investigadora Principal

Afiliação – Instituto de Investigação e Inovação em Saúde, Universidade do Porto; Instituto de Patologia e Genética Molecular da Universidade do Porto, Porto Portugal

O trabalho apresentado nesta tese foi realizado no Instituto de Patologia e Imunologia Molecular da Universidade do Porto (IPATIMUP) e no Instituto de Investigação e Inovação em Saúde da Universidade do Porto (i3S).





Este trabalho foi financiado pelos projetos “Spinit-crispr: deteção específica de ácidos nucleicos para diagnóstico point-of-care de doenças tropicais” (POCI-01-0247-FEDER-033778; projeto em co-promoção com as companhias Biosurfit S.A. e Stab Vida Lda) financiado pela ANI – Agência Nacional de Inovação e “Development of a fast and cheap SARS-CoV-2 diagnostic tool based on CRISPR-Cas13a” (109_596696487_Research4COVID19) financiado pela FCT - Fundação para a Ciência e a Tecnologia)



Declaração de Honra

Declaro que a presente tese é de minha autoria e não foi utilizada previamente noutro curso ou unidade curricular, desta ou de outra instituição. As referências a outros autores (afirmações, ideias, pensamentos) respeitam escrupulosamente as regras da atribuição, e encontram-se devidamente indicadas no texto e nas referências bibliográficas, de acordo com as normas de referenciação. Tenho consciência de que a prática de plágio e auto-plágio constitui um ilícito académico.



Preceitos Legais

According to the paragraph d) of the article 3 of the general regulations of the third cycle of studies of the University of Porto (alínea "d" do artigo 3.º do regulamento Geral dos Terceiros Ciclos de estudos da Universidade do Porto), the author declares that this thesis used the results of the published and in preparation articles indicated below. In compliance with the legislation, the author of this thesis declares that she actively participated in the conception, execution, analysis, and discussion of the results, as well as in the elaboration of the publications, under the name Magalhães AC. The author clarifies that in Paper III she was responsible for the acquisition and interpretation of the results of the drugs that could be used as treatment, and for the preparation of the respective section in the manuscript. In Papers I, II and IV, the author was responsible for the execution of the laboratorial analyses, as well as writing of the manuscript together with the supervisor, and with the collaboration of all authors. Papers II and III, published by MDPI (Basel, Switzerland) are open access, and do not require authorization by the journal for reuse, according to the "Creative Common CC BY license" disposed on the website https://www.mdpi.com/openaccess.

Paper I. **Magalhães AC**, Pinto RJ, and Pereira L. Testing of CRISPR-Cas13a based point-of-care diagnostic tools for DENV and SARS-CoV-2. *In preparation*.

Paper II. **Magalhães AC**, Ricardo S, Moreira AC, Nunes M, Tavares M, Pinto RJ, Gomes MS, Pereira L. 2022. InfectionCMA: A Cell MicroArray Approach for Efficient Biomarker Screening in In Vitro Infection Assays. *Pathogens* 2022, 11, 313

Paper III. Sierra B, **Magalhães AC**, Soares D, Cavadas B, Perez AB, Alvarez M, Aguirre E, Bracho C, Pereira L, Guzman MG. 2021. Multi-tissue transcriptomic-informed in silico investigation of drugs for the treatment of dengue fever disease. *Viruses* 2021, 13, 1540.

Paper IV. **Magalhães AC**, Moreira AC, Gomes MS, Pereira L. Endocytic pathways as pharmacological targets for DENV and SARS-CoV-2 infection. *In preparation*.

Acknowledgements

Aos meus pais, por toda a paciência, dedicação e amor incondicional, sempre. Por me terem dado a oportunidade e a liberdade de poder fazer as minhas escolhas e por sempre me apoiarem nas minhas decisões. Por fazerem de mim o que sou hoje.

À Luísa, por me ter aceite e acolhido no seu grupo e por ter embarcado comigo nesta insana aventura que é fazer um doutoramento. Pela presença constante e por todo o apoio ao longo destes quatro intensos anos. Pela sua coragem e pela sua capacidade de fazer as coisas acontecerem, que foram fundamentais para termos conseguido completar todo este trabalho durante uma pandemia. Por ser uma orientadora excepcional e dedicada e por, genuinamente, ter feito tudo ao seu alcance para o meu sucesso nesta jornada.

À Carolina, por todo o companheirismo e disponibilidade durante o trabalho árduo no P3. Pelas longas horas passadas nas condições mais inóspitas do instituto, com fatos e máscaras desconfortáveis, seja de manhazinha, seja em vésperas de feriado intermináveis. Por sempre adaptar a sua vida em função das minhas experiências. Por todas as conversas, toda a orientação, motivação e força ao longo destes anos. Mas principalmente por se ter tornado, mais que uma colega, mais que uma "chega-me isso" profissional, por se ter tonado uma amiga para a vida.

A todos os membros do grupo Diversidade Genética. Ao Ricardo, pela ajuda constante, por todas as imagens feitas, sem nunca reclamar, mesmo com todos os pedidos de alterações até à última. À Nicole por toda o auxílio dado e pela disponibilidade em ser a minha companheira de reserva nas idas ao P3. Ao Bruno, pela ajuda na integração e por todo o trabalho no artigo em conjunto. Aos três, à Verónica, à Joana, e à mais novinha, à Carla, por junto com a Luísa, proporcionarem um ambiente de qualidade e descontração no dia a dia do trabalho no laboratório.

À Nocas, por todo o apoio e compreensão desde o primeiro minuto. Por crescer comigo na vida e me acompanhar de perto em todos os momentos. À Mariana por sempre viver as minhas alegrias e acreditar em mim. À Guida, pelas corridas de domingo, que serviram de momentos de desabafo da semana e que tão importantes foram nestes anos.

À Isabel, à Rita, à Ana e à Sílvia, que me acompanham desde o início da minha caminhada em investigação. Primeiro como colegas de trabalho, mas que rapidamente passaram a amigas e companheiras de belas gargalhadas e viagens. Por, apesar dos caminhos distintos na vida profissional, estarem sempre presentes. Ao Miguel e à Maria, porque também fazem parte da minha primeira família em investigação e participaram neste meu caminho.

A todos os amigos, família e colegas que, de uma forma ou de outra, contribuíram para que este dia chegasse.

Abstract

In recent years, the World Health Organization (WHO) raised concerns to the risk of emergent viruses and the diseases they cause. These risks are accelerated by the high and ease mobility of people across the globe, the climate alterations enlarging dispersion of vectors, and the interference with natural habitats promoting jumps of viruses between species. The transition to the 21st century testified the wider dispersion of dengue virus (DENV), and the emergence of related flavivirus Zika (ZIKV). But the emergence of the severe acute respiratory syndrome coronavirus 2 (SARS-CoV-2) at the end of 2019, and the soon associated global pandemic coronavirus disease 2019 (COVID-19), was the hardest human lesson of contemporary times. In this thesis, we explored recently available molecular tools, and *in silico* and *in vitro* modelling, in order to contribute insights into the disease mechanisms caused by DENV and SARS-CoV-2, aiming at improving diagnosis and treatment.

In terms of improving the molecular diagnosis, we tried to establish the CRISPR-Cas13a-based (clustered regularly interspaced short palindromic repeats-associated endoribonuclease) method Sherlock. We conceived two point-of-care (POC) tests for DENV and SARS-CoV-2, best suited for endemic and pandemic scenarios, respectively. We concluded that the isothermal recombinase polymerase amplification (RPA; step 1 of the Sherlock method) was a fragile and limiting step in the method. RPA did not allow higher yield than the traditional polymerase reaction amplification, it implied a risky dependency on reagents availability as only one company sells the kit at a worldwide scale, and the end result was far less sensitive than the traditional quantitative real time (qRT-PCR) amplification based methods. Our results, supported by other meanwhile published results, render more promising attempts to improve the fluorescence readout (step 2 of the Sherlock method). We proved this was possible by including multi-RNA guides (crRNAs) in the same reaction, and other authors advise also to use tandem CRISPR nucleases. The more recent POC tests explore microfluidic volumes, and we confirmed that these can also improve the fluorescence readout by decreasing the volume of the reaction. We agree that the CRISPR-Cas13a based technology is interesting, but the easiness of establishment and extreme sensitivity promised by the original authors did not hold up against the COVID-19 challenges.

The COVID-19 pressure also made us aware of the importance to design efficient *in vitro* set-ups to evaluate infectious kinetics and associated biomarker screening. We were extremely conditioned to pursue extended experiments in biosecurity level 3 (BSL3) conditions, due to constant lockdowns, isolations, distance measures in labs and access to reagents. Thus, we tested the efficiency of the cell microarray (CMA) methodology in SARS-CoV-2 infection, by establishing two InfectionCMAs: one to compare multiplicity of infection (MOI) levels and infection kinetics in one cell line (12 observation-points); the other to compare infection in diverse cell lines (18 observation-points). The InfectionCMAs were easy to implement, and led to substantial savings against a traditional approach, in slides needed to be prepared and in antibodies amounts for immunocytochemistry (ICC), as well as one against 2.5 BSL3 experimental procedures. If the maximum of the 5 x 7 mould for the InfectionCMA was used (34 observational-points), the gains would be 30 versus 510 slides, and 17 times lower antibodies amounts. Additionally, the InfectionCMA slides could be easily stored for future screening of additional markers, and be shipped to other laboratories unable to conduct viral experiments. One additional important finding from our ICC on host cell surface proteins was the tendency for decrease of expression in neuropilin-1 (NRP1) alongside the angiotensin-converting enzyme 2 (ACE2), throughout the SARS-CoV-2 infection course. This is our *in vitro* evidence that SARS-CoV-2 can use several surface receptors to infect human cells.

In terms of treatment applications, we applied first an *in silico* approach on big data, in order to highlight a few candidate drugs to be further tested *in vitro*. This part of the thesis was initiated before the COVID-19 pandemic, and so was restricted to DENV, and soon similar *in silico* approaches were applied by others to SARS-CoV-2. We analyzed transcriptomic data in liver (published), spleen (our own data) and blood (published) tissues and verified that tissue specialization led to transcriptomic differences. Nevertheless, the common mechanisms of action "Adrenergic receptor antagonist", "ATPase inhibitor", "NF-kB pathway inhibitor" and "Serotonin receptor antagonist" were found to be druggable to oppose the effects of severe Dengue infection across all these tissues. These are potential candidates for future functional evaluation and clinical trials.

We also wanted to implement the *in vitro* testing of drugs in our viral models. Building up on our results, we tested drugs affecting various endocytosis mechanisms, one of which (chlorpromazine) is a "serotonin receptor antagonist", highlighted by our *in silico* analysis. We established the intervals of concentrations

to be used for each drug, after confirming their impact in cell viability (chlorpromazine should be decreased around 15 times in relation to rosuvastatin and amiloride). In general, as DENV2 was more efficient in infecting all cell lines than the alpha variant of SARS-CoV-2, the half-maximal inhibitory concentration (IC50)-relative infection values were higher for DENV2 than SARS-CoV-2. The “serotonin receptor antagonist” chlorpromazine drug had a significant high impact in DENV viral production, but in general the three drugs led to lower viral production for both DENV and SARS-CoV-2, calling for follow-up studies.

Resumo

Nos últimos anos, a Organização Mundial de Saúde (OMS) manifestou preocupação com o risco dos vírus emergentes e as doenças que estes provocam. Estes riscos são acelerados pela elevada e fácil mobilidade global das pessoas, pelas alterações climáticas que aumentam a dispersão de vetores e pela interferência com habitats naturais que promovem saltos de vírus entre espécies. A transição para o século XXI testemunhou a dispersão mais ampla do vírus da dengue (DENV) e a emergência do vírus Zika (ZIKV). Mas o aparecimento do coronavírus da síndrome respiratória aguda grave 2 (SARS-CoV-2) no final de 2019, e da pandemia global coronavírus 2019 (COVID-19), foi a lição humana mais difícil no período contemporâneo. Nesta tese, explorámos ferramentas moleculares recentemente disponíveis, *in silico* e modelação *in vitro*, a fim de contribuir para a compreensão dos mecanismos de doença causados pelo DENV e SARS-CoV-2, visando melhorar o diagnóstico e o tratamento.

Em termos de melhoria do diagnóstico molecular, tentámos estabelecer o método Sherlock baseado em CRISPR-Cas13a (do inglês *clustered regularly interspaced short palindromic repeats-associated endoribonuclease*). Concebemos dois testes rápidos (*point-of-care*, POC) para DENV e SARS-CoV-2, adequados a cenários endémicos e pandémicos, respetivamente. Concluímos que a amplificação da polimerase isotérmica recombinante (RPA; etapa 1 do método Sherlock) era uma etapa frágil e limitativa do método. A RPA não permitiu um rendimento mais elevado do que a tradicional reação de amplificação da polimerase, implicou uma dependência arriscada da disponibilidade de reagentes (uma vez que apenas uma empresa vende o kit a nível mundial) e o resultado final foi muito menos sensível do que os métodos tradicionais baseados na amplificação quantitativa em tempo real (qRT-PCR). Os nossos resultados, apoiados por outros entretanto publicados, tornam mais promissoras as tentativas de melhorar a leitura da fluorescência (passo 2 do método Sherlock). Provámos que tal melhoria seria possível ao incluir múltiplos guias-RNA (crRNAs) na mesma reação e outros autores aconselham também a utilização de múltiplas nucleases CRISPR. Os testes POC mais recentes exploram volumes microfluídicos e confirmamos que estes também podem melhorar a leitura da fluorescência ao diminuir o volume da reação. Em suma, concordamos que a tecnologia baseada no CRISPR-Cas13a é interessante, mas a

facilidade de estabelecimento e a extrema sensibilidade prometidas pelos autores originais não se confirmaram face aos desafios da COVID-19.

A pressão gerada pela COVID-19 também nos sensibilizou para a importância de conceber testes *in vitro* eficientes para avaliar a cinética da infeção e o rastreio de biomarcadores associados. Estivemos extremamente condicionados na realização de experiências extensas em condições de biossegurança de nível 3 (BSL3), devido a constantes confinamentos, isolamentos, distanciamento em laboratórios e acesso a reagentes. Assim, testámos a eficiência da metodologia de *microarray* celular (CMA) na infeção por SARS-CoV-2, estabelecendo dois InfectionCMAs: um para comparar doses de multiplicidade de infeção (MOI) e a cinética da infeção numa linha celular (12 pontos de observação); o outro para comparar a infeção em diversas linhas celulares (18 pontos de observação). Os InfectionCMAs foram fáceis de implementar e levaram a poupanças substanciais quando comparados com uma abordagem tradicional, em termos de lâminas necessárias a preparar, quantidades de anticorpos para imunocitoquímica (ICC), bem como um em vez de 2,5 procedimentos experimentais BSL3. Se fosse utilizado o máximo do molde 5 x 7 para o InfectionCMA (34 pontos de observação), os ganhos seriam de 30 contra 510 lâminas e 17 vezes menos anticorpos. Além disso, as lâminas do InfectionCMA podem ser facilmente armazenadas para futura triagem de marcadores adicionais e ser enviadas para outros laboratórios incapazes de realizar experiências virais. Uma descoberta adicional importante da ICC sobre as proteínas da superfície das células hospedeiras foi a tendência para a diminuição da expressão da neuropilina-1 (NRP1) juntamente com a enzima conversora de angiotensina 2 (ACE2), durante o curso de infeção por SARS-CoV-2. Esta é a nossa prova *in vitro* de que o SARS-CoV-2 pode utilizar vários recetores de superfície para infetar células humanas.

Em termos de aplicações de tratamento, aplicámos primeiro uma abordagem *in silico* em *big data*, a fim de destacar alguns medicamentos candidatos a serem testados *in vitro*. Esta parte da tese foi iniciada antes da pandemia COVID-19, pelo que se restringiu ao DENV, mas outros autores aplicaram abordagens semelhantes ao SARS-CoV-2. Analisámos dados transcriptómicos em tecidos de fígado (publicado), baço (nosso) e sangue (publicado) e verificámos que a especialização dos tecidos levou a diferenças transcriptómicas. No entanto, os tecidos partilham os mecanismos de ação "Antagonista do recetor adrenérgico", "inibidor da ATPase", "inibidor da via NF-kB" e "antagonista do recetor da serotonina" como drogáveis de

modo a oporem os efeitos da infeção grave pela dengue. Estes são bons candidatos para uma futura avaliação funcional e ensaios clínicos.

Também quisemos implementar os testes *in vitro* de drogas nos nossos modelos virais. Com base nos nossos resultados, testámos drogas que afetam vários mecanismos de endocitose, um dos quais (clorpromazina) é um "antagonista dos recetores de serotonina", realçado pela nossa análise *in silico.* Estabelecemos os intervalos de concentrações a utilizar para cada fármaco, após confirmar o seu impacto na viabilidade celular (a clorpromazina deve ser diminuída cerca de 15 vezes em relação à rosuvastatina e amilorida). Em geral, como o DENV2 foi mais eficiente em infetar todas as linhas celulares do que a variante alfa do SARS-CoV-2, os valores de infeção relativos a metade da concentração inibitória máxima (IC50) foram mais elevados para o DENV2 do que para o SARS-CoV-2. A droga "antagonista dos recetores de serotonina" clorpromazina teve um impacto significativo na produção viral de DENV, mas em geral as três drogas diminuíram a produção viral de DENV e SARS-CoV-2, justificando a realização de estudos futuros.

Table of Contents

DECLARAÇÃO DE HONRA 7

PRECEITOS LEGAIS 9

ACKNOWLEDGEMENTS 11

ABSTRACT 13

RESUMO 17

TABLE OF CONTENTS 21

ABBREVIATIONS 23

LIST OF FIGURES 27

LIST OF TABLES 36

I. INTRODUCTION 39

1. VIRUSES 41

1.1. Organization of the viruses *41*

1.2. Classification and taxonomy of viruses *43*

1.3. The replication cycle of viruses *45*

1.3.1. Attachment and entrance into cells 46

1.3.2. Replication and transcription of the viruses 48

1.3.3. Assembly and release into the extracellular space 51

1.4. DENV as an example of neglected tropical virus *52*

1.4.1. Cell cycle of DENV 53

1.4.2. Endemic and epidemic status 55

1.4.3. Characterization of Dengue fever disease 57

1.4.4. Vaccines and treatment 57

1.5. SARS-CoV-2 as an example of a recently emerged virus *59*

1.5.2. Cell cycle of SARS-CoV-2 60

1.5.3. Pandemic status and variants of concern 62

1.5.4. COVID-19 characterisation 64

1.5.5. Vaccines and treatment 65

2. TRANSLATIONAL APPLICATION IN THE FIELD OF INFECTIOUS DISEASES 67

2.1. Molecular diagnosis *67*

2.2. Preliminary steps in drug testing: in silico and in vitro approaches *69*

II. AIMS 73

III. RESEARCH WORK 77

PAPER I – TESTING OF CRISPR-CAS13A BASED POINT-OF-CARE DIAGNOSTIC TOOLS FOR DENV AND SARS-COV-2. 79

PAPER II – INFECTIONCMA: A CELL MICROARRAY APPROACH FOR EFFICIENT BIOMARKER SCREENING IN IN VITRO INFECTION ASSAYS. 107

PAPER III – MULTI-TISSUE TRANSCRIPTOMIC-INFORMED IN SILICO INVESTIGATION OF DRUGS FOR THE TREATMENT OF DENGUE FEVER DISEASE 129

PAPER IV - ENDOCYTIC PATHWAYS AS PHARMACOLOGICAL TARGETS FOR DENV AND SARS-COV-2 INFECTION 145

IV. CONCLUDING REMARKS 165

REFERENCES 173

APPENDICES 205

APPENDIX A - SUPPLEMENTARY INFORMATION FROM PAPER II 207

APPENDIX B - SUPPLEMENTARY INFORMATION FROM PAPER III 213

APPENDIX C - SUPPLEMENTARY INFORMATION FROM PAPER IV 223

Abbreviations

3D – Three-dimension

ACE2 – Angiotensin converting enzyme 2

ADE - Antibody-dependent enhancement

BSL3 - Biosafety level 3

Cas13a - CRISPR-associated endoribonuclease 13a

CCIM - Clathrin-caveolae-independent mechanisms

CMA – Cell microarray

CMap – Connectivity Map

CME - Clathrin-mediated endocytosis

CoV - Coronaviruses

COVID-19 - Coronavirus disease 2019

C protein - Capsid protein

CRISPR - Clustered regularly interspaced short palindromic repeats

crRNA - Guide RNA

Ct - Threshold cycle

DENV - dengue virus (DENV1 to DENV4 – recognized dengue virus strains 1, 2, 3 and 4)

DF - Dengue fever

DHF - Dengue haemorrhagic fever

DMVs - Double-membrane vesicles

dsDNA - double-stranded DNA

dsRNA - double-stranded RNA

DSS - Dengue shock syndrome

EMA – European Medicines Agency

E protein - Envelope protein

ER - endoplasmic reticulum

FDA - Food and Drug Administration

HCoVs - Human-infecting coronavirus

HCV – Hepatitis C virus

HIV-1/2 - Human immunodeficiency virus type ½

HPV – Human papillomavirus

Hsp90 - Heat shock protein 90

HSV-1 - Herpes simplex virus type 1

HTS – High-throughput screening

IC50 - Half maximal inhibitory concentration

ICC – Immunocytochemistry

ICTV - International Committee on Taxonomy of Viruses

IFNs – Interferons

Ig – Immunoglobulin

IL-1 Interleukin1

IL-6 Interleukin 6

ISGs - IFN-stimulated genes

Kb - Kilobase

LME - Lipid raft/caveolae-mediated endocytosis

MERS - Middle East respiratory syndrome

MERS-CoV - Middle East respiratory syndrome coronavirus

MPC – Macropinocytosis

M protein - Membrane protein

MOI - Multiplicity of infection

N protein – Nucleoprotein

NLM – National Library of Medicine

NRP1 - Neuropilin 1

ORF - Open reading frame

pgRNA - pregenomic RNA

prM - premembrane protein

POC – Point-of-care

qRT-PCR - quantitative real time PCR

RBD - Receptor-binding domain

RdRp - RNA-dependent RNA polymerase

RNase H - Ribonuclease H

RPA – Recombinase polymerase amplification

RT – Reverse transcriptase

SARS - Severe acute respiratory syndrome

SARS-CoV - severe acute respiratory syndrome coronavirus

SARS-CoV-2 - Severe acute respiratory syndrome coronavirus 2

S protein – Spike protein

ssDNA - Single-stranded DNA

(+)ssRNA - Positive-sense single stranded RNA

(-)ssRNA - Negative -sense single stranded RNA

TMPRSS2 - Transmembrane serine protease 2

VOC - Variants of concern

WHO – World Health Organization

YFV – Yellow fever virus

ZIKV - Zika virus

List of Figures

Introduction

Figure 1 - The basic organization of virions. On the left, representation of a non-enveloped virus, and on the right, an enveloped virus. Adapted from (Payne 2017)……..42

Figure 2 - The main steps of the viral infectious cycle: (1) attachment and entry; (2) genome replication and transcription and (3) assembly and release. Adapted from (Payne 2017)……45

Figure 3 - Scheme representative of the seven pathways from viral genomes to mRNA that is the base of the Baltimore classification. Adapted from (Flint et al. 2020)……..48

Figure 4 - Representation of the DENV genome, illustrating the order of the genes coding for structural (capsid - C, premembrane – prM, and envelope - E) and non-structural (NS1, NS2A, NS2B, NS3, NS4A, NS4B, NS5) proteins. Adapted from (Guzman et al. 2016)……53

Figure 5 - DENV infection cell cycle. The cycle begins with the viral binding to host cell receptors and internalization into the cell. DENV can enter the cells via various endocytic routes. Inside the cell, the virus is transported in vesicles/endosomes, that will suffer pH-dependent rearrangements leading to disassembling and release of the viral RNA genome. The replication and translation occur on the ER, and translated viral proteins are assembled forming an immature particle, that is transported to the Golgi, where it undergoes a maturation process into virion that can infect new host cells, after exocytosis. Adapted from (Nanaware et al. 2021)..54

Figure 6 - World incidence of dengue between 1990-2017 – Source WHO (online dengue data application https://ntdhq.shinyapps.io/dengue5/, accessed on 28.02.22)……..56

Figure 7 - Representation of SARS-CoV-2 genome, illustrating the order of the genes coding for non-structural (comprised of open reading frame 1a and 1b) and structural (S, E, M, N, and accessory) proteins. Adapted from (Kim et al. 2020)……60

Figure 8 - SARS-CoV-2 infection cell cycle. After the binding to the cell host receptors, the virus fuses with the plasma membrane, and releases its RNA genome directly into the cytoplasm, where the host ribosomes start translating the viral

RNA into non-structural proteins. The replication occurs on the ER, that suffers structural rearrangements into DMVs. After assembly is complete, the virus will exit the cell through the Golgi or lysosomes. A final maturation process is executed by the host enzyme furin. Adapted from (Scudellari 2021)……61

Figure 9 – Emergence over time of SARS-CoV-2 variants of concern……62

Figure 10 - SHERLOCK detection method, starting with the isothermal amplification of the specific target, and followed by its detection with Cas13a-crRNA that begins to cleave the target and other added RNA fluorescent reporters. Adapted from (Kellner et al. 2019)……68

Paper I

Figure 1- Designing POC test models in epidemic and pandemic. On Top: schematic representation of the CRISPR-Cas13a based test diagnosis for inactive viral samples extracted from blood or nasopharyngeal swab, in which step 1 consists in the recombinase polymerase amplification (RPA), and step 2 in the Cas13a action and detection of lateral fluorescence. Below, right: the LOD platform for an endemic situation, illustrated for the diagnosis of DENV and identification of the strain (DENV1-4; and human control gene). Below, left: the plate-fluorescence reader platform for a pandemic situation, illustrated for the SARS-CoV-2 diagnosis based on two viral genes (and human control gene), in 96-well (29 samples) and 384-well (125 samples) plates……91

Figure 2- The main protein purification steps (panel A) and the respective SDS-PAGE images (panel B). The columns in the gels represent the following samples: L – ladder; **Gel 1**, 1- uninduced, 2- induced; **Gel 2**, 1- cell lysate; 2- cleared cell lysate, 3- cell pellet after clearing of lysate, 4- after 1h resin, 5- flow-through resin, 6- wash 1, 7- wash 2, 8- wash 3, 9- eluted fraction, 10- final resin; **Gel 3**, 1- filtered eluted fraction from gel 2, 2-to-12- fractions 17-to-28; **Gel 4**, 1- pool of positive fractions from cation exchange FPLC, 2-to-7- fractions 5-to-10 from size exchange FPLC; **Gel 5**, 1- final concentrated protein, 2- flow-through filter……92

Figure 3 – Specificity tests of the DENV crRNAs in PCR amplified synthetic positive controls and by performing step 2 of the Sherlock method. (A) crRNA designed to identify DENV independently of the strain (B) crRNAs specifically designed to detect one strain: DENV1, DENV2, DENV3 or DENV4. B represents the non-template control……96

Figure 4 – Tests of the SARS-CoV-2 crRNAs in PCR amplified synthetic positive controls and by performing step 2 of the Sherlock method. (A) crRNAs for various genes of SARS-CoV-2 in the presence of the respective synthetic standards (B) Mismatch of the crRNA and synthetic positive controls for Orf1ab and S genes. B represents the non-template control……97

Figure 5 – Sensitivity tests for step 2 of the Sherlock method with ten-fold serial dilutions of the synthetic positive targets for SARS-CoV-2 and human genes. B represents the non-template control……98

Figure 6 - Comparison with the DENV4 crRNA, between performing PCR or step 1 of the Sherlock method. B represents the non-template control……98

Figure 7 – Sensitivity tests for step 1 (RPA) + step 2 of the Sherlock method with ten-fold serial dilutions of the synthetic positive targets for SARS-CoV-2 (Orf1ab and S) and human (RnaseP20) genes. B represents the non-template control……99

Figure 8 - Fluorescence read-outs for SARS-CoV-2 Orf1ab gene alone (left) and in combination with SARS-CoV-2 E gene (right), with only step 2 Sherlock method. B represents the non-template control……100

Figure 9 - Fluorescence read-outs for SARS-CoV-2 combined Orf1ab and E1 genes in extracted positive and negative RNA samples. S represents sample (- negative or + positive by qRT-PCR) and B the non-template control……100

Figure 10 - Fluorescence read-outs for SARS-CoV-2 combined Orf1ab and E1 genes and testing lyophilisation. (A) Testing lyophilization of step 2 reagents, either for the complete Cas13a reaction (left) or lyophilized Cas13a reaction without the complex Cas13a+crRNAs (right), that that was added after. S+ represents a positive sample by qRT-PCR and B the non-template control……101

Paper II

Figure 1 - Schematic representation of the procedure to establish the InfectionCMA. The infection assay can have variable timelines depending on the experimental assay. The manual establishm assay and immune processing of the InfectionCMA take around 5-7 days. A 1-2 cm pellet of infected of infected cells guarantees 30 slides from each InfectionCMA. This biological resource can be used for the expression evaluation of several markers of interest, through diverse techniques such as immunocytochemistry (ICC) and in situ hybridization (ISH)……115

Figure 2 - Comparison of the design and outputs between the InfectionCMA and the traditional vitro infection assay for the first infection kinetics test performed here.....116

Figure 3 - ICC results for SARS-CoV-2 spike and nucleocapsid proteins in infected Vero cells, at various time points (4 h, 24 h, 48 h and 72 h), for MOI 0.001 and MOI 0.01. (A) Microscopic images with 50 μm scale bar. The last column represents zoomed-in images of the sections highlighted within a red square in the respective rows. Both viral proteins were located in the cytoplasm of the infected cells. (B) Heat map for the percentage of cells stained (0–1%, >1–10%, >10–25%, >25–50%, >50–75%, and >75%). (C) Infectious viral particles produced at the various time points (in ffu/mL – focus forming units pel mL).....117

Figure 4 – ICC results for ACE2 and NRP1 proteins in SARS-CoV-2-infected Vero cells, at various time points (4 h, 24 h, 48 h and 72 h), for mock (non-infected), MOI 0.001 and MOI 0.01. (A) Microscopic images with a 50 µm scale bar. The last column represents zoomed-in images of the sections highlighted within a red square in the respective rows. Both viral proteins were located in the cytoplasm of the infected cells. ACE2 was localized in the membrane, and NRP1 in the membrane and in the cytoplasm. (B) Heat map for the percentage of cells stained (0–1%, > 1–10%, > 10–25%, > 25–50%, > 50–75%, and > 75%).....118

Figure 5 - Characterization of SARS-CoV-2 spike expression in the human (Caco-2 and Huh-7) and Vero cell lines, at various time points after infection with MOI 1, by ICC ((A) microscopic images with 100 µm scale bar, including zooms of the red inserts; (B) heat map), and ISH ((C) microscopic images, including zooms of the red inserts; (D) heat map). The spike protein had a cytoplasmic location in all the infected cell lines. (E) Infectious viral particles produced at the vari-ous time points (in ffu/mL—focus forming units per mL). (F) Western blots and graphs representing the spike quantifi-cation in cells and the infectious viral particles produced in these independent experiments. In the graphs, data represent means ± SD of three independent experiments, and significant Student's *t*-test *p*-values are indicated (*< 0.05).....120

Figure 6 - Characterization of ACE2 expression in the human (Caco-2 and Huh-7) and Vero cell lines, at various time points after infection with MOI 1, by ICC ((A) microscopic images with 100µm scale bar, including zooms of the red in-serts; (B) heat map), Western blot (C), and qRT-PCR (D). In the graphs, data represent means

± SD of three independent experiments, and significant Student's t-test p-values are indicated (** < 0.01). The ACE2 was placed in the membrane of all the infected cell lines……..121

Figure 7 - Characterization of NRP1 expression in the human (Caco-2 and Huh-7) and Vero cell lines, at various time points after infection with MOI 1, by ICC ((A) microscopic images with 50 µm scale bar, including zooms of the red in-serts; (B) heat map) and Western blot (C). In the graphs, data represent means ± SD of three independent experiments, and significant Student's t-test p-values are indicated (* < 0.05). The NRP1 was expressed in the membrane and in the cytoplasm of all the infected cell lines……..122

Figure 8 - Characterization of Ki-67 and BCL-2 expression in the human (Caco-2 and Huh-7) and Vero cell lines, at 72 h after infection with MOI 1, by ICC (A-microscopic images with 50µm scale bar, including zooms of the red inserts in the last row; B–heat map). The Ki-67 displayed a nuclear and BCL-2 cytoplasmic localizations……..123

Paper III

Figure 1 - Top 20 Gene Ontology Biological Process (GO-BP) pathways in the (A) spleen and (B) liver cells (cut-off values: nominal p-value < 0.05 and FDR < 0.25). Positive normalized enrichment score (NES; in purple) represents upregulated pathways in the infected individuals versus controls, while negative NES values (in green) represent downregulated pathways in the infected individuals versus controls……136

Figure 2 - Top 20 Gene Ontology Biological Process (GO-BP) in the two blood datasets: (A) GSE18090 and (B) GSE51808 pathways (cut-off values: nominal p-value < 0.05 and FDR < 0.25). Positive NES (in purple) represents upregulated pathways in the infected individuals versus controls, while negative NES values (in green) represent downregulated pathways in the infected individuals versus controls…137

Figure 3 - CMap-identified compounds (score equal to or below −90) that potentially impact Dengue haemorrhagic fever treatment, according to their mechanism of action in the blood, spleen and liver. (A) Bar plot of the distribution of drugs by broad pharmacological classification; (B) heatmap of drugs per mechanism identified in one or more tissues; (C) circus plot of common mechanisms of action……..138

Paper IV

Figure 1- *In vitro* testing of the effect of the chlorpromazine, rosuvastatin and amiloride drugs in cell viability, in the absence of infection. A. Schematic representation of the main effect of each drug in the endocytic pathways: chlorpromazine (serotonin antagonist receptor) inhibiting clathrin-mediated endocytosis; rosuvastatin (statin) involved in depletion of cholesterol in cell membranes; and amiloride (inhibitor of sodium-proton exchange), blocking macropinocytosis. B. Schematic representation of the in vitro test. Cells were seeded in 96 well plates, treated with six concentrations of the three drugs, and incubated for 48 hours. After fixation of the cells, DAPI staining measured in IN Cell Analyzer 2000 informed on the cell number. C. Plots represent the dose-response curves of the effect of the chlorpromazine, rosuvastatin and amiloride drugs in cell viability for Vero, Huh-7 and NCI-H2110 cell lines, with respective IC50 values indicated. Data are plotted as percentage compared with DMSO only control wells (100%). Values represent mean and standard deviation of three independent experiments.....157

Figure 2- *In vitro* testing of the effect of the chlorpromazine, rosuvastatin and amiloride drugs in cell viability, in the presence of infection. **A.** Schematic representation of the *in vitro* test. Cells were seeded in 96 well plates and treated with six concentrations of the three drugs. One hour later, the cells were infected (in the BSL3) with DENV2 or SARS-CoV-2 at MOI 1, and incubated for 48h. After fixation of the cells, the viral infection rate was evaluated by immunofluorescence (IF) detection of DENV envelope protein or SARS-CoV-2 spike protein in IN Cell Analyzer 2000. DAPI staining informed on the cell viability rate. **B.** Plots represent the dose-response curve for each drug (chlorpromazine, rosuvastatin and amiloride) in the Vero cell line, in terms of cell viability (red lines) and relative infection (green lines), with respective IC50 values indicated in corresponding colours. Data are plotted as percentage compared with DMSO only control wells (100%). Values represent mean and standard deviation of three independent experiments. The lateral panels consist in the microscope images of the viral protein staining (green) inside cells. The corresponding DAPI-stained cell nuclei images are shown in Supplementary Figure S1.....158

Figure 3- Viral titre measurement after treating the Vero, Huh-7 and NCI-H2110 cell lines independently with the three drugs (chlorpromazine, rosuvastatin and amiloride) at the respective IC50-relative infection value (5µM, 20µM, and 100 or

50μM, respectively). Supernatant aliquots were collected at three time-points post-infection with DENV or SARS-CoV-2 (1h, 24h and 48h post-infection). The controls consisted in the infected cells in the absence of drugs. In the graphs, data represent means ± SD of three independent experiments, and significant Student's t test p-values are indicated (*≤0.05)……160

Appendix A

Supplementary Figure S1 - ICC for the spike, nucleocapsid, ACE2, NRP1, Ki-67 and BCL2, and ISH for the spike, in the tumour tissue cores of kidney and liver. Scale bar 50μm……209

Supplementary Figure S2 - Controls for the characterization of SARS-CoV-2 spike mRNA expression in the human (Caco-2 and Huh-7) and Vero cell lines, at different time-points, by ISH. Microscopic images with 100μm scale bar……209

Supplementary Figure S3 - Characterization of SARS-CoV-2 nucleocapsid expression in the human (Caco-2 and Huh-7) and Vero cell lines, at different time-points after infection with MOI 1, by ICC (A- light microscopic images with 100μm scale bar; B- heat map)……210

Supplementary Figure S4 - Characterization of Ki-67 expression in the human (Caco-2 and Huh- 7) and Vero cell lines, at different time-points after infection with MOI 1, by ICC (A- light microscopic images with 50μm scale bar; B- heat map)….211

Supplementary Figure S5 - Characterization of BCL-2 expression in the human (Caco-2 and Huh-7) and Vero cell lines, at different time-points after infection with MOI 1, by ICC (A- light microscopic images with 50μm scale bar; B- heat map)….212

Appendix B

Figure S1 - PCA plot (PC1 explaining 81.4% of variation vs. PC2 explaining 6.2% of variation) of the human transcriptomic profile of the spleen, liver and encephalon tissues……216

Figure S2 - Volcano plots for the gene differential expression in the (A) spleen and (B) liver cell datasets. The points represented on red are the statistically significant genes. The negative side of the graph refers to downregulated genes in patients

when compared to controls; the positive side of the graph refers to upregulated genes in patients when compared to controls……216

Figure S3 - Top 20 Gene Ontology Cellular Component (GO-CC) pathways in the (A) Spleen and (B) Liver cells (cut-off value; nominal p-value < 0.05 and FDR < 0.25). Positive NES (in purple) show upregulated pathways in the infected individuals versus controls, while negative NES values (in green) mean downregulated pathways in the infected individuals versus controls……217

Figure S4 - Top 20 Gene Ontology Molecular Function (GO-MF) pathways in the (A) Spleen and (B) Liver cells (cut-off value; nominal p-value < 0.05 and FDR < 0.25). Positive NES (in purple) show upregulated pathways in the infected individuals versus controls, while negative NES values (in green) mean downregulated pathways in the infected individuals versus controls……217

Figure S5 - Top 20 significantly enriched KEGG pathways in the (A) Spleen and (B) Liver cells (cut-off value; nominal p-value < 0.05 and FDR < 0.25). Positive NES (in purple) show upregulated pathways in the infected individuals versus controls, while negative NES values (in green) mean downregulated pathways in the infected individuals versus controls……217

Figure S6 - Dendrograms for the gene expression profiles in the two blood datasets: (A) GSE18090 and (B) GSE51808. The red points indicate the infected dengue haemorrhagic fever individuals (DHF), while the blue points indicate control samples……218

Figure S7 - Volcano plots for the gene differential expression in the two blood datasets: (A) GSE18090 and (B) GSE51808. The points represented in red are the statistically significant genes. The negative side of the graph refers to downregulated genes in patients when compared to controls; the positive side of the graph refers to upregulated genes in patients when compared to controls….219

Figure S8 - Venn diagrams of the upregulated (A) and downregulated (B) genes in the two blood datasets……219

Figure S9 - Top 20 Gene Ontology Cellular Component (GO-CC) pathways in the (A) GSE18090 and (B) GSE51808 (cut-off value; nominal p-value < 0.05 and FDR < 0.25). Positive NES (in purple) show upregulated pathways in the infected individuals versus controls, while negative NES values (in green) mean downregulated pathways in the infected individuals versus controls……220

Figure S10 - Top 20 Gene Ontology Molecular Function (GO-MF) pathways in the (A) GSE18090 and (B) GSE51808 (cut-off value; nominal p-value < 0.05 and FDR < 0.25). Positive NES (in purple) show upregulated pathways in the infected individuals versus controls, while negative NES values (in green) mean downregulated pathways in the infected individuals versus controls……..220

Figure S11- Top 20 significantly enriched KEGG pathways in the (A) GSE18090 and (B) GSE51808 (cut- off value; nominal p-value < 0.05 and FDR < 0.25). Positive NES (in purple) show upregulated pathways in the infected individuals versus controls, while negative NES values (in green) mean downregulated pathways in the infected individuals versus controls……221

Appendix C

Supplementary Figure S1- Microscope images for the evaluation of cell viability rate by immunofluorescence detection (in the IN Cell Analyzer 2000) of the DAPI staining (red), when performing the *in vitro* testing of the effect of the chlorpromazine, rosuvastatin and amiloride drugs in the presence of infection with DENV2 (left panel) and SARS-CoV-2 (right panel)……225

List of Tables

Introduction

Table 1 - Overview of the ICTV 2020 virus taxonomy release, with indication of the type of nucleic acid, names of families, genome size, and major hosts.....44

Paper I

Table 1 – Sequences of primers (FW – forward; RV – reverse), crRNAs and synthetic positive targets.....93

Appendix B

Table S1- Additional information on the individuals from whom samples were collected for transcriptomics.....215

Table S2 - Differentially expressed genes between infected and control cohorts for the spleen tissue samples (adjusted p-value<0.05).....https://cloud.i3s.up.pt/index.php/s/X8k4neAXPqc5Bpo

Table S3 - Differentially expressed genes between infected and control cohorts for the liver single cell dataset (adjusted p-value < 0.05).....https://cloud.i3s.up.pt/index.php/s/G9GWbxqM5ynsfe2

Table S4 - Differentially expressed genes between infected and control cohorts for the GSE18090 dataset (adjusted p-value < 0.05).....https://cloud.i3s.up.pt/index.php/s/mJt2M8nESG6Qw46

Table S5- Differentially expressed genes between infected and control cohorts for the GSE51808 dataset (adjusted p-value < 0.05).....https://cloud.i3s.up.pt/index.php/s/sRK2aDTmWLCoHLE

Table S6 - CMap results for the blood microarray data. Table contains score, name and mechanism of action for the outputted drugs with a Cmap score above 90 and below -90 indicating similar or opposing signatures between a given perturbagen's and the query, respectively.....https://cloud.i3s.up.pt/index.php/s/S2fWtLidPYFJG6Z

Table S7 - CMap results for the spleen tissue data. Table contains score, name and mechanism of action for the outputted drugs with a Cmap score above 90 and below -90 indicating similar or opposing signatures between a given perturbagen's

and the query, respectively……
……..https://cloud.i3s.up.pt/index.php/s/xJj5Wbk6qiXkTWb

Table S8 - CMap results for the liver cell data. Table contains score, name and mechanism of action for the outputted drugs with a Cmap score above 90 and below -90 indicating similar or opposing signatures between a given perturbagen's and the query, respectively……
……https://cloud.i3s.up.pt/index.php/s/5rdbL9XZkjDG8rk

I. Introduction

1. Viruses

Viruses have been causing human diseases since thousands of years ago, as directly testified by the successful retrieving of ancient hepatitis B virus genomes from human remains dating back 4,500 years old (Mühlemann et al. 2018). However, viruses were only shown to be filterable, and hence identified as sub-microscopic particles different from bacteria, by the end of the 19th century (reviewed in (Sankaran 2018)), and were first visualized through the electron microscope by Ruska, Kausche and Pfankuch in 1939 (reviewed in (Goldsmith and Miller 2009)). Modern biotechnology contributed substantially with knowledge on viruses, and virology is currently a vast field, comprising: molecular biology of virus replication; structure of viruses; genomics and evolution of viruses; interactions of viruses and hosts; viral infectious diseases and clinical aspects; virus epidemiology, the ecological niche occupied by viruses and how they spread from victim to victim; viral diagnosis; and prevention of viral disease by vaccination, drugs, or other methods.

It is well established that viruses infect most organisms, including bacteria, blue-green algae, fungi, plants, insects, and vertebrates (Berman 2019). Median values for virus-to-microbe ratios in the various Earth biomes allowed theoretically to estimate an amount of 4.8×10^{31} virus-like particles on Earth, of which 2.80×10^{22} are human-associated (Cobián Güemes et al. 2016). In this thesis, we are interested in two viruses that are important human disease agents: DENV and SARS-CoV-2.

1.1. Organization of the viruses

Viruses are obligate intracellular parasites that make use of the host cell machinery to replicate and originate new progeny. When outside the cells, the mature virus particle is called virion (Figure 1), and contains the viral genome, which can be DNA or RNA. Viruses can have large genomes that consequently encode high numbers of proteins, compatible with more complex life cycles (Strauss and Strauss 2008). The largest known RNA viruses are the coronaviruses (CoV; family *Coronaviridae*), whose genomes attain 30 kilobase (kb), and the largest DNA viruses, the poxviruses (family *Poxviridae*), have sizes up to 375kb. The viruses with smaller genomes, like the *Picornaviridae* family, are restricted to 7.1-8.5kb. There are other

subcellular infectious agents that are even “smaller” than viruses, namely satellite viruses, which are dependent for their replication on other viruses; viroids, small (~300 nucleotide) RNAs that are not translated and have no capsid; and prions, infectious agents whose identity remains controversial (Das and Zou 2016). Nevertheless, the largest viral genomes are still small compared to the median size of a bacterial genome (2000kb), and minuscule compared to the size of the human genome (diploid size of 6×10^6kb).

The viral genome is surrounded by a protein coat, named capsid or nucleocapsid, sometimes containing a lipid envelope, whose purpose is to protect the viral genome in the extracellular space and to enable its entry into a new cell. This protection is important because the viral genome contains all the information required for the viral replication and production of new virions. The virions bind to receptors present on the surface of the cells, then the viral genome is released into the cytoplasm, and reprograms the cell to replicate and produce progeny virions. Thus, the virus uses the cellular machinery in its benefit to produce energy and for the translation of the viral mRNA in proteins, among other proposes (Payne 2017; Walsh and Mohr 2011).

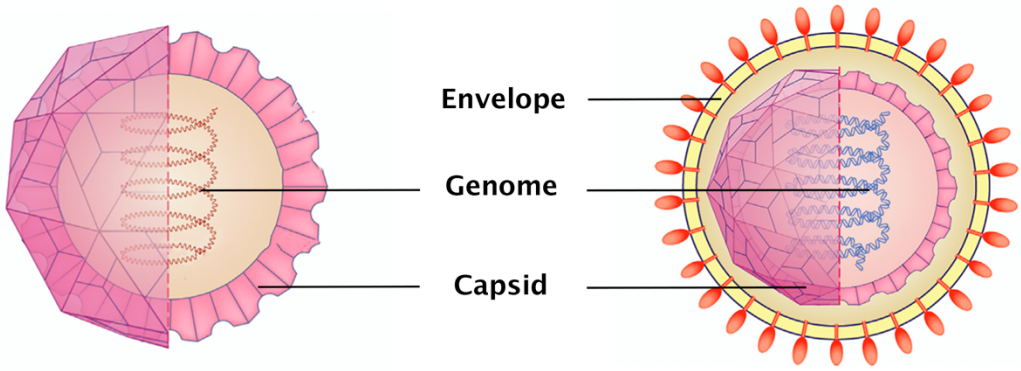


Figure 1 – The basic organization of virions. On the left, representation of a non-enveloped virus, and on the right, an enveloped virus. Adapted from (Payne 2017).

The viral genome encodes three main classes of proteins (Strauss and Strauss 2008): (1) enzymes required for replication of the genome and the production of; (2) proteins that are used in the assembly of new viruses; and (3) proteins that

interfere with the defence mechanisms of the host. Detailed information will be provided for the first class of enzymes in the section *1.3.2.* of this introduction. For the assembly, some simple viruses encode a small number of structural proteins that assemble themselves with the genome to form the progeny virion. While more complex viruses can encode scaffolding proteins that are required for the assembly, but that are not present in the virion. Depending on the number of protein subunits and their interconnection, the virus can present different shapes and sizes, with two types of symmetry been recognized: icosahedral (e.g. DENV) and helical (e.g. Influenza virus). Other viruses can present an asymmetrical structure and be recognized as complex, such as the poxviruses (Burrell et al. 2017). Regarding the third class of viral proteins, various viruses encode proteins that interfere with the defence mechanisms of the host, namely the secretion of interferons (IFNs), which are essential for the innate immunity and have critical impact on adaptive immune responses. The host cell pattern recognition receptors recognize the virion particles and induce the activation of several signalling cascades, leading to the production and secretion of IFNs. IFN signalling, in turn, prompts transcription of hundreds of IFN-stimulated genes (ISGs) that culminate into the immune response against the viral infection (Mesev et al. 2019).

1.2. Classification and taxonomy of viruses

Two classification systems for viruses are commonly used: the International Committee on Taxonomy of Viruses (ICTV) and the Baltimore.

The ICTV was created in 1966 to establish a single and universal system for the classification and nomenclature of all viruses. This classification system is related to the classification of cellular organisms, and organizes viruses in orders (-virales), families (-viridae), subfamilies (-virinae), genera (-virus), and species (Gorbalenya et al. 2020). Viruses are classified into species based on a close relationship, although a species usually contains many different strains that may differ significantly (>10%). Species with a close relationship are grouped into a genus, and genera are grouped into families, based on the genome type/size, the virion structure, and the strategy of replication/genome organization of the virus. In the 2020 virus taxonomy release (Table 1), there were 9110 viral species, 2224 genera and 189 families.

Table 1 – Overview of the ICTV 2020 virus taxonomy release, with indication of the type of nucleic acid, names of families, genome size, and major hosts.

Nucleic Acid	Family	Genome Size	Major Hosts
dsDNA	*Poxviridae*	130-375kb	Vertebrates, insects
	Hespesviridae	120-220kb	Vertebrate
	Baculoviridae	80-180kb	Insects
	Adenoviridae	28-48kb	Vertebrates
	Papillomaviridae	6.8-8.4kb	Vertebrates
	Polyomaviridae	5kb	Vertebrates
ssDNA	*Parvoviridae*	4-6kb	Vertebrates, insects
dsRNA	*Reoviridae*	20-30kb	Vertebrates, insects, and plants
	Birnaviridae	5.9kb	Vertebrates (non-humans) and insects
(+)ssRNA	*Coronaviridae*	28-33kb	Vertebrates
	Togaviridae	10-13kb	Vertebrates and insect vectors
	Flaviviridae	10-12kb	Vertebrates and some insect vectors
	Picornaviridae	7-8.5kb	Vertebrates
	Astroviridae	7-8kb	Vertebrates
	Caliciviridae	8kb	Vertebrates
	Hepeviridae	7.2kb	Vertebrates
(-)ssRNA	*Filoviridae*	19kb	Vertebrates
	Paramyxoviridae	15-16kb	Vertebrates
	Rhabdoviridae	11-16kb	Vertebrates, invertebrates, and plants
	Orthomyoxiviridae	10-15kb	Vertebrates
	Bunyaviridae	12-23kb	Vertebrates, insect vector and plants
	Arenaviridae	11kb	Vertebrates
ssRNA RT	*Retroviridae*	7-10kb	Vertebrates (DNA Intermediate)
dsDNA RT	*Caulinoviridae*	8kb	Plants (RNA intermediate)
	Hepadnaviridae	3kb	Vertebrates (RNA intermediate)

In 1971, David Baltimore (Baltimore 1971) presented a simplified classification system, known as the Baltimore system. This system clusters viruses into families depending on the type of genome, regardless evolutionary relationships. This non-hierarchical classification is widely used due to its concise and functional

organization. It contains seven classes of viruses: (1) Class I - double-stranded DNA viruses (dsDNA); (2) Class II - single-stranded DNA viruses (ssDNA); (3) Class III - double-stranded RNA viruses (dsRNA); (4) Class IV - positive-sense RNA viruses ((+)ssRNA); (5) Class V - negative-sense RNA viruses ((-)ssRNA); (6) Class VI - RNA viruses that reverse transcribe; and (7) Class VII - DNA viruses that reverse transcribe.

1.3. The replication cycle of viruses

The infection cycle of viruses involves several steps (Figure 2), which can be organized in three main phases: attachment and entrance into the host cells; replication and transcription; assembling and release into the extracellular space.

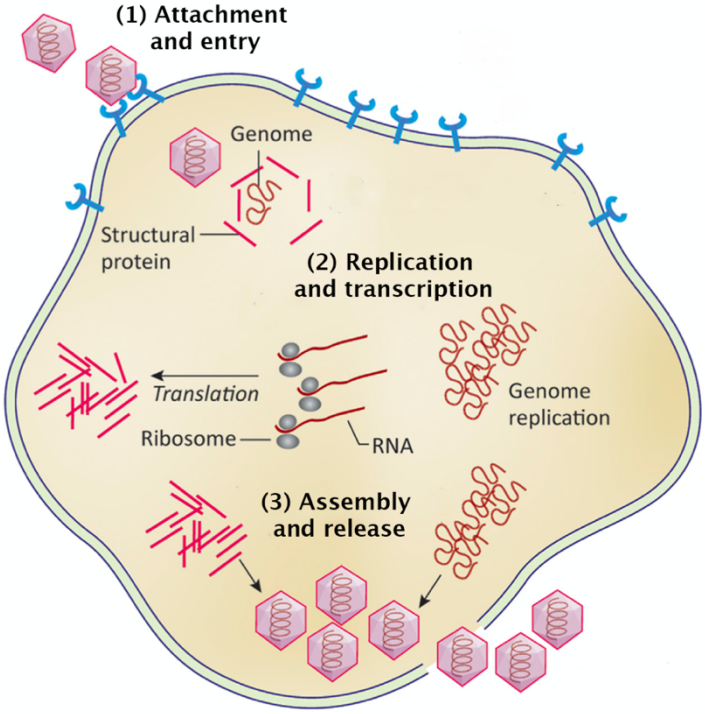


Figure 2 - The main steps of the viral infectious cycle: (1) attachment and entry; (2) genome replication and transcription and (3) assembly and release. Adapted from (Payne 2017).

1.3.1. Attachment and entrance into cells

The viral replication cycle initiates with the binding by external proteins of the virion to a receptor on the surface of the host cell. This binding presents affinity and specificity, and governs which species can be infected by a certain virus (the host range), the tissue tropism, and the pathology of the caused disease (Maginnis 2018). The binding process can involve several other host proteins besides the main receptor, as accessory receptors that accelerate the process but are not essential for it, and coreceptors that are required after the virus-main receptor link. Examples of these host proteins are many members of the immunoglobulin (Ig) superfamily, as CD155 (for poliovirus; (Bowers et al. 2017)) and CD4 (for human immunodeficiency virus type 1 or HIV-1; (Bour et al. 1995)), as primary receptors, the glycosaminoglycan heparan sulfate (for *Herpesviridae* family; (Shukla and Spear 2001)) as accessory receptor, and chemokines as CCR5 (for HIV; (Blanpain et al. 2002)) as coreceptor. In general, viruses from the same family use identical receptors, but in some cases unrelated viruses can use the same receptors and related viruses can use different receptors. Also, some host proteins can serve as primary receptors in one virus and as accessories or coreceptors for another virus. This is the case of the referred heparan sulfate, which serves as accessory receptor for the herpes simplex virus type 1 (HSV-1) and is recognized as primary receptor for DENV and Yellow Fever virus (YFV) (Cruz-Oliveira et al. 2015; Germi et al. 2002).

After the attachment, the next step is the penetration of the viral genome into the cytoplasm of the cell. For some viruses this can occur with the introduction of only the viral nuclei acid, while for others, a subviral particle comprising the nucleic acid (e.g. nucleocapsid) enters the cell. The entry is supported by viral proteins that may be the same used in the binding to the receptors or other proteins present in the virions. In most cases, the insertion into the cytoplasm implicates the fusion with the plasma membrane or other intracellular membranes (Dimitrov 2004). When the fusion with the host cell plasma membrane occurs, the viruses are internalized through a variety of endocytic pathways (Cossart and Helenius 2014): clathrin-mediated endocytosis (CME); Lipid raft/caveolae-mediated endocytosis (LME); macropinocytosis (MPC); and clathrin-caveolae-independent mechanisms (CCIM).

In CME, the virion attachment to the host receptor leads to the binding of accessory and adaptor proteins to the receptor, and subsequently the binding to clathrin. On the intracellular side of the plasma membrane, clathrin will form characteristic

invaginations known as clathrin-coated pits, that will be pinched off the host membrane by scissor proteins (like dynamin), releasing the clathrin-coated vesicles to the cytoplasm. The clathrin is subsequently released from the vesicles, and these will deliver their viral content to early endosomes (Mercer et al. 2010; Shi et al. 2021). Several viruses have been reported to use CME as the main cell entry pathway, including HIV-1 (Daecke et al. 2005), hepatitis C virus (HCV) (Blanchard et al. 2006), HSV-1 (Praena et al. 2020), ZIKV (Li et al. 2020), DENV (Piccini et al. 2015), SARS-CoV-2 (Bayati et al. 2021), among others.

The LME endocytosis involves the binding of the virus to a host receptor, but in this case by invagination of lipid-enriched domains within the host plasma membrane. Internalization can occur with the assembly of specific lipids, usually sphingolipids and cholesterol, or via caveolae, which are specialized lipid rafts that form invaginations which contain a coat protein known as caveolin (Pelkmans 2005; Ripa et al. 2021). LME has been reported to be used by numerous viruses, such as: Human Coronavirus 229E (Nomura et al. 2004), Influenza A virus (Verma et al. 2018), Simian virus 40 (Chen et al. 2019), and flaviviruses like DENV, ZIKV, YFV, and West Nile virus (Osuna-Ramos et al. 2018).

MPC is a nonspecific endocytic pathway that is initiated by external stimulus and not by the cargo binding to specific cell surface receptors. This endocytic pathway can be triggered by growth factors that lead to the activation of Rho GTPases (Rac1 and/or Cdc42), myosins, and kinases such as PAK1, PI3 kinase, and PKC, and initiate a signalling cascade that leads to changes in the dynamics of actin filaments in the membrane. The generation of cell membrane protrusions known as membrane ruffles, that can present several shapes like filopodia, lamellopodia, circular ruffles, or blebs, will lead to the formation of large and uncoated vacuoles, the macropinosomes (Mercer and Helenius 2009). Different viruses exploit this non-specific entry route: Epstein-Barr virus (Tugizov et al. 2013), respiratory syncytial virus (Krzyzaniak et al. 2013), Vaccinia virus (Mercer and Helenius 2008), Ebola virus (Nanbo et al. 2010).

Some viruses can enter into host cells by CCIM, such as human rhinovirus 14 (Khan et al. 2010), human papillomavirus (HPV) type 16 (Spoden et al. 2008), and Lassa virus (Kunz 2009). Instead of clathrin and caveolin, this mechanism uses other proteins, such as tetraspanins used by HPV16 (Spoden et al. 2008). Tetraspanins are transmembrane proteins that interact laterally with each other and with other transmembrane proteins (like proteoglycans, integrins, growth factor receptors) to

form tetraspanin-enriched microdomains. These microdomains can modulate intercellular interactions and are involved in intracellular protein transport, as well as in endocytosis and exocytosis. Although the microdomains are enriched in cholesterol, they are different from conventional lipid rafts.

1.3.2. Replication and transcription of the viruses

Once the viral genome is released in the cytoplasm, the transcription and replication steps can be initiated, and they are dependent on the organization of the viral genome (Figure 3).

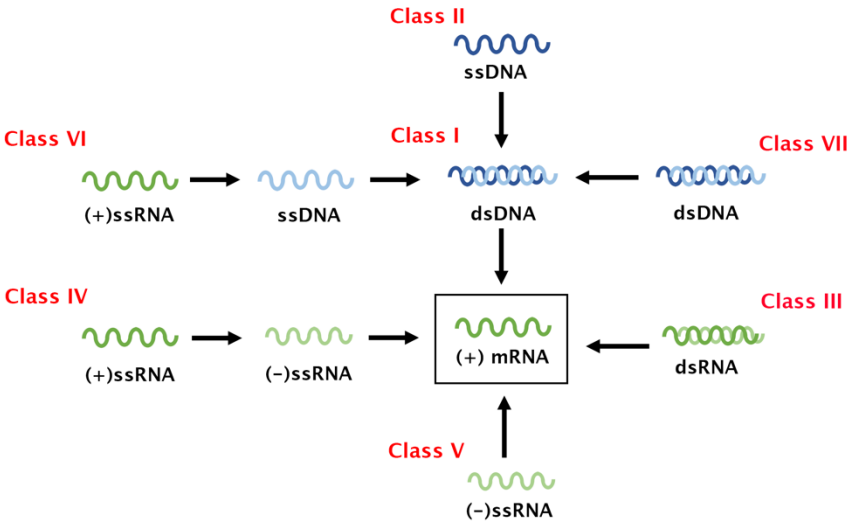


Figure 3 – Scheme representative of the seven pathways from viral genomes to mRNA that is the base of the Baltimore classification. Adapted from (Flint et al. 2020).

The Baltimore Classes I and II viruses contain DNA genomes that are replicated by direct DNA-DNA copying, similarly to eukaryotic organisms. These classes include viruses from the *Adenoviridae*, *Herpesviridae*, *Papillomaviridae*, *Polyomaviridae*, and *Poxiviridae* families (Louten 2016). The first event in their replication is the production of mRNAs. For most dsDNA viruses (except the cytoplasm-replicated poxviruses), the viral genome is transported to the nucleus where it is transcribed by the host RNA polymerase (Pasdeloup et al. 2009). The viral mRNAs are then translated by host ribosomes in the cytoplasm, at different times into early and late

genes. The early genes code viral proteins involved in the viral genome replication and further transcription, such as DNA polymerases. The late genes code most of the structural proteins required for viral assembly, maturation and release from the cell (Strauss and Strauss 2008). The resulting proteins are transported back to the nucleus, where the DNA replication is performed by cellular (polyomaviruses and papillomaviruses) or viral (most of the remaining dsDNA viruses) DNA polymerases (Louten 2016). The ssDNA viruses are the simplest and smallest known viruses, encoding only a few genes and depending completely on host cell enzymes for genome replication and transcription (Malathi and Renuka Devi 2019). The genome replication occurs at the nucleus of the host cell, where at first the ssDNA viral genome is converted to dsDNA by the DNA polymerase. When the ssDNA genome becomes double-stranded, the RNA polymerase can transcribe the viral genes, which are then translated into viral proteins (Malathi and Renuka Devi 2019).

The big group of RNA viruses that replicate by direct RNA-RNA copying (Classes III to V) do not usually enter the nucleus of the infected cell. They must carry or encode their RNA-dependent RNA polymerase (RdRp) to transcribe viral mRNA in the cytoplasm (Louten 2016). Some differences are observed between the thee classes (Poltronieri et al. 2015):

dsRNA (class III - e.g. *Reoviridae*) viruses have mRNA synthesis in the partially uncoated capsid that entered the cell. The transcribed mRNAs will pass through the capsid pores, into the cytoplasm where they associate with host ribosomes for translation of structural and nonstructural viral proteins. As new capsids are forming, a viral mRNA becomes enclosed within the capsid, along with the RdRp protein. Within the capsid, the RdRp synthesizes each mRNA transcript just once to create the complementary negative strand, thereby creating the dsRNA genome in the newly produced capsid (Tao and Ye 2010).

(+)ssRNA (class IV; e.g. CoVs, flaviviruses, and picornaviruses) viral genome is a mRNA molecule that is translated by host ribosomes into a long polyprotein, to be further on cleaved into several smaller proteins. As the replication proteins of +ssRNA viruses are produced, they tend to gather at or within certain membranes (as endoplasmic reticulum (ER) or secretory vesicles) in the cell, building replication complexes (den Boon et al. 2010) that may facilitate the replication processes and protect the viral ssRNA from intracellular immune responses (Ravindran et al. 2016; Richards et al. 2014). The viral genome of +ssRNA viruses serves to create a

complementary negative strand, the antigenomic RNA, that is used as a template to generate many copies of the +ssRNA genome (Louten 2016).

(-)ssRNA (class V; e.g. *Paramyxoviridae*) viruses have an anti-messenger sense genome, which must be first transcribed by the viral RdRp into mRNA, which is then translated into viral proteins. As with (+)ssRNA viruses, the produced antigenomic RNA serves as template for replication of the genome, but in this case, the complementary antigenomic RNA is +ssRNA. During the viral replication, the RdRp switch from mRNA transcription to genome replication with the help of several translated viral proteins that bind to the (-)ssRNA genome at sites that would normally stop the polymerase, allowing it to continue copying the entire genome (Burrell et al. 2017; Louten 2016). Some viruses in this class have ambisense viral genomes (e.g. family *Arenaviridae*), with both messenger and anti-messenger sense regions (Nguyen and Haenni 2003). The positive-sense portion is not directly infectious, and it must be copied into an antigenome segment that is used to generate the viral mRNA and replicate similarly to (-)ssRNA viruses.

Another group of RNA viruses have an RNA to DNA step (RNA-DNA-RNA) in their life cycle (Class VI; e.g. *Retroviridae*), and consequently must encode a reverse transcriptase (RT), being known as reverse-transcribing viruses. The retrovirus genome is a positive single strand RNA that does not serve as mRNA (Ryu 2017). First, on the cytoplasm, replication is initiated with the production of a double-strand DNA copy from the viral ssRNA genome. This step requires two enzymes present in its virion: RT, which synthesizes DNA from either a DNA or an RNA template; and the ribonuclease H (RNase H), which degrades the RNA strand of a DNA–RNA duplex. The double-strand DNA copy of the genome is transported to the nucleus, where it integrates into the host DNA, an event catalyzed by another protein present in the virus, called integrase. The integrated DNA copy, called a provirus, is transcribed by cellular RNA polymerases, rather than a viral RdRp, to produce an RNA that is identical to the viral genome. This RNA is exported to the cytoplasm, either unspliced or as one or more spliced mRNAs, and acts as a messenger for the translation of a set of polyproteins, which contain the translation products of the gag, pro and pol genes, responsible for the formation of the viral capsid, the polyprotein precursors, and the RT, RNase H, and integrase proteins, respectively.

To finalise, other viruses contain double stranded DNA, and their genomes replicate through an RNA intermediate (DNA-RNA-DNA) (Class VII; e.g.

Hepadnaviridae) (Berman 2019). Contrarily to retroviruses, the reverse transcription step occurs at the end of their replication cycle to generate their DNA genomes (Strauss and Strauss 2008). The viral genome is transported to the nucleus where it is converted to a double-strand DNA, which does not integrate into the host genome, persisting in the nucleus as a nonreplicating episome. It is transcribed by cellular RNA polymerases, leading to the production of a series of RNAs to be exported to the cytoplasm where they serve as mRNAs. One of these RNAs, called the pregenomic RNA (pgRNA), serves as template for the reverse transcription into DNA, performed by the translated RT and RNase H enzymes at a core particle (assembled from viral capsid proteins, the viral enzymes, and pgRNA).

1.3.3. Assembly and release into the extracellular space

After the synthesis of the viral genome and all the viral proteins, the viral components need to be assembled to generate the new mature viruses (Strauss and Strauss 2008). The assembly process can occur alongside maturation and release, and the location will depend upon the virus. It can take place within the nucleus of the cell, at the plasma membrane, or at a variety of intracellular membranes. Most nonenveloped DNA viruses assemble in the nucleus, where the genome replication occurs, with the aid of viral proteins that are imported through nuclear pores. Smaller assembled DNA viruses will fit through the nuclear pores and cross the double-membraned nuclear envelope, but larger ones will not fit, and have to induce cell lysis or apoptosis to escape the nucleus. On the other hand, enveloped viruses derived from the plasma membrane usually assemble there, or in other intracellular membranes in the cytoplasm, such as ER and Golgi complex (Louten 2016; Zhu et al. 2021).

After or during assembly, some viruses go through maturation processes, transforming an immature virion in an infectious virion. These processes are mediated by host or virus-encoded enzymes (Rampersad and Tennant 2018). A good example is the influenza hemagglutinin protein that is involved in the attachment to the cell surface receptor. The hemagglutinin protein must be cleaved by cell proteases into two portions, so that the virion becomes infectious (Dou et al. 2018). Another example occurs in the CoVs, that synthetize an inactive precursor of the spike protein after entering host cells, which must be cleaved to be able to fusion to the membrane surface receptor. One of the hypotheses is that

this cleavage occurs in the maturation phase by the action of the host furin enzyme (Peacock et al. 2021; Wu and Zhao 2021).

The release of the virion into the extracellular environment is the final step of the viral replication cycle and can occur in different manners such as cell lysis, budding, or exocytosis (Payne 2017). Cell lysis results in cell death and can happen in cytolytic viruses such as variola virus (Priyamvada and Satheshkumar 2021). Budding occurs typically with enveloped viruses and consists of wrapping the virus in cell membranes, leading to the formation of vesicles through which viruses will be released to the outside. Viruses that acquire their envelope from the plasma membrane generally assemble embedding into the inside layer of this membrane. The constant interaction of the viral capsid proteins with the plasma membrane leads to the budding, and subsequently to the viral release. Viruses budding from other membranes in the cell, including ER, Golgi complex or even the nuclear envelope, generally undergo direct exocytosis (Cann 2008; Stass et al. 2019).

1.4. DENV as an example of neglected tropical virus

DENV is an arbovirus, transmitted by an arthropod vector, which due to globalization and climate changes has become a worldwide major concern, leading to outbreaks in atypic locations (Mayer et al. 2017). Two mosquito species are responsible for DENV transmission to humans, *Aedes aegypti* and *Aedes albopictus*, which are also responsible for spreading other arboviruses like the YFV, ZKV and Chikungunya viruses (Kraemer et al. 2019). After being exposed to the virus, an incubation period of 4-7 days ensues, and then the patient can either go asymptomatic or develop symptoms that range from a flu-like disease to a more severe case (Guzman et al. 2016).

DENV is an enveloped virus with a (+)ssRNA genome, that belongs to the family *Flaviviridae*, and can be genetically differented in four serotypes (DENV-1, DENV-2, DENV-3 and DENV-4) that nevertheless share epidemiological characteristics (Vasilakis et al. 2011). DENV has a genome of approximately 11kb of length (Figure 4), encoding three structural proteins (capsid - C, premembrane – prM, and envelope - E), and seven non-structural (NS) proteins (NS1, NS2A, NS2B, NS3, NS4A, NS4B, NS5) (Guzman et al. 2016).

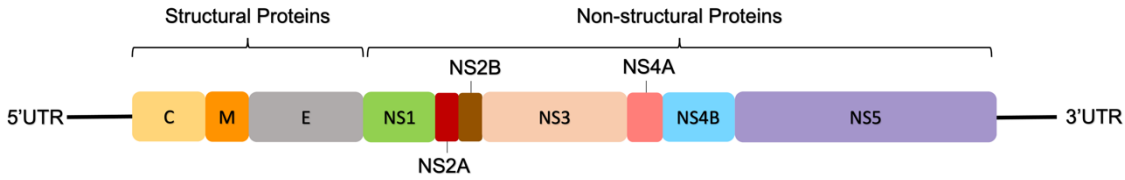


Figure 4 – Representation of the DENV genome, illustrating the order of the genes coding for structural (capsid - C, premembrane – prM, and envelope - E) and non-structural (NS1, NS2A, NS2B, NS3, NS4A, NS4B, NS5) proteins. Adapted from (Guzman et al. 2016).

1.4.1. Cell cycle of DENV

DENV is inoculated in a human host during the feed of an infected mosquito. After the injection of the virus in the dermis or directly into the bloodstream, macrophages and dendritic cells are the primary targets of the virus (Durbin et al. 2008; Wu et al. 2000). These cells can then migrate to the lymph nodes, which trigger the recruitment of monocytes and macrophages, leading to the dissemination of the infection. Evidences revealed that DENV is able to replicate in macrophages in lymph nodes, in peripheral blood monocytes, as well as in liver and spleen (Jessie et al. 2004).

It has been demonstrated *in vitro* that DENV is able to infect numerous cell lines, an evidence that the virus must bind to a ubiquitous cell receptor or to various receptors, in order to enter cells (Rodenhuis-Zybert et al. 2010). Throughout the years, several putative receptors have been recognized such as: heparan sulfate (Chen et al. 1997), heat shock protein 90 (Hsp90) (Reyes-Del Valle et al. 2005), CD14 (Chen et al. 1999), DC-SIGN (Lozach et al. 2005; Tassaneetrithep et al. 2003), mannose receptor (Miller et al. 2008), GRP78/BiP (Jindadamrongwech et al. 2004), and the 37/67-kDa high-affinity laminin receptor (Thepparit and Smith 2004).

The DENV infection life cycle (Figure 5) begins with the attachment to host cells by binding of the E protein to the host cell receptor, the consequent fusion with the host plasma membrane, and internalization into cell. DENV can enter the cells via all the different routes mentioned before, CLE, LME, MCP and CCIM (Acosta et al. 2009; Suksanpaisan et al. 2009; van der Schaar et al. 2008).

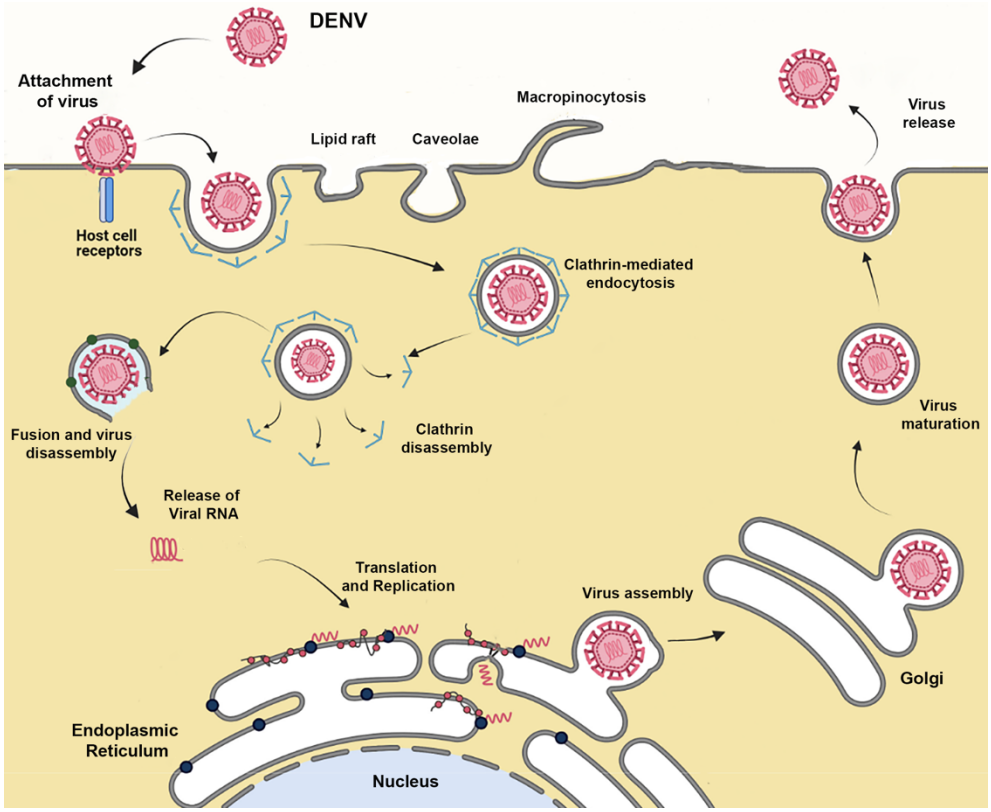


Figure 5 – DENV infection cell cycle. The cycle begins with the viral binding to host cell receptors and internalization into the cell. DENV can enter the cells via various endocytic routes. Inside the cell, the virus is transported in vesicles/endosomes, that will suffer pH-dependent rearrangements leading to disassembling and release of the viral RNA genome. The replication and translation occur on the ER, and translated viral proteins are assembled forming an immature particle, that is transported to the Golgi, where it undergoes a maturation process into virion that can infect new host cells, after exocytosis. Adapted from (Nanaware et al. 2021).

Once inside the host cell, the vesicle/endosome where the virus is transported, undergoes pH-dependent rearrangements, triggered in some cases by Rab5 and Rab7 proteins (van der Schaar et al. 2008). These rearrangements cause the fusion of the viral envelope and endosomal membranes, and lead to the release of the nucleocapsid. After disassembling, the viral RNA genome is translated into a polyprotein and cleaved by viral non-structural and host proteases into individual proteins, and then routed to the site of replication on the ER. The replicated genome and translated viral proteins are assembled with the prM and the E protein, embedding into the ER membrane and enclosing the newly formed nucleocapsid to form an immature particle. This immature virus is transported to the Golgi

apparatus, where the prM undergoes furin-mediated cleavage that leads to maturation into membrane (M) protein, enabling the virion to infect new host cells (Mukherjee et al. 2016; Zybert et al. 2008). The virion is then released from the infected cell by exocytosis (Nanaware et al. 2021).

1.4.2. Endemic and epidemic status

DENV is the most predominant arbovirus in the world. In the last two decades, the list of endemic countries enlarged, and the cases reported to WHO grew dramatically, with increasing numbers from around 500 thousand cases in 2000 to over 5.2 million in 2019. The deaths reported also raised from 960 in 2000 to 4,032 in 2015, with the younger ages being more affected (WHO 2022). A significant number of cases are asymptomatic or mild, and occasionally misdiagnosed as other febrile diseases circulating in the endemic zones, which means that the actual numbers of dengue cases are under-reported. The prevalence studies estimate the occurrence of 390 million dengue virus infections per year, of which 96 million have clinical manifestations (with any severity of disease) (Bhatt et al. 2013), and 3.9 billion people are at risk of infection in 128 countries (Brady et al. 2012).

Currently, WHO classifies as endemic more than 100 countries (Figure 6), meaning that the occurrence of dengue disease is constant in those geographic areas (Porta 2008). The endemic regions more affected are in South-East Asia and Western Pacific, corresponding to 70% of the actual burden, and having reported multiple outbreaks in 2020 (Bhatt et al. 2013; WHO 2022). As every year there is at least one outbreak (increase of number of cases, above the normally expected, in a limited geographic area (Porta 2008)), the adult population has been already in contact with DENV serotypes, and only young children become newly infected. Therefore, new Dengue cases in Asia occur in children and in tourists from naïve regions (Guzman et al. 2016).

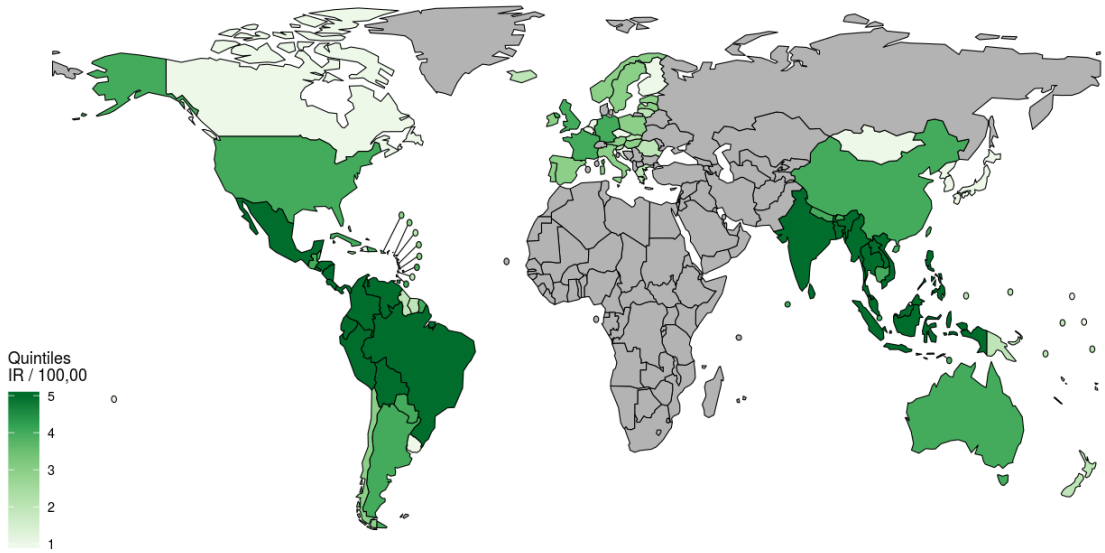


Figure 6 – World incidence of dengue between 1990-2017 – Source WHO (online dengue data application https://ntdhq.shinyapps.io/dengue5/, accessed on 28.02.22).

Latin America is also an endemic region where the concern with the occurrence of DENV has been raising, with epidemic or more circumscribe outbreaks occurring yearly (Bhatt et al. 2013; Gubler 2011; Ramos-Castañeda et al. 2017). The increase in dengue cases has been also observed in Africa, in the Pacific and Indian Oceans, where the disease burden is known to be underestimated due to the lack of occurrence data communication, and to dengue being misdiagnosed with other diseases with similar symptoms (Gainor et al. 2022; Humphrey et al. 2016).

The increasing expansion of the mosquito species that transmit the virus, and the lack of effective vector control has raised global health concern (Kraemer et al. 2015). In fact, several cases in the last years have occurred in naïve regions, including Europe, the most significant of which was the outbreak of 2,000 cases occurring in Madeira Islands, Portugal, in 2012 (Wilder-Smith et al. 2014).

With the SARS-CoV-2 pandemic, the incidence of Dengue decreased 44·1% in endemic regions due to COVID-19-related lockdowns, such as the closure of schools and reduced time spent in non-residential areas, and the decrease in the global population mobility (Chen et al. 2022). Besides that, in some countries, the COVID-19 disruptions made the surveillance of DENV infections get worse, especially due to the reduced availability of laboratory testing for dengue (Lu et al. 2021; Olive et al. 2020; Silva et al. 2021).

1.4.3. Characterization of Dengue fever disease

Most of the DENV infection cases are asymptomatic, but the severest forms can lead to potentially deadly complications (Guzman et al. 2016). The milder form of the disease is known as Dengue Fever (DF) and is characterized by a rapid onset of fever, accompanied by severe headaches, myalgias, arthralgias and gastrointestinal discomfort. These symptoms can last between 7 and 14 days, after which homeostasis is normally restored (Diamond and Pierson 2015). The more severe cases, known as Dengue Haemorrhagic Fever (DHF), are characterized by the DF symptoms combined with coagulopathy, spontaneous bleeding, low to moderate liver injury and increased vascular fragility and permeability. DHF can eventually evolve to an even more severe case, identified as Dengue Shock Syndrome (DSS) and characterized by rapid fluid loss that result in severe hypotension and haemorrhagic episodes, mainly bleedings in the skin and the gastrointestinal tract. These symptoms can sometimes lead to death (Wilder-Smith, Ooi, et al. 2019).

The DENV infection has the particularity that a first infection does not confer immune protection to a second infection with another serotype and can even increase the risk of severe disease. This phenomenon is called antibody-dependent enhancement (ADE), and was firstly described in 1970 (Halstead et al. 1970). It consists in pre-existing antibodies present in the body, from a primary infection with DENV, recognizing and binding to a viral particle from a second infection with a different dengue serotype (Shukla et al. 2020). Instead of promoting viral neutralization, these pre-existing antibodies enhance viral infectivity through internalization of virus-containing immunocomplexes by cells bearing Fc receptors, such as mononuclear phagocytes (Murphy and Whitehead 2011). The ADE cause an increase in both the total number of infected cells and the amount of virus produced, leading to an exacerbated response of the immune system, with a storm of cytokine production (Guzman et al. 2013). The non-neutralizing antibodies can also result from low concentrations of dengue antibodies of maternal origin in the infant sera (Murphy and Whitehead 2011).

1.4.4. Vaccines and treatment

Currently, there is no treatment available against DENV infection, and medical doctors can only try to minimize symptoms and complications (Wilder-Smith, Ooi,

et al. 2019). In mild cases, to reduce the pain and fever, the antipyretics are the first line of treatment, avoiding in this way the use of corticosteroids and other nonsteroidal anti-inflammatory drugs, which have shown no improved results, and have the risk of causing bleeding. Solutions of mineral salts and water-soluble molecules, known as crystalloids, are employed to keep intravascular volume, blood pressure and urine formation at normal levels. In severe cases, like DHF and DSS, volume expanders are used for the re-establishment of intravascular volume, blood pressure and tissue perfusion (Rajapakse et al. 2012).

The HMG-CoA reductase inhibitors, known as statins, are commonly used in the treatment of patients with hyperlipidaemia. Several *in vitro* studies have investigated their possible role against DENV infection, given the lipid metabolism action in viral infections and their effect on the endothelial function (Martinez-Gutierrez et al. 2014; Martínez-Gutierrez et al. 2011). Despite the good tolerance to statins treatment by infected patients, the promising *in vitro* results were not replicated in clinical trials, and no beneficial effects in diminishing symptoms or viremia were observed (Chia et al. 2018; Whitehorn et al. 2016).

Metformin, a first line drug used for the treatment of type 2 diabetes, has shown *in vitro* and *in vivo* antiviral effect against DENV infection by activating 5' adenosine monophosphate-activated protein kinase, an essential regulator of cell metabolism, and reducing HMG-CoA reductase activity (Cheang et al. 2021; Farfan-Morales et al. 2021). Currently, there is a phase 1 clinical trial aiming to investigate the possible role of metformin as host-directed therapy in obese/overweight patients with dengue disease and to evaluate the safety and tolerability to this drug (National Library of Medicine (NLM, NCT04377451)).

Recently, a promising pan-serotype dengue virus inhibitor has been described: JNJ-A07 (Kaptein et al. 2021). The mechanism of action involves the targeting of the NS3–NS4B viral proteins interaction, preventing the formation of the viral replication complex, and showing activity against 21 clinical isolates representative of the genetic diversity of DENV. The compound showed efficacy in prophylactic and in therapeutic models, and it is currently in phase 2 clinical trials, sponsored by Janssen (NLM, NCT04906980).

There is only one authorized vaccine to fight Dengue disease: the Dengvaxia commercialized by Sanofi Pasteur (FDA 2019). The live-attenuated vaccine was approved for the prevention of the disease caused by the four DENV serotypes in

endemic regions, and its administration is limited to people who have had a previous infection with DENV (Sridhar et al. 2018). This limitation was imposed because, when this vaccine was introduced in some endemic countries like Philippines, its general use has caused an additional risk of hospitalization for severe dengue, mostly in children who had not had a previous dengue infection (Wilder-Smith, Flasche, et al. 2019). Other vaccine candidates against Dengue have been under investigation and enrolled in clinical trials, including the live-attenuated tetravalent chimeric vaccine by Takeda (Osorio et al. 2016), that is in phase 3 (NLM, NCT02747927) ; and a recombinant tetravalent vaccine by Merck (Manoff et al. 2019), that finished phase 1 (NLM, NCT01477580).

1.5. SARS-CoV-2 as an example of a recently emerged virus

In December 2019, an outbreak due to a novel coronavirus, named as SARS-CoV-2, began in Wuhan, China (Wu et al. 2020). COVID-19 was the name given to the disease triggered by the infection with this new virus. The human-to-human transmission was reported to occur through respiratory droplets or direct contact with the infected patients (Chan et al. 2020).

The first SARS-CoV-2 genome sequences to be available were obtained from one (Wu et al. 2020) and nine (Lu et al. 2020) Chinese patients early on in the epidemic. The sequences showed relatedness to other beta-CoVs of bat origin, indicating that these animals were the likely reservoir hosts (Wu et al. 2020; Zhou et al. 2020). This new human-infecting CoV (HCoV) adds to a previous list made of: SARS-CoV that emerged in Guangdong, China during 2002–03 (Chan-Yeung and Xu 2003); the Middle East respiratory syndrome (MERS) CoV (MERS-CoV), first detected in Saudi Arabia in 2012 (Zaki et al. 2012); few other HCoVs that only cause mild flu-like symptoms (Lu et al. 2020).

As other viruses of the *Coronaviridae* family (Chen et al. 2020), SARS-CoV-2 is an enveloped (+)ssRNA virus. CoVs are common in birds (gamma- and delta-CoV genera) and mammals (alpha- and beta-CoV genera), including domesticates as dogs, cats, pigs and cows (Lu et al. 2020). CoVs have large genomes (Figure 7), with 26-32 kb in length, that encode for non-structural and structural proteins. The structural proteins spike (S), E, M and nucleoprotein (N) are key pieces to the entry and replication of the virus in the host cells (Chen et al. 2020).

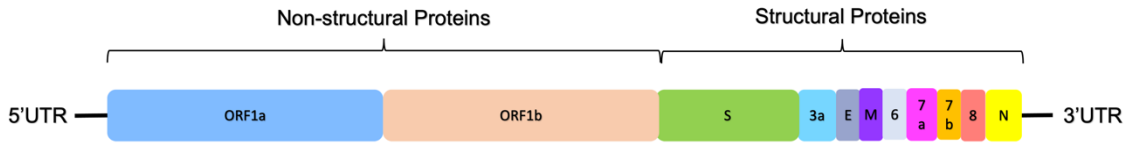


Figure 7 - Representation of SARS-CoV-2 genome, illustrating the order of the genes coding for non-structural (comprised of open reading frame 1a and 1b) and structural (S, E, M, N, and accessory) proteins. Adapted from (Kim et al. 2020).

1.5.2. Cell cycle of SARS-CoV-2

Early in the beginning of the pandemic, evidence showed that SARS-CoV-2 and SARS-CoV share the same main human cellular receptor, ACE2 (Andersen et al. 2020). The interaction of the receptor-binding domain (RBD) from the S protein of SARS-CoV-2 with the host ACE2 is required for membrane fusion and viral entry into the target cell. After the binding to the ACE2 (Figure 8), the virus efficiently uses the host transmembrane serine protease 2 (TMPRSS2), an enzyme that is present in high amounts on the extracellular space of respiratory cells. TMPRSS2 cleaves the spike protein on the S2 subunit and exposes parts that fuse the viral membrane with the host membrane (Hoffmann, Kleine-Weber, Schroeder, et al. 2020). By mainly using the TMPRSS2 route, SARS-CoV-2 infects faster than SARS-CoV. This latter virus preferentially uses the host protease cathepsin L through endosomes, a route that is more easily trapped by antiviral proteins (Peacock et al. 2021).

After membranes fusion, the virus releases its RNA genome directly into the cell. Once in the cytoplasm, host ribosomes will start translation of the viral RNA into non-structural proteins, which will be responsible for the suppression of host mRNA translation (Schubert et al. 2020). This viral hijacking of the host machinery includes the remodelling of the ER into double-membrane vesicles (DMVs), providing special conditions for more viral RNA to be replicated and translated (Klein et al. 2020). In parallel, cellular mRNA will be prevented from getting out of the nucleus, impeding the release of signaling proteins (like interferons) to alert the immune system of the presence of an infection (Thoms et al. 2020; Zhang, Miorin, et al. 2021). SARS-Cov-2 is more efficient than other respiratory viruses in

preventing the human immune system from recognizing and combating the infection in the initial phases, silently proliferating. When the immune system senses the presence of SARS-CoV-2 , an exacerbated reaction will then take place, causing more damage to human cells (Blanco-Melo et al. 2020).

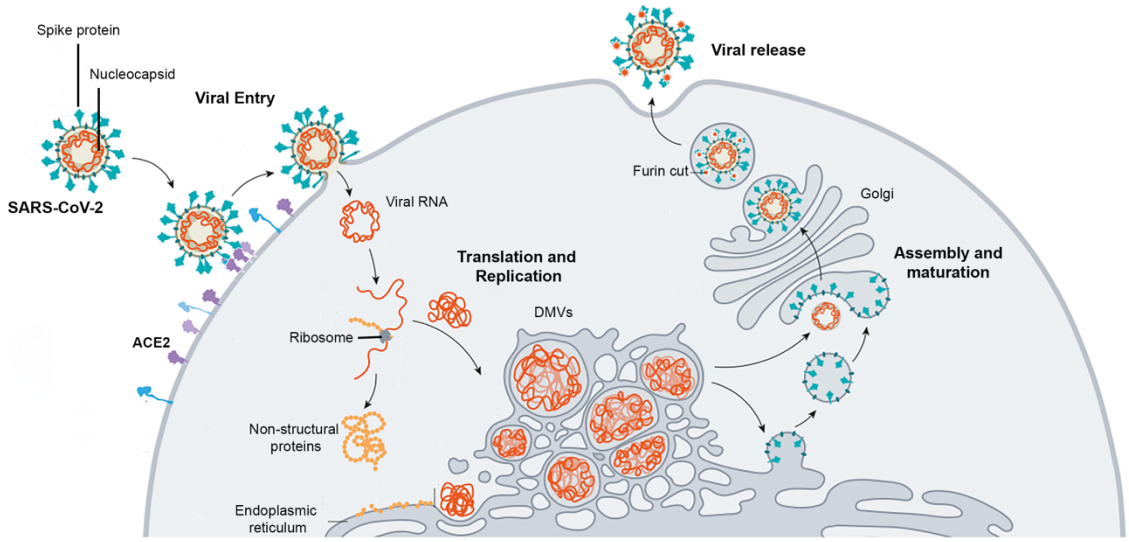


Figure 8 - SARS-CoV-2 infection cell cycle. After the binding to the cell host receptors, the virus fuses with the plasma membrane, and releases its RNA genome directly into the cytoplasm, where the host ribosomes start translating the viral RNA into non-structural proteins. The replication occurs on the ER, that suffers structural rearrangements into DMVs. After assembly is complete, the virus will exit the cell through the Golgi or lysosomes. A final maturation process is executed by the host enzyme furin. Adapted from (Scudellari 2021).

With the host protein translation significantly reduced, only the proteins with viral tag will be translated, and viral synthesis will proceed without limitations (Finkel et al. 2021). New viral RNAs will be generated which will code structural proteins and lead to the production of new virus particles, like the spike and accessory proteins. Once the newly made molecules assemble into a complete virus particle, they will exit the cell through the Golgi apparatus or lysosomes (Ghosh et al. 2020), the exact route being not clearly elucidated. A final process during the virion assembly or just before release is performed by a host enzyme named furin. This enzyme makes an essential cut at a site of five amino acids on the spike protein, which

prepares the virus to attack another cell (Hoffmann, Kleine-Weber and Pöhlmann 2020).

1.5.3. Pandemic status and variants of concern

Emerging viruses are recurrent tests to society, and SARS-CoV-2 has been especially challenging. The pandemic status was declared on March 2020 by WHO, after epidemic occurrence increased over a wide area, crossing international boundaries, and affecting a large number of people. Two years after, by March 2022, SARS-CoV-2 has already infected 460 million people and caused more than 6 million deaths around the world (Dong et al. 2020).

These two years of pandemic saw the emergence of several SARS-CoV-2 variants of concern (VOC) (Figure 9), which have recurrently put in question the efficacy of the vaccines and drugs that have become available (Hirabara et al. 2021). The first VOC, containing the D614G mutation in the spike gene, spread dramatically in Europe in mid-2020 (Korber et al. 2020). This mutation in the *S* gene was associated to a higher viral load and a better binding to the ACE2 receptor (Plante et al. 2021; Volz, Hill, et al. 2021).

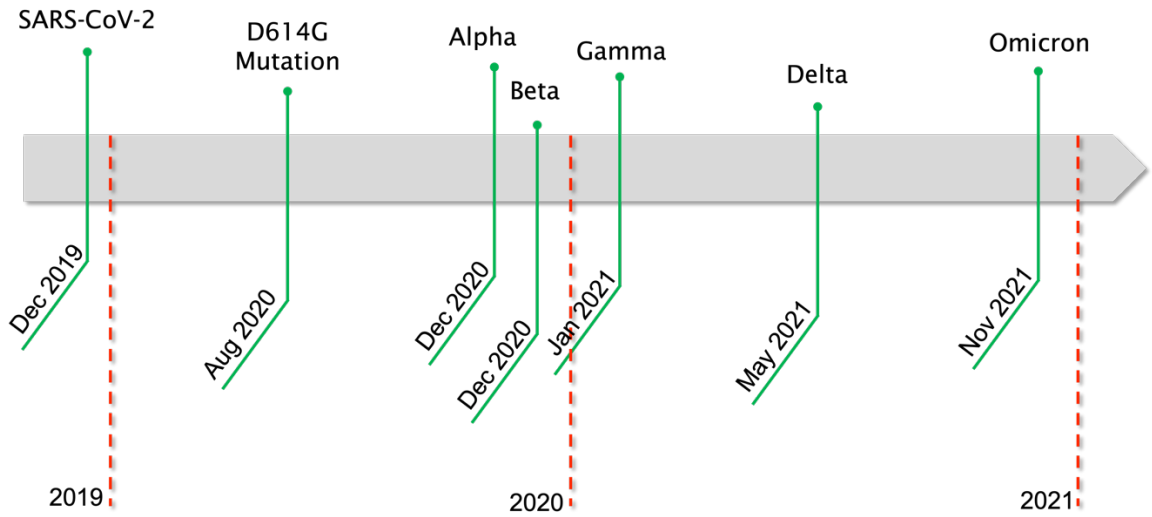


Figure 9 - Emergence over time of SARS-CoV-2 variants of concern

Late in 2020, the Alpha variant (20I/501Y.V1 or B.1.1.7 lineage) was firstly identified in the United Kingdom, but had a rapid spread to the rest of Europe and the globe, and was also associated to higher viral loads and higher number of deaths (Challen et al. 2021; Davies et al. 2021; Volz, Mishra, et al. 2021). This VOC has several mutations in the *S*, *N*, *ORF-1* and *ORF-8* genes, with the main mutations occurring in the S protein including the N501Y, A570D, P681H, T716I, S982A, D1118H, and the deletions ΔH69/ΔV70 (Zhang, Cui, et al. 2021).

At the same time, the Beta VOC (20H/501Y.V2 or B.1.351 lineage) was detected in South-Africa, and had a fast spread across the world (Tegally et al. 2021). This variant has several structural and nonstructural mutations, including eight mutations in the spike protein, particularly with K417N, E484K, and N501Y mutation in the RBD region. These RBD mutations increased the binding affinity to ACE2 and were critical to exacerbate the immune escape from neutralizing antibodies and consequently reduce vaccine effectivity against infection (Zhang, Cui, et al. 2021).

In the beginning of 2021, the Gama VOC (20J/501Y.V3 or P.1 lineage) was identified in Brazil (Faria et al. 2021), causing high mortality (Buss et al. 2021). Two mutations (E484K and N501Y) in the RBD were shared with Beta VOC, with the addition of the K417T (Zhang, Cui, et al. 2021). This lineage has also increased ACE2 receptor binding affinity, transmissibility, and resistance to immune response, although the neutralization resistance of the Gamma VOC was less robust than the resistance of Beta VOC (Zhang, Cui, et al. 2021).

The Delta VOC (21A, 21I, 21J or B.1.617.2 lineage) was first identified in late 2020 in India, but by mid-2021 it was the most dominant one in several countries around the world (Cherian et al. 2021; Ferreira et al. 2021; Mlcochova et al. 2021). This variant bears nine mutations in the spike protein. *In vitro* studies showed that Delta was less sensitive to neutralizing antibodies and had a higher replication efficiency than Alpha VOC (Mlcochova et al. 2021).

The Delta VOC was prevalent until the end of 2021, when it was replaced by the Omicron VOC (21K, 21L, 21M or B.1.1.529 lineage). The latter was first described in South Africa and Botswana (Viana et al. 2022), and presented more than 30 mutations on the spike protein of the virus. The K417N along with E484A mutation, like in Beta VOC, was expected to make Omicron more likely to escape vaccine protection. The loss of inhibitory activity of highly neutralizing anti-RBD antibodies

against Omicron, could explain the observed rise in symptomatic infections in vaccinated individuals, by the possible decrease in the antibody response generated after vaccination (VanBlargan et al. 2022).

1.5.4. COVID-19 characterisation

Like other HCoVs, SARS-CoV-2 is primarily transmitted through respiratory droplets from an infected individual. The incubation period is estimated to be 5-6 days and the patients can develop symptoms within 11-12 days of infection (Chan et al. 2020; Lauer et al. 2020). Although a high frequency of infections is asymptomatic (Cohen et al. 2022; Ma et al. 2021), the most frequent clinical presentation is a mild respiratory tract infection, associated with fever, cough, myalgia and loss of smell and taste. But the disease can evolve to severe forms, with patients presenting an atypical pneumonia, and requiring supplemental oxygen or even artificial ventilation, that can progress to organs failure and death (Guan et al. 2020). The risk of developing severe forms of Covid-19 is increased in aged people and when comorbidities are associated, such as diabetes, hypertension, and obesity (Booth et al. 2021).

The cytokine storm was frequently pointed as the cause of severe outcome in COVID-19 patients (Chen et al. 2021). In fact, these patients presented increased proinflammatory cytokines (e.g., IL-1 and IL-6 (Qin et al. 2020)) along with elevation of inflammatory chemokines (e.g., CCL2 (Xiong et al. 2020)), with consequent severe lung pathology. When SARS-CoV-2 enters the cells, and establishes a sustained infection, it is detected by cytosolic sensors from the innate immune system, which will lead to the production of IFNs and proinflammatory mediators. The activation of these pathways in this disease will lead to an impaired increase of inflammatory cytokines/chemokines and, consequently, the damage of tissues through endothelial dysfunction and vasodilation, which will amplify the recruitment of immune cells promoting a hypoxic environment and rapid progression of respiratory failure (Harrison et al. 2020). The exacerbation of the immune system is one of the main treatment strategies explored in this disease (Hwang et al. 2022).

1.5.5. Vaccines and treatment

At the end of 2020, four vaccines have been approved by the regulatory authorities (Food and Drug Administration (FDA) in United States and European Medicines Agency (EMA) in Europe) for emergency use: two based in mRNA technology, containing a synthetic part of the SARS-CoV-2 genetic material (Pfizer BioNtech and Moderna); and the other two based on the viral vector technology, where the SARS-CoV-2 genetic code was packed in a carrier virus (Astrazeneca and Jonhson & Jonhson). Both approaches lead to the production of key viral proteins in the vaccinated individual that can trigger an immune response (**Error! Hyperlink reference not valid.**). By March 2022, there are at least 340 vaccine candidates, 122 in clinical testing, and 30 in use (Shrotri et al. 2021)

During the pandemic, several clinical trials were started, and various drugs have been tested. Unfortunately, some drugs with *in vitro* promising results showed no effect when used in patients and have been abandoned, such as the case of chloroquine, hydroxychloroquine and ivermectin (Altulea et al. 2021; Lim et al. 2022). Others are still in use, as the antiviral remdesivir (Veklury) and the glucocorticoid dexamethasone. The remdesivir is an adenosine analogue that competes with the substrate for the incorporation by RNA polymerase into viral RNA, leading to inhibition of the viral replication, and has been used in cases of moderate to severe disease (Gottlieb et al. 2021; Kokic et al. 2021). Dexamethasone is a synthetic glucocorticoid, with anti-inflammatory and immunosuppressive effects, and has been used as supportive treatment in patients with severe and critical disease (Horby et al. 2021).

More recently, alternative therapeutics have been approved (EMA 2022). For the treatment of mild to moderate disease, two antivirals have been approved: Paxlovid and Lagevrio. The Paxlovid combines two compounds: the PF-07321332, a 3CL protease inhibitor of SARS-CoV-2, and the ritonavir, recognized as an inhibitor of HIV-1 and HIV-2 proteases, that here acts as an inhibitor of cytochrome P450 3A and CYP2D6, that will inhibit the metabolism of PF-07321332, allowing the administration of lower doses of the substance (Boras et al. 2021; Eng et al. 2022; Saravolatz et al. 2022). The molnupiravir (Lagevrio) is an antiviral that, once inside the body, is converted into a synthetic cytidine nucleoside, which introduces errors on the genetic material of the RNA viruses during the replication. These alterations

will origin nonfunctional viral components resulting in an antiviral effect (Jayk Bernal et al. 2021; Saravolatz et al. 2022).

Monoclonal antibodies have also been approved as treatment drugs. They are synthetic proteins that mimic the immune system capacity to combat infectious agents (Hwang et al. 2022; Salazar et al. 2017). During the pandemic these treatments were strongly explored as emergence use, and currently five have been approved for COVID-19 disease: sotrovimab (Xevudy) regdanvimab (Regkirona) imdevimab + casirivimab (Ronapreve), tocilizumab (RoActemra), and anakinra (Kineret) (EMA 2022). The sotrovimab (Gupta et al. 2021), regdanvimab (Lee et al. 2022), and the combination of imdevimab with casirivimab (Razonable et al. 2021) are used in patients with mild to moderate disease and have a common mechanism of action: hamper SARS-CoV-2 infection by binding to different epitopes in RBD. Although, sotrovimab does not compete with human ACE2 receptor binding, regdanvimab and imdevimab-casirivimab combination block the interaction of RBD with ACE2 (**Error! Hyperlink reference not valid.**). The tocilizumab (Rosas et al. 2021) and anakinra (Kyriazopoulou et al. 2021) are used in severe and critical cases. The first binds specifically to the receptors for IL-6, impeding the subsequent signalling pathway and decreasing the pro-inflammatory effect of IL-6. The second, blocks the activity of IL-1, also affecting the pro-inflammatory process (**Error! Hyperlink reference not valid.**).

Recently, the FDA approved a combination of two monoclonal antibodies, tixagevimab and cilgavimab, as pre-exposure prevention of COVID-19 in immune compromised individuals, who may not develop an adequate immune response to COVID-19 vaccination (FDA 2021). Tixagevimab and cilgavimab are long-acting monoclonal antibodies that bind to specific non-overlapping sites on SARS-CoV-2 spike protein, and are expected to inhibit the attachment and entry of the virus into human cells (Loo et al. 2022).

2. Translational application in the field of infectious diseases

2.1. Molecular diagnosis

The conventional methods to diagnose viral infections are complex and time-consuming, and usually imply specialized technicians and a lab environment. In fact, most routine diagnosis of viral infections are still based on qRT-PCR, in which the DNA amplification is monitored in real time through a fluorescence read-out measured after each cycle (Holland et al. 1991). In the first cycles, the fluorescence signal is too low to be distinguishable from the background, but when the fluorescence intensity increases above the detectable level, the cycle corresponds proportionally to the initial number of template DNA molecules in the sample and is called the threshold cycle (Ct). The lower the Ct the higher the concentration of the nucleic acid in the sample. This Ct metric became widely known, also by the general public, during the COVID-19 pandemic, but the variability in Ct values with the kits and machines used, as well as between labs, made diagnostic labs cautious to not report it (Binnicker and Kraft 2020; Rhoads et al. 2020).

The qRT-PCR presents high sensibility and, importantly, high reproducibility (Espy et al. 2006), it was therefore elected as the main test by health systems along most the COVID-19 pandemic (Baldanti et al. 2022), till the emergence of the Omicron VOC and its vast numbers of infected people. The pressure put on confirmatory diagnosis, and the indications of higher viral loads in nasopharyngeal samples with this VOC compared with previous ones (Salvagno et al. 2022), led finally to the acceptance of positive results from fast antigen tests, while suspicious negative ones have to do the qRT-PCR (Osterman et al. 2022). These fast antigen tests that can be done by the user are based on antibody reaction. They are less sensitive than the qRT-PCR and the probability of cross-reaction with other pathogens is higher, being less specific than nucleic acid-based methods (Adnan et al. 2021).

Therefore, it remains vital to develop high sensitivity, practical and faster methods based on the detection of the pathogen nucleic acid. These improvements would answer the demand for POC tests, which are diagnostic tests performed at or near the place of collection of the sample, leading to a result within minutes and of easy interpretation (Vashist 2017). One limitation of the traditional PCR and qRT-PCR for automation and simplification is the need of alteration between temperatures in each cycle (Almassian et al. 2013). In recent years, several isothermal amplification

methods have been described (Zhao et al. 2015). One of this is RPA (Piepenburg et al. 2006) for which the exponential isothermal amplification of specific DNA fragments is achieved by the cyclic repetition of the following reactions: recombinase-primer complexes scan double-stranded DNA and facilitate strand exchange at cognate sites; the resulting structures are stabilized by single-stranded DNA binding proteins interacting with the displaced template strand; recombinase disassembly leaves the 3'-end of the oligonucleotide accessible to a strand displacing DNA polymerase; and, primer extension ensues.

Several researchers have been exploring the joining of isothermal amplification with easy and fast detection systems (Oliveira et al. 2021). An example of such was introduced in 2017 (Gootenberg et al. 2017), being named as SHERLOCK (Figure 10). This new genetic-based diagnostic method that uses Cas13a was first described for diagnosis of DENV and ZIKV. The CRISPR-Cas13a is a programmable endonuclease by crRNAs for specific RNA sensing. After recognizing its RNA target, Cas13a starts to cleave nearby non-targeted RNAs, as a collateral effect. The discovery group took advantage of this effect and designed the Sherlock method to detect nucleic acids with high sensitivity, by using isothermal amplification and the cleavage mediated by Cas13a of a fluorescently labeled reporter RNA. This method is an interesting discovery, since it is possible to design targets for any pathogen with known genomic sequence (Gootenberg et al. 2017; Kaminski et al. 2021).

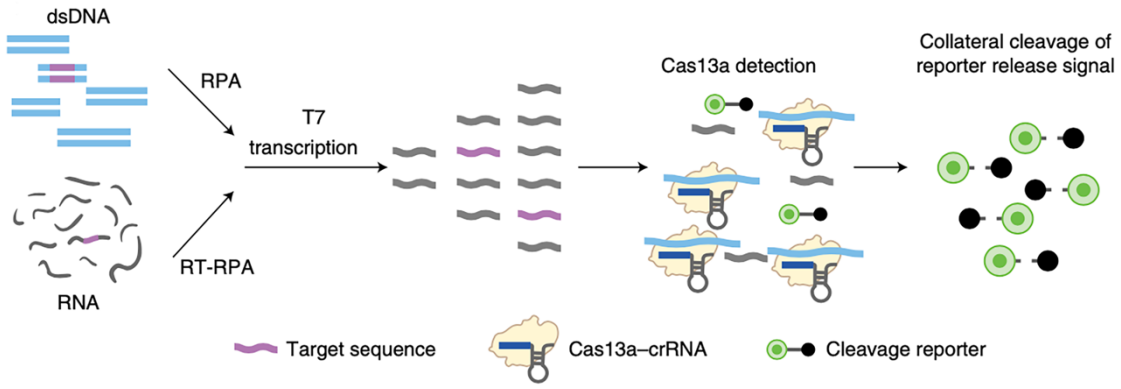


Figure-10 – SHERLOCK detection method, starting with the isothermal amplification of the specific target, and followed by its detection with Cas13a-crRNA that begins to cleave the target and other added RNA fluorescent reporters. Adapted from (Kellner et al. 2019).

2.2. Preliminary steps in drug testing: *in silico* and *in vitro* approaches

The traditional process from the discovery of a new drug until its introduction to the market is very long (Salazar and Gormley 2017). Thus, the option to recur to the repurposing of known drugs has several advantages and has been an attractive direction in the treatment of diseases (Pushpakom et al. 2019). In fact, approved drugs, and even some investigational compounds, have already been tested in humans, and essential information of safe doses and side effects is known, which leads to shorter development timelines and lower overall costs. Time and costs can be further reduced with a combination of *in silico* and subsequent *in vitro* approaches.

With the advances of omics techniques, several databases have been available for transcriptomics, proteomics, and pathogen-host interactomics data, and are continually being explored for the *in silico*–informed selection of drugs. These progresses are transforming the development and repurposing of drugs (Loging et al. 2007), allowing a preliminary guided selection of candidate drugs to be further tested *in vitro*. In general, this selection relies on the search of common biological targets between diseases and on the pleiotropic mechanism of actions of drugs. The COVID-19 pandemic has highlighted the importance of this type of approach (Gordon et al. 2020), since there was a need of a quick and effective response.

An example of a mining tool used for *in silico* drug discovery is the Connectivity Map (CMap), which was developed using gene expression profiles from tissues treated with many molecules (Lamb et al. 2006). Recently, CMap has been updated for the so called L1000 platform (Subramanian et al. 2017), where the number of profiles was increased to 1,319,138 from 42,080 perturbagens, which correspond to 25,200 biological entities for a total of 473,647 signatures. Users can enter information about the up- and downregulated genes in a specific disease into this mining tool to obtain the drugs related to gene expression patterns using data mining and pattern searching algorithms. The CMap tool has been used in the research for treatment of different diseases, such as cancer, (Uva et al. 2021; Vengoji et al. 2021; Yang et al. 2022), neurological (Lee et al. 2019; Soleimani Zakeri et al. 2021), cardiovascular (Tanaka et al. 2021; Wan et al. 2022) and infectious diseases (Amemiya et al. 2019; Le et al. 2021). In the latter case, CMap allowed to identify eight drug candidates (estradiol, etoposide, simvastatin, resveratrol, sirolimus, valproic acid, vorinostat and Y-27632 compound) for DHF

treatment, when applied to blood transcriptomic, proteomic and protein–protein interaction datasets (Amemiya et al. 2019). For COVID-19, the CMap tool (Le et al. 2021) enabled to identify 102 hits, from which 25 were identified in at least two of the signatures, several of which have been enrolled in clinical trials.

The *in vitro* tests are valuable tools for validation of the *in silico* approaches. This is the case of the above mentioned work on COVID-19 (Le et al. 2021), where the group validated 16 of the promising hits recurring to in vitro assays in the lung human cell line Calu-3 infected with SARS-CoV-2. They obtained encouraging preliminary results, with 11 of the 16 compounds tested, such as clofazimine and haloperidol, showing antiviral activity against SARS-CoV-2.

The *in vitro* testing can also be done dissociated from the *in silico* evaluation. Traditionally, these cell-based assays were used for testing just a small number of compounds to validate hypotheses and mechanisms of action. In fact, the same pathway can be involved in the development of different diseases. Therefore, when a drug is recognized to have an effect on one disease it has a good chance to be effective in other diseases, and the *in vitro* tests are suitable and fast methods to evaluate these possibilities. In one study (Leela et al. 2016), the research group explored the evidence that some antibiotics have showed effects against DENV infection, and tested lomefloxacin, netilmicin, and minocycline, three FDA-approved antibiotics, against DENV in the liver cells HepG2. They observed that minocycline reduced DENV infection for all the four serotypes and suggested that it acts by decreasing the phosphorylation of ERK and subsequently upregulating antiviral gene expression. Another group (Xu et al. 2017) took advantage of the findings that Sofosbuvir (an FDA-approved drug treatment for HCV infections) has demonstrated inhibition of viral RNA polymerases of other +ssRNA viruses, including ZIKV, in cell culture and in an animal model, and tested it *in vitro* against DENV infection. They found that Sofosbuvir has anti-DENV activity in cell culture, and the active triphosphate of the drug was an inhibitor of DENV NS5 polymerase activity.

More recently, in vitro testing *per se* is being applied as direct high-throughput screening (HTS) of thousands of components (**Error! Hyperlink reference not valid.**). In a first phase, the HTS is generally performed in a simple condition using an appropriated 2D cell line, where different concentrations of the compounds are tested in plates of 96-, 384-, or 1536-well formats, to select putative hits among the thousands of compounds tested. In a second phase, the identified hits (drugs

with the desired effect) are tested in other cell models more representative of the disease in the study. A good example of a HTS study was published recently for COVID-19, (Riva et al. 2020), testing 12000 clinical-stage or FDA-approved small molecules in Vero E6 cells. The screening identified 100 molecules that inhibit the SARS-CoV-2 replication. Of these, thirteen molecules were selected, including the PIKfyve kinase inhibitor apilimod and the cysteine protease inhibitors MDL-28170, Z LVG CHN2, VBY-825 and ONO 5334, for further efficacy on the human cell lines Huh-7 and HEK293T cells transduced with ACE2. The MDL-28170, ONO 5334 and apilimod presented better results, and were subsequently validated in more complex representative models: human induced pluripotent stem cell derived pneumocyte-like cell, and in an ex vivo lung culture system. The MDL-28170, ONO 5334 and apilimod showed viral replication inhibition, and apilimod also revealed antiviral efficacy in a primary human lung explant model.

A recent improvement into the *in vitro* models consists in the development of three-dimension (3D) cultures or organoids from primary or immortalized cells and tissues. Although they have the limitation of not resembling the entire complexity of a whole organism, they best mimic tissue multicellularity, are inexpensive, fast, and straightforward, allowing the study of several cellular targets, which would otherwise be difficult to assess in a macroscopic system (Rosa et al. 2021). These 3D models are a hopeful solution to reduce the use of animal models, address the associated ethical issues, and answer relevant questions in the disease's mechanisms of action.

II. Aims

The main aims of this thesis were to explore recently available molecular tools, together with *in vitro* and *in silico* modelling, to contribute with insights into the disease mechanisms that could be applied afterwards to improve diagnosis and treatment of viral diseases. We began by focusing on the dengue virus, but the emergence of the SARS-CoV-2 created an opportunity to extend our investigation to an unprecedented modern-era pandemic scenario. Specifically, the research work of this thesis was divided in the following goals:

1. **Testing of CRISPR-Cas13a based point-of-care diagnostic tools for DENV and SARS-CoV-2**

We tested the implementation of the CRISPR-Cas13a method Sherlock in two POC tests for DENV and SARS-CoV-2, specifically designed to address demands on an endemic versus pandemic scenarios, respectively. This work began before the COVID-19 pandemic, when one research group presented the method as extremely promising and easy to implement. Soon the pressure due to COVID-19 pandemic revealed serious constrains and needed improvements in the implementation.

2. **Combining *in vitro* infection assays, CMAs and immunocytochemistry to evaluate infection kinetics**

The COVID-19 pandemic made us especially aware how essential is to design efficient *in vitro* set-ups due to the: (a) pressure on acquiring real-time knowledge on SARS-CoV-2 infection; (b) huge restrictions in access to and transport of reagents; (c) interruptions due to the obligatory quarantines that necessarily impacted complex experiments. We explored the advantages of the simple automation technique CMA, widely used in the field of histology, when applied to model infection kinetics. We evaluated the practicability and efficiency of this InfectionCMA against traditional *in vitro* infection assays in two SARS-CoV-2 situations: effect of viral load in infection kinetics on Vero cells; infection kinetics in human cell lines and Vero cells.

3. **Multi-tissue transcriptomic-informed *in silico* investigation of drugs for the treatment of dengue fever disease**

The complexity and durability of the clinical trials of drugs led to investment on improving the preliminary steps of *in silico* and *in vitro* testing, so that fewer and

more promising drugs follow up in the screening. A type of powerful computer tools for the identification of drugs effective on a phenotype departs from transcriptomic data, such as the CMap tool. We applied a multi-tissue (liver, spleen and blood) transcriptomic-informed *in silico* investigation in dengue fever, by using the CMap tool and interpreted the results in the light of altered molecular pathways (inferred from the transcriptomics) and preliminary pin-point *in vitro* drug test results.

4. In vitro pharmacological inhibition of the main endocytic pathways in DENV and SARS-CoV-2 infection models

Drugs interfering with the biology of the host are very attractive for the possible treatment of emergent viruses. Within the biology of the host, endocytosis is a key function to be explored for antiviral drugs, although promising *in vitro* results have unfortunately not translated in clinical trials. Better understanding of the biological mechanisms governing endocytosis are needed. We aimed at providing insights contributing to elucidate the endocytosis mechanism used by DENV (strain 2) and SARS-CoV-2 (alpha variant) in diverse cell models, and by direct probing endocytosis via pharmacological inhibitors.

III. Research work

Paper I – Testing of CRISPR-Cas13a based point-of-care diagnostic tools for DENV and SARS-CoV-2.

Testing of CRISPR-Cas13a based point-of-care diagnostic tools for DENV and SARS-CoV-2

Ana C. Magalhães[1,2,3], Ricardo J. Pinto[1,2,3], Luisa Pereira[1,2,*]

[1] i3S - Instituto de Investigação e Inovação em Saúde, Universidade do Porto, 4200-135 Porto, Portugal; acmagalhaes@ipatimup.pt (A.C.M.); rjpinto@ipatimup.pt (R.J.P.)

[2] Ipatimup - Instituto de Patologia e Imunologia Molecular, Universidade do Porto, 4200-135 Porto, Portugal

[3] ICBAS - Instituto de Ciências Biomédicas Abel Salazar, Universidade do Porto, 4050-313 Porto, Portugal

* Correspondence: luisap@ipatimup.pt

Keywords: Point-of-care tests; CRISPR-Cas13a method; recombinase polymerase amplification; lab-on-a-disk; dengue virus; SARS-CoV-2

Abstract

We report our experience in trying to establish two point-of-care (POC) tests based on the CRISPR-Cas13a method Sherlock, for two viruses, DENV and SARS-CoV-2, which represent endemic versus pandemic scenarios, respectively. We began this work before the COVID-19 pandemic, when the method seemed extremely promising although still under the domain of one research group, and soon the pressure put by SARS-CoV-2 with revealed constrains and further testing needs. This learning process contributed informative insights that we will pursue for a successful use of the Sherlock methodology in POC testing of viruses. Namely, (1) to eliminate the isothermal amplification step, as it would save precious time, money and simplify design of the platforms; (2) improve the fluorescence readout by testing tandem CRISPR nucleases and multi-crRNAs in the same reaction; (3) test efficient microfluidic strategies, to decrease the volume of the reaction.

Introduction

POC tests, by definition, are diagnostic tests performed at or near the place of collection of the specimen, leading to a result within minutes rather than hours. These tests are witnessing large advances in recent years, as improvements in biosensors, microfluidic, bioanalytical platforms, assay formats, lab-on-a-chip technologies, and complementary technologies continue to lead innovation applied to health [1]. The impact of the COVID-19 pandemic on the POC diagnostics market has been tremendous, with projections of increase from USD 29.5 billion in 2020 to USD 50.6 billion by 2025, at a compound annual growth rate of 11.4% [2]. The rising incidence of infectious diseases will continue to feed this growth path. POC tests can greatly improve the management of infectious diseases, and avoid epidemic outbreaks by allowing the fast application of controlling measures, as we are testifying in COVID-19 pandemic [3, 4] and recent Ebola outbreaks [5]. This is a major issue in developing countries, where access to timely medical care is challenging, and the healthcare infrastructures are sparse [6].

Amongst POCs, Nucleic Acid Amplification Tests (NAAT) for the specific detection of the pathogen genome, continue to be basilar in human infections diagnosis. In recent years, isothermal or recombinase polymerase amplification (RPA)-based methods [7] are being tested as alternatives to the now traditional reverse transcription polymerase chain reaction (RT-PCR), such as: Nicking endonuclease amplification reaction (NEAR), Transcription mediated amplification (TMA), Loop-mediated isothermal amplification (LAMP), Helicase-dependent amplification (HDA), Clustered regularly interspaced short palindromic repeats (CRISPR), and Strand displacement amplification (SDA). RPA methods, by performing amplification of nucleic acids at a constant temperature, are amenable to be coupled with friendly-to-use/portable detection systems, allowing processing by personnel with minimum laboratory experience [8]. This is precisely the case of the SHERLOCK method (meaning Specific High-Sensitivity Enzymatic Reporter UnLOCKing) implemented by Gootenberg et al. [9], in which the CRISPR effector Cas13a enzyme is activated by guide RNAs (crRNAs) that specifically and sensitively (attomolar sensitivity) recognise the pathogen, in a fast as 1h period when coupled to RPA. The procedure includes reverse transcription of the viral RNA, amplification by RPA, transcription of DNA back to RNA and activation of the Cas13a enzyme by the specific viral RNA guide with detection of the result by fluorescence reading. All reactions may be performed at 37°C, allowing its easy implementation in tropical and subtropical places. The original paper applied

the method to detect viruses (namely, dengue fever virus or DENV) and bacteria, and to distinguish between strains/isolates. Since then, protocols were improved [10], multiplexed for the simultaneous differentiation of 169 human-associated viruses (and renamed as CARMEN - Combinatorial Arrayed Reactions for Multiplexed Evaluation of Nucleic acids; [11]), and, since the beginning of the COVID-19 pandemic, also applied to the diagnosis of SARS-CoV-2 [12, 13].

Various platforms can be used for conducting the SHERLOCK method, in order to match specifications of the diagnosis design (reviewed in [14]). Reactions can take place in multi-well plates with readout in the form of fluorescence reading in a machine reader, taking advantage of RNA or DNA reporter molecules carrying a fluorophore and a quencher. This format allows the testing of many samples at once, optimal for a pandemic situation, and implies a minimal lab set-up, compatible for instance with hospital or private diagnosis centres. Another interesting format is lateral-flow assay, as the commercially available system Millenia 1T (Milenia biotec, Giessen, Germany), in which reporter molecules carrying biotin and fluorescein amidite (FAM) bind to anti-fluorescein isothiocyanate (FITC) antibodies coupled to gold nanoparticles in the sample pad area of the strip. Although these lateral-flow assays are compatible with a self-use, in this case, the preparation of the sample for the SHERLOCK method would also need a minimal lab set-up, but with less investment in the detection part. During the last two decades we have seen centrifugal microfluidics as an advanced diagnostics platform, typically taking the shape of a compact disc (CD; lab-on-a-disk or LOD) with interconnected fluidic channels and chambers [15]. The combination of SHERLOCK and LOD has been tested successfully for the detection of human papillomavirus (HPV) strains 16 and 18 [16].

In this manuscript, we report the conceptualisation and attempts to establish two POC tests based on the CRISPR-Cas13a method Sherlock, for two viruses, DENV and SARS-CoV-2. We devised the POC test for DENV to be used in an endemic situation, while the one for SARS-CoV-2 was adapted to a pandemic scenario, reflecting current reality. Interestingly, the real pressure due to the COVID-19 pandemic was paramount in exposing serious constrains on dependence on reagents and heterogeneity of viral load in samples to be diagnosed.

Material and methods

1. Production and purification of the Cas13a protein

The Cas13a bacterial expression vector pC013 - Twinstrep-SUMO-huLwCas13a (Plasmid #90097) was purchase from Addgene (Watertown, MA, USA), the repository where the original authors [9] deposited it. This plasmid is provided in a Rosetta 2(DE3)pLysS Singles bacterial stab, which was used to streak bacteria onto Luria broth (LB)-agar plates (GRiSP Research Solutions, Porto, Portugal), with ampicillin (100ug/ml) and chloramphenicol (25 ug/ml; NZYTech, Lisboa, Portugal), and to obtain single colonies (incubation at 37ºC). The single colonies were used to inoculate an overnight liquid culture to grow enough bacteria for plasmid DNA purification and for creating glycerol stocks (for long storage at -80ºC). The plasmid DNA purification was performed by miniprep with the NZYMiniprep kit (NZYTech, Lisboa, Portugal), followed by verification by Sanger sequencing, using T7 promoter (5'-TAATACGACTCACTATAGGG-3') and T7 terminator (5'-GCTAGTTATTGCTCAGCGG-3') primers.

A 50 mL starter culture, from the glycerol stock of LwCas13a expression plasmid, was first grown overnight in Terrific Broth (TB) growth media (T0918; Merck, Darmstadt, Germany), with ampicillin and chloramphenicol, and then 5ml/L of the overnight culture was used to inoculate 4L of TB for growth at 37ºC and shaking at 200 RPM until an optical density (OD, 600nm) of 0.4-0.6. At this time, culture flasks were transferred to 4ºC for 30 min to allow cooling before induction, and an aliquot was collected for sodium dodecyl sulphate–polyacrylamide gel electrophoresis (SDS-PAGE) analysis (uninduced sample). Then, protein expression was induced by supplementation with 1ml/L 0.5M IPTG (Merck, Darmstadt, Germany), and the culture shacked for 16h at 150-160 RPM in a pre-chilled 21ºC biological shaker. An aliquot of the induced culture was collected for SDS-PAGE analysis (induced sample). Cells were harvested by spinning the culture down at 4000 RPM for 15 min at 4ºC (High Speed Centrifuge Avanti J-26 XP with a JLA-8.1000 rotor; Beckman Coulter, Brea, CA, USA) and stored at -80ºC for later purification. The uninduced and induced culture aliquots were loaded onto a 12% SDS-PAGE gel (Gel 1) and visualized with PageBlue Protein Staining Solution (Thermo Fisher, Waltham, MA, USA).

For the protein purification, the frozen cell pellet was crushed and resuspended in 4x (wt/vol) lysis buffer (20mM Tris-HCl, 500mM NaCl, 1mM DTT; pH 8.0) supplemented with protease inhibitors (Complete Ultra EDTA-free tablets), lysozyme, and

benzonase, by stirring the mixture at 4ºC for 30 min on a magnetic stir table. After this step, cells were rupture on ice using sonication (Sonifier 250; Branson, Danbury, CT, USA) with the following conditions: amplitude setting of 5, duty cycle 50 for 10 sec (hence 10 pulses) on and 30 sec off, a total of 10 times. A fraction was collected for SDS-PAGE analysis (lysate sample). Lysate was cleared by centrifugation for 40 min at 18,500 RPM at 4°C (High Speed Centrifuge Avanti J-25, with a JA 25-50 rotor, Beckman Coulter, Brea, CA, USA). The supernatant was decanted into a conical 250 ml tube and fractions of supernatant and pellet were collected for SDS-PAGE analysis (cleared cell lysate sample, and cell pellet after clearing of lysate sample). The supernatant was filtered through a 0.45µm filter (Merck, Darmstadt, Germany), and then applied to 5ml StrepTactin Sepharose resin (GE Healthcare, Chicago, IL, USA) and incubated with rotation for 1h (4ºC). A fraction was collected for SDS-PAGE analysis (after 1h resin sample). The protein-bound StrepTactin resin was washed three times in lysis buffer, and a fraction was collected for SDS-PAGE analysis (flow-through resin sample). The resin was resuspended in SUMO protease cleavage solution (lysis buffer with 250ul of SUMO protease and 22.5ul of NP-40 detergent) and incubated overnight at 4˚C with rotation (gently shaking). The column was drained, and the cleavage solution was collected into a separate 50-ml Falcon tube (eluted fraction sample for SDS-PAGE). The remaining sample was washed three times with 5ml of lysis buffer, to ensure complete transfer of the cleaved or untagged LwCas13a protein (a sample for SDS-PAGE was collected from each wash, wash 1, wash 2 and wash 3 samples, and the resin, final resin sample). All these samples were run in SDS-PAGE Gel 2.

The protein was then purified by fast protein liquid chromatography (FPLC; AKTAprime plus; Cytiva, Marlborough, MA, USA), using first a 5mL HiTrap SP HP cation exchange column (GE Healthcare, Chicago, IL, USA), by following the published protocol [10]. The resulting fractions were tested for the presence of LwCas13a by SDS-PAGE (Gel 3), and the ones identified as containing the protein were then pooled in 15ml centrifugal spin filter unit (50 MWCO; Merck, Darmstadt, Germany) and concentrated to 1mL final volume by centrifugation for 15 min at 13000 RPM at 4°C. A further purification was performed (Biologic Duoflow system; Bio-Rad Laboratories, Hercules, CA, USA), by using a Superdex 200 Increase 10/300 GL size-exclusion chromatography column (GE Healthcare, Chicago, IL, USA), and following the published protocol [10]. The resulting fractions from gel filtration were analyzed by SDS-PAGE (Gel 4), and fractions containing LwCas13a were pooled and concentrated as referred before. The buffer containing the protein was replaced by Storage Buffer (SB; 600 mM NaCl, 50 mM TrisHCl pH 7.5, 5% glycerol, 2mM DTT), for preservation

and last SDS-PAGE (final concentrated protein and flow-through filter samples; Gel 5). The final protein concentration was measured in NanoDrop1000 (Thermo Fisher, Waltham, MA, USA), diluted to 2 mg/mL in protein SB, and stored as 5µL aliquots in PCR strip tubes at -80ºC until use.

2. Designing of primers, crRNAs and synthetic positive targets

RPA primers were designed in NCBI Primer-BLAST [17], using default parameters, except for: amplicon size (between 100 and 190 nt); primer melting temperatures (between 54˚C and 67˚C); and primer size (between 25 and 35 nt). All the forward primers included the T7 RNA polymerase promoter sequence (GAAATTAATACGACTCACTATAGGG) at the 5'end. Primers were then ordered as DNA sequence (Integrated DNA Technologies, Coralville, IA, USA; STAB VIDA, Caparica, Portugal). The reference genomes used for each virus and strain were: DENV – NC_001477.1; DENV2 – KM204118.1; DENV3 – KU050695.1; DENV4 – JQ822247.1; SARS-CoV-2 - NC_045512.2.

The crRNAs contain a 5' direct repeat sequence (GAUUUAGACUACCCCAAAAACGAAGGGGACUAAAAC) and a 28nt spacer sequence designed by us as the reverse complement of the target site in the transcribed RNA (avoiding overlap with RPA primers to reduce off-target amplification products). These constructs were chemically synthesized (Integrated DNA Technologies, Coralville, IA, USA).

To create synthetic positive targets, we selected ~200 bp sequences from the viral genomic DNAs that included the respective amplified segments. These targets were ordered as gBlocks (Integrated DNA Technologies, Coralville, IA, USA), with the T7 RNA polymerase promoter sequence added to the 5' end. The targets were initially diluted in UltraPure DNase/RNase-Free Distilled Water (ref. 10977035; Thermo Fisher, Waltham, MA, USA) to obtain original stocks at 1ug/ul concentration. Then the original stocks were submitted to serial ten-fold dilutions till a concentration of $1x10^{-7}$ ug/ul (1 to $1x10^{-7}$ in the figures), for the sensitivity test.

3. The COVID-19 human samples

Nasopharyngeal samples from suspected COVID-19 patients were processed for molecular diagnosis by qRT-PCR. For the extraction of the nucleic acids and inactivation of viral RNA, the FOSUN Ultrapure NA Nucleic Acid Extraction and

Purification kit (Fosun Pharma USA Inc., Princeton, NJ, USA) was used. The qRT-PCR kit included three SARS-CoV-2 genes (ORF1ab, E and N - Fosun COVID-19 RT-PCR Detection Kit; Fosun Pharma USA Inc., Princeton, NJ, USA), and the protocol recommended by the company was followed. The samples were run in a 7500 Fast RT-PCR instrument (Thermo Fisher, Waltham, MA, USA), with the following program: 95°C during 3min, followed by 50 cycles of a 5s denaturation step at 95°C and a 40s annealing/elongation step at 60°C. Whenever the nasopharyngeal samples were not immediately processed, they were stored at -80ºC, in order to avoid degradation of the viral RNA. The nucleic acids were quantified in the extracted samples in the Qubit® 3.0 Fluorometer (Thermo Fisher, Waltham, MA, USA).

4. PCR and RPA – step 1 of Sherlock method

Conventional PCR amplification of each target was performed by using the pairs of primers referred to in Table 1, the NZYTaq II DNA polymerase (NZYTech, Lisboa, Portugal), and the following program: initial denaturation at 94°C during 5min; 40 cycles of 1min denaturation at 94°C, 1min annealing at primers specific temperature and 1min elongation at 72°C; and final extension of 20min at 72°C.
For the isothermal method, RPA, the reactions were run as instructed with TwistAmp® Basic kit (Twistdx, Maidenhead, UK) with adaptations. The reaction mixture was prepared on ice by adding 10µM of each primer, the TwistAmp Rehydration Buffer, and ultra-pure water to the lyophilized pellet provided on the kit. After the resuspension of the pellet, magnesium acetate was added at a concentration of 280mM, to obtain a final master mix. In general, one single pellet allowed the preparation of four individual RPA reactions following previous indications [10]. The reaction was run in a pre-heated PCR thermocycler at 37°C for 25-30min. The amplified products were kept on ice until further processing.

5. Fluorescence-based readout of Cas13a reaction – step 2 of Sherlock method

The detection assays were performed by first preparing a master mix containing the following components: 63,3 ug/ml purified LwCas13a, 10ng/µl crRNA, 40 U/µl Murine RNase inhibitor (New England Biolabs, Ipswich, MA, USA), 2µM RNAse Alert v2 (Thermo Fisher, Waltham, MA, USA), NTP Buffer Mix (25mM each; New England Biolabs, Ipswich, MA, USA), 5U/ µl T7 polymerase mix (New England Biolabs, Ipswich, MA, USA), 1M MgCl2 and ultra-pure water. Next, the master mix was distributed to a

384 well black plate (Greiner, Kremsmunster, Austria), and the sample was added to the respective well. The plates were placed in a fluorescent plate reader, Synergy2 (Agilent, Santa Clara, CA, USA) and reactions were allowed to proceed for 1-3h at 37˚C (Excitation/Emission: 490/520nm). Until data acquisition, the reactions were kept on ice. The initial fluorescence of the samples was subtracted to the final fluorescence, to eliminate the background.

6. Lyophilisation of reagents

The lyophilisation of reagents was performed using a freeze dryer, VirTis BenchTop Pro with Omnitronics (SP; Warminster, PA, USA). Briefly, the Cas13a reaction was prepared as described above, with or without the addition of the complex Cas13a + crRNA, and placed in a 384 well plate. The plate was then transferred to the freeze dryer and left overnight to complete the process at a condenser surface temperature of −80˚C.

Results

1. Designing the POC test models for DENV and SARS-CoV-2, in epidemic and pandemic scenarios, respectively

The CRISPR-Cas13a method (Figure 1, top panel) consists in two steps: step 1 is the recombinase polymerase amplification (RPA); step 2 is the Cas13a reaction and detection of lateral fluorescence.

We envisioned a POC test model for DENV, in an epidemic situation, based on a LOD platform that would allow the diagnosis and strain identification, from DENV1 to DENV4 (Figure 1, lower left panel). We report here the establishment of the molecular test, while the development of the LOD platform and microfluidic adaptation will be the responsibility of the commercial partner Biosurfit (Azambuja, Portugal). Exemplifying with the DENV1 strain diagnosis, the testing sample is placed in a chamber (already extracted or a blood drop whose cells are lysed here) and moves to another chamber that will receive the reagents for RPA to take place (step 1). There is a parallel chamber where RPA is conducted for the synthetic positive target for DENV1. The resulting products from the two RPA chambers move after to other two parallel chambers, for the Cas13a reaction and detection of the fluorescence reporter (step 2). Thus, the reagents for both steps for each DENV strain have to be halved, one for the test blood sample, and the other for the synthetic positive target for the specific DENV strain. The sets of chambers for detection of each DENV strain have to be independent (four sets of independent chambers), and a fourth set of chambers has to be dedicated to the human gene that functions as a positive control for the diagnosis. The Biosurfit machine will maintain temperature around 37ºC and have fluorescence detectors that read each of the reading chambers.

For SARS-CoV-2, emerged to create the COVID-19 pandemic, a platform allowing testing of various samples at once would be more adequate. Plate-based platforms for screening of two SARS-CoV-2 genes and one human gene, enable to include either 29 samples (96-well plate) or 125 samples (384-well plate), plus a blank and a positive control (Figure 1, lower right panel).

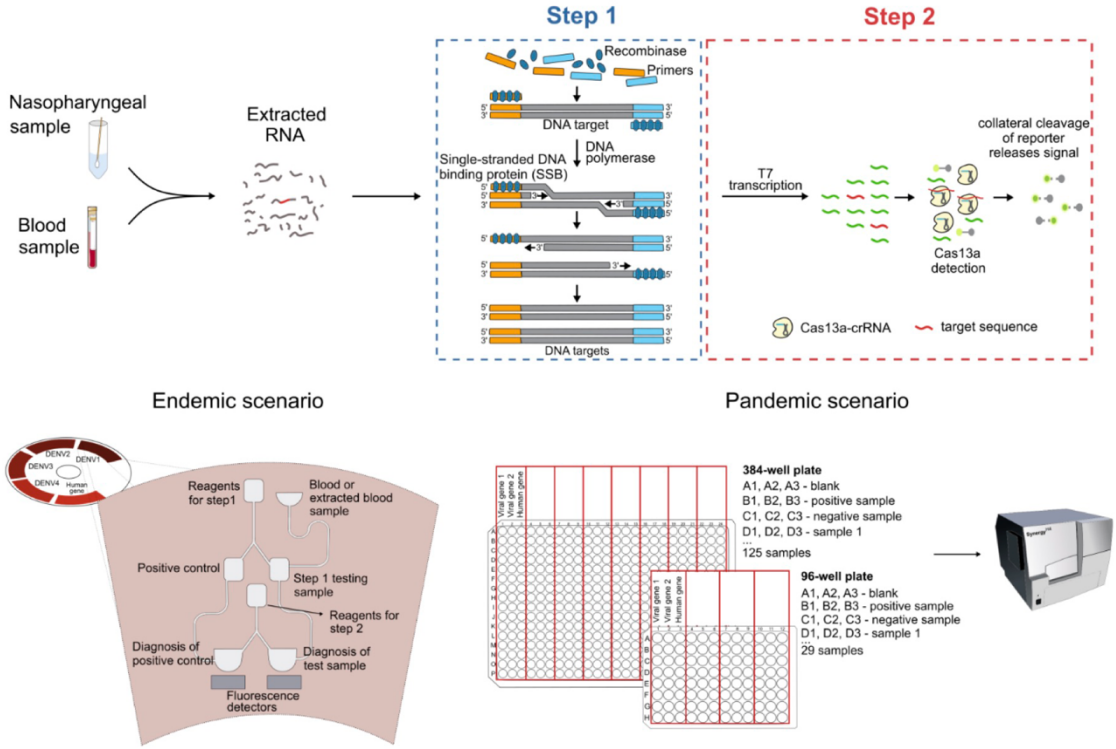


Figure 1- Designing POC test models in epidemic and pandemic. On Top: schematic representation of the CRISPR-Cas13a based test diagnosis for inactive viral samples extracted from blood or nasopharyngeal swab, in which step 1 consists in the recombinase polymerase amplification (RPA), and step 2 in the Cas13a action and detection of lateral fluorescence. Below, right: the LOD platform for an endemic situation, illustrated for the diagnosis of DENV and identification of the strain (DENV1-4; and human control gene). Below, left: the plate-fluorescence reader platform for a pandemic situation, illustrated for the SARS-CoV-2 diagnosis based on two viral genes (and human control gene), in 96-well (29 samples) and 384-well (125 samples) plates.

2. The purified Cas13a protein

By the time we began this work, there was no company commercializing the Cas13a protein, so we had to produce and purify the protein from the Cas13a bacterial expression vector pC013 - Twinstrep-SUMO-huLwCas13a (Plasmid #90097), provided by the original authors [9] to the repository Addgene (Watertown, MA, USA). The vector is provided in the competent Rosetta 2(DE3)pLysS Singles bacteria that must be grown for large-scale expression of the protein, and then the expressed protein must be further untagged and purified by FPLC (combined cation exchange and size exclusion; Figure 2A). The presence of the protein was confirmed along the various

steps by SDS-PAGE (Figure 2B). Departing from the same quantities indicated in [10], we obtained a final yield of ~2mg of LwCas13a pure protein (comparable to their ~0.5-1 mg). This amount of protein is enables to perform thousands of individual Cas13a-SHERLOCK reactions.

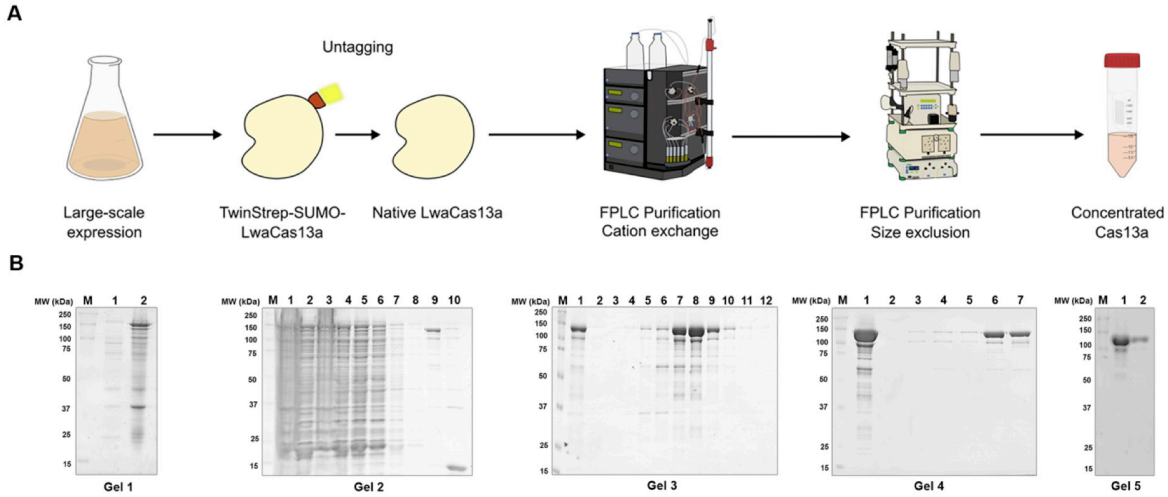


Figure 2- The main protein purification steps (panel A) and the respective SDS-PAGE images (panel B). The columns in the gels represent the following samples: M – ladder; **Gel 1**, 1- uninduced, 2- induced; **Gel 2**, 1- cell lysate; 2- cleared cell lysate, 3- cell pellet after clearing of lysate, 4- after 1h resin, 5- flow-through resin, 6- wash 1, 7- wash 2, 8- wash 3, 9- eluted fraction, 10- final resin; **Gel 3**, 1- filtered eluted fraction from gel 2, 2-to-12- fractions 17-to-28; **Gel 4**, 1- pool of positive fractions from cation exchange FPLC, 2-to-7- fractions 5-to-10 from size exchange FPLC; **Gel 5**, 1- final concentrated protein, 2- flow-through filter.

3. Designing of primers, crRNAs and synthetic standards

For DENV, we aimed that our POC test distinguished between the four well-recognized strains, DENV1-4, and that it would not be misdiagnosed with other viruses co-circulating in tropical and sub-tropical regions, as the related arboviruses Zika and Chikungunya. We first downloaded several sequences for the four DENV strains (89 total sequences), Zika (24 sequences) and Chikungunya (22 sequences) from the VIPR database [18], and made diverse alignments in CATCH (Compact Aggregation of Targets for Comprehensive Hybridization) tool [19]: all together, per strain, only DENV. This allowed us to select the regions for the primers and crRNAs from the DENV genomes to include in our POC test, in the region around 10,300-10,700 nt, in the 3'UTR (Table 1), a common region to another publication [19].

For SARS-CoV-2, we followed options selected by others for the SHERLOCK method (SARS-CoV-2 Orf1ab and S genes; consulted on 4th April 2020; https://www.broadinstitute.org/files/publications/special/COVID-19%20detection%20(updated).pdf) and for qRT-PCR (SARS-CoV-2 rdp and E genes and human RnaseP gene-subunit P20 gene; consulted on 4th April 2020; https://www.who.int/docs/default-source/coronaviruse/whoinhouseassays.pdf). In both cases, we copied the genomic regions to CATCH, in order to verify or select adequate sequences for the primers and crRNAs and ended up designing our own sequences (Table 1).

Table 1 – Sequences of primers (FW – forward; RV – reverse), crRNAs and synthetic positive targets.

Name		Sequences
DENV1	Primers	FW: GAAATTAATACGACTCACTATAGGGATGGAAGCTGTACGCATGGGGTAGCA
		RV: TCTCTGGTCTCTCCCAGCGTCAATATG
	crRNA	GGGGAUUUAGACUACCCCAAAAACGAAGGGGACUAAAACCUCCUCUAACCUCUAGUCCUUACCACCA
	Synthetic positive target	GAAATTAATACGACTCACTATAGGGCGGGAGGCTGCAAACCATGGAAGCTGTACGCATGGGGTAGCAGAC TAGTGGTTAGAGGAGACCCCTCCCAAGACACAACGCAGCAGCGGGGCCCAACACCAGGGGAAGCTGTACC CTGGTGGTAAGGACTAGAGGTTAGAGGAGACCCCCCGCACAACAACAAACAGCATATTGACGCTGGGAGA GACCAGAGATCCTGCTGTCTCTACAGCATCATTCCAGGCACAGAACGCCAAAAAATGGAATGGTGCTGTT GAATCAACAGGTTCT
DENV2	Primers	FW: GAAATTAATACGACTCACTATAGGGCCTTACAGATCGCAGCAACAATGGGGG
		RV: TCTCTGGTCTCTCCCAGCGTCAATATG
	crRNA	GGGGAUUUAGACUACCCCAAAAACGAAGGGGACUAAAACGUCCUUCCAGUGAGACUACAGCUUCAUC
	Synthetic positive target	GAAATTAATACGACTCACTATAGGGAAATCTGGGAGGCCACAAACCATGGAAGCTGTACGCATGGCGTAG TGGACTAGCGGTTAGAGGAGACCCCTCCCTTACAAATCGCAGCAACAATGGGGGCCCAAGGTGAGATGAA GCTGTAGTCTCACTGGAAGGACTAGAGGTTAGAGGAGACCCCCCCAAAACAAAAAACAGCATATTGACGC TGGGAAAGACCAGAGATCCTGCTGTCTCCTCAGCATCATTCCAGGCACAGAACGCCAGAAAATGGAATGG TGCTGTTGAATCAACAGGTTCT
DENV3	Primers	FW: GAAATTAATACGACTCACTATAGGGCACAGTGTAGCAGACTAGCGGTTAGAG
		RV: TCTCTGGTCTCTCCCAGCGTCAATATG
	crRNA	GGGGAUUUAGACUACCCCAAAAACGAAGGGGACUAAAACCUCGGGCCCCGCUGCUGCGUUGUGUCAU
	Synthetic positive target	GAAATTAATACGACTCACTATAGGGCCGTGGAAGCTGTACGCACGGTGTAGCAGACTAGTGGTTAGAGGA GACCCCTCCCATGACACAACGCAGCAGCGGGGCCCGAGCACTGAGGGAAGCTGTACCTCCTTGCAAAGGA CTAGAGGTTATAGGAGACCCCCCGCAAACAAAAACAGCATATTGACGCTGGGAGAGACCAGAGATCCTGC TGTCTCCTCAGCATCATTCCAGGCACAGAACGCCAGAAAATGGAATGGTGCTGTTGAATCAACAGGTTCT
DENV4	Primers	FW: GAAATTAATACGACTCACTATAGGGCCTCCCATCACTGACAAAACGCAGC
		RV: TCTCTGGTCTCTCCCAGCGTCAATATG
	crRNA	GGGGAUUUAGACUACCCCAAAAACGAAGGGGACUAAAACGUACAGCUUCCUCCUGGCUUCGGGCCCC

	Synthetic positive target	GAAATTAATACGACTCACTATAGGGGCTGTACGCGTGGCATATTGGACTAGCGGTTAGAGGAGACCCCTC CCATCACTGACAAAACGCAGCAAAAAAGGGGGCCCGAAGCCAGGAGGAAGCTGTACTCCTGGTGGAAGGA CTAGAGGTTAGAGGAGACCCCCCCAACACAAAAACAGCATATTGACGCTGGGAAAGACCAGAGATCCTGC TGTCTCTGCAACATCAATCCAGGCACAGAGCGCCGCGAGATGGATTGGTGTTGTTGATCCAACAGGTTCT
DENV	Primers	FW: GAAATTAATACGACTCACTATAGGGATGGAAGCTGTACGCATGGGGTAGCA
		RV: TCTCTGGTCTCTCCCAGCGTCAATATG
	crRNA	GGGGAUUUAGACUACCCCAAAAACGAAGGGGACUAAAACGGGGGGUCUCCUCUAACCUCUAGUCCUU
	Synthetic positive target	GAAATTAATACGACTCACTATAGGGCGGGAGGCTGCAAACCATGGAAGCTGTACGCATGGGGTAGCAGAC TAGTGGTTAGAGGAGACCCCTCCCAAGACACAACGCAGCAGCGGGGCCCAACACCAGGGGAAGCTGTACC CTGGTGGTAAGGACTAGAGGTTAGAGGAGACCCCCCCGCACAACAACAAACAGCATATTGACGCTGGGAGA GACCAGAGATCCTGCTGTCTCTACAGCATCATTCCAGGCACAGAACGCCAAAAAATGGAATGGTGCTGTT GAATCAACAGGTTCT
Orf1ab	Primers	FW: GAAATTAATACGACTCACTATAGGGCAGTCTCTGAAGAAGTAGTGGAAAATC
		RV: GACTAGAATTGTCTACATAAGCAGCCA
	crRNA	GAUUUAGACUACCCCAAAAACGAAGGGGACUAAAACCCAACCUCUUCUGUAAUUUUUAAACUAU
	Synthetic positive target	GAAATTAATACGACTCACTATAGGGAATCTTGCCTGCGAAGATCTAAAACCAGTCTCTGAAGAAGTAGTGG AAAATCCTACCATACAGAAAGACGTTCTTGAGTGTAATGTGAAAACTACCGAAGTTGTAGGAGACATTATA CTTAAACCAGCAAATAATAGTTTAAAAATTACAGAAGAGGTTGGCCACACAGATCTAATGGCTGCTTATGT AGACAATTCTAGTCTTACTATTAAGAAACCTAATGAATT
S	Primers	FW: GAAATTAATACGACTCACTATAGGGGCCAATAGGTATTAACATCACTAGGTTTC
		RV: ACAGTCTACAGCATCTGTAATGGTTCC
	crRNA	GAUUUAGACUACCCCAAAAACGAAGGGGACUAAAACGCAGCACCAGCUGUCCAACCUGAAGAAG
	Synthetic positive target	GAAATTAATACGACTCACTATAGGGCGGCTTTAGAACCATTGGTAGATTTGCCAATAGGTATTAACATCAC TAGGTTTCAAACTTTACTTGCTTTACATAGAAGTTATTTGACTCCTGGTGATTCTTCTTCAGGTTGGACAGC TGGTGCTGCAGCTTATTATGTGGGTTATCTTCAACCTAGGACTTTTCTATTAAAATATAATGAAAATGGAA CCATTACAGATGCTGTAGACTGTGCACTTGACCCTCTCTCAGAAACAA
E1	Primers	FW: GAAATTAATACGACTCACTATAGGGGTAAAACCTTCTTTTTACGTTTACTCTCG
		RV: GGTAATAGTACCGTTGGAATCTGCCAT
	crRNA	GGGGAUUUAGACUACCCCAAAAACGAAGGGGACUAAAACAGAUCAGGAACUCUAGAAGAAUUCAGAU
	Synthetic positive target	GAAATTAATACGACTCACTATAGGGCTGCAATATTGTTAACGTGAGTCTTGTAAAACCTTCTTTTTACGTTT ACTCTCGTGTTAAAAATCTGAATTCTTCTAGAGTTCCTGATCTTCTGGTCTAAACGAACTAAATATTATATT AGTTTTTCTGTTTGGAACTTTAATTTTAGCCATGGCAGATTCCAACGGTACTATTACCGTTGAAGAGCTTAA AAAGCTCCTT
E2	Primers	FW: GAAATTAATACGACTCACTATAGGGACACTAGCCATCCTTACTGCGCTTCG
		RV: AGACCAGAAGATCAGGAACTCTAGAAGA
	crRNA	GGGGAUUUAGACUACCCCAAAAACGAAGGGGACUAAAACAACGUAAAAAGAAGGUUUUACAAGACUC
	Synthetic positive target	GAAATTAATACGACTCACTATAGGGTGCTTTCGTGGTATTCTTGCTAGTTACACTAGCCATCCTTACTGCG CTTCGATTGTGTGCGTACTGCTGCAATATTGTTAACGTGAGTCTTGTAAAACCTTCTTTTTACGTTTACTCT CGTGTTAAAAATCTGAATTCTTCTAGAGTTCCTGATCTTCTGGTCTAAACGAACTAAATATTATATTAGTT
Rdrp1	Primers	FW: GAAATTAATACGACTCACTATAGGGAGCATGGCCTCTTATTGTAACAGCTTTA
		RV: AAGCTAACGCATTGTCATCAGTGCAAG
	crRNA	GGGGAUUUAGACUACCCCAAAAACGAAGGGGACUAAAACGUAGUACCGGCAGCACAAGACAUCUGUC
	Synthetic positive target	GAAATTAATACGACTCACTATAGGGTTAGTATGGACAATTCACCTAATTTAGCATGGCCTCTTATTGTAAC AGCTTTAAGGGCCAATTCTGCTGTCAAATTACAGAATAATGAGCTTAGTCCTGTTGCACTACGACAGATGT

		CTTGTGCTGCCGGTACTACACAAACTGCTTGCACTGATGACAATGCGTTAGCTTACTACAACACAACAAAG GGAGGTAGG
Rdrp2	**Primers**	FW: GAAATTAATACGACTCACTATAGGGACACTAGCCATCCTTACTGCGCTTCG
		RV: AGCCCTGGTCAAGGTTAATATAGGCAT
	crRNA	GGGGAUUUAGACUACCCCAAAAACGAAGGGGACUAAAACACUCCACUACCUGGCGUGGUUUGUAUGA
	Synthetic positive target	GAAATTAATACGACTCACTATAGGGGTGTACTGACATTAGATAATCAAGATCTCAATGGTAACTGGTATGA TTTCGGTGATTTCATACAAACCACGCCAGGTAGTGGAGTTCCTGTTGTAGATTCTTATTATTCATTGTTAAT GCCTATATTAACCTTGACCAGGGCTTTAACTGCAGAGTCACATGTTGACA
RnaseP20	**Primers**	FW:GAAATTAATACGACTCACTATAGGGTTGATGAGCTGGAGCCAGAGACCGACACA
		RV: ATATCACGGAGGGGATAAGTGGAGGAGTG
	crRNA	GGGGAUUUAGACUACCCCAAAAACGAAGGGGACUAAAACAAUUACUUGGGUGUGACCCUGAAGACUC
	Synthetic positive target	GAAATTAATACGACTCACTATAGGGGCCAATACCTCCACCGTGGAGCTTGTTGATGAGCTGGAGCCAGAG ACCGACACACGGGAGCCACTGACTCGGATCCGCAACAACTCAGCCATCCACATCCGAGTCTTCAGGGTCA CACCCAAGTAATTGAAAAGACACTCCTCCACTTATCCCCTCCGTGATATGGCTCTTCGCATGCTGAGTACT GGAC

4. Implementation of the SHERLOCK method with synthetic positive targets

We began by testing the specificity of the crRNAs for DENV and SARS-CoV-2 in the synthetic positive targets amplified by PCR and by performing the step 2 of the Sherlock method. Since amplification by PCR is routine at our lab, we avoided issues due to the needed optimization for the RPA. We verified that the crRNA designed to identify DENV independently of the strain (specific for DENV) led to a positive reaction when independently tested for the synthetic positive targets for DENV1, DENV2, DENV3 and DENV4 (Figure 3A). For the crRNAs specifically designed to just detect one strain (specific for each DENV strain), DENV2, DENV3 and DENV4 crRNAs only detected the specific strain, but DENV1 crRNA was not specific, leading to a positive reaction when in the presence of DENV1, DENV2 and DENV4 (signal was weak for the DENV3 synthetic target; Figure 3B).

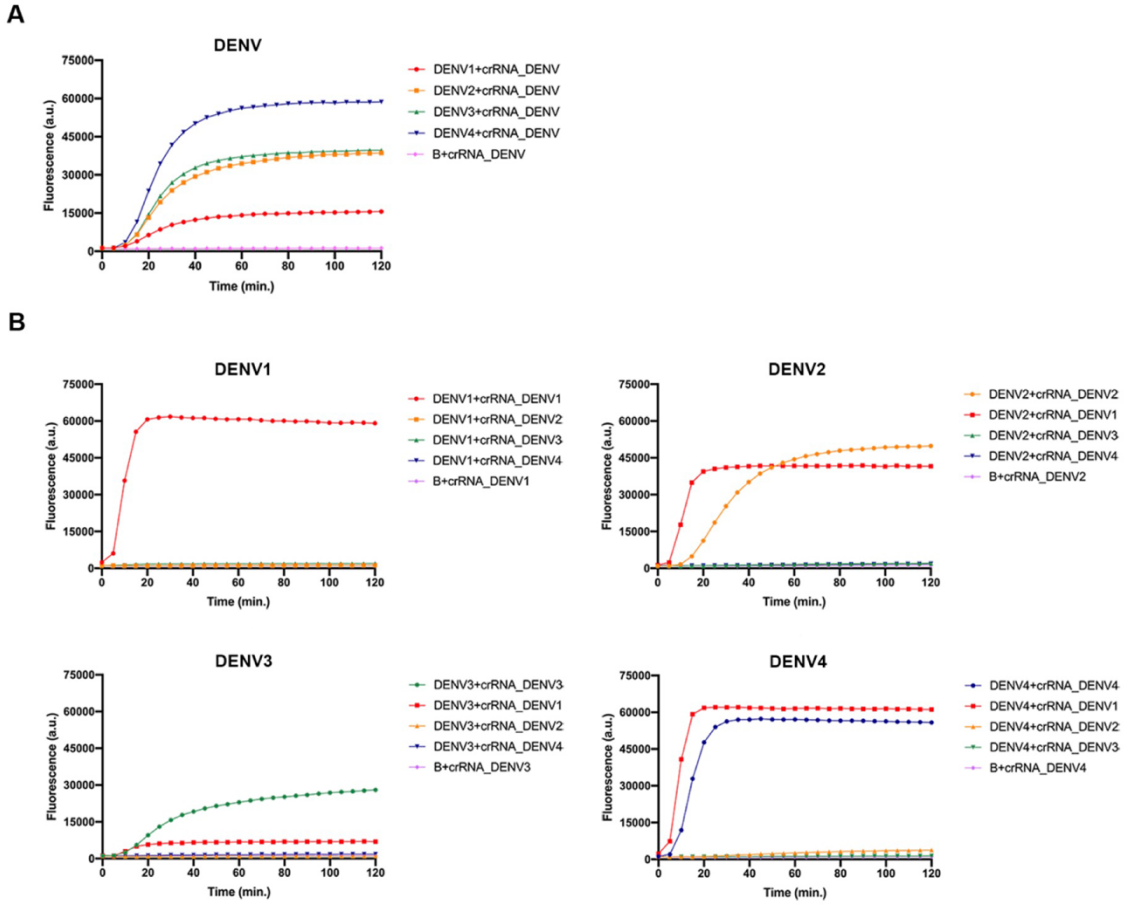


Figure 3 – Specificity tests of the DENV crRNAs in PCR amplified synthetic positive controls and by performing step 2 of the Sherlock method. (A) crRNA designed to identify DENV independently of the strain (B) crRNAs specifically designed to detect one strain: DENV1, DENV2, DENV3 or DENV4. B represents the non-template control.

For SARS-CoV-2, a 2019 emergent virus, there were no issues with strain/variant specificity by the time we did these tests, thus we only assayed if the various crRNAs would lead to a positive signal in the presence of the respective synthetic positive controls (Figure 4A). Comparing between the SARS-CoV-2 crRNAs tested, Orf1ab, Rdrp1, Rdrp2 and E2 (although there was a noise background in the E2 non-template control, probably due to an unspecific bind of the crRNA) seemed to allow a higher output yield than the S and E1 crRNAs (Figure 4A). As the crRNAs aligned in very different regions of the viral genome, it would be highly improbable to obtain a reaction with a mismatched crRNA, and we further verified this by mismatching Orf1ab and S crRNAs and synthetic positive controls (Figure 4B).

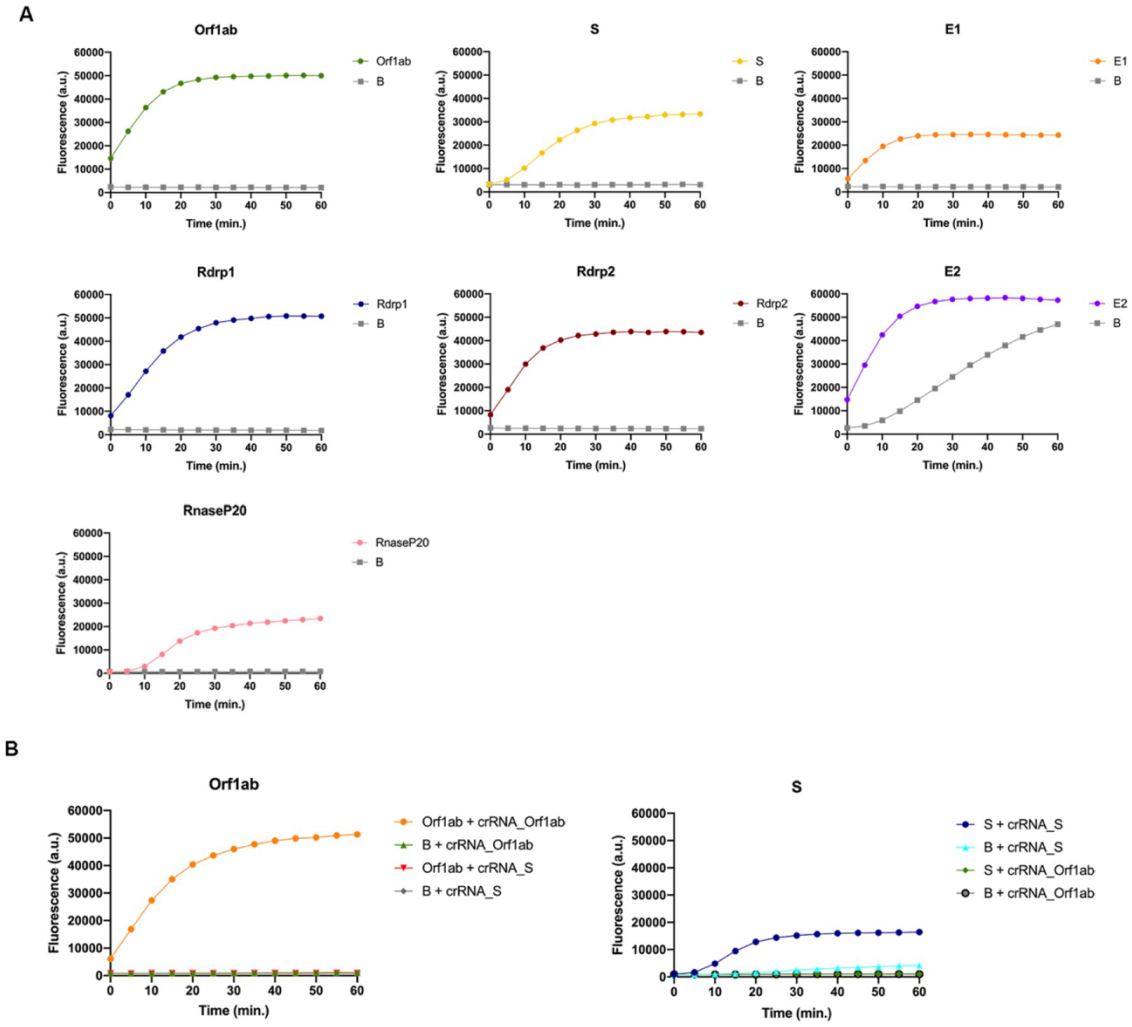


Figure 4 – Tests of the SARS-CoV-2 crRNAs in PCR amplified synthetic positive controls and by performing step 2 of the Sherlock method. (A) crRNAs for various genes of SARS-CoV-2 in the presence of the respective synthetic standards (B) Mismatch of the crRNA and synthetic positive controls for Orf1ab and S genes. B represents the non-template control.

From the results just stated, we proved at the same time that the produced and purified Cas13a was functioning, guaranteeing that step 2 of the Sherlock reaction was working. We further tested the sensitivity of step 2 alone through serial dilutions of the synthetic positive targets for SARS-CoV-2 crRNAs (Figure 5). We found that the limit of detection by doing only step 2 (no amplification, either by PCR or RPA) was the dilution of 10^{-7} for the Rdrp2 gene. For most of the others, the limit was around 10^{-4}. The sensitivity for the S viral gene and the human gene were consistently worse.

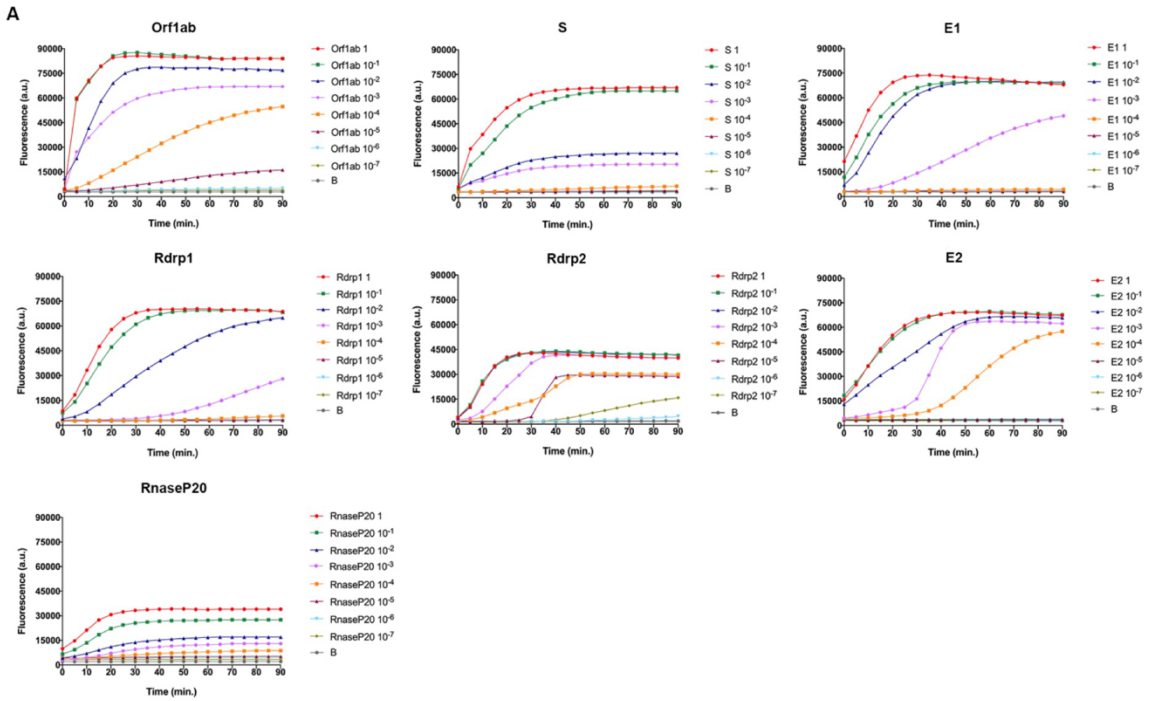


Figure 5 – Sensitivity tests for step 2 of the Sherlock method with ten-fold serial dilutions of the synthetic positive targets for SARS-CoV-2 and human genes. B represents the non-template control.

Then we tried to optimize the RPA reaction, or step 1 of the Sherlock method. We did a first comparison with the DENV4 crRNA, between performing PCR or step 1 of the Sherlock method. The PCR reaction produced a 1.5 times higher output yield than the RPA (Figure 6).

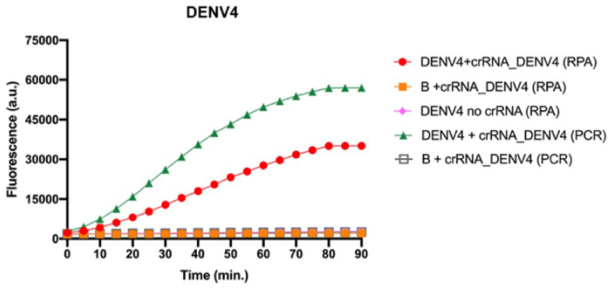


Figure 6 - Comparison with the DENV4 crRNA, between performing PCR or step 1 of the Sherlock method. B represents the non-template control.

We further tried to assay if we could improve the yield of the above mentioned sensitivity tests for SARS-CoV-2 (only step 2) by now doing the Sherlock method with the RPA amplification. We did it for Orf1ab, S and the human genes (Figure 7), but the results were identical when doing the two steps and when omitting the RPA reaction. We concluded that the RPA or step 1 was not working properly.

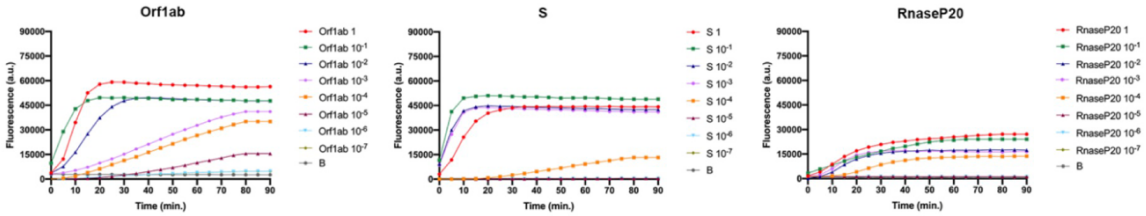


Figure 7 – Sensitivity tests for step 1 (RPA) + step 2 of the Sherlock method with ten-fold serial dilutions of the synthetic positive targets for SARS-CoV-2 (Orf1ab and S) and human (RnaseP20) genes. B represents the non-template control.

Two options were left: a) try to improve the RPA reaction; or b) try to avoid it. At this time, three reasons led us to choose the second path. We were facing serious delays in acquiring the RPA kit from the only British company (TwistDx) producing it. We also tried to acquire the individual proteins to reproduce the RPA kit at-home, but only one American company sold all the proteins, and after delays in shipping, the period spent in customs was too long and dangerous for the integrity of the reagents. But the real support for our decision to avoid the RPA step came from other authors attempts [20], were the trick was to include at least two viral crRNAs in the same tube in order to increase sensitivity of the Cas13a reaction. We experimented the use of more than one crRNA and confirmed that the value of fluorescence increased when using serial dilutions of positive controls (Figure 8). With the combination of SARS-CoV-2 Orf1ab and E1 genes, we could detect a read-out of 10^{-5} and 10^{-6} dilutions, improving it from 10^{-4} and 10^{-5}.

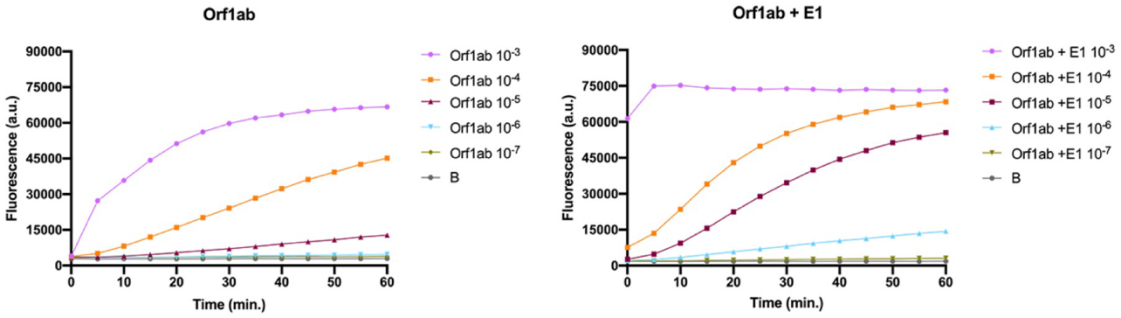


Figure 8 - Fluorescence read-outs for SARS-CoV-2 Orf1ab gene alone (left) and in combination with SARS-CoV-2 E gene (right), with only step 2 Sherlock method. B represents the non-template control.

5. Testing of the SHERLOCK method with case samples

Given the availability of samples for SARS-CoV-2 infected people due to the COVID-19 pandemic, we began the tests with human samples by recurring to nasopharyngeal samples of these cases. We first confirmed the positive and negative samples for SARS-CoV-2 by traditional qRT-PCR. The test that we assayed consisted only in step 2 Sherlock with two crRNAs in the reaction (Orf1ab+E). As can be seen in Figure 9, the test failed in the extracted samples that had been diagnosed as positive by the RT-PCR test.

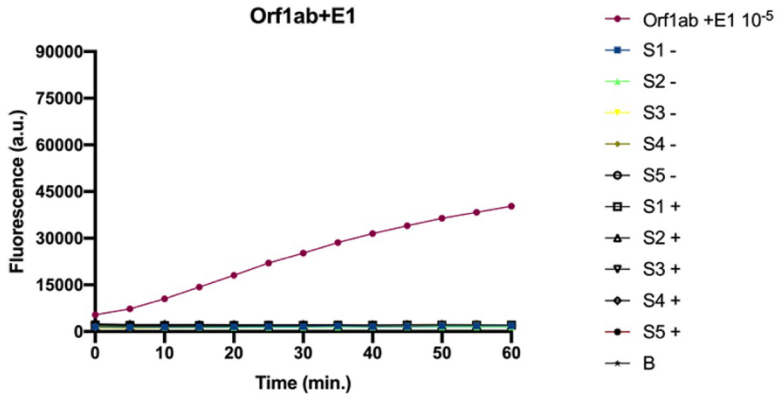


Figure 9 - Fluorescence read-outs for SARS-CoV-2 combined Orf1ab and E1 genes in extracted positive and negative RNA samples. S represents sample (- negative or + positive by qRT-PCR) and B the non-template control.

We next tried to increase the sensitivity of the detection by concentrating the Cas13a reaction through lyophilisation (Figure 10). In fact, the reduction of the volume of the Cas13a reaction (so that the added sample would not be so diluted) would also have the advantages of the microfluidic adaptation needed for the LOD platform, and better conservation and transportation of the pre-prepared plate platform. We tried first to lyophilize the Cas13a reaction, but verified that the long process of lyophilization led the loss of function of the enzyme. This limitation could be circumvented by lyophilization of all reagents except the Cas13a+crRNAs complex that could be added afterwards with the sample. Unfortunately, the positive sample was still bellow detection level.

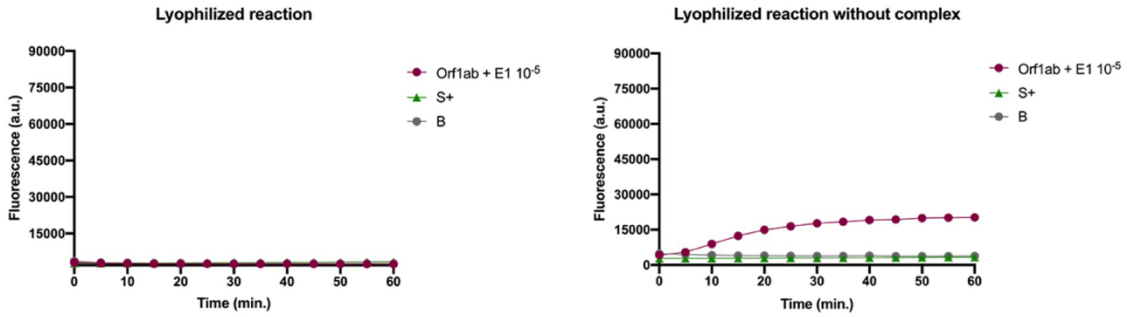


Figure 10 - Fluorescence read-outs for SARS-CoV-2 combined Orf1ab and E1 genes and testing lyophilisation. (A) Testing lyophilization of step 2 reagents, either for the complete Cas13a reaction (left) or lyophilized Cas13a reaction without the complex Cas13a+crRNAs (right), that that was added after. S+ represents a positive sample by qRT-PCR and B the non-template control.

Conclusions

All the implemented steps that we managed to establish in adaptation of the CRISPR-Cas13a method to SARS-CoV-2 diagnosis ended up being far less sensitive than current routine qRT-PCR methods. It is a fact that the test would still be faster, but the loss of sensitivity does not justify its implementation, as it is, at a large scale. It is possible that the amount of the viral RNA in the samples is too low for the level of detection we managed to attain with the single step 2 Sherlock method and two added crRNAs. It is a fact that when we tried to quantify the level of nucleic acids in the nasopharyngeal samples in the Qubit system, it was below the linear detection range of 0.2-100 ng capacity of the machine. Our limit of detection for the synthetic positive targets was around 0.1 ng, close to the limit of the Qubit detection. Unfortunately, due to the COVID-19 pandemic our efforts to obtain DENV positive samples were unsuccessful, so we could not ascertain if the level of detection attained would allow the diagnosis of DENV in blood samples.

The initial publications of the Sherlock method reported sensitivities at the attomolar level [9, 21], several orders of magnitude lower than ours. Of note they performed the method by including the RPA amplification, which we could not successfully implement. Indirectly, the COVID-19 pandemic exposed serious issues in basing a diagnosis on RPA amplification: the kit is produced by one company at a worldwide scale, creating serious bottlenecks in access to reagents; the company terminated their RPA kit for RNA, which included a transcriptase reverse step, implying the need to include a further cDNA production step in the POCs for RNA viruses; no comparison of efficiency between kits from different companies could be performed. For sure the authors of the first protocol online for the SHERLOCK method also had some concerns, as they made some alterations during the evolution of the pandemic [22, 23], introducing Cas12 instead of Cas13a, and changing the RPA by the LAMP-RT amplification. But even so, the LAMP-RT based method that was tested in the Great Manchester area (denominated Operation Moonshot; [24]) showed to miss more than 50% of the positive cases. This observation raises some concerns on the reliability of isothermal amplification methods.

Additionally, some papers describing a successful adaptation of the Sherlock method to SARS-CoV-2 use only a very small number of patient samples with high viral concentration (very low CT values for the qRT-PCR tests). For instance, Patchsung et al. [25] used 154 patient samples, but they could detect only 78 out of 81 positive COVID-19 samples by fluorescence readouts and they specifically mentioned “stored

RNA samples at −80°C to reduce degradation and always performed SHERLOCK validation experiments onsite at Hospital, to eliminate the possibility of sample degradation during transport". So, conditions of collection and transportation of samples seem to be serious limiting factors for this method. Our samples were collected elsewhere, and transported at 4ºC to our lab, with variable hours of interval. We also cannot currently ascertain if the Cas13a that we produced at home is working with top-efficiency. Before the pandemic there was no company selling Cas13a protein leading us to do it at-home. Since the pandemic started, one company began to sell it, but the prices are prohibitive as they oblige to buy a large amount of the protein. If our Cas13a protein is less efficient, this could justify our worse sensitivity results with the synthetic positive targets. A recent publication [26] supports our concerns on the efficiency of Cas13a, as the authors are adding another CRISPR nuclease in step 2, called Csm6, to increase the fluorescence readout. Now, this enzyme is not commercialized and must be produced and purified at-home, as we did for Cas13a.

The difficulties we faced in adapting Sherlock method to our POC platforms contradict extensively the promising claims that this technique is easy to implement and especially adaptable to the poor conditions in developing countries [9]. We will definitely pursue in its establishment, and we will focus on the following strategies: (1) eliminate the amplification step, especially do not recur to RPA; (2) improve the fluorescence readout by testing using tandem CRISPR nucleases, together and independently of using multi-crRNAs in the same reaction; (3) test better microfluidic strategies, to decrease the volume of the reaction.

Acknowledgements

This work was financed by the following projects: POCI-01-0247-FEDER-033778 supported by FEDER through COMPETE 2020 and Portugal 2020; and Research4COVID19 project 109_596696487 granted by the Portuguese Foundation for Science and Technology (FCT). FCT also financed the PhD grant to R.J.P. (SFRH/BD/145217/2019). i3S is supported by FEDER funds through the COMPETE 2020, Portugal 2020, and by Portuguese funds through FCT/Ministério da Ciência, Tecnologia e Inovação in the framework of the project 'Institute for Research and Innovation in Health Sciences' (PO-CI-01-0145-FEDER-007274).

References

1. Vashist, S.K., *Point-of-Care Diagnostics: Recent Advances and Trends.* Biosensors (Basel), 2017. **7**(4).
2. Market., P.-o.-C.D., *Available online: https://www.marketsandmarkets.com/MarketReports/point-of-care-diagnostic-market-106829185.html (accessed on 10 November 2021).*
3. Rezaei, M., et al., *Point of Care Diagnostics in the Age of COVID-19.* Diagnostics (Basel), 2020. **11**(1): p. 9.
4. Valera, E., et al., *COVID-19 Point-of-Care Diagnostics: Present and Future.* ACS Nano, 2021. **15**(5): p. 7899-7906.
5. Kost, G.J., et al., *Molecular detection and point-of-care testing in Ebola virus disease and other threats: a new global public health framework to stop outbreaks.* Expert Rev Mol Diagn, 2015. **15**(10): p. 1245-59.
6. Duchesne, L. and K. Lacombe, *Innovative technologies for point-of-care testing of viral hepatitis in low-resource and decentralized settings.* J Viral Hepat, 2018. **25**(2): p. 108-117.
7. Piepenburg, O., et al., *DNA detection using recombination proteins.* PLoS Biol, 2006. **4**(7): p. e204.
8. Almassian, D.R., L.M. Cockrell, and W.M. Nelson, *Portable nucleic acid thermocyclers.* Chem Soc Rev, 2013. **42**(22): p. 8769-98.
9. Gootenberg, J.S., et al., *Nucleic acid detection with CRISPR-Cas13a/C2c2.* Science, 2017. **356**(6336): p. 438-442.
10. Kellner, M.J., et al., *SHERLOCK: nucleic acid detection with CRISPR nucleases.* Nat Protoc, 2019. **14**(10): p. 2986-3012.
11. Ackerman, C.M., et al., *Massively multiplexed nucleic acid detection with Cas13.* Nature, 2020. **582**(7811): p. 277-282.

12. Arizti-Sanz, J., et al., *Streamlined inactivation, amplification, and Cas13-based detection of SARS-CoV-2.* Nat Commun, 2020. **11**(1): p. 5921.
13. Broughton, J.P., et al., *CRISPR-Cas12-based detection of SARS-CoV-2.* Nat Biotechnol, 2020. **38**(7): p. 870-874.
14. Kaminski, M.M., et al., *CRISPR-based diagnostics.* Nat Biomed Eng, 2021. **5**(7): p. 643-656.
15. Kong, L.X., et al., *Lab-on-a-CD: A Fully Integrated Molecular Diagnostic System.* J Lab Autom, 2016. **21**(3): p. 323-55.
16. Liu, F.X., et al., *Microfluidics-enabled digital isothermal Cas13a assay.* medRxiv, 2021. **2021.08.18.21262201**.
17. Ye, J., et al., *Primer-BLAST: a tool to design target-specific primers for polymerase chain reaction.* BMC Bioinformatics, 2012. **13**: p. 134.
18. Pickett, B.E., et al., *ViPR: an open bioinformatics database and analysis resource for virology research.* Nucleic Acids Res, 2012. **40**(Database issue): p. D593-8.
19. Myhrvold, C., et al., *Field-deployable viral diagnostics using CRISPR-Cas13.* Science, 2018. **360**(6387): p. 444-448.
20. Fozouni, P., et al., *Amplification-free detection of SARS-CoV-2 with CRISPR-Cas13a and mobile phone microscopy.* Cell, 2021. **184**(2): p. 323-333 e9.
21. Gootenberg, J.S., et al., *Multiplexed and portable nucleic acid detection platform with Cas13, Cas12a, and Csm6.* 2018. **360**(6387): p. 439-444.
22. Joung, J., et al., *Point-of-care testing for COVID-19 using SHERLOCK diagnostics.* medRxiv, 2020. **2020.05.04.20091231**.
23. Schermer, B., et al., *Rapid SARS-CoV-2 testing in primary material based on a novel multiplex RT-LAMP assay.* PLoS One, 2020. **15**(11): p. e0238612.
24. Deeks, J.J., A.J. Brookes, and A.M. Pollock, *Operation Moonshot proposals are scientifically unsound.* BMJ, 2020. **370**: p. m3699.
25. Patchsung, M., et al., *Clinical validation of a Cas13-based assay for the detection of SARS-CoV-2 RNA.* Nat Biomed Eng, 2020. **4**(12): p. 1140-1149.
26. Liu, T.Y., et al., *Accelerated RNA detection using tandem CRISPR nucleases.* Nat Chem Biol, 2021. **17**(9): p. 982-988.

Paper II – InfectionCMA: A Cell MicroArray Approach for Efficient Biomarker Screening in In Vitro Infection Assays.

pathogens

MDPI

Article

InfectionCMA: A Cell MicroArray Approach for Efficient Biomarker Screening in In Vitro Infection Assays

Ana C. Magalhães [1,2,3], Sara Ricardo [1,2,4], Ana C. Moreira [1,3,5], Mariana Nunes [1,2,3], Margarida Tavares [6,7,8], Ricardo J. Pinto [1,2,3], Maria Salomé Gomes [1,3,5] and Luisa Pereira [1,2,*]

1 i3S–Instituto de Investigação e Inovação em Saúde, Universidade do Porto, 4200-135 Porto, Portugal; acmagalhaes@ipatimup.pt (A.C.M.); sricardo@ipatimup.pt (S.R.); ana.s.moreira@ibmc.up.pt (A.C.M.); mnunes@ipatimup.pt (M.N.); rjpinto@ipatimup.pt (R.J.P.); sgomes@ibmc.up.pt (M.S.G.)
2 Ipatimup–Instituto de Patologia e Imunologia Molecular, Universidade do Porto, 4200-135 Porto, Portugal
3 ICBAS–Instituto de Ciências Biomédicas Abel Salazar, Universidade do Porto, 4050-313 Porto, Portugal
4 TOXRUN, Toxicology Research Unit, University Institute of Health Sciences, Advanced Polytechnic and University Cooperative (CESPU), 4585-116 Gandra, Portugal
5 IBMC–Instituto de Biologia Molecular e Celular, Universidade do Porto, 4200-319 Porto, Portugal
6 Department of Infectious Diseases and Emerging Infectious Disease Unit, CHUSJ–Centro Hospitalar Universitário S. João, 4200-319 Porto, Portugal; margarida.tavares@chsj.min-saude.pt
7 Public Health and Forensic Sciences and Medical Education Department, FMUP–Faculdade de Medicina, Universidade do Porto, 4200-319 Porto, Portugal
8 EPIUnit–Instituto de Saúde Pública, Universidade do Porto, 4050-091 Porto, Portugal
* Correspondence: luisap@ipatimup.pt

Abstract: The recently emerged severe acute respiratory syndrome coronavirus 2 (SARS-CoV-2) has forced the scientific community to acquire knowledge in real-time, when total lockdowns and the interruption of flights severely limited access to reagents as the global pandemic became established. This unique reality made researchers aware of the importance of designing efficient in vitro set-ups to evaluate infectious kinetics. Here, we propose a histology-based method to evaluate infection kinetics grounded in cell microarray (CMA) construction, immunocytochemistry and in situ hybridization techniques. We demonstrate that the chip-like organization of the InfectionCMA has several advantages, allowing side-by-side comparisons between diverse cell lines, infection time points, and biomarker expression and cytolocalization evaluation in the same slide. In addition, this methodology has the potential to be easily adapted for drug screening.

Keywords: in vitro infectious assays; cell microarrays; immunocytochemistry; SARS-CoV-2; human receptors for viruses; cell cycle and apoptosis

check for updates

Citation: Magalhães, A.C.; Ricardo, S.; Moreira, A.C.; Nunes, M.; Tavares, M.; Pinto, R.J.; Gomes, M.S.; Pereira, L. InfectionCMA: A Cell MicroArray Approach for Efficient Biomarker Screening in In Vitro Infection Assays. *Pathogens* **2022**, *11*, 313. https://doi.org/10.3390/pathogens11030313

Academic Editors: Timokratis Karamitros, Tara Patricia Hurst and Lemonia Skoura

Received: 7 February 2022
Accepted: 1 March 2022
Published: 3 March 2022

Publisher's Note: MDPI stays neutral with regard to jurisdictional claims in published maps and institutional affiliations.

Copyright: © 2022 by the authors. Licensee MDPI, Basel, Switzerland. This article is an open access article distributed under the terms and conditions of the Creative Commons Attribution (CC BY) license (https://creativecommons.org/licenses/by/4.0/).

1. Introduction

In vitro modelling is one of the first research steps in the field of infectious diseases, allowing scientists to investigate, amongst other things, which host cell types are permissive to infection, which molecular mechanisms govern the entrance of pathogens into cells and their replication within, and what alterations are induced in the host cell metabolism and viability due to infection [1–3]. This modelling is also the first step in the preclinical evaluation of novel or repurposed drugs and compounds, saving precious time and money at the in vivo testing and clinical trial levels [1,4,5]. The value of in vitro modelling justifies the various efforts being made in improving settings, aiming to better mimic the complex biological systems, such as, for example, recurring stem-cell differentiation, establishing co-culture assays, and implementing three-dimensional organoids [6]. The global coronavirus disease 2019 (COVID-19) pandemic is the perfect illustrative example of the vital importance of in vitro modelling as a research and translational tool. COVID-19 is a viral respiratory disease that newly emerged by the end of 2019 in Wuhan,

China, which rapidly spread worldwide. By the end of the year 2021, conservative estimates point to 290 million SARS-CoV-2 infections and 5.4 million related deaths globally (https://coronavirus.jhu.edu/map.html, accessed on 31 December 2021). Meanwhile, in vitro modelling allowed scientists to elucidate several aspects of the SARS-CoV-2 cycle in the host cells [7–26]. The viral spike protein binds to the human receptor ACE2 and is cleaved by the transmembrane serine protease 2 (TMPRSS2), allowing the fusion of the viral and host membranes for entrance into the cell. The translation of the viral RNA into non-structural proteins suppresses the translation of host mRNAs in favor of the viral mRNAs for the production of virions. Further transformations of the host cells include the endoplasmic reticulum being modified into double-membrane vesicles, where more viral RNA can be replicated and translated. The exit of the new virus particles occurs via Golgi and/or lysosomes, and at the same time the host furin protein cuts the spike protein, preparing the virus to infect another cell. In vitro modelling has also been key for preliminary drug screenings [27–29] of FDA-approved drugs, leading to the identification of several compounds that show in vitro antiviral properties against SARS-CoV-2.

The pressure regarding acquiring real-time knowledge on SARS-CoV-2 infection, and the huge restrictions in access to reagents in the beginning of the pandemic, also demonstrated how essential it is to design efficient in vitro set-ups. Simple solutions can be available in a specific research field, but they do not often cross to other fields. This is the case of a simple automation technique used in the field of histology, the CMA. Cultured cells, namely fixed infected cells, can be included in paraffin-embedded blocks similarly to the formalin-fixed paraffin-embedded (FFPE) tissues from surgical pathology specimens (reviewed in [30]). Then, CMAs can be created, consisting of several tens to hundreds of cores from one or various individual cell blocks, integrated into a microarray form, on a single or various slides. CMAs allow various ancillary studies to be performed, such as the rapid and high-throughput analysis of molecular targets through immunocytochemistry (ICC) [31,32] and in situ hybridization (ISH) [33]. The CMA block can be easily archived for retrospective studies [34]. Additionally, the ICC processing can be further automatized by the integration of microfluidic techniques [35], enabling further reductions in reagent quantities and process time, the precise control of assay conditions, and ease of multiplexing.

In this work, we want to demonstrate to the infectious disease research community the advantages of the CMA. We call this CMA design InfectionCMA due to its ability to model infection kinetics. We demonstrate the practicability and efficiency of the InfectionCMA compared to traditional in vitro infection assays in two SARS-CoV-2 investigations, with the first aiming to compare the effect of viral load in infection kinetics on Vero cells, and the second aiming to compare the infection kinetics between human cell lines and Vero cells. Although the establishment of the InfectionCMA implies additional preparation time and reagents, this extensively compensates for the more complex, laborious and reagent-consuming infectious assays in biosafety level 3 (BSL3) conditions, ICC preparations and microscopic observations needed to obtain the same output through a traditional in vitro infection assay.

2. Materials and Methods

2.1. Cell Lines

Vero cells from the kidney of African green monkey (ATCC, #CCL-81; ATCC, Manassas, VA, USA), Caco-2 cells from human primary colorectal adenocarcinoma (in-house cell bank) and Huh-7 cells from human hepatocellular carcinoma (kindly gifted by Tiago Duarte) were used in this work after confirmation of a mycoplasma-negative status. The cell lines were propagated in Dulbecco's modified Eagle medium (DMEM, Thermo Scientific, Waltham, MA, USA) supplemented with 10% fetal bovine serum (FBS, Labclinics, Barcelona, Spain), 100 U/mL of penicillin, and 100 ug/mL of streptomycin. Cells were maintained at 37 °C, under a 5% CO_2 humidified atmosphere.

2.2. Isolation of the SARS-CoV-2

SARS-CoV-2 was isolated from the nasopharyngeal sample of a hospitalized symptomatic patient from North Portugal in the spring of 2020. The molecular diagnosis was confirmed by RT-PCR for three SARS-CoV-2 genes (ORF1ab, E and N–Fosun COVID-19 RT-PCR Detection Kit; Fosun Pharma USA Inc., Princeton, NJ, USA). The nasopharyngeal sample was preserved at −80 °C in the hospital, until being transferred to our lab (distance of 1 km from the hospital) 15 days later, for immediate isolation of the virus.

The isolation was performed by inoculation in Vero cells, and the resultant supernatants were filtered and used as virus stocks preserved at −80 °C. Titers were determined by the focus forming assay (FFA). Briefly, ten-fold dilutions of viral supernatants were inoculated in Vero cells, seeded 24 h prior to infection in 96-well plates. After 1 h of incubation, an overlay medium of DMEM with 4% FBS and 3% carboxymethyl cellulose (CMC) in a ratio of 1:1 was added to the inoculum, and the infected monolayer was incubated for 48 h at 37 °C in 5% CO_2. Cells were fixed with 4% paraformaldehyde at room temperature (RT), permeabilized with 0.2% Triton-X 100 (Sigma, St. Louis, MO, USA) for 10 min, blocked with 1% bovine serum albumin (BSA–Sigma, St. Louis, MO, USA) for 10 min, and incubated with a mouse SARS-CoV-2 spike antibody (GTX632604, GeneTex, Irvine, CA, USA) for 1 h at RT. Afterwards, cells were incubated with anti-mouse Alexa 488-conjugated secondary antibody for 1 h (Thermo Scientific, Waltham, MA, USA), followed by nuclear staining with 4′,6-diamidino-2-phenylindole (DAPI–BioRad, Hercules, CA, USA) for 10 min, before analysis. Images of each well were acquired on the IN Cell Analyzer 2000 (Cytiva, Marlborough, MA, USA), using an appropriate magnifying objective, and the fluorescent focus units (FFU) were counted.

All experiments involving infectious SARS-CoV-2 were performed in BSL3 conditions in accordance with institutional guidelines.

2.3. Viral Whole Genome Sequencing

The viral whole-genome sequencing was performed on extracted RNA from the isolated virus. Briefly, this protocol [36,37] consisted of: reverse-transcription with the SuperScriptTM VILOTM cDNA synthesis Kit (Thermo Fisher Scientific, Waltham, MA, USA); PCR enrichment of the SARS-CoV-2 genome and five human gene expression controls with the Ion AmpliSeqTM SARS-CoV-2 Research Panel; library construction with the Ion AmpliSeqTM Library Kit Plus; library quantification and size range verification at the 2200 TapeStation Automated Electrophoresis System, using the High Sensitivity DNA ScreenTape (Agilent Technologies, Santa Clara, CA, USA); next-generation sequencing (NGS) on the Ion S5XL system with the Ion 530™ chip; and raw data extracted with the Ion Torrent pipeline.

The bioinformatic pipeline consisted of: alignment of the raw data versus the reference genome (severe acute respiratory syndrome coronavirus 2 isolate Wuhan-Hu-1; accession number NC_045512.2; [38]) with BWA tool; variant calling with three tools, FreeBayes, BCFtools and GATK, with editing of variants identified in at least two; variant annotation with SnpEff; consensus sequence was inferred with Bcftools.

2.4. In Vitro Infection Assays

For the CMA construction, cells were seeded 24 h prior to infection in T-25 flasks at a density of 7×10^5/flask. On the infection day, the cell culture medium in each flask was discarded and cell monolayers were inoculated with SARS-CoV-2 (diluted appropriately in serum free DMEM) with a multiplicity of infection (MOI) of 0.01 and 0.001 for the first CMA construction test with Vero cells only, and an MOI of 1 for the remaining experiments with the human and Vero cell lines. Viral infection was allowed to proceed for 1 h at 37 °C in 5% CO_2, and after that, DMEM with 2% of FBS was added to the flasks. Cells were collected at various time points: for the first InfectionCMA at 4 h, 24 h, 48 h and 72 h; and for the second InfectionCMA at 16 h, 36 h and 72 h.

The proteins and RNA for the Western blotting and qRT-PCR were obtained by conducting three independent infection assays in 6-well plates, with a cell density of 1×10^5/well, following the same conditions as described above. Cells were collected at 16 h, 48 h and 96 h.

In order to confirm that infectious viral particles were produced after the infection assays, the viral yields were determined by FFA, as described in Section 2.1, at each observation-point.

2.5. InfectionCMA Construction

The establishment of the InfectionCMA followed the published protocols [32]. For the various time point controls and infected cell cultures, before fixation, the medium/supernatant was removed and cells were washed with PBS 1×, thus discarding remnants of medium and non-internalized viruses. Then, cells were independently collected by scraping them from the flask with PBS 1×, followed by centrifugation and fixation with 10% neutral-buffered formalin. After fixation, each cell pellet was embedded in HistoGel (Thermo Scientific, Waltham, MA, USA) according to the manufacturer's instructions, followed by standard histological processing and paraffin embedding. Each cell block (donor block) was sectioned, and hematoxylin and eosin (H&E) stained for morphology control. Microscopic visualization of these H&E slides guided the selection of cell-rich sections for punching the 1.5 mm diameter cores. For CMA arrangement, we organized the cell lines (controls and infected) per lines, and the time points after infection per columns, or the other way around depending on whether we had more cell lines or infection time points. Then, the cores from each donor block were collected and transported to the previously defined position in the recipient paraffin block. The recipient block used had 35 cores with 1.5 mm diameter (5 lines × 7 columns) and was constructed with liquid paraffin and microarray molds. If the cores exceeded the number of samples, the empty ones were filled with paraffin. After construction, the InfectionCMAs were homogenized at 37 °C overnight and sectioned with a standard microtome (3–4 µm thickness) into slides.

2.6. Immunocytochemistry

After deparaffinization, heat-induced (98 °C) antigen retrieval was performed with a citrate buffer (pH 6.0) or EDTA buffer, and slides were incubated with hydrogen peroxide 3%. The InfectionCMAs were immunostained with the following primary antibodies: SARS-CoV-2 spike [1A9] (mouse; GTX632604, Genetex, Irvine, CA, USA), SARS-CoV-2 nucleocapsid [6H3] (mouse; GTX632269, Genetex, Irvine, CA, USA), ACE2 (mouse; MA5-31395, Thermo Scientific, Waltham, MA, USA), Neuropilin 1 [EPR3113] (rabbit; ab183495, Abcam, Cambridge, UK), Ki-67 (rabbit; MA5–14520, Thermo Scientific, Waltham, MA, USA) and BCL2 (rabbit; AB196495; Abcam, Cambridge, UK). Primary antibodies were detected using a secondary antibody with horseradish peroxidase (HRP) polymer (Dako–Agilent, Santa Clara, CA, USA) and visualization of the reaction was performed using diaminobenzidine (DAB) according to the manufacturer's instructions. The DAB brown coloration represents the positive staining, and the hematoxylin (blue coloration) was used as nuclear counterstain, dehydrated, and mounted. We confirmed that the tested human proteins were expressed in the tissues (from kidney and liver) represented by the used monkey and human cell lines (Supplementary Figure S1), while the viral ones were not expressed (confirming the SARS-CoV-2 specificity, as tissues were collected before the pandemic).

ICC images were evaluated in an Olympus Cx31 microscope (Olympus Lifesciences, Tokyo, Japan) by two independent observers (ACMagalhães and SR). The cytolocalization (nuclear, cytoplasm or membrane) of the staining was identified, and the relative percentage of the stained cells (in the entire core field) was registered in the following categories: 0–1%, >1–10%, >10–25%, >25–50%, >50–75%, and >75%. Digitalization of the InfectionCMA slides was obtained in NanoZoomer 2.0 HT (Hamamatsu Photonics, Hamamatsu City, Japan) with a magnification of 40×, and the high-resolution digital images were visualized in the associated NDP.view2 software in order to select representative figures.

2.7. mRNA In Situ Hybridization Assay

The mRNA ISH was performed using the RNAScope® Probe-V-nCoV2019-S (848561, Advanced Cell Diagnostics, Newark, CA, USA) directed against SARS-CoV-2, targeting the segment between nucleotides 21,631 and 23,303 of the reference sequence. This RNAScope probe is an antisense probe that detects the sense (positive strand). The tumor tissue cores (from before the pandemic) and the non-infected cells were used as negative controls, and a probe to the housekeeping gene peptidylprolyl isomerase B (PPIB–313901, Advanced Cell Diagnostics, Newark, CA, USA) was used to check RNA integrity. The RNAscope 2.5 HD Detection Kit-Brown was used on CMA sections (4 μm) according to the manufacturer's recommendations. Briefly, InfectionCMAs retrieval was performed at 98 °C for 20 min followed by incubation with RNAscope protease for 30 min at 40 °C. Probes were added and hybridized for 2 h at 40 °C, followed by incubation with AMP1 (30 min at 40 °C), AMP2 (15 min at 40 °C), AMP3 (30 min at 40 °C), AMP4 (15 min at 40 °C), AMP5 (30 min at RT), AMP6 (15 min at RT), and DAB (10 min at RT). Sections were counterstained with hematoxylin, dehydrated and mounted. All incubations at 40 °C were performed in a HybEZ hybridization oven (Advanced Cell Diagnostics, Newark, CA, USA). We confirmed that the tested viral mRNA probe was not expressed on the human tissues (Supplementary Figure S1) and in the mock experiments for Vero and human cells (Supplementary Figure S2).

2.8. Western Blotting

Cells were lysed with RIPA buffer (Sigma, St. Louis, MO, USA) supplemented with a protease-inhibitor cocktail (Roche, Basel, Switzerland). Samples were incubated for 30 min at 4 °C. After clearing by centrifugation (17,000× *g*, 15 min), protein concentrations were determined using the DC Protein Assay (Bio Rad, Hercules, CA, USA). Equivalent amounts of protein were separated by electrophoresis in 12.5% SDS-polyacrylamide gels, transferred to nitrocellulose (Amersham Protan, Cytiva, Marlborough, MA, USA) using a wet system (BioRad, Hercules, CA, USA), and analyzed by immunoblotting. The membranes were blocked with 5% BSA and incubated with the specific primary antibodies (the ones used in ICC), and mouse or rabbit HRP-conjugated secondary antibodies. GAPDH (mouse; GTX627408, Genetex, Irvine, CA, USA) and Actin (rabbit; ab8227, Abcam, Cambridge, UK) were used as loading controls. Finally, the membranes were incubated with the Luminata Crescendo Western HRP substrate (Millipore, Burlington, MA, USA), imaged with the ChemiDoc system, and analyzed with associated ImageLab software (Bio-Rad, Hercules, CA, USA). Student's *t*-tests were applied for pairwise comparisons.

2.9. RNA Extraction, cDNA Synthesis and qRT-PCR

In order to evaluate the expression of ACE2 gene, total RNA was isolated with the NZY Total RNA Isolation kit (Nzytech, Lisbon, Portugal), quantified in the NanoDrop 1000 (Thermo Scientific, Waltham, MA, USA), and reverse transcribed to cDNA with the M-MuLV kit (Nzytech, Lisbon, Portugal). The qRT-PCR reaction was performed in triplicate, with the NZYSupreme qPCR Probe Master Mix (Nzytech, Lisbon, Portugal) and predesigned qPCR assay (Hs.PT.58.27645933; IDT, Coralville, IA, USA), run and analyzed in the Applied Biosystems® 7500 Real-Time PCR System (Applied Biosystems, Waltham, MA, USA). TATA-box-binding protein (TBP; no. 4326322E-0705006; Applied Biosystems, Waltham, MA, USA) was used as a housekeeping gene. Data analysis was performed using the $2-\Delta\Delta CT$ method. Student's *t*-tests were applied for pairwise comparisons.

3. Results

3.1. Sequencing of the SARS-CoV-2 Isolate

The sequencing of the isolated viral specimen revealed its affiliation in the B.1.1.29 lineage, with C241T-C3037T-C14408T-T19521C-A20742C-A23403G-G28881A-G28882A-G28883C variants in relation to the reference sequence NC_045512.2. This specimen was common in Europe during the spring of 2020. As this virus was isolated from a hospitalized symptomatic individual, it has pathogenic competence, and could be used in the in vitro infection

evaluation. This competence was additionally confirmed through viral titration in each infection assay performed here.

3.2. Establishment of an InfectionCMA and Evaluation of Its Efficiency Versus a Traditional Approach

We decided to illustrate the establishment of an InfectionCMA with the following specific infection kinetic test for SARS-CoV-2: Vero cells infected with the SARS-CoV-2 isolate at two MOIs (MOI 0.01 and MOI 0.001) and control non-infected cells (mock) were grown until four time points after infection (4 h, 24 h, 48 h and 72 h), giving a total of 12 observation-points. These low MOIs are usually used in Vero cells to grow the virus for establishing stocks. The infection assay in BSL3 conditions took three days, and could be done in T-25 flasks, with eight independent infections. After fixation that inactivates SARS-CoV-2, samples were brought out of the BSL3 for the manual establishment of the InfectionCMA and ICC processing, a process that took 5–7 days in total (Figure 1). In a first phase, the cells from the 12 observation points had to be independently processed and included in 12 paraffin blocks; these 12 blocks were sectioned and H&E stained to check morphology and cell orientation in the paraffin blocks; and finally, each of the 12 blocks was individually punched to remove a 1.5 mm-diameter core to build the microarray arrangement in the 5 line $\times$ 7 column mold. In a second phase, with the 12 independent points already in a microarray format, the block could be cut in a single slide, for ICC or ISH. This block can be stored for an infinite period of time, and be posteriorly cut several times depending on the initial number of cells. In this specific case, for the initial number of cells used, we could retrieve a 1–2 cm pellet, at each time point, guaranteeing enough amount to obtain 30 slides from the InfectionCMA. This biological resource can be used to evaluate the expression of several markers of interest, specifically 30–90 proteins in total, depending on singleplexing or multiplexing the antibodies (1 to 3 proteins per slide).

To evaluate the efficiency of the InfectionCMA for this test, in quantitative terms, we estimated the required conditions in a traditional in vitro infection assay in order to obtain identical outputs (Figure 2). Usually, the output from the traditional in vitro infection assay can be improved by increasing the number of cells, viruses, plates and independent infection points, which result in obvious constraints on management, reproducibility, time consumption and used reagents. In the specific case, in order to keep the experiment manageable, we envisioned using double the number of cells and viruses in 12-well plates, implying 8 $\times$ 12 independent infections instead of eight. We used 12 independent points each copied 12 times, and all must be processed at the same or within a limited period of time, as the conservation of fixed cells at 4 °C or −20 °C, in several plates, is not practical and is prone to contamination. If we combine the 12 observation points two-by-two in the same slide, we end up with six slides to replicate the InfectionCMA single slide. This implies using a six times greater quantity of primary and secondary antibodies per protein, and also the process to acquire microscopic images multiplies by six. The twelve repetitions imply the simultaneous processing of 72 slides, allowing to ICC only 12 to 36 proteins. In order to obtain the same output of the 30 slides cut from the InfectionCMA, the traditional in vitro infection assay would need to be performed again 1.5×. This would give a final number of 180 slides to be processed.

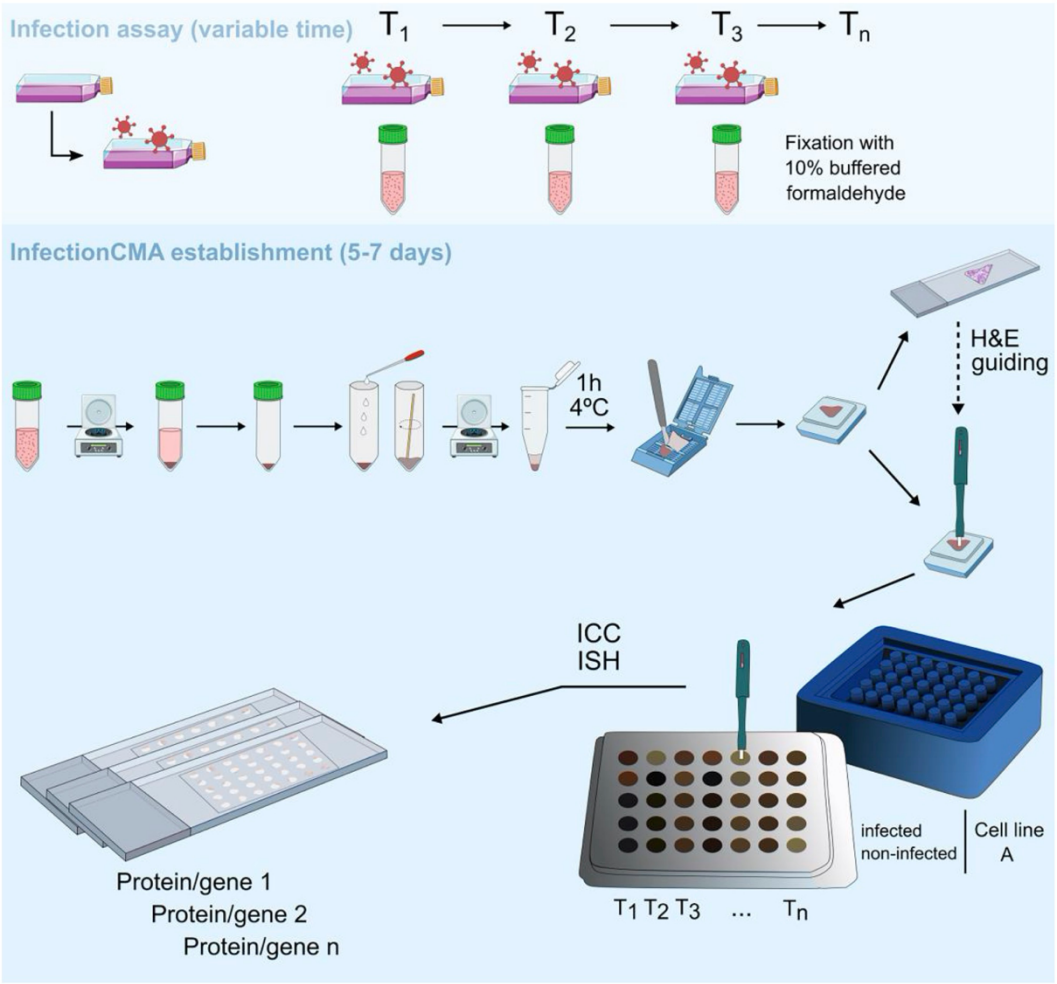


Figure 1. Schematic representation of the procedure to establish the InfectionCMA. The infection assay can have variable timelines depending on the experimental assay. The manual establishment and immune processing of the InfectionCMA take around 5–7 days. A 1–2 cm pellet of infected cells guarantees 30 slides from each InfectionCMA. This biological resource can be used for the expression evaluation of several markers of interest, through diverse techniques such as immunocytochemistry (ICC) and in situ hybridization (ISH).

Note that we only used 12 of the 35 cores available in the 5 × 7 mold for the InfectionCMA. The higher the number of cores used, the higher the efficiency of the InfectionCMA compared with the traditional in vitro infection assay.

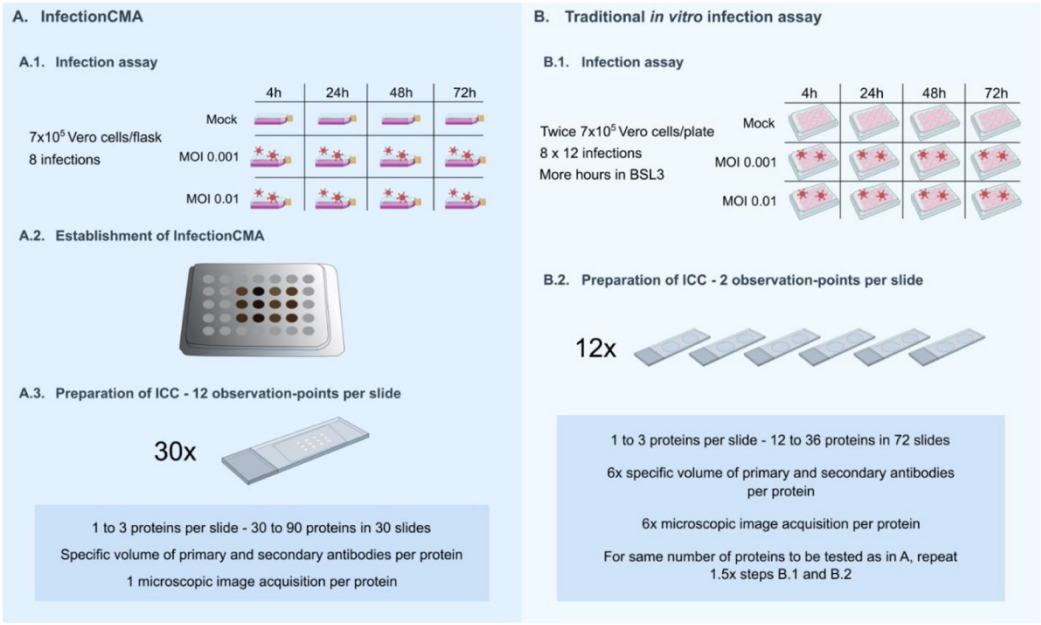


Figure 2. Comparison of the design and outputs between the InfectionCMA and the traditional in vitro infection assay for the first infection kinetics test performed here.

3.3. Evaluation of SARS-CoV-2 Infection Kinetics in Vero Cells

The SARS-CoV-2 infection kinetics in Vero cells was evaluated through the application of ICC for specific SARS-CoV-2 proteins (spike and nucleocapsid) in the InfectionCMA slides (Figure 3). It was possible to observe in the microscopic images that the viral spike and nucleocapsid proteins were located in the cytoplasm of the infected cells. A possible explanation for the signal for the nucleocapsid being stronger than the one for the spike is the former being more abundantly produced than the latter, when the virus is replicating, as observed by others [39]. This can lead to the impression that the nucleocapsid is being produced in more cells than the spike, when in fact it is being detected earlier in cells that are beginning to replicate the virus. At the higher MOI, infection was already visible in the Vero cells at 24 h (between 10 and 20% of infected cells), while at the lower MOI, the same level of infection was only observable at 48 h. Similar time points were observed in other studies [40]. For both MOIs, the rate of infected cells was already higher than 75% around a day later. At the beginning of the infection course, most cells have a low viral load, but by 72 h, most cells have a high viral load, visible by the intense spike staining.

ICC was also used for the evaluation of the expression of the human receptors involved in SARS-CoV-2 entrance into cells: NRP1 and ACE2 genes. ACE2 was localized in the membrane, and NRP1 in the membrane and in the cytoplasm (Figure 4). The cells were collected by scraping and were not trypsinized, allowing us to keep alterations to membrane receptors as low as possible. A higher percentage of Vero cells were positive for NRP1 (>75%) than for ACE2 (~25%) expression. As already described in the literature [41,42], the expression of ACE2 protein significantly decreased as the SARS-CoV-2 infection progressed. Concordantly with the results for spike and nucleocapsid evaluation, the decrease in the ACE2 protein was visible earlier for the higher MOI (at 24 h–10–25%) than for the lower MOI (at 48 h–10–25%), but at 72 h it was not detected in any of the MOIs. No differences in NRP1 expression in the Vero cells were observable over time in any of the MOIs.

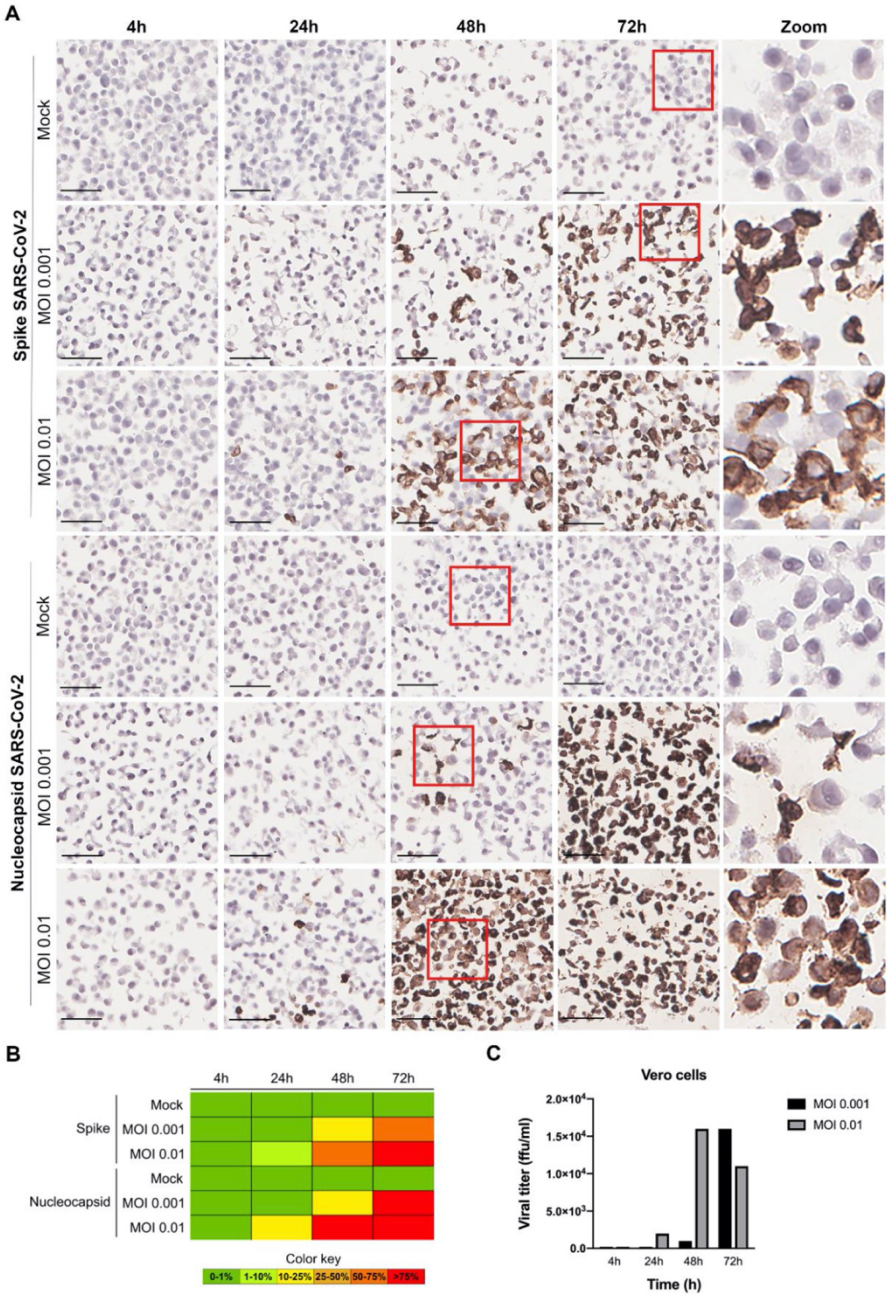


Figure 3. ICC results for SARS-CoV-2 spike and nucleocapsid proteins in infected Vero cells, at various time points (4 h, 24 h, 48 h and 72 h), for MOI 0.001 and MOI 0.01. (**A**) Microscopic images with 50 µm scale bar. The last column represents zoomed-in images of the sections highlighted within a red square in the respective rows. Both viral proteins were located in the cytoplasm of the infected cells. (**B**) Heat map for the percentage of cells stained (0–1%, >1–10%, >10–25%, >25–50%, >50–75%, and >75%). (**C**) Infectious viral particles produced at the various time points (in ffu/mL—focus forming units per mL).

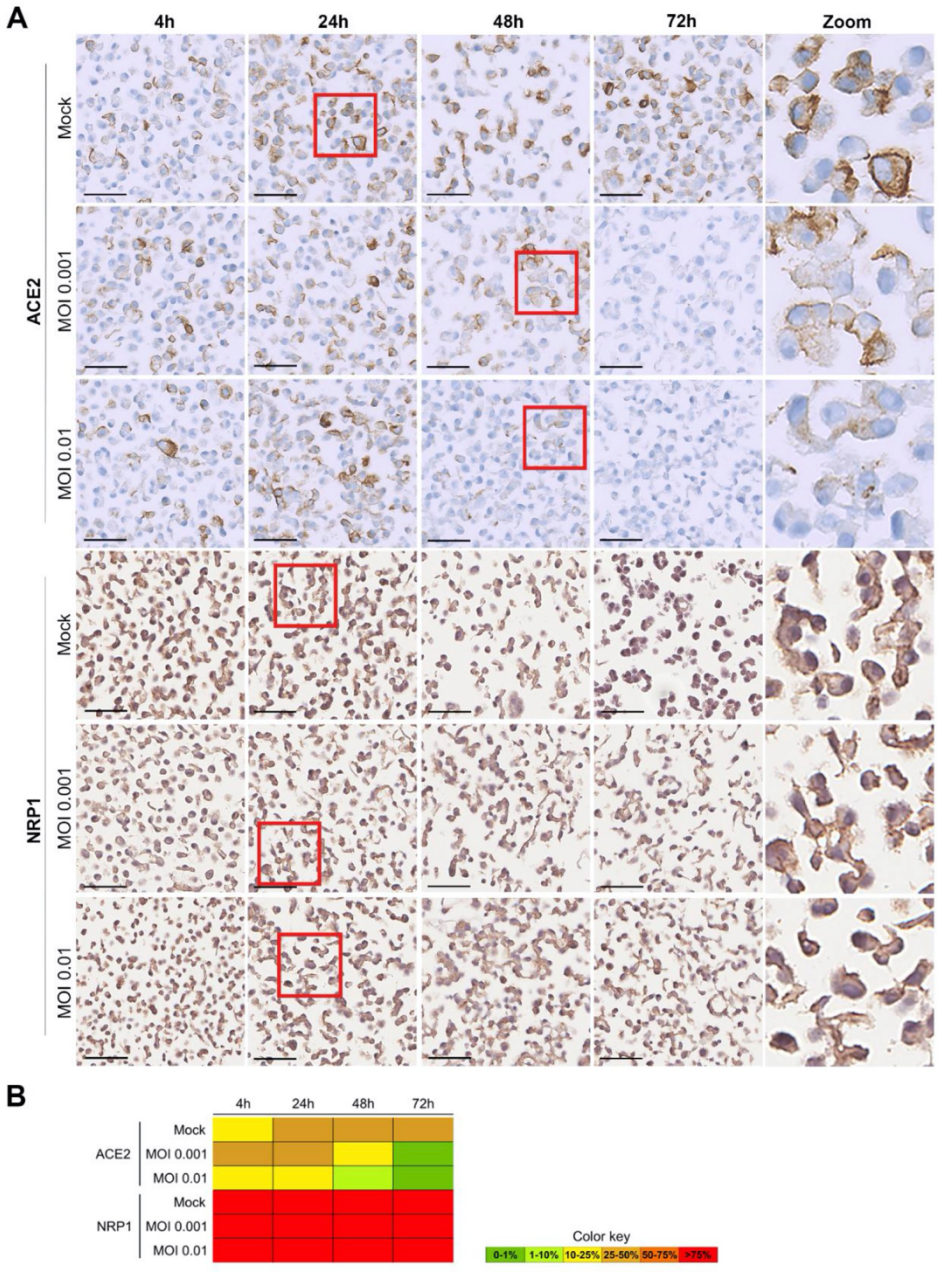


Figure 4. ICC results for ACE2 and NRP1 proteins in SARS-CoV-2-infected Vero cells, at various time points (4 h, 24 h, 48 h and 72 h), for mock (non-infected), MOI 0.001 and MOI 0.01. (**A**) Microscopic images with a 50 µm scale bar. The last column represents zoomed-in images of the sections highlighted within a red square in the respective rows. Both viral proteins were located in the cytoplasm of the infected cells. ACE2 was localized in the membrane, and NRP1 in the membrane and in the cytoplasm. (**B**) Heat map for the percentage of cells stained (0–1%, >1–10%, >10–25%, >25–50%, >50–75%, and >75%).

3.4. Evaluation of SARS-CoV-2 Infection Kinetics in Human Cell Lines

In order to investigate the SARS-CoV-2 infection kinetics in human cell lines, we established an InfectionCMA for Caco-2 and Huh-7 (in parallel with Vero cells, for comparison). Since Vero cells allow higher viral replication rates due to their lack of genes encoding type I interferons, we increased MOI to 1 in this assay. This was conducted in one experiment for each cell line, with two conditions (mock and MOI 1) for three time points. The resulting InfectionCMA contained 18 observation points, rendering it more efficient than the first kinetic infection test: a total of 30 slides for the InfectionCMA in comparison with 270 slides for the traditional in vitro infection assay; nine times lower quantities of primary and secondary antibodies; and 9 versus 9 × 12 infections.

Figure 5 shows the results for the quantification of the viral spike protein and mRNA levels. For this high MOI, the ICC results indicate that the Vero cells displayed a high infection rate (>75%) already at 16 h, and the viral titer was higher at 36 h, decreasing significantly at 72 h (Figure 5E; while in Figure 3C, at MOI 0.001, the viral titer was still increasing at this time period, but already decreasing for MOI 0.01). These results show that with a high MOI, the infection rate is very high, and the viral cycle is very fast in the Vero cell lines. Additionally, as ACE2 expression decreases along the infection course, the virions will be less able to reinfect cells, and new replication will begin to decrease (so, decreasing viral titer). In the liver Huh-7 cell line, viral replication was slower (10–25% of cells were positive for the spike protein at 16 h) and showed a steady infection rate of 25–50% along the infection course. In the intestinal Caco-2 cell line, viral replication was even slower (<10% positive cells at 16 h) but reached a higher infection rate at 72 h (50–75%). For both human cell lines, the higher values of viral release to the medium were observed only at 72 h (Figure 5E), testifying the slower infection rate in these cells in relation to Vero cells. These ICC results were broadly supported by the ISH (which is more sensitive than ICC) and the Western blot results for spike, as well as by the ICC results for the nucleocapsid (Supplementary Figure S3). In conclusion, the two human cell lines Huh-7 and Caco-2 are susceptible to infection by SARS-CoV-2 and can be used as in vitro models of infection by this new emergent virus. The evaluation of viral replication kinetics by InfectionCMA and ICC gave reliable results, as compared to well-established techniques such as Western blot and qRT-PCR.

Then, we conducted ICC of the human receptors, ACE2 (Figure 6) and NRP1 (Figure 7). NRP1 presented high expression in the non-infected Vero and human cells lines (>75%), while ACE2 proportions was present in 10–25% of all cells. Again, for MOI 1, the decrease in the expression of ACE2 protein as the virus replicated within the human cell lines was clear, being already significant (in relation to the control) at 16 h after infection for the Vero and Huh-7 cells, and only at the time point of 48 h for Caco-2. The decrease with infection was also observable for the ACE2 mRNA when quantified by qRT-PCR. Interestingly, for this higher MOI, NRP1 (Figure 7) followed the same tendency of a decrease in protein expression with the SARS-CoV-2 infection course, but values were overall not statistically significant, probably reflecting the initial higher proportion of NRP1 than ACE2 in all cells.

We did not detect visual loss of cell integrity in the course of infection in the Vero and human cell lines. However, in order to evaluate possible alterations in cell viability or proliferation related to viral replication, we performed ICC for two additional markers (Figure 8 and Supplementary Figures S4 and S5): Ki-67, a nuclear protein associated with cellular proliferation [43]; BCL-2 a biomarker of the intrinsic apoptosis pathway [44]. The microscopic images allowed us to confirm the nuclear location of Ki-67 and cytoplasmic localization of BCL-2. There were no statistically significant alterations in proliferation (Ki-67) and in apoptosis (BCL-2) amongst the Vero and human cell lines along the infection course. All cells were homogeneously proliferating, and non-apoptotic (Figure 7 and Supplementary Figures S3 and S4).

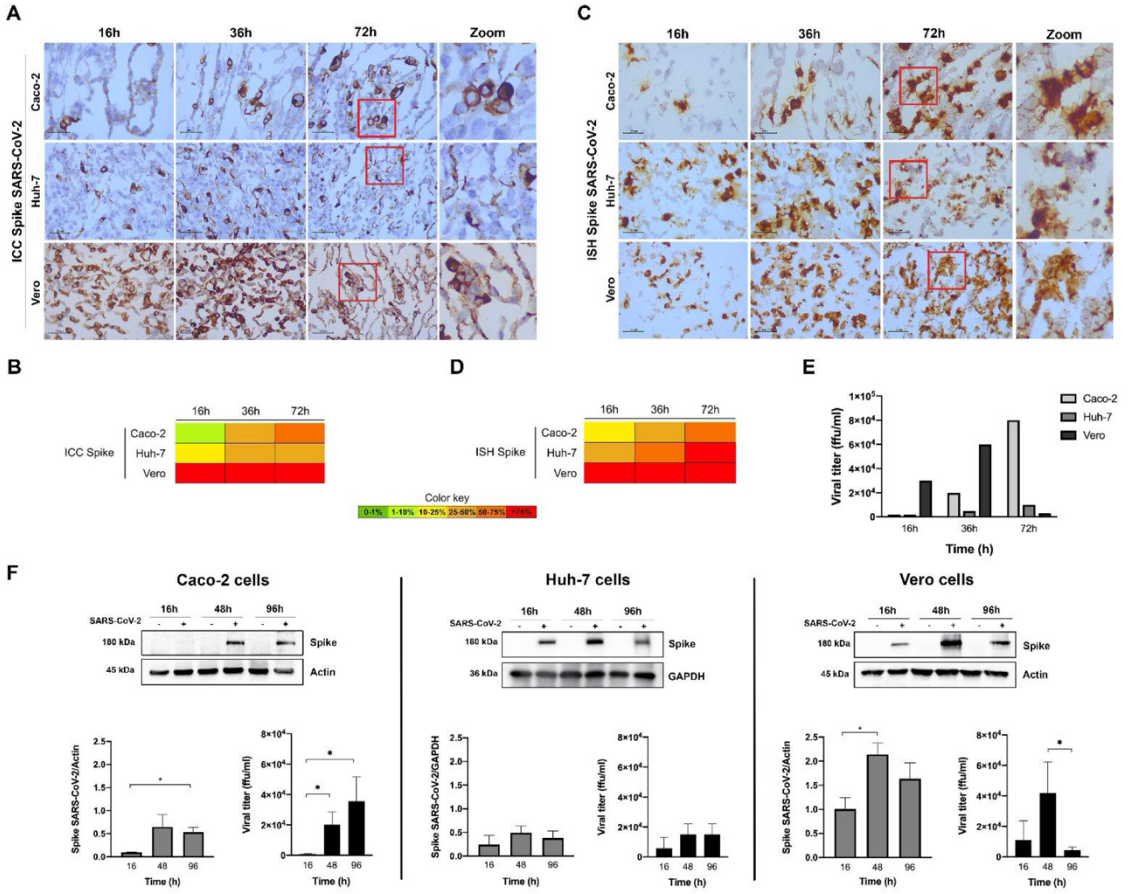


Figure 5. Characterization of SARS-CoV-2 spike expression in the human (Caco-2 and Huh-7) and Vero cell lines, at various time points after infection with MOI 1, by ICC ((**A**) microscopic images with 100 µm scale bar, including zooms of the red inserts; (**B**) heat map), and ISH ((**C**) microscopic images, including zooms of the red inserts; (**D**) heat map). The spike protein had a cytoplasmic location in all the infected cell lines. (**E**) Infectious viral particles produced at the various time points (in ffu/mL —focus forming units per mL). (**F**) Western blots and graphs representing the spike quantification in cells and the infectious viral particles produced in these independent experiments. In the graphs, data represent means ± SD of three independent experiments, and significant Student's *t*-test *p*-values are indicated (* < 0.05).

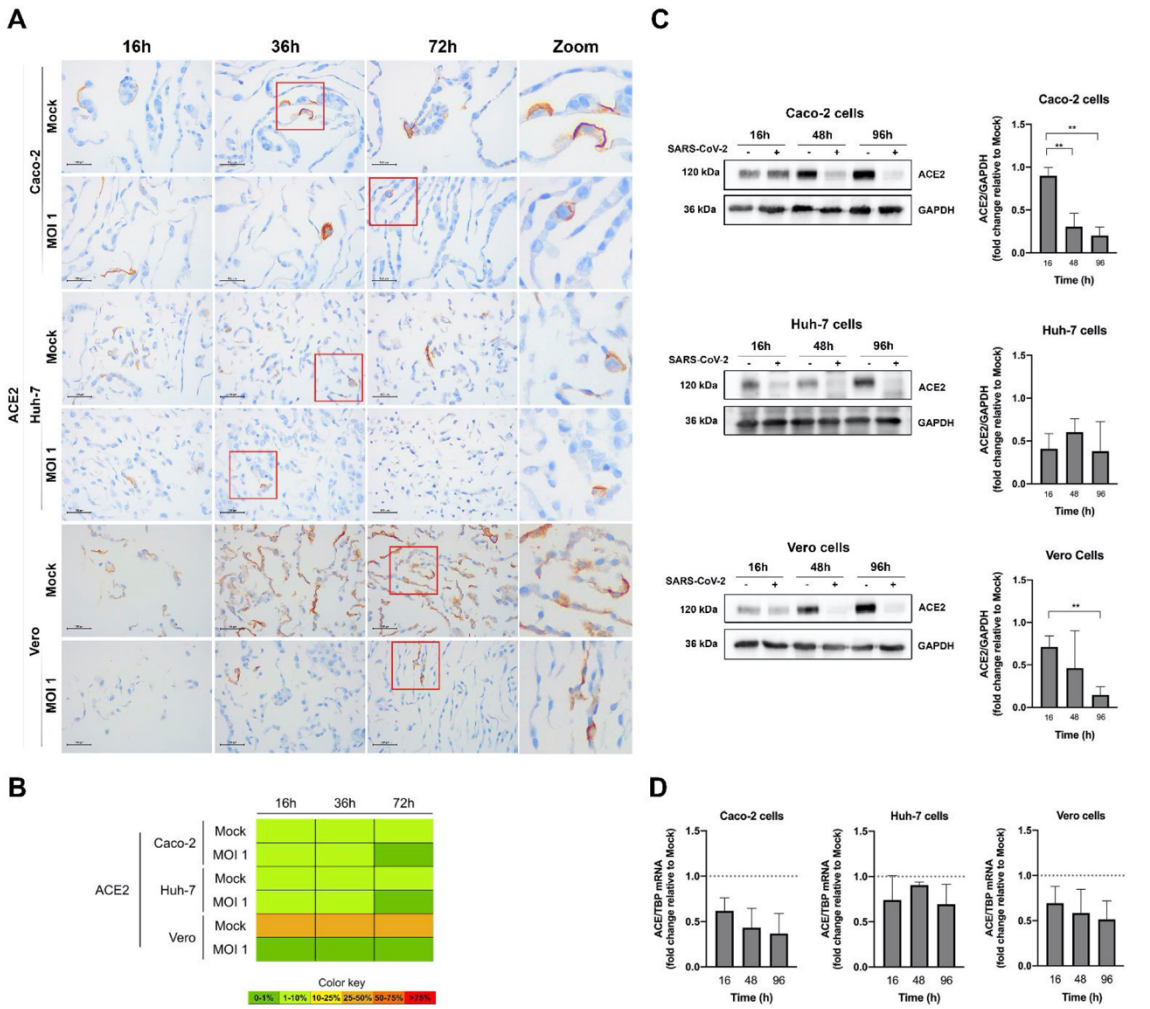


Figure 6. Characterization of ACE2 expression in the human (Caco-2 and Huh-7) and Vero cell lines, at various time points after infection with MOI 1, by ICC ((**A**) microscopic images with 100 µm scale bar, including zooms of the red inserts; (**B**) heat map), Western blot (**C**), and qRT-PCR (**D**). In the graphs, data represent means ± SD of three independent experiments, and significant Student's *t*-test *p*-values are indicated (** < 0.01). The ACE2 was placed in the membrane of all the infected cell lines.

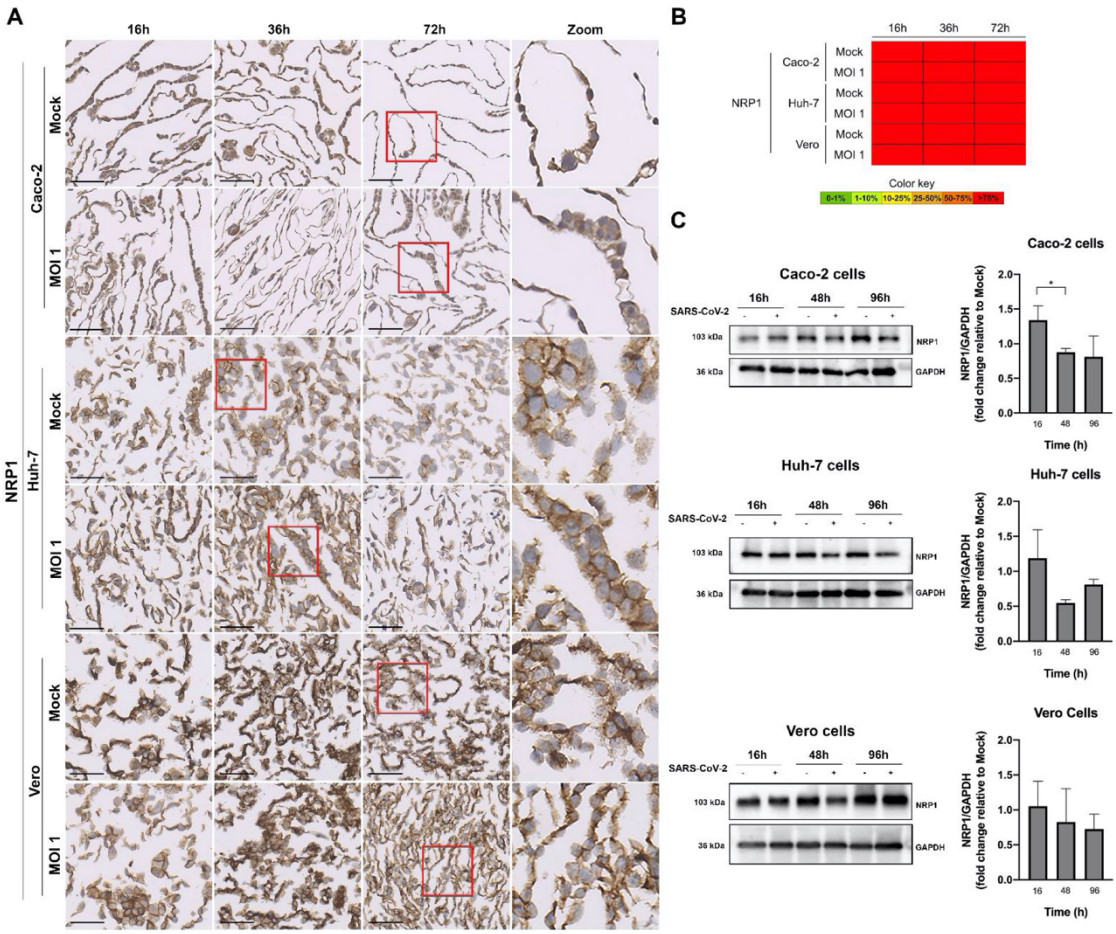


Figure 7. Characterization of NRP1 expression in the human (Caco-2 and Huh-7) and Vero cell lines, at various time points after infection with MOI 1, by ICC ((**A**) microscopic images with 50 µm scale bar, including zooms of the red inserts; (**B**) heat map) and Western blot (**C**). In the graphs, data represent means ± SD of three independent experiments, and significant Student's *t*-test *p*-values are indicated (* < 0.05). The NRP1 was expressed in the membrane and in the cytoplasm of all the infected cell lines.

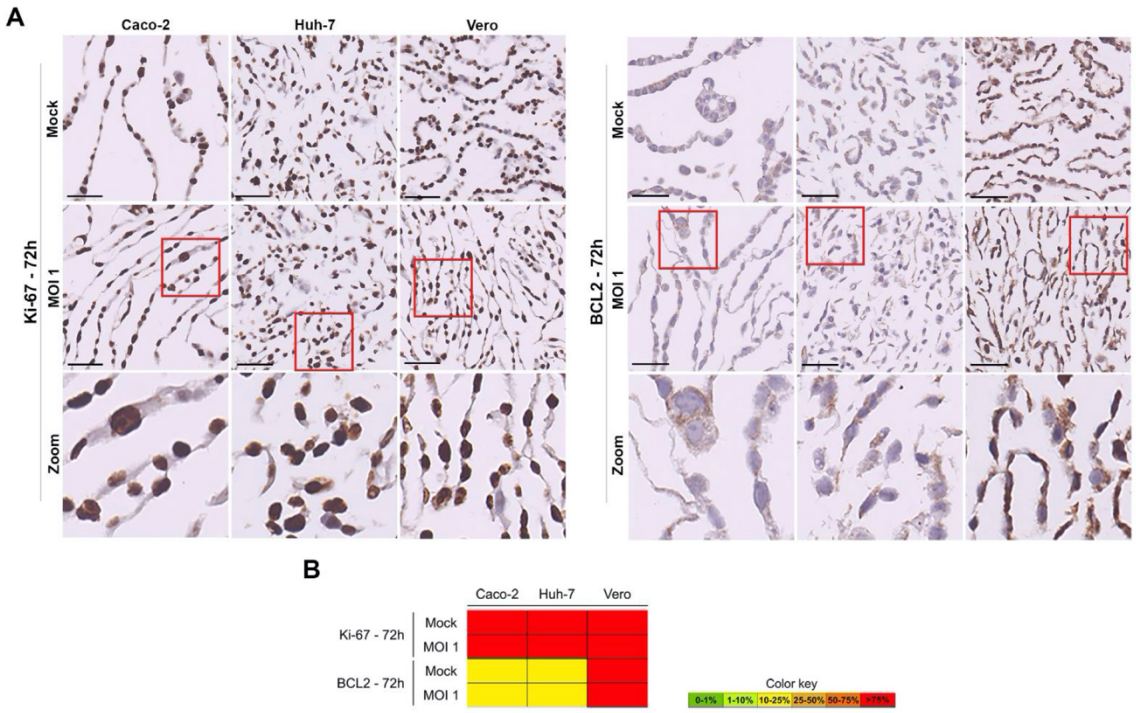


Figure 8. Characterization of Ki-67 and BCL-2 expression in the human (Caco-2 and Huh-7) and Vero cell lines, at 72 h after infection with MOI 1, by ICC ((**A**)—microscopic images with 50 µm scale bar, including zooms of the red inserts in the last row; (**B**)—heat map). The Ki-67 displayed a nuclear and BCL-2 cytoplasmic localizations.

4. Conclusions

In this work, we illustrate the efficiency of the InfectionCMAs as tools to investigate the infection kinetics of a pathogen, namely SARS-CoV-2. This approach significantly increases the applicability of histology-based methods in virology/infectious diseases field, which traditionally was limited to the viral detection in FFPE samples [45]. The two InfectionCMAs established in this work were easy to implement, and despite not using the maximum output allowed by a 5 × 7 mold, led to substantial gains against a traditional approach: for the 12 observation-point InfectionCMA, it provided 30 slides versus 180 slides and a saving of six times the antibody amounts; for the 18 observation-point InfectionCMA, it provided 30 slides versus 270 slides and a saving of nine times the antibody amounts; and for both, only one compared to 2.5× BSL3 experimental procedures. If the maximum capacity of the 5 × 7 mold was used (an even number of 34 observation-points), the gains would be 30 versus 510 slides and 17 times lower antibody amounts. There are larger molds available, allowing even better outputs. Thus, we demonstrated the added value of InfectionCMA in overcoming difficulties raised by the otherwise complex traditional in vitro infection assays, where improvements in outputs imply increasing the number of cells, viruses, plates and independent infection points. In addition, the InfectionCMA block and slides could be easily stored, and allowed testing of additional markers without the need to conduct a new experiment in biosafety BSL3 conditions. They can also be easily and safely sent to other laboratories, who do not dispose of conditions for viral experiments, for local screening of biomarkers.

Importantly, the evaluation of each marker cytolocalization combined with the morphologic assessment of the infected cell is a powerful tool for a comprehensive histological

evaluation of the SARS-CoV-2 infection process and of its key biological players. We confirmed the capacity of SARS-CoV-2 (isolate B.1.1.29) to efficiently infect the monkey Vero and the human Huh-7 and Caco-2 cells. As verified previously [40], Caco-2 were more susceptible than Huh-7. We verified that a significant decrease occurred in the mRNA and protein expressions of ACE2 along the infection course, as observed by others [41,42]. ACE2 is known to be the main human receptor for SARS-CoV-2, and this may explain the fast viral cycle in the permissive Vero cell line at high MOI: the significant decrease in ACE2 expression impaired the reinfection of cells by virions at 72 h (inferred from the decreasing viral titer). However, SARS-CoV-2 can use other host receptors, as demonstrated by Daly et al. [46], when the suppression of NRP1 expression by short hairpin RNA greatly reduced SARS-CoV-2 infection at both 7 h and 16 h after infection in Caco-2 cells. Interestingly, we observed the same tendency of NRP1 protein for decreased expression with infection in the three cell types, when the MOI was high. To the best of our knowledge, this decrease in NRP1 expression with SARS-CoV-2 infection has not been described previously in the literature, probably due to its considerable overall higher expression than ACE2 in most cells and tissues (as can be confirmed in protein atlas and GTEx websites; https://www.proteinatlas.org/ and https://gtexportal.org/home/, accessed on 31 December 2021). This confirmation strengthens the implication that cell types which do not express ACE2 can even so be infected by SARS-CoV-2, either through alternative surface receptors [47] or receptor-independent mechanisms of entry [48]. Additionally, as SARS-CoV-2 acquires further mutations, it can become more efficient in exploring the alternative receptors and mechanisms.

Even at the higher MOI 1, we did not observe significant cell death over the course of infection, for as long as 72 h. Similar observations were reported in comparison studies between SARS-CoV-2 and SARS-CoV infectivity, which found that SARS-CoV-2 replicates to higher levels without inducing substantial host cell damage, while SARS-CoV showed more restricted tropism and higher pathogenicity [40]. This behavior might contribute to prolonged COVID-19 in patients whose immune system is not efficient in fighting SARS-CoV-2.

Supplementary Materials: The following are available online at: https://www.mdpi.com/article/10.3390/pathogens11030313/s1, Figure S1: ICC for the spike, nucleocapsid, ACE2, NRP1, Ki-67 and BCL2 in the tumor tissue cores of kidney and liver. Scale bar 50 µm. Figure S2: Characterization of SARS-CoV-2 nucleocapsid expression in the human (Caco-2 and Huh-7) and Vero cell lines, at different time points after infection with MOI 1, by ICC (A–light microscopic images with 100 µm scale bar; B–heat map). Figure S3: Characterization of Ki-67 expression in the human (Caco-2 and Huh-7) and Vero cell lines, at different time points after infection with MOI 1, by ICC (A–light microscopic images with 50 µm scale bar; B–heat map). Figure S4: Characterization of BCL-2 expression in the human (Caco-2 and Huh-7) and Vero cell lines, at different time points after infection with MOI 1, by ICC (A–light microscopic images with 50 µm scale bar; B–heat map).

Author Contributions: Conceptualization, A.C.M. (Ana C. Magalhães), S.R. and L.P.; methodology, A.C.M. (Ana C. Magalhães), S.R., A.C.M. (Ana C. Moreira), M.N., M.T., R.J.P.; formal analysis, A.C.M. (Ana C. Magalhães), S.R., M.S.G.; supervision, L.P.; writing, A.C.M. (Ana C. Magalhães) and L.P. All authors have read and agreed to the published version of the manuscript.

Funding: The Portuguese Foundation for Science and Technology (FCT) funded this project through the Research4COVID19 projects 109_596696487 and RESEARCH COVID-19 projects Ref. 510. FCT also financed the Ph.D. grant to R.J.P. (SFRH/BD/145217/2019) and M.N. (2020.04720.BD). i3S is supported by FEDER–Fundo Europeu de Desenvolvimento Regional funds through the COMPETE 2020–Operational Program for Competitiveness and Internationalization (POCI), Portugal 2020, and by Portuguese funds through FCT/Ministério da Ciência, Tecnologia e Inovação in the framework of the project 'Institute for Research and Innovation in Health Sciences' (POCI-01-0145-FEDER-007274).

Institutional Review Board Statement: Not applicable.

Informed Consent Statement: Not applicable.

Data Availability Statement: The data presented in this study are available in the main text, figures, tables and Supplementary Materials.

Acknowledgments: We thank Leonor David, Fernando Schmitt and Paula Soares for access to reagents.

Conflicts of Interest: The authors declare no conflict of interest. The funders had no role in the design of the study; in the collection, analyses, or interpretation of data; in the writing of the manuscript, or in the decision to publish the results.

References

1. Bente, D.A.; Rico-Hesse, R. Models of dengue virus infection. *Drug Discov. Today Dis. Models* **2006**, *3*, 97–103. [CrossRef] [PubMed]
2. Pena, L.J.; Miranda Guarines, K.; Duarte Silva, A.J.; Sales Leal, L.R.; Mendes Félix, D.; Silva, A.; de Oliveira, S.A.; Junqueira Ayres, C.F.; Júnior, A.S.; de Freitas, A.C. In vitro and in vivo models for studying Zika virus biology. *J. Gen. Virol.* **2018**, *99*, 1529–1550. [CrossRef] [PubMed]
3. Last, A.; Maurer, M.; Mosig, A.S.; Gresnigt, M.S.; Hube, B. In vitro infection models to study fungal-host interactions. *FEMS Microbiol. Rev.* **2021**, *45*, fuab005. [CrossRef] [PubMed]
4. Parish, T. In vitro drug discovery models for Mycobacterium tuberculosis relevant for host infection. *Expert Opin. Drug Discov.* **2020**, *15*, 349–358. [CrossRef] [PubMed]
5. Andrews, K.A.; Wesche, D.; McCarthy, J.; Möhrle, J.J.; Tarning, J.; Phillips, L.; Kern, S.; Grasela, T. Model-Informed Drug Development for Malaria Therapeutics. *Annu. Rev. Pharmacol. Toxicol.* **2018**, *58*, 567–582. [CrossRef]
6. Benam, K.H.; Dauth, S.; Hassell, B.; Herland, A.; Jain, A.; Jang, K.J.; Karalis, K.; Kim, H.J.; MacQueen, L.; Mahmoodian, R.; et al. Engineered in vitro disease models. *Annu. Rev. Pathol.* **2015**, *10*, 195–262. [CrossRef]
7. Casalino, L.; Gaieb, Z.; Goldsmith, J.A.; Hjorth, C.K.; Dommer, A.C.; Harbison, A.M.; Fogarty, C.A.; Barros, E.P.; Taylor, B.C.; McLellan, J.S.; et al. Beyond Shielding: The Roles of Glycans in the SARS-CoV-2 Spike Protein. *ACS Cent. Sci.* **2020**, *6*, 1722–1734. [CrossRef]
8. Ke, Z.; Oton, J.; Qu, K.; Cortese, M.; Zila, V.; McKeane, L.; Nakane, T.; Zivanov, J.; Neufeldt, C.J.; Cerikan, B.; et al. Structures and distributions of SARS-CoV-2 spike proteins on intact virions. *Nature* **2020**, *588*, 498–502. [CrossRef]
9. Turoňová, B.; Sikora, M.; Schürmann, C.; Hagen, W.J.H.; Welsch, S.; Blanc, F.E.C.; von Bülow, S.; Gecht, M.; Bagola, K.; Hörner, C.; et al. In situ structural analysis of SARS-CoV-2 spike reveals flexibility mediated by three hinges. *Science* **2020**, *370*, 203–208. [CrossRef]
10. Nguyen, H.L.; Lan, P.D.; Thai, N.Q.; Nissley, D.A.; O'Brien, E.P.; Li, M.S. Does SARS-CoV-2 Bind to Human ACE2 More Strongly Than Does SARS-CoV? *J. Phys. Chem. B* **2020**, *124*, 7336–7347. [CrossRef]
11. Shang, J.; Ye, G.; Shi, K.; Wan, Y.; Luo, C.; Aihara, H.; Geng, Q.; Auerbach, A.; Li, F. Structural basis of receptor recognition by SARS-CoV-2. *Nature* **2020**, *581*, 221–224. [CrossRef]
12. Gobeil, S.M.; Janowska, K.; McDowell, S.; Mansouri, K.; Parks, R.; Stalls, V.; Kopp, M.F.; Manne, K.; Li, D.; Wiehe, K.; et al. Effect of natural mutations of SARS-CoV-2 on spike structure, conformation, and antigenicity. *Science* **2021**, *373*, eabi6226. [CrossRef] [PubMed]
13. Hoffmann, M.; Kleine-Weber, H.; Schroeder, S.; Krüger, N.; Herrler, T.; Erichsen, S.; Schiergens, T.S.; Herrler, G.; Wu, N.H.; Nitsche, A.; et al. SARS-CoV-2 Cell Entry Depends on ACE2 and TMPRSS2 and Is Blocked by a Clinically Proven Protease Inhibitor. *Cell* **2020**, *181*, 271–280.e8. [CrossRef] [PubMed]
14. Peacock, T.P.; Goldhill, D.H.; Zhou, J.; Baillon, L.; Frise, R.; Swann, O.C.; Kugathasan, R.; Penn, R.; Brown, J.C.; Sanchez-David, R.Y.; et al. The furin cleavage site in the SARS-CoV-2 spike protein is required for transmission in ferrets. *Nat. Microbiol.* **2021**, *6*, 899–909. [CrossRef] [PubMed]
15. Finkel, Y.; Gluck, A.; Nachshon, A.; Winkler, R.; Fisher, T.; Rozman, B.; Mizrahi, O.; Lubelsky, Y.; Zuckerman, B.; Slobodin, B.; et al. SARS-CoV-2 uses a multipronged strategy to impede host protein synthesis. *Nature* **2021**, *594*, 240–245. [CrossRef] [PubMed]
16. Schubert, K.; Karousis, E.D.; Jomaa, A.; Scaiola, A.; Echeverria, B.; Gurzeler, L.A.; Leibundgut, M.; Thiel, V.; Mühlemann, O.; Ban, N. SARS-CoV-2 Nsp1 binds the ribosomal mRNA channel to inhibit translation. *Nat. Struct. Mol. Biol.* **2020**, *27*, 959–966. [CrossRef]
17. Thoms, M.; Buschauer, R.; Ameismeier, M.; Koepke, L.; Denk, T.; Hirschenberger, M.; Kratzat, H.; Hayn, M.; Mackens-Kiani, T.; Cheng, J.; et al. Structural basis for translational shutdown and immune evasion by the Nsp1 protein of SARS-CoV-2. *Science* **2020**, *369*, 1249–1255. [CrossRef]
18. Zhang, K.; Miorin, L.; Makio, T.; Dehghan, I.; Gao, S.; Xie, Y.; Zhong, H.; Esparza, M.; Kehrer, T.; Kumar, A.; et al. Nsp1 protein of SARS-CoV-2 disrupts the mRNA export machinery to inhibit host gene expression. *Sci. Adv.* **2021**, *7*, eabe7386. [CrossRef]
19. Zhang, Z.; Zheng, Y.; Niu, Z.; Zhang, B.; Wang, C.; Yao, X.; Peng, H.; Franca, D.N.; Wang, Y.; Zhu, Y.; et al. SARS-CoV-2 spike protein dictates syncytium-mediated lymphocyte elimination. *Cell Death Differ.* **2021**, *28*, 2765–2777. [CrossRef]
20. Trimarco, J.D.; Heaton, B.E.; Chaparian, R.R.; Burke, K.N.; Binder, R.A.; Gray, G.C.; Smith, C.M.; Menachery, V.D.; Heaton, N.S. TMEM41B is a host factor required for the replication of diverse coronaviruses including SARS-CoV-2. *PLoS Pathog.* **2021**, *17*, e1009599. [CrossRef]
21. Wolff, G.; Limpens, R.; Zevenhoven-Dobbe, J.C.; Laugks, U.; Zheng, S.; de Jong, A.W.M.; Koning, R.I.; Agard, D.A.; Grünewald, K.; Koster, A.J.; et al. A molecular pore spans the double membrane of the coronavirus replication organelle. *Science* **2020**, *369*, 1395–1398. [CrossRef] [PubMed]

22. Ghosh, S.; Dellibovi-Ragheb, T.A.; Kerviel, A.; Pak, E.; Qiu, Q.; Fisher, M.; Takvorian, P.M.; Bleck, C.; Hsu, V.W.; Fehr, A.R.; et al. β-Coronaviruses Use Lysosomes for Egress Instead of the Biosynthetic Secretory Pathway. *Cell* **2020**, *183*, 1520–1535 e1514. [CrossRef] [PubMed]
23. Hoffmann, M.; Kleine-Weber, H.; Pöhlmann, S. A Multibasic Cleavage Site in the Spike Protein of SARS-CoV-2 Is Essential for Infection of Human Lung Cells. *Mol. Cell* **2020**, *78*, 779–784 e775. [CrossRef] [PubMed]
24. Mykytyn, A.Z.; Breugem, T.I.; Riesebosch, S.; Schipper, D.; van den Doel, P.B.; Rottier, R.J.; Lamers, M.M.; Haagmans, B.L. SARS-CoV-2 entry into human airway organoids is serine protease-mediated and facilitated by the multibasic cleavage site. *eLife* **2021**, *10*, e64508. [CrossRef] [PubMed]
25. Gordon, D.E.; Jang, G.M.; Bouhaddou, M.; Xu, J.; Obernier, K.; White, K.M.; O'Meara, M.J.; Rezelj, V.V.; Guo, J.Z.; Swaney, D.L.; et al. A SARS-CoV-2 protein interaction map reveals targets for drug repurposing. *Nature* **2020**, *583*, 459–468. [CrossRef] [PubMed]
26. Braga, L.; Ali, H.; Secco, I.; Chiavacci, E.; Neves, G.; Goldhill, D.; Penn, R.; Jimenez-Guardeño, J.M.; Ortega-Prieto, A.M.; Bussani, R.; et al. Drugs that inhibit TMEM16 proteins block SARS-CoV-2 spike-induced syncytia. *Nature* **2021**, *594*, 88–93. [CrossRef]
27. Ku, K.B.; Shin, H.J.; Kim, H.S.; Kim, B.T.; Kim, S.J.; Kim, C. Repurposing Screens of FDA-Approved Drugs Identify 29 Inhibitors of SARS-CoV-2. *J. Microbiol. Biotechnol.* **2020**, *30*, 1843–1853. [CrossRef]
28. Chen, C.Z.; Shinn, P.; Itkin, Z.; Eastman, R.T.; Bostwick, R.; Rasmussen, L.; Huang, R.; Shen, M.; Hu, X.; Wilson, K.M.; et al. Drug Repurposing Screen for Compounds Inhibiting the Cytopathic Effect of SARS-CoV-2. *Front. Pharmacol.* **2020**, *11*, 592737. [CrossRef]
29. Biering, S.B.; Van Dis, E.; Wehri, E.; Yamashiro, L.H.; Nguyenla, X.; Dugast-Darzacq, C.; Graham, T.G.W.; Stroumza, J.R.; Golovkine, G.R.; Roberts, A.W.; et al. Screening a Library of FDA-Approved and Bioactive Compounds for Antiviral Activity against SARS-CoV-2. *ACS Infect. Dis.* **2021**, *7*, 2337–2351. [CrossRef]
30. Shidham, V.B. CellBlockistry: Chemistry and art of cell-block making—A detailed review of various historical options with recent advances. *CytoJournal* **2019**, *16*, 12. [CrossRef]
31. Ricardo, S.A.; Milanezi, F.; Carvalho, S.T.; Leitão, D.R.; Schmitt, F.C. HER2 evaluation using the novel rabbit monoclonal antibody SP3 and CISH in tissue microarrays of invasive breast carcinomas. *J. Clin. Pathol.* **2007**, *60*, 1001–1005. [CrossRef] [PubMed]
32. Coelho, R.; Marcos-Silva, L.; Mendes, N.; Pereira, D.; Brito, C.; Jacob, F.; Steentoft, C.; Mandel, U.; Clausen, H.; David, L.; et al. Mucins and Truncated O-Glycans Unveil Phenotypic Discrepancies between Serous Ovarian Cancer Cell Lines and Primary Tumours. *Int. J. Mol. Sci.* **2018**, *19*, 2045. [CrossRef] [PubMed]
33. Kononen, J.; Bubendorf, L.; Kallioniemi, A.; Bärlund, M.; Schraml, P.; Leighton, S.; Torhorst, J.; Mihatsch, M.J.; Sauter, G.; Kallioniemi, O.P. Tissue microarrays for high-throughput molecular profiling of tumor specimens. *Nat. Med.* **1998**, *4*, 844–847. [CrossRef] [PubMed]
34. Liu, D.; He, J.; Yuan, Z.; Wang, S.; Peng, R.; Shi, Y.; Teng, X.; Qin, T. EGFR expression correlates with decreased disease-free survival in triple-negative breast cancer: A retrospective analysis based on a tissue microarray. *Med. Oncol.* **2012**, *29*, 401–405. [CrossRef] [PubMed]
35. Cho, C.H.; Cho, M.; Park, J.K. Biomarker barcodes: Multiplexed microfluidic immunohistochemistry enables high-throughput analysis of tissue microarray. *Lab A Chip* **2021**, *21*, 3471–3482. [CrossRef] [PubMed]
36. Pedro, N.; Silva, C.N.; Magalhães, A.C.; Cavadas, B.; Rocha, A.M.; Moreira, A.C.; Gomes, M.S.; Silva, D.; Sobrinho-Simões, J.; Ramos, A.; et al. Dynamics of a dual SARS-CoV-2 lineage co-infection on a prolonged viral shedding COVID-19 case: Insights into clinical severity and disease duration. *Microorganisms* **2021**, *9*, 300. [CrossRef]
37. Pedro, N.; Fernandes, V.; Cavadas, B.; Guimarães, J.T.; Barros, H.; Tavares, M.; Pereira, L. Field and Molecular Epidemiology: How Viral Sequencing Changed Transmission Inferences in the First Portuguese SARS-CoV-2 Infection Cluster. *Viruses* **2021**, *13*, 1116. [CrossRef]
38. Wu, F.; Zhao, S.; Yu, B.; Chen, Y.M.; Wang, W.; Song, Z.G.; Hu, Y.; Tao, Z.W.; Tian, J.H.; Pei, Y.Y.; et al. A new coronavirus associated with human respiratory disease in China. *Nature* **2020**, *579*, 265–269. [CrossRef]
39. Kim, D.; Lee, J.Y.; Yang, J.S.; Kim, J.W.; Kim, V.N.; Chang, H. The Architecture of SARS-CoV-2 Transcriptome. *Cell* **2020**, *181*, 914–921.e910. [CrossRef]
40. Chu, H.; Chan, J.F.; Yuen, T.T.; Shuai, H.; Yuan, S.; Wang, Y.; Hu, B.; Yip, C.C.; Tsang, J.O.; Huang, X.; et al. Comparative tropism, replication kinetics, and cell damage profiling of SARS-CoV-2 and SARS-CoV with implications for clinical manifestations, transmissibility, and laboratory studies of COVID-19: An observational study. *Lancet Microbe* **2020**, *1*, e14–e23. [CrossRef]
41. Zhou, P.; Yang, X.L.; Wang, X.G.; Hu, B.; Zhang, L.; Zhang, W.; Si, H.R.; Zhu, Y.; Li, B.; Huang, C.L.; et al. A pneumonia outbreak associated with a new coronavirus of probable bat origin. *Nature* **2020**, *579*, 270–273. [CrossRef] [PubMed]
42. Glowacka, I.; Bertram, S.; Herzog, P.; Pfefferle, S.; Steffen, I.; Muench, M.O.; Simmons, G.; Hofmann, H.; Kuri, T.; Weber, F.; et al. Differential downregulation of ACE2 by the spike proteins of severe acute respiratory syndrome coronavirus and human coronavirus NL63. *J. Virol.* **2010**, *84*, 1198–1205. [CrossRef] [PubMed]
43. Gerdes, J.; Schwab, U.; Lemke, H.; Stein, H. Production of a mouse monoclonal antibody reactive with a human nuclear antigen associated with cell proliferation. *Int. J. Cancer* **1983**, *31*, 13–20. [CrossRef] [PubMed]
44. Ashkenazi, A.; Fairbrother, W.J.; Leverson, J.D.; Souers, A.J. From basic apoptosis discoveries to advanced selective BCL-2 family inhibitors. *Nat. Rev. Drug Discov.* **2017**, *16*, 273–284. [CrossRef] [PubMed]
45. Bodewes, R.; van Run, P.R.; Schürch, A.C.; Koopmans, M.P.; Osterhaus, A.D.; Baumgärtner, W.; Kuiken, T.; Smits, S.L. Virus characterization and discovery in formalin-fixed paraffin-embedded tissues. *J. Virol. Methods* **2015**, *214*, 54–59. [CrossRef]

46. Daly, J.L.; Simonetti, B.; Klein, K.; Chen, K.E.; Williamson, M.K.; Antón-Plágaro, C.; Shoemark, D.K.; Simón-Gracia, L.; Bauer, M.; Hollandi, R.; et al. Neuropilin-1 is a host factor for SARS-CoV-2 infection. *Science* **2020**, *370*, 861–865. [CrossRef] [PubMed]
47. Peng, R.; Wu, L.A.; Wang, Q.; Qi, J.; Gao, G.F. Cell entry by SARS-CoV-2. *Trends Biochem. Sci.* **2021**, *46*, 848–860. [CrossRef] [PubMed]
48. Murgolo, N.; Therien, A.G.; Howell, B.; Klein, D.; Koeplinger, K.; Lieberman, L.A.; Adam, G.C.; Flynn, J.; McKenna, P.; Swaminathan, G.; et al. SARS-CoV-2 tropism, entry, replication, and propagation: Considerations for drug discovery and development. *PLoS Pathog.* **2021**, *17*, e1009225. [CrossRef]

Paper III – Multi-tissue transcriptomic-informed in silico investigation of drugs for the treatment of dengue fever disease

viruses

MDPI

Article

Multi-Tissue Transcriptomic-Informed In Silico Investigation of Drugs for the Treatment of Dengue Fever Disease

Beatriz Sierra [1], Ana Cristina Magalhães [2,3,4], Daniel Soares [2,3], Bruno Cavadas [2,3], Ana B. Perez [1], Mayling Alvarez [1], Eglis Aguirre [1], Claudia Bracho [1], Luisa Pereira [2,3,*] and Maria G. Guzman [1]

[1] Virology Department, PAHO/WHO Collaborating Center for the Study of Dengue and its Vector, Pedro Kourí Institute of Tropical Medicine (IPK), Havana 11400, Cuba; siebet@ipk.sld.cu (B.S.); anab@ipk.sld.cu (A.B.P.); mayling@ipk.sld.cu (M.A.); eglis@ipk.sld.cu (E.A.); cbracho@ipk.sld.cu (C.B.); lupe@ipk.sld.cu (M.G.G.)
[2] i3S-Instituto de Investigação e Inovação em Saúde, Universidade do Porto, 4200-135 Porto, Portugal; acmagalhaes@ipatimup.pt (A.C.M.); danielcarpinteirosoares@gmail.com (D.S.); bcavadas@ipatimup.pt (B.C.)
[3] IPATIMUP—Instituto de Patologia e Imunologia Molecular, Universidade do Porto, 4200-135 Porto, Portugal
[4] ICBAS—Instituto de Ciências Biomédicas Abel Salazar, Universidade do Porto, 4050-313 Porto, Portugal
* Correspondence: luisap@ipatimup.pt; Tel.: +351-22-607-4900

Abstract: Transcriptomics, proteomics and pathogen-host interactomics data are being explored for the in silico–informed selection of drugs, prior to their functional evaluation. The effectiveness of this kind of strategy has been put to the test in the current COVID-19 pandemic, and it has been paying off, leading to a few drugs being rapidly repurposed as treatment against SARS-CoV-2 infection. Several neglected tropical diseases, for which treatment remains unavailable, would benefit from informed in silico investigations of drugs, as performed in this work for Dengue fever disease. We analyzed transcriptomic data in the key tissues of liver, spleen and blood profiles and verified that despite transcriptomic differences due to tissue specialization, the common mechanisms of action, "Adrenergic receptor antagonist", "ATPase inhibitor", "NF-kB pathway inhibitor" and "Serotonin receptor antagonist", were identified as druggable (e.g., oxprenolol, digoxin, auranofin and palonosetron, respectively) to oppose the effects of severe Dengue infection in these tissues. These are good candidates for future functional evaluation and clinical trials.

Keywords: Dengue fever disease; multi-tissue transcriptomics; in silico evaluation of drugs; tissue specialization; common mechanisms of action

check for updates

Citation: Sierra, B.; Magalhães, A.C.; Soares, D.; Cavadas, B.; Perez, A.B.; Alvarez, M.; Aguirre, E.; Bracho, C.; Pereira, L.; Guzman, M.G. Multi-Tissue Transcriptomic-Informed In Silico Investigation of Drugs for the Treatment of Dengue Fever Disease. *Viruses* **2021**, *13*, 1540. https://doi.org/10.3390/v13081540

Academic Editors: Oliver Planz, Stephan Ludwig and Stephan Pleschka

Received: 7 July 2021
Accepted: 31 July 2021
Published: 4 August 2021

Publisher's Note: MDPI stays neutral with regard to jurisdictional claims in published maps and institutional affiliations.

Copyright: © 2021 by the authors. Licensee MDPI, Basel, Switzerland. This article is an open access article distributed under the terms and conditions of the Creative Commons Attribution (CC BY) license (https://creativecommons.org/licenses/by/4.0/).

1. Introduction

Dengue virus (DENV) is an arbovirus (Flaviviridae family) with four genetically distinguishable serotypes (DENV-1 to DENV-4), whose rapid worldwide spread is a major health problem [1]. The virus is transmitted to humans through the bite of infected *Aedes aegypti* or *Aedes albopictus* mosquitoes [2]. It is estimated that Dengue has an incidence of 390 million infections per year, of which 96 million people manifest the disease clinically and more than 20,000 die [3], contributing to a total annual global burden of 8.9 billion dollars [4]. Increases in Dengue global incidence and geographical distribution are expected due to the rise of global temperature, the increase of worldwide travel and the rapid growth of densely populated zones [5].

After being infected by the virus, patients can either be asymptomatic (~75% of cases) or, after a 4–10 day incubation period, develop symptoms that range from those of a mild flu to more severe symptoms [1]. The milder form of the disease (Dengue Fever—DF) is characterized by a rapid onset of fever accompanied by severe headaches, myalgias, arthralgias and gastrointestinal discomfort that last 7–14 days, after which homeostasis is normally restored. The more severe cases (Dengue Haemorrhagic Fever—DHF) present coagulopathy, spontaneous bleeding, low to moderate liver injury and increased vascular fragility and permeability. DHF can eventually progress to an even more severe case

(Dengue Shock Syndrome—DSS), characterized by rapid fluid loss that leads to severe hypotension and haemorrhagic episodes, mainly bleeding in the skin and the gastrointestinal tract. DHF and DSS can sometimes lead to death. Several factors can contribute to this plasticity of phenotypes, namely the antibody-dependent enhancement (ADE) [6]. A patient infected for the first time with a DENV serotype becomes immunized against that serotype and usually develops DF in a milder form; if a secondary infection by another serotype occurs, the previously formed memory T-cells are activated, being ineffective in combatting the new serotype, and leading to the production of high concentrations of inflammatory cytokines (IFN-γ, TFN-α and IL-13) and a low concentration of anti-inflammatory ones (IL-10). Consequently, the patient usually develops more aggressive phenotypes (DHF or even DSS). Host genetic factors are also associated with susceptibility to DENV, including immune system factors such as HLA-I and HLA-II, TNF-α, Fc receptor, TAP and DC-SIGN (reviewed in [7]); immune system and endothelial homeostasis genes *MICB* and *PLCE1* [8]; genes controlling lipid (*OSBPL10* and *RXRA* [9]) and xenobiotic metabolism (*PLCB4*, *CHST10*, *AHRR*, *PPP2R5E* and *GRIP1* [10]). A metanalysis of several of these genes across worldwide populations [11] made it possible to infer a preliminary worldwide map of host susceptibility to Dengue disease: sub-Saharan Africans and descendants are best protected against severe forms; Europeans and close neighbours are best protected against DF but not against severe forms; Northeast and Southeast Asians are less protected against mild and severe forms.

Dengue disease symptoms reflect the various alterations occurring after infection in key organs like the liver, spleen and encephalon, and further studies are needed to fully elucidate the local mechanisms. The liver displays signs of auto-immune response, circulatory compromising, hypoxia and hypotension caused by vascular leakage, hepatomegaly and a rise of transaminase enzyme levels [12,13]. Sudden spleen ruptures have been reported in the early acute and convalescent phases, which can be fatal if not treated immediately through surgery [14]. A comparison of transcriptomic profiles between infected and control groups provides meaningful insights into the human and pathogen interactions in diverse tissues and may help in understanding the pathophysiology of the disease. Regarding Dengue, a few transcriptomic analyses have been conducted in Asian and South American populations for diverse phenotypes or phases of the disease, but all were in blood samples or in cancer cell lines and not in tissues from patients [15–20]. It would be very informative to analyze Dengue-affected tissues, since the transcriptome profiles differ with tissue/organ specialization.

No antiviral treatment is available against Dengue infection, and, essentially, infected patients receive treatment to minimize and manage the symptoms [21]: antipyretics are used to reduce pain and fever in mild cases; crystalloids are used to maintain intravascular volume, blood pressure and normal urine formation; and volume expanders are used for the restauration of intravascular volume, blood pressure and tissue perfusion in DHF and DSS. Treatment with immunomodulators, corticosteroids and other nonsteroidal anti-inflammatory drugs has shown no results and should be avoided [21]. Statins, a group of drugs known as HMG-CoA reductase inhibitors, which are administrated to patients with hyperlipidaemia, have been investigated in the Dengue context, given the lipid metabolism importance in viral infections and their effect on the endothelial function. Promising in vitro (reduced DENV virion assembly; [22]) and in vivo (increased survival rate and decreased DENV viremia in DENV-infected mice treated with Lovastatin; [23]) results were unfortunately not replicated in clinical trials [24,25]: statins were well tolerated by infected patients but provided no beneficial effects in reducing symptoms or viremia. Disappointingly, the Sanofi Pasteur vaccine, which had been introduced in some endemic countries, had its general use hampered by fatalities of children with severe Dengue in the Philippines [26].

Recent developments in mining big data are revolutionizing the development and repurposing of drugs [27], making it possible to narrow down candidate drugs to be tested, and leading to significant reductions in time and costs. Drug repurposing, the process of

finding new uses for approved pharmaceutical drugs or investigational compounds by relying on the biological targets shared between diseases and the pleiotropic actions of drugs, further simplifies the process. In fact, as these repurposed drugs have already been tested in humans, doses and side effects are known. The current COVID-19 pandemic testifies to the high impact of this type of approach [28]. CMap is an example of a mining tool for in silico drug discovery that was built on genetic expression profiles from tissues treated with many molecules [29]. The second phase of CMap, called L1000 [30], includes 1,319,138 profiles from 42,080 perturbagens, corresponding to 25,200 biological entities for a total of 473,647 signatures. Users can input information on up- and downregulated genes in a certain disease into the CMap tool and obtain the drugs related to that gene expression pattern via data mining and pattern searching algorithms. Successful examples of CMap use have been published in cancer research [31,32]. In Dengue [33], CMap analysis of blood transcriptomics was combined with other miners on blood-based proteomic and protein–protein interaction datasets, making it possible to infer eight candidate drugs: estradiol, etoposide, simvastatin, resveratrol, sirolimus, valproic acid, vorinostat and Y-27632 compound (kinase inhibitor).

In this work, we aimed to identify drugs that could be effective against Dengue disease by applying a multi-tissue transcriptomic-informed in silico investigation. First, we analyzed the transcriptome from liver (published data), spleen (our own data) and blood (published). We checked for significantly differentially expressed genes in the pairwise comparisons and evaluated which molecular pathways were significantly changed. Second, we evaluated through CMap which drugs could interfere with the expression profiles from each of the tissues in the Dengue context.

2. Materials and Methods

2.1. Biological Samples, Laboratorial Processing and Raw Data Analysis

Tissue samples from liver, spleen and encephalon were post-mortem collected from deceased Cuban individuals that died from Dengue (case cohort: IDs 875, 900, 37478, 39538 and 39539; cases 875 and 900 did not include encephalon sample) or traffic accidents (control cohort obtained at the Cuban Institute of Legal Medicine during routine autopsy examination: IDs F1, F2 and F4). Additional information on the individuals is included in Table S1. The study was approved 20 February 2018 by the Institutional Ethical Review Committee of the Institute of Tropical Medicine Pedro Kourí (IPK), with the number CEI-IPK 30-18, for studies with Arbovirus with medical importance in Cuba, 2017–2021, including Dengue fatal cases and controls. The consent for using tissue samples in this research was verbally provided by relatives of the deceased cases prior to the necropsy. This consent procedure was also included in the ethics approval. Tissue fragments sized 5×5 mm^3 (20–30 mg approximately) were collected and immersed in RNAlater at 4 °C overnight, then stored at −80 °C the following day. The frozen tissues from Dengue-deceased cases arrived at the IPK's National Reference Laboratory for Arbovirus 72 h after the patient's death, while the control cases arrived 24 h after death. For RNA isolation, tissues were disrupted using the Tissue Lyser II kit (QIAGEN), and RNA was extracted using a column-based method (RNeasyProtect Mini kit, Qiagen, Hilden, Germany). For the DENV detection in tissue samples, two methods were used: a conventional capsid and premembrane gene (C-prM) RT-PCR protocol for samples from 2014 [34] and the CDC Dengue multiplex real-time qRT-PCR assay (four serotypes) targeting the capsid (C) gene [35].

Gene expression evaluation was done by Next Generation Sequencing (NGS), using the Ion AmpliSeq Transcriptome Human Gene Expression Kit, Ion 550TM Chip kit and Ion S5TM XL System (Thermo Fisher Scientific, Waltham, MA, USA). This kit contains one amplicon per 20,812 protein-coding genes. The total raw reads allowed in the chip for each sample were around 10.8 million reads.

Raw fastq files were checked for quality control using FastQC software, by evaluating the overall sequence quality scores, the base sequence content, the sequence GC content and

the presence of duplicated or overrepresented sequences. Low-quality bases were further filtered by a sliding window (four nucleotides with a mean average below 15). A minimum length of 40 bases was set to decrease multi-mapping. Alignment was performed in Bowtie2 with the "local-sensitive" flag against the human hg19 reference. After alignment, reads were sorted and converted using samtools [36] and counted using HTSeq, exclusively for the amplified regions.

2.2. Published Datasets

Two microarray-based transcriptomic datasets from Dengue-infected patients and healthy controls were retrieved from the Gene Expression Omnibus (GEO) database [37], identified by IDs GSE18090 [15] and GSE51808 [19]. GSE18090 contained data from Peripheral Blood Mononuclear Cells (PBMCs) collected from Brazilian adults, while GSE51808 referred to whole blood samples from Thai children and adults. The arrays used for GSE18090 and GSE51808 were Affymetrix Human Genome U133 Plus 2.0 and Affymetrix HT HG-U133+ PM Array Plate, respectively. Samples included in the analysis belonged to DHF patient and healthy control groups; convalescent individuals (only in the GSE51808 dataset) and DF (milder form) were excluded from analysis. Outlier samples in both datasets were removed after principal component analysis (PCA; three samples for GSE18090 and two samples for GSE51808). Final numbers of individuals were seven controls and eight DHF for GSE18090 and nine controls and eight DHF for GSE51808. As the microarrays have multiple probes per gene, data were filtered in R with the "genefilter" package featureFilter function (which keeps the probe with the highest expression variance for each gene).

A publicly available viscRNA-Seq dataset (virus-including single cell RNA-seq) [38], referring to the transcriptome of individual human hepatoma (Huh7) cells infected by DENV, was downloaded from GEO (ID: GSE110496). The two groups considered for analyses were non-infected (after quality control, 67 single cells were considered) and infected at an MOI (multiplicity of infection) of 10 and collected after 48 h of infection (75 single cells included).

2.3. Differential Expression Evaluation and Gene Set Enrichment Analysis

For the AmpliSeq dataset, differential expression analysis between the infected and controls was carried for each tissue individually, using the DESeq2 R package [39]. DESeq2 applies a negative binomial distribution to model gene counts and test for differential expression.

Gene expression profiles from the microarray datasets were normalized through the Robust Multi-array Average (RMA) algorithm using the R oligo package. To increase sensitivity, low-intensity probes were removed from the normalized probe intensity values. Probes were then collapsed to the genes for gene differential expression (DE) analysis, using functions from the limma package [40].

Raw single cell counts were analyzed by the SingleCellExperiment R package. The data were filtered using the following parameters: gene present in >3 cells, cell with >4000 genes, total number of counts above 1×10^5, and percent of mitochondrial genes <10%. After filtering, counts were log normalized, and a tSNE was performed with a perplexity of 10 for the identification and removal of visual outliers. Raw counts from single cells that passed these filters were loaded into DESeq2 [39] and processed as for the Ampliseq dataset.

An adjusted p-value < 0.05 was used for attributing a differentially expressed gene status. Enrichment analysis was done using GSEA [41] for Gene Ontology (CC, BP and MF) and KEGG pathway databases. The pre-ranking option was used, taking into account an ordered list of genes for the differential expression. Volcano plots for the expression profiles were created using the R packages "ggplot2" and "ggrepel". Venn diagrams with common upregulated and downregulated genes between datasets were generated in "VennDiagram" R package.

2.4. Drug Repurposing

For the drug repurposing step, the CMap Query tool from clue.io (https://clue.io/query; accessed on 27 January 2021) was used. For the blood information, the first 150 (this number is a limitation from the tool) genes that were significantly up- and down-regulated (false discovery rate, FDR values) between patients and controls, in at least one dataset, were uploaded in an ordered way according to the highest absolute mean fold change value across the two datasets. In the case of the AmpliSeq and Huh7 single cell data, query analyses were made independently for each tissue, inputting the 150 upregulated and downregulated genes ranked by the lowest *p*-values (even if they were not statistically significant).

We queried the CMap Touchstone dataset containing perturbation data for 2837 compounds tested in nine human cell lines: A375 (malignant melanoma), A549 (non-small cell lung carcinoma), HCC515 (non-small cell lung adenocarcinoma), HEPG2 (hepatocellular carcinoma cell line), MCF7 (breast adenocarcinoma), PC3 (prostate adenocarcinoma), VCAP (metastatic prostate cancer), HT29 (colorectal adenocarcinoma), and HA1E (kidney epithelial immortalized). The CMap query output consists of a list of perturbagens rank-ordered by the similarity of differentially expressed gene sets to the query gene set. These results come in the form of a connectivity map score, tau (τ), ranging from -100 to 100, which compares the observed enrichment score seen in the inputted data with all others in the reference database. τ applies a weighted connectivity score based on the weighted Kolmogorov–Smirnov enrichment statistic, normalized across cell types and perturbations. A τ of 90 indicates that only 10% of reference perturbations showed stronger connectivity to that query. A positive score indicates there is similarity between a given perturbagen's signature and that of the query, while a negative score indicates that the two signatures are opposing. Thus, we considered scores of below -90 as drugs that could potentially treat Dengue disease. The drugs are complemented with information for their molecular mechanism of action. We then classified these drugs into seven main groups of actions: antineoplastic, antibiotic, antiparasitic, immunosuppressant, cardiovascular, anti-inflammatory, antiviral and other. This classification was based on information contained in several databases: Inxight: Drugs (https://drugs.ncats.io/; accessed on 27 January 2021); PubChem [42]; Drugbank [43]; FDA (https://www.fda.gov/; accessed on 27 January 2021); EMA (https://www.ema.europa.eu/en; accessed on 27 January 2021); ClinicalTrials (https://clinicaltrials.gov/; accessed on 27 January 2021). Some molecular mechanisms of action can be affiliated to more than one main group of action. The bar plots created for demonstrating the distribution of drugs among different groups of action were created using the "ggplot2" package from R.

3. Results

3.1. Expression Profiles in the Liver, Spleen and Encephalon Dengue Cohorts

The AmpliSeq characterization of the extracted RNA from the tissues aimed at approximately 10 million reads per sample, but the initial amount of reads obtained was lower, varying between 1,410,487 and 9,239,028, with a mean of 5,412,203. There was no effect of the tissue analyzed, as the mean of initial reads was similar between tissues: 5,987,967 in spleen, 5,136,132 in encephalon and 5,077,912 in liver. An initial quality control, based on the distribution of GC content, showed that the available tissue samples (liver and spleen) from cases 900 and 875 did not follow the theoretical unimodal distribution, presenting bimodal distributions. Since bimodal distributions are a common indicator of some form of contamination, these samples were removed from further analyses.

To evaluate if the clustering of samples mirrored the tissue of origin, a PCA was conducted (Supplementary Figure S1). Spleen samples were clustered, with some differentiation between infected and control samples, but encephalon and liver samples presented a high variance, with no clustering with infection status. The time elapsing between death and collection of tissue may have interfered with the RNA quality in encephalon and liver, which are known to degrade fast [44]. We conducted a bibliographic search in order to

check whether there were transcriptome datasets that had been published that could be compared with/replace our tissue data for encephalon and liver, and verified that a recent study was available only for a liver cell line infected by DENV [38]. We decided to proceed with the analysis of our tissue data for spleen, replace the tissue data for liver with the data available from the in vitro infection of the liver cell line, and remove encephalon from the analysis.

The differential expression analyses revealed the following values of significantly upregulated and downregulated genes (Supplementary Figure S2; Supplementary Tables S2 and S3): 23 and 89 in spleen and 1069 and 1319 in the liver single cell dataset. A careful survey of the top differentially expressed genes and pathways in the two tissues indicated signals that make sense in the context of infection, supporting the reliability of the results obtained here.

The spleen tissue of the infected patients showed upregulation of the *AVPR2* gene (vasopressin receptor), which increases retention of water by increasing cyclic AMP [45], and the *TYRO3* gene, which activates the AKT survival pathway and mediates the clearance of apoptotic cells [46]. Pathway enrichment analysis for the spleen tissue (Figure 1A; Supplementary Figures S3–S5) revealed a downregulation of immune components related with the phosphorylation of the STAT protein, type I interferon, autophagy and RIG-I-like receptor signaling pathway; the latter is a target of DENV that regulates RIG-I-directed IFN induction to successfully replicate and spread [47]. Dimerization of STATs is essential for the establishment of classical JAK-STAT signaling pathways, which have an important role in the control of immune responses. A downregulation of signaling pathways related to the response to angiotensin was also detected. On the other hand, the upregulation of insulin and cholesterol metabolic pathways could also be distinguished.

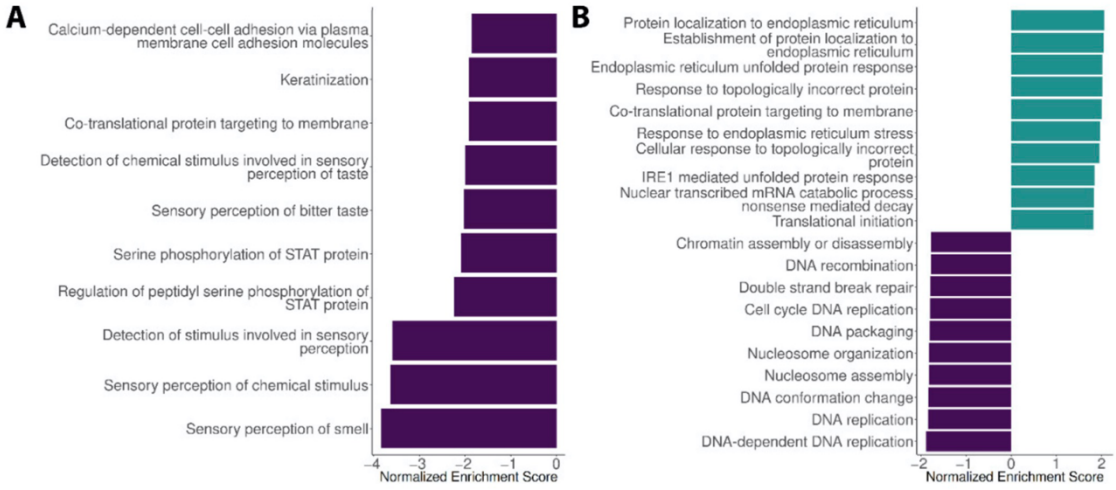


Figure 1. Top 20 Gene Ontology Biological Process (GO-BP) pathways in the (**A**) spleen and (**B**) liver cells (cut-off values: nominal *p*-value < 0.05 and FDR < 0.25). Positive normalized enrichment score (NES; in purple) represents upregulated pathways in the infected individuals versus controls, while negative NES values (in green) represent downregulated pathways in the infected individuals versus controls.

In the liver cells, we noticed an upregulation of *ATF3*, a activating transcription factor 3, which is a suppressor of pro-inflammatory responses [48] and has been considered a hub of the cellular adaptative response [49]. Other transcription factors responsible for the pro-inflammatory response, such as *TNFRSF9* and *MXD1*, were also found upregulated. Pathway enrichment analysis in the liver cells (Figure 1B; Supplementary Figures S3–S5) showed a downregulation of cell cycle pathways, an observation previously made [38]. Hepatic manifestations may be the result of cell cycle arrest, which through the inhibition

of cell death may allow immune evasion and/or help promote viral assembly. In the literature, it has been shown that HepG2 (liver) cells were significantly more permissive for both infection and virus production in the G(2) phase than Vero (kidney) cells [50].

3.2. Expression Profiles in the Blood Dengue Cohorts

The blood Dengue cohorts showed a strong partition in gene expression between the infected and control clusters (Supplementary Figure S6). Several genes were differentially expressed (Supplementary Figure S7; full information provided in Supplementary Tables S4 and S5), especially in the GSE51808 dataset from whole blood (9230 differentially expressed genes), in contrast with GSE18090 from PBMCs only (311). The heterogeneity in the original blood cells could explain the discrepancy between datasets. When applying Venn diagrams to the upregulated and the downregulated sets of these genes (Supplementary Figure S8), 208 upregulated and 54 downregulated genes were shared between datasets. To investigate which type of pathways were upregulated and downregulated, gene set enrichment analysis was conducted in each dataset. Figure 2 represents the top-20 significantly enriched pathways, when using the database KEGG (results with GO database significantly enriched pathways are reported in Supplementary Figures S9–S11). As can be observed in the figure, the infected group displayed downregulation of biological pathways related with the immune system and response to pathogens, and upregulation in biological pathways related with cell cycle and repair mechanisms, an observation previously made for PBMC samples in Nicaraguan children [17].

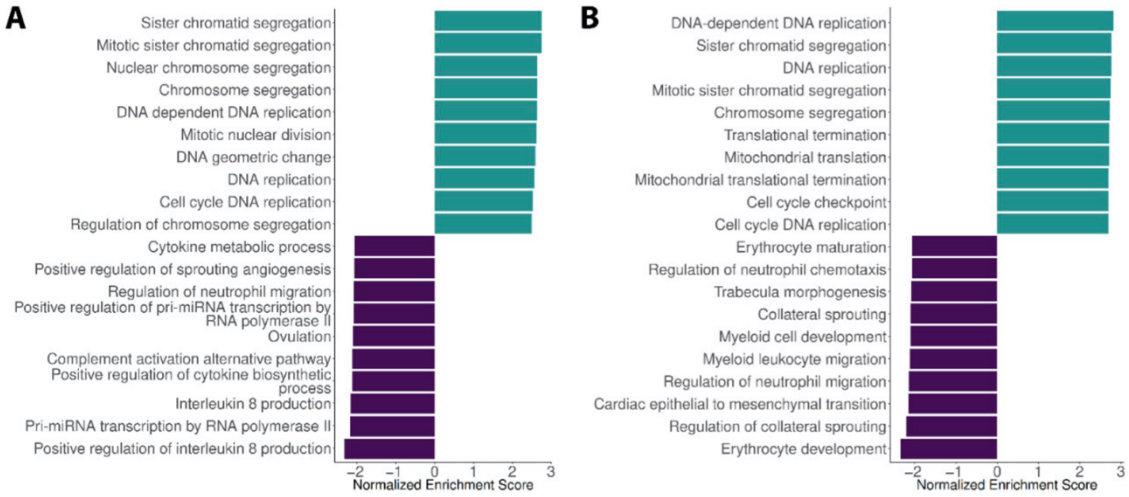


Figure 2. Top 20 Gene Ontology Biological Process (GO-BP) in the two blood datasets: (**A**) GSE18090 and (**B**) GSE51808 pathways (cut-off values: nominal p-value < 0.05 and FDR < 0.25). Positive NES (in purple) represents upregulated pathways in the infected individuals versus controls, while negative NES values (in green) represent downregulated pathways in the infected individuals versus controls.

3.3. Drug Repurposing

The CMap tool results for the drug discovery in the blood cohort indicated a total of 203 known compounds that were inferred (CMap score inferior to −90) as having a potential impact in Dengue hemorrhagic fever treatment (Supplementary Table S6). These drugs were spread across seven main different mechanisms of action: antineoplastic (120), antibiotic (11), antiparasitic (2), immunosuppressant (6), cardiovascular (11), anti-inflammatory (9) and antiviral drugs (7). Among these, some compounds have already been shown to have some action against DENV or the mechanism of action taken by flavivirus. Some examples are the purvalanol A and palbociclib, both cyclin-dependent

kinase inhibitors, which have shown anti-flavivirus activity [51]. Mycophenolic acid, a drug currently used as an immunosuppressive agent, has been shown to inhibit flavivirus infection by preventing synthesis and accumulation of viral RNA [52].

When analyzing the CMap results for all tissues included in this work (Figure 3; Supplementary Tables S7 and S8), we observed a similar pattern as the one identified in the blood, with some variations between tissues. Forskolin, an antihypertensive agent and a platelet aggregation inhibitor with an anti-viral effect against HIV [53], also detected in the liver, was the only drug observed in more than one tissue. Norethindrone is used as a contraceptive, and it might confer some protection against Dengue, since pregnant women have an increased risk of developing severe Dengue infections [54]. In the liver, atorvastatin (statin), dexamethasone (corticosteroids) and prostaglandin A1 (anti-viral) has shown effects on cholesterol metabolism, immune response, and viral replication, respectively. In the spleen, geldanamycin, an inhibitor of Hsp90, which has a role in viral replication, has shown some effect in the reduction of Dengue viral infection [55].

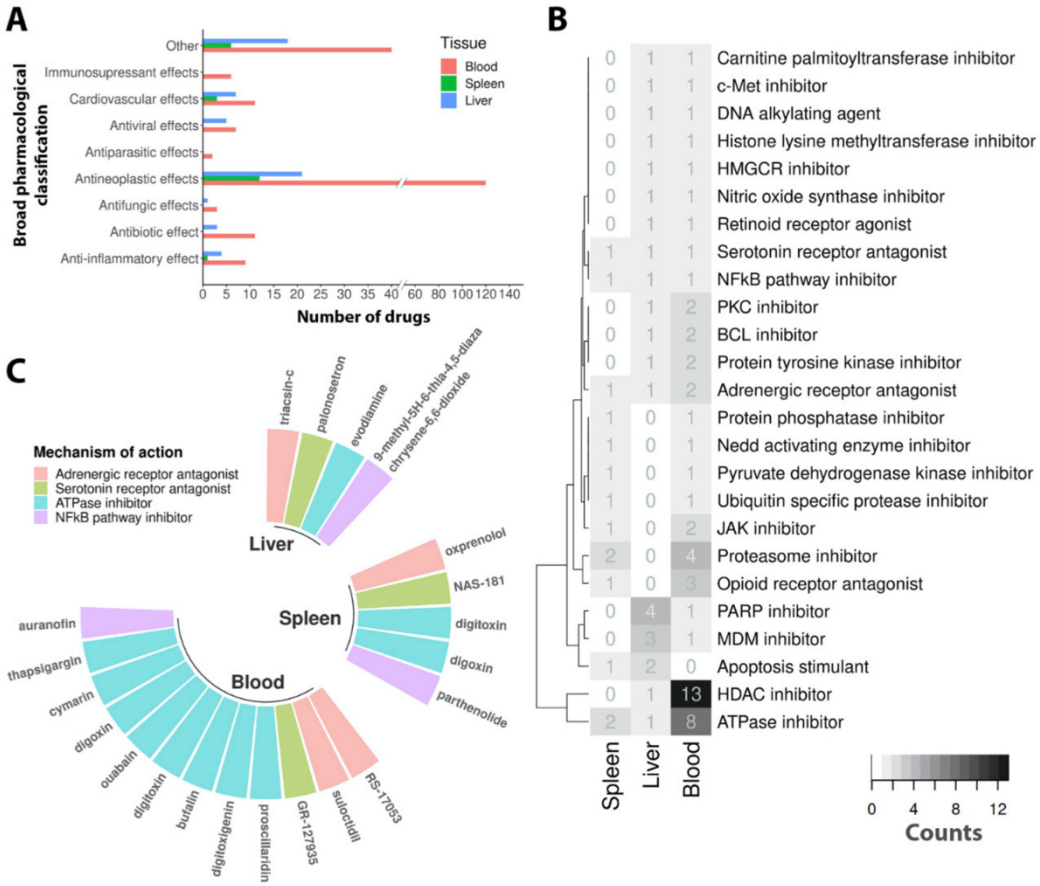


Figure 3. CMap-identified compounds (score equal to or below −90) that potentially impact Dengue haemorrhagic fever treatment, according to their mechanism of action in the blood, spleen and liver. (**A**) Bar plot of the distribution of drugs by broad pharmacological classification; (**B**) heatmap of drugs per mechanism identified in one or more tissues; (**C**) circus plot of common mechanisms of action.

Given the high stochasticity in identifying a drug from a connectivity map including 1,000,000 profiles, we instead based the comparison between tissues on the CMap molecular mechanism of action. Four mechanisms of action were found to be common to all tissues:

"Adrenergic receptor antagonist", "ATPase inhibitor", "NF-kB pathway inhibitor" and "Serotonin receptor antagonist".

4. Discussion

The gene expression profiles that have been perturbed pharmacologically and have been obtained in vitro, such as the second phase of CMap, known as L1000 [30], are beginning to shed light on gene function and on understanding the molecular basis of diseases [56]. A first attempt was conducted on blood expression profiles of Dengue patients against CMap [33], but a broader picture for other affected tissues was needed and seemed a good aim to pursue in this work. A first step consisted of obtaining post mortem human tissue samples for studying the patterns of gene expression underlying tissue specificity, as sampling many tissues from living individuals would be impossible. However, a drawback of the post mortem human tissue samples is the significant reduction of RNA, which degrades quickly upon death [57]. As we saw in this work, despite the careful steps we took in collecting the samples as soon as possible after autopsies, degradation affected the liver and encephalon tissues, leading us to exclude the transcriptomic data for these tissues.

By referring to our own transcriptomic dataset on the spleen and complementing with published datasets for the blood and liver of Dengue patients, we identified some heterogeneity in molecular pathways between tissues. The dissimilarity in the results reflecting tissue specificity could initially indicate that a cocktail-based treatment would be more suitable to address this diversity. However, given the high connectivity between molecular networks in the body, and the multi-effects of drugs, some candidate drugs can be effective in the various tissues for Dengue disease. Notably, drugs sharing the mechanism of actions in the "NF-kB pathway inhibitor", "ATPase inhibitor", "Adrenergic receptor antagonist" and "Serotonin receptor antagonist" seem to be promising candidates in Dengue treatment, and some previous pin-point functional tests have contributed evidence supporting the antiviral action of some of these mechanisms. By pharmacologically inhibiting NF-kB activation, Cheng et al. [58] observed that the potential role of NF-kB in oxidative signaling is prevented during Dengue infection through the abolishment of iNOS/NO biosynthesis and TNF-α production. Interestingly, the NF-kB pathway inhibitor compounds identified in this work, auranofin and parthenolide, have previously been shown to successfully inhibit flavivirus infection [59,60]. ATPase inhibitors, such as evodiamine, digoxin and digitoxin, also present strong anti-inflammatory responses. Evodiamine inhibits nitric oxide production by interfering with the interferon-gamma and inhibiting the action of NF-kB signal events [61]. The impact of evodiamine in the inhibition of viral replication, much like digitoxin, is still limited to influenza A [62,63]. Digitoxin administration to influenza A virus (IAV)–infected cotton rats has been shown to lower pro-inflammatory cytokine levels of TNFα, GRO/KC, MIP2, MCP1, and IFN-γ in lungs, commonly associated with cytokine storm [63]. Since high levels of inflammatory cytokines are observed in severe Dengue infection, digitoxin might have a therapeutic potential. Besides digitoxin, digoxin, another cardiac glycoside, displays antiviral effects against Zika virus [59]. Other authors [64] have identified a group of small molecules that inhibit infection with Dengue and other flaviviruses, and interestingly those molecules were similar in structure to tricyclic antipsychotic compounds, which act as antagonists of serotonin and dopamine receptors. Further knockdown of dopamine receptor D4 reduced DENV replication via inhibition of epidermal growth factor receptor (EGFR)–related kinase (ERK) phosphorylation. Although the involvement of receptors that are mainly located in neurons seems unexpected, it has been shown that dopamine receptors are expressed on rodent and human macrophages, a primary target cell of DENV infection. These macrophage-related dopamine receptors may be the ones being influenced by DENV.

Other mechanisms seem promising druggable targets in certain tissues. This is the case for the inhibition of histone deacetylases (HDAC) in blood, as this class of enzymes is essential in normal hematopoiesis, namely in the cell differentiation and proliferation [65]. The HDAC inhibitor valproic acid has been previously shown to downregulate cytokine

expression on Dengue-infected macrophages [66]; the CMap tool identified this drug both in our results and in another data mining work [33]. The signal we detected in spleen and blood for the proteasome inhibition was previously demonstrated functionally [67] in human monocytic cells and in mice infected with DENV; the drug acting in this mechanism inhibited infectious DENV production in primary monocytes and the spread of DENV in the spleen. Poly (ADR-ribose) polymerase (PARP) seems to be a key mediator of liver inflammation and fibrosis [68], suggesting the possible process by which a PARP inhibitor would be effective in controlling DENV in the liver, as identified here.

At first instance, there were not many indications of lipid-related drugs in the CMap results. This may be because of the late stage of the disease analyzed in this work, while lipids may be more important in the first stages of entrance of the virus into the cells and in their replication in the acute phase [9]. Even so, a "LXR agonist" mechanism was identified in the spleen, and statins (atorvastatin and simvastatin, respectively) were highlighted in the liver and blood. These results call for a continuation of trials with statins (bigger sample sizes; different concentrations of intake; different times of intake), as the few clinical trials already performed [24,25] showed that treatment or continuation of statin intake has no negative effects on Dengue patients.

The development of a new drug takes several years before it can become accessible for treatment of patients or prophylactic protection. On the other hand, repurposed drugs can skip several steps in the process of approval and commercialization, as safety, toxicity and risk assessment tests have already been conducted in human clinical trials. This second class of drugs can be highly valuable for a faster battle against Dengue disease and its complications, decreasing the pressure due to the increasing incidence of DENV infection and its rapid spread across the world.

5. Conclusions

Our results showed that despite some tissue heterogeneity in the response to DENV, drugs acting on "Adrenergic receptor antagonist", "ATPase inhibitor", "NF-kB pathway inhibitor" and "Serotonin receptor antagonist" mechanisms would be effective across tissues. Some of these candidate drugs have been pinpointedly described in the literature to have an impact against DENV or other viruses affiliated with the flavivirus family. Our work advances considerably the knowledge in this area by demonstrating that these four molecular mechanisms can be pharmaceutically modulated across the tissues most affected by Dengue disease.

Supplementary Materials: The following are available online at https://www.mdpi.com/article/10.3390/v13081540/s1, Table S1: Additional information on the individuals from whom samples were collected for transcriptomics; Figure S1: PCA plot (PC1 explaining 81.4% of variation vs. PC2 explaining 6.2% of variation) of the human transcriptomic profile of the spleen, liver and encephalon tissues; Figure S2: Volcano plots for the gene differential expression in the (A) spleen and (B) liver cell datasets; Table S2: Differentially expressed genes between infected and control cohorts for the spleen tissue samples (adjusted p-value < 0.05); Table S3: Differentially expressed genes between infected and control cohorts for the liver single cell dataset (adjusted p-value < 0.05); Figure S3: Top 20 Gene Ontology Cellular Component (GO-CC) pathways in the (A) spleen and (B) liver cells; Figure S4: Top 20 Gene Ontology Molecular Function (GO-MF) pathways in the (A) spleen and (B) liver cells; Figure S5: Top 20 significantly enriched KEGG pathways in the (A) spleen and (B) liver cells; Figure S6: Dendrograms for the gene expression profiles in the two blood datasets: (A) GSE18090 and (B) GSE51808; Figure S7: Volcano plots for the gene differential expression in the two blood datasets: (A) GSE18090 and (B) GSE51808; Table S4: Differentially expressed genes between infected and control cohorts for the GSE18090 dataset (adjusted p-value < 0.05); Table S5: Differentially expressed genes between infected and control cohorts for the GSE51808 dataset (adjusted p-value < 0.05); Figure S8: Venn diagrams of the upregulated (A) and downregulated (B) genes in the two blood datasets; Figure S9: Top 20 Gene Ontology Cellular Component (GO-CC) pathways in the (A) GSE18090 and (B) GSE51808; Figure S10: Top 20 Gene Ontology Molecular Function (GO-MF) pathways in the (A) GSE18090 and (B) GSE51808; Figure S11: Top 20 significantly enriched KEGG pathways in the

(A) GSE18090 and (B) GSE51808; Table S6: CMap results for the blood microarray data; Table S7: CMap results for the spleen tissue data; Table S8: CMap results for the liver cell data.

Author Contributions: All authors declare that everyone contributed adequately to the experimental procedures and writing of the manuscript. Conceptualization, B.S., L.P. and M.G.G.; methodology, B.S., A.C.M., D.S., B.C., A.B.P., M.A., E.A. and C.B.; formal analysis, A.C.M., B.C., D.S. and L.P.; writing, B.S., A.C.M., B.C. and L.P. All authors have read and agreed to the published version of the manuscript.

Funding: Funding was provided by FEDER, Fundo Europeu de Desenvolvimento Regional funds, through the COMPETE 2020, Competitiveness and Internationalization Operational Programme (POCI), Portugal 2020, and by Portuguese funds through FCT/Ministério da Ciência, Tecnologia e Inovação, in the framework of the project "Institute for Research and Innovation in Health Sciences" (POCI-01-0145-FEDER-007274).

Institutional Review Board Statement: The study was approved by the Institutional Ethical Review Committee of the Institute of Tropical Medicine Pedro Kourí (IPK), with the number CEI-IPK 30-18, for studies with Arbovirus.

Informed Consent Statement: The consent for using tissue samples in this research was verbally provided by relatives of the deceased cases prior to the necropsy. This consent procedure was also included in the ethics approval.

Data Availability Statement: Raw data are publicly available at the European Nucleotide Archive (ENA), with Accession Number PRJEB46564.

Acknowledgments: We thank the families of the deceased individuals who gave consent for their post-mortem material to be included in this research work.

Conflicts of Interest: The authors declare no conflict of interest. The funders had no role in the design of the study; in the collection, analyses, or interpretation of data; in the writing of the manuscript, or in the decision to publish the results.

References

1. Guzman, M.G.; Gubler, D.J.; Izquierdo, A.; Martinez, E.; Halstead, S.B. Dengue infection. *Nat. Rev. Dis. Primers* **2016**, *2*, 16055. [CrossRef] [PubMed]
2. Mayer, S.V.; Tesh, R.B.; Vasilakis, N. The emergence of arthropod-borne viral diseases: A global prospective on dengue, chikungunya and zika fevers. *Acta Trop.* **2017**, *166*, 155–163. [CrossRef] [PubMed]
3. Bhatt, S.; Gething, P.W.; Brady, O.J.; Messina, J.P.; Farlow, A.W.; Moyes, C.L.; Drake, J.M.; Brownstein, J.S.; Hoen, A.G.; Sankoh, O.; et al. The global distribution and burden of dengue. *Nature* **2013**, *496*, 504–507. [CrossRef] [PubMed]
4. Shepard, D.S.; Undurraga, E.A.; Halasa, Y.A.; Stanaway, J.D. The global economic burden of dengue: A systematic analysis. *Lancet Infect. Dis.* **2016**, *16*, 935–941. [CrossRef]
5. Kraemer, M.U.; Sinka, M.E.; Duda, K.A.; Mylne, A.Q.; Shearer, F.M.; Barker, C.M.; Moore, C.G.; Carvalho, R.G.; Coelho, G.E.; Van Bortel, W.; et al. The global distribution of the arbovirus vectors Aedes aegypti and Ae. albopictus. *Elife* **2015**, *4*, e08347. [CrossRef] [PubMed]
6. Halstead, S.B.; Mahalingam, S.; Marovich, M.A.; Ubol, S.; Mosser, D.M. Intrinsic antibody-dependent enhancement of microbial infection in macrophages: Disease regulation by immune complexes. *Lancet Infect. Dis.* **2010**, *10*, 712–722. [CrossRef]
7. Oliveira, M.; Ferreira, J.; Fernandes, V.; Sakuntabhai, A.; Pereira, L. Host ancestry and dengue fever: From mapping of candidate genes to prediction of worldwide genetic risk. *Future Virol.* **2018**, *13*, 647–655. [CrossRef]
8. Khor, C.C.; Chau, T.N.; Pang, J.; Davila, S.; Long, H.T.; Ong, R.T.; Dunstan, S.J.; Wills, B.; Farrar, J.; Van Tram, T.; et al. Genome-wide association study identifies susceptibility loci for dengue shock syndrome at MICB and PLCE1. *Nat. Genet.* **2011**, *43*, 1139–1141. [CrossRef] [PubMed]
9. Sierra, B.; Triska, P.; Soares, P.; Garcia, G.; Perez, A.B.; Aguirre, E.; Oliveira, M. OSBPL10, RXRA and lipid metabolism confer African-ancestry protection against dengue haemorrhagic fever in admixed Cubans. *PLoS Pathog.* **2017**, *13*, e1006220. [CrossRef] [PubMed]
10. Oliveira, M.; Lert-Itthiporn, W.; Cavadas, B.; Fernandes, V.; Chuansumrit, A.; Anunciação, O.; Casademont, I.; Koeth, F.; Penova, M.; Tangnararatchakit, K.; et al. Joint ancestry and association test indicate two distinct pathogenic pathways involved in classical dengue fever and dengue shock syndrome. *PLoS Negl. Trop. Dis.* **2018**, *12*, e0006202. [CrossRef]
11. Oliveira, M.; Saraiva, D.P.; Cavadas, B.; Fernandes, V.; Pedro, N.; Casademont, I.; Koeth, F.; Alshamali, F.; Harich, N.; Cherni, L.; et al. Population genetics-informed meta-analysis in seven genes associated with risk to dengue fever disease. *Infect. Genet. Evol.* **2018**, *62*, 60–72. [CrossRef] [PubMed]

12. Trung, D.T.; Thao, L.T.T.; Hien, T.T.; Hung, N.T.; Vinh, N.N.; Hien, P.T.; Chinh, N.T.; Simmons, C.; Wills, B. Liver involvement associated with dengue infection in adults in Vietnam. *Am. J. Trop. Med. Hyg.* **2010**, *83*, 774–780. [CrossRef] [PubMed]
13. Samanta, J.; Sharma, V. Dengue and its effects on liver. *World J. Clin. Cases* **2015**, *3*, 125–131. [CrossRef]
14. de Silva, W.T.; Gunasekera, M. Spontaneous splenic rupture during the recovery phase of dengue fever. *BMC Res. Notes* **2015**, *8*, 286. [CrossRef] [PubMed]
15. Nascimento, E.J.; Braga-Neto, U.; Calzavara-Silva, C.E.; Gomes, A.L.; Abath, F.G.; Brito, C.A.; Cordeiro, M.T.; Silva, A.M.; Magalhães, C.; Andrade, R.; et al. Gene expression profiling during early acute febrile stage of dengue infection can predict the disease outcome. *PLoS ONE* **2009**, *4*, e7892. [CrossRef]
16. Loke, P.; Hammond, S.N.; Leung, J.M.; Kim, C.C.; Batra, S.; Rocha, C.; Balmaseda, A.; Harris, E. Gene expression patterns of dengue virus-infected children from nicaragua reveal a distinct signature of increased metabolism. *PLoS Negl. Trop. Dis.* **2010**, *4*, e710. [CrossRef] [PubMed]
17. Popper, S.J.; Gordon, A.; Liu, M.; Balmaseda, A.; Harris, E.; Relman, D.A. Temporal dynamics of the transcriptional response to dengue virus infection in Nicaraguan children. *PLoS Negl. Trop. Dis.* **2012**, *6*, e1966. [CrossRef] [PubMed]
18. Sessions, O.M.; Tan, Y.; Goh, K.C.; Liu, Y.; Tan, P.; Rozen, S.; Ooi, E.E. Host cell transcriptome profile during wild-type and attenuated dengue virus infection. *PLoS Negl. Trop. Dis.* **2013**, *7*, e2107. [CrossRef]
19. Kwissa, M.; Nakaya, H.I.; Onlamoon, N.; Wrammert, J.; Villinger, F.; Perng, G.C.; Yoksan, S.; Pattanapanyasat, K.; Chokephaibulkit, K.; Ahmed, R.; et al. Dengue virus infection induces expansion of a CD14(+)CD16(+) monocyte population that stimulates plasmablast differentiation. *Cell Host Microbe* **2014**, *16*, 115–127. [CrossRef] [PubMed]
20. Long, H.T.; Hibberd, M.L.; Hien, T.T.; Dung, N.M.; Van Ngoc, T.; Farrar, J.; Wills, B.; Simmons, C.P. Patterns of gene transcript abundance in the blood of children with severe or uncomplicated dengue highlight differences in disease evolution and host response to dengue virus infection. *J. Infect. Dis.* **2009**, *199*, 537–546. [CrossRef]
21. Rajapakse, S.; Rodrigo, C.; Rajapakse, A. Treatment of dengue fever. *Infect Drug Resist.* **2012**, *5*, 103–112. [CrossRef] [PubMed]
22. Martínez-Gutierrez, M.; Castellanos, J.E.; Gallego-Gómez, J.C. Statins reduce dengue virus production via decreased virion assembly. *Intervirology* **2011**, *54*, 202–216. [CrossRef]
23. Martinez-Gutierrez, M.; Correa-Londoño, L.A.; Castellanos, J.E.; Gallego-Gómez, J.C.; Osorio, J.E. Lovastatin delays infection and increases survival rates in AG129 mice infected with dengue virus serotype 2. *PLoS ONE* **2014**, *9*, e87412. [CrossRef]
24. Whitehorn, J.; Nguyen, C.V.V.; Khanh, L.P.; Kien, D.T.H.; Quyen, N.T.H.; Tran, N.T.T.; Hang, N.T.; Truong, N.T.; Hue Tai, L.T.; Cam Huong, N.T.; et al. Lovastatin for the Treatment of Adult Patients With Dengue: A Randomized, Double-Blind, Placebo-Controlled Trial. *Clin. Infect. Dis.* **2016**, *62*, 468–476. [CrossRef] [PubMed]
25. Chia, P.Y.; Htun, H.L.; Ling, W.P.; Leo, Y.S.; Yeo, T.W.; Lye, D.C.B. Hyperlipidemia, statin use and dengue severity. *Sci. Rep.* **2018**, *8*, 17147. [CrossRef]
26. Wilder-Smith, A.; Flasche, S.; Smith, P.G. Vaccine-attributable severe dengue in the Philippines. *Lancet* **2019**, *394*, 2151–2152. [CrossRef]
27. Loging, W.; Harland, L.; Williams-Jones, B. High-throughput electronic biology: Mining information for drug discovery. *Nat. Rev. Drug. Discov.* **2007**, *6*, 220–230. [CrossRef]
28. Gordon, D.E.; Hiatt, J.; Bouhaddou, M.; Rezelj, V.V.; Ulferts, S.; Braberg, H.; Jureka, A.S.; Obernier, K.; Guo, J.Z.; Batra, J.; et al. Comparative host-coronavirus protein interaction networks reveal pan-viral disease mechanisms. *Science* **2020**, *370*, 6521. [CrossRef]
29. Lamb, J.; Crawford, E.D.; Peck, D.; Modell, J.W.; Blat, I.C.; Wrobel, M.J.; Lerner, J.; Brunet, J.P.; Subramanian, A.; Ross, K.N.; et al. The Connectivity Map: Using gene-expression signatures to connect small molecules, genes, and disease. *Science* **2006**, *313*, 1929–1935. [CrossRef]
30. Subramanian, A.; Narayan, R.; Corsello, S.M.; Peck, D.D.; Natoli, T.E.; Lu, X.; Gould, J.; Davis, J.F.; Tubelli, A.A.; Asiedu, J.K.; et al. A Next Generation Connectivity Map: L1000 Platform and the First 1,000,000 Profiles. *Cell* **2017**, *171*, 1437–1452.e1417. [CrossRef]
31. Agren, R.; Mardinoglu, A.; Asplund, A.; Kampf, C.; Uhlen, M.; Nielsen, J. Identification of anticancer drugs for hepatocellular carcinoma through personalized genome-scale metabolic modeling. *Mol. Syst. Biol.* **2014**, *10*, 721. [CrossRef]
32. Uhlen, M.; Zhang, C.; Lee, S.; Sjöstedt, E.; Fagerberg, L.; Bidkhori, G.; Benfeitas, R.; Arif, M.; Liu, Z.; Edfors, F.; et al. A pathology atlas of the human cancer transcriptome. *Science* **2017**, *357*, 6352. [CrossRef]
33. Amemiya, T.; Gromiha, M.M.; Horimoto, K.; Fukui, K. Drug repositioning for dengue haemorrhagic fever by integrating multiple omics analyses. *Sci. Rep.* **2019**, *9*, 523. [CrossRef]
34. Lanciotti, R.S.; Calisher, C.H.; Gubler, D.J.; Chang, G.J.; Vorndam, A.V. Rapid detection and typing of dengue viruses from clinical samples by using reverse transcriptase-polymerase chain reaction. *J. Clin. Microbiol.* **1992**, *30*, 545–551. [CrossRef]
35. Santiago, G.A.; Vergne, E.; Quiles, Y.; Cosme, J.; Vazquez, J.; Medina, J.F.; Medina, F.; Colón, C.; Margolis, H.; Muñoz-Jordán, J.L. Analytical and clinical performance of the CDC real time RT-PCR assay for detection and typing of dengue virus. *PLoS Negl. Trop. Dis.* **2013**, *7*, e2311. [CrossRef]
36. Li, H.; Handsaker, B.; Wysoker, A.; Fennell, T.; Ruan, J.; Homer, N.; Marth, G.; Abecasis, G.; Durbin, R. The Sequence Alignment/Map format and SAMtools. *Bioinformatics* **2009**, *25*, 2078–2079. [CrossRef] [PubMed]
37. Barrett, T.; Wilhite, S.E.; Ledoux, P.; Evangelista, C.; Kim, I.F.; Tomashevsky, M.; Marshall, K.A.; Phillippy, K.H.; Sherman, P.M.; Holko, M.; et al. NCBI GEO: Archive for functional genomics data sets–update. *Nucleic Acids Res.* **2013**, *41*, D991-995. [CrossRef] [PubMed]

63. Pollard, B.S.; JC, B.L.; Pollard, J.R. Classical Drug Digitoxin Inhibits Influenza Cytokine Storm, With Implications for Covid-19 Therapy. *In Vivo* **2020**, *34*, 3723–3730. [CrossRef] [PubMed]
64. Smith, J.L.; Stein, D.A.; Shum, D.; Fischer, M.A.; Radu, C.; Bhinder, B.; Djaballah, H.; Nelson, J.A.; Früh, K.; Hirsch, A.J. Inhibition of dengue virus replication by a class of small-molecule compounds that antagonize dopamine receptor d4 and downstream mitogen-activated protein kinase signaling. *J. Virol.* **2014**, *88*, 5533–5542. [CrossRef]
65. Wang, P.; Wang, Z.; Liu, J. Role of HDACs in normal and malignant hematopoiesis. *Mol. Cancer* **2020**, *19*, 5. [CrossRef]
66. Delgado, F.G.; Cárdenas, P.; Castellanos, J.E. Valproic Acid Downregulates Cytokine Expression in Human Macrophages Infected with Dengue Virus. *Diseases* **2018**, *6*, 59. [CrossRef] [PubMed]
67. Choy, M.M.; Zhang, S.L.; Costa, V.V.; Tan, H.C.; Horrevorts, S.; Ooi, E.E. Proteasome Inhibition Suppresses Dengue Virus Egress in Antibody Dependent Infection. *PLoS Negl. Trop. Dis.* **2015**, *9*, e0004058. [CrossRef]
68. Mukhopadhyay, P.; Rajesh, M.; Cao, Z.; Horváth, B.; Park, O.; Wang, H.; Erdelyi, K.; Holovac, E.; Wang, Y.; Liaudet, L.; et al. Poly (ADP-ribose) polymerase-1 is a key mediator of liver inflammation and fibrosis. *Hepatology* **2014**, *59*, 1998–2009. [CrossRef]

Paper IV - Endocytic pathways as pharmacological targets for DENV and SARS-CoV-2 infection

Endocytic pathways as pharmacological targets for DENV and SARS-CoV-2 infection

Ana C. Magalhaes[1,2,3], Ana C. Moreira[1,2,4], Maria S. Gomes[1,2,4], Luísa Pereira[1,3]

[1]i3S – Instituto de Investigação e Inovação em Saúde, Universidade do Porto, Porto, Portugal

[2]ICBAS - Instituto de Ciências Biomédicas Abel Salazar, Universidade do Porto, Porto, Portugal

[3]IPATIMUP - Instituto de Patologia e Imunologia Molecular, Universidade do Porto, Porto, Portugal

[4]IBMC- Instituto de Biologia Molecular e Celular, Universidade do Porto, Porto, Portugal

Keywords: Endocytosis; Dengue virus; SARS-CoV-2; pharmacological inhibition; *in vitro* modeling

Summary

Endocytosis, the basic cellular process used by cells to internalize a variety of molecules, is also hijacked by bacteria and viruses to enter in the host cell. Therefore, the entry mechanisms are important for viral infectivity and pathogenesis, and key targets for drug control. In this work, we explored the role of pharmacological inhibition of three main endocytic pathways: clathrin-mediated endocytosis (CME) lipid raft/caveolae-mediated endocytosis (LME), macropinocytosis (MPC). We infected Vero, Huh7 and NCI-H2110 cells with dengue (DENV - strain 2) and SARS-CoV-2 (alpha variant). From the three drugs tested (chlorpromazine, rosuvastatin and amiloride), only chlorpromazine needed lower concentration (15 times) to be safe in absence of infection. The three drugs led to decrease in viral production for both viruses, indicating that endocytic mechanisms are important pathways that should be explored in the pursuit of new intervention strategies.

1. Introduction

Viruses are intracellular pathogens that need to enter into the host cells to use the cell machinery to replicate the viral genome and construct new virions that can infect new cells. They can exploit the various endocytosis mechanisms for host cell entry, hence the entry mechanisms are important for viral infectivity and pathogenesis [1]. Clathrin-mediated endocytosis (CME) is mostly used by small and medium-size viruses. CME is characteristic of the receptor-mediated endocytosis type: a specific protein of the virus binds to a specific receptor(s) of the host membrane, and both are invaginated in the clathrin-coated pit; additionally, a number of adaptor and accessory molecules are necessary for controlling different steps in the assembly and maturation of the coated pits, such as the PI(4,5)P2 complex, amphiphysin and dynamin guanosine triphosphatase (GTPase) [1]. Another endocytosis pathway, known as lipid raft/caveolae-mediated endocytosis (LME), also involves the binding of the virus to a host receptor, but followed by invagination of cholesterol-enriched microdomains within the plasma membrane that may contain a coat protein known as caveolin; it involves dynamin activity and tyrosine kinase signalling [1]. Macropinocytosis (MPC) is a nonspecific (non-receptor) endocytic pathway [2], involving the activation of Rho GTPases (Rac1 and/or Cdc42), myosins, and kinases such as PAK1, PI3 kinase, and PKC, that trigger downstream signaling cascades resulting in transient, global changes in actin dynamics that lead to cell-wide plasma membrane ruffling in the form of filopodia, lamellopodia, circular ruffles, or blebs, and formation of large and uncoated vacuoles (macropinosomes).

The development of drugs against viruses targets either host molecules or viral molecules. The first has the essential advantages of: (a) the relative immutability of the host cell compared to the virus avoiding acquisition of drug resistance [3]; (b) a general mechanism used by several viruses guarantees a broad-spectrum antiviral effect [4]; and (c) rapid availability for possible treatment of newly emerged viruses. These advantages can compensate the higher potential for undesired side effects of interfering in natural mechanisms of the host, essential for several other functions. Within the biology of the host, endocytosis is a key function to be explored for antiviral drugs and has been extensively investigated.

Several molecules are known to efficiently inhibit endocytosis. Accumulated evidence shows that all popular inhibitors of different endocytic pathways have no absolute specificity [5]. Chlorpromazine, a cationic amphipathic drug that inhibits CME of various plasma membrane proteins (through the loss of clathrin and the AP2 adaptor

complex on cell surfaces), does not interfere with LME but can affect the formation of macropinosomes. The statin rosuvastatin, a competitive inhibitor of the enzyme HMG-CoA (3-hydroxy-3-methylglutaryl coenzyme A) reductase, interferes with cholesterol (constituent of rafts and caveolae) biosynthesis, and possibly also affects CME and MPC. Amiloride, an inhibitor of sodium-proton exchange, blocks MPC, but was also shown to interfere with CME and to attenuate LME. These drugs are useful tools in probing endocytosis, and in interfering with viral infection. Furthermore, given that they are already being used in treatment of certain pathologies, their side effects and doses are well known, rendering it unnecessary to perform extensive testing to ascertain these. In fact, chlorpromazine is since the 1950s a benchmark treatment for people with schizophrenia [6], rosuvastatin is provided against hypercholesterolemia and mixed dyslipidemia [7], and amiloride has been given for treatment of hypertension, congestive heart failure and hepatic cirrhosis with ascites [8].

Host-directed antivirals have been tested in the past. Although promising results were obtained *in vitro*, they have unfortunately failed when evaluated in clinical trials due to several factors such as on-target toxicity and limited in vivo activity [9]. This has been the case with the DENV [10] and, more recently, with SARS-CoV-2 [11, 12]. The older DENV evolved to bind several receptors (as heparin sulphate, DC-SIGN, mannose receptor and CD14), a capacity that allowed it to increase infectivity [13]. Several studies showed that LME is an important mechanism for DENV to enter in human cells [14], and in vitro and clinical studies have tried to test the efficiency of statin drugs as antiviral against DENV [10, 15]. Drugs used to control lipid metabolism were also identified as potential antiviral agents in a combined transcriptomic-in silico approach comparing advanced dengue with controls [16], although the main signatures were associated with the anti-inflammatory response, probably due to the advanced stages of the disease. It makes sense that endocytosis controlling drugs are more important as prophylactic and at the first stages of the infection, rather than for treatment of later advanced stages when the immune system is not coping with the disease. For the recent SARS-CoV-2, ACE2 is accepted as the main receptor (e.g. [17]), but the broad cellular tropism and high transmission rate of this virus soon raised the possibility that it uses alternative pathways and receptors, and the list is already extensive [18]. Some of these receptors for SARS-CoV-2 match DENV-binding molecules, adding evidence for the overlapping in entrance mechanisms used by both viruses [19].

In this work, we want to provide insights contributing to elucidate the endocytosis mechanism used by DENV (strain 2) and SARS-CoV-2 (alpha variant) in diverse cell models, and by direct probing endocytosis via pharmacological inhibitors.

2. Material and Methods

2.1. Cell lines, viruses and drugs

Vero cells from the kidney of African green monkey (ATCC, #CCL-81; ATCC, Manassas, VA, USA), Huh-7 cells from human hepatocellular carcinoma (kindly gifted by Tiago Duarte) and NCI-H2110 cells from human non-small cell lung cancer (ATCC, #CRL-5924; ATCC, Manassas, VA, US) were used in this work after confirmation of mycoplasma negative status. The Vero and Huh-7 cell lines were propagated in Dulbecco's Modified Eagle Medium (DMEM - Thermo Scientific, Waltham, MA, USA), and NCI-H2110 in Roswell Park Memorial Institute (RPMI) 1640 (RPMI - Thermo Scientific, Waltham, MA, USA), both supplemented with 10% fetal bovine serum (FBS - Labclinics, Barcelona, Spain), 100 U/ml of penicillin, and 100 ug/ml of streptomycin. Cells were maintained at 37ºC, under a 5% CO2 humidified atmosphere.

DENV2 was acquired from ATCC (strain New Guinea C, #VR-1584, ATCC, Manassas, VA, USA). SARS-CoV-2 was isolated from a positive nasopharyngeal sample diagnosed in a Portuguese individual in January 2021. The molecular diagnosis was confirmed by RT-PCR for three SARS-CoV-2 genes (ORF1ab, E and N - Fosun COVID-19 RT-PCR Detection Kit; Fosun Pharma USA Inc., Princeton, NJ, USA). The nasopharyngeal sample was stored at -80ºC in our lab prior virus isolation. The isolation was performed by inoculation in Vero cells, and the viral sequencing was performed by next-generation sequencing as described in detail previously [20], allowing to confirm that it could be affiliated in B.1.1.7 variant, according to PANGO nomenclature, or alpha variant according to the OMS classification. All experiments involving infectious DENV2 and SARS-CoV-2 were performed in BSL3 conditions in accordance with institutional guidelines.

Rosuvastatin (#18813), chlorpromazine (#16129) and amiloride (#14409) were purchase from Cayman Chemical (Ann Arbor, MI, USA). The drugs were prepared as 10 mM stock solutions in dimethyl sulfoxide (DMSO; Merck, Darmstadt, Germany).

2.2. Viral titration

Titters were determined by focus forming assay (FFA). Briefly, ten-fold dilutions of viral supernatants, either DENV2 or SARS-CoV-2, were independently inoculated in Vero cells, seeded 24h prior to infection in 96 well plates. After 1h incubation, an

overlay medium of DMEM with 4% FBS and 3% carboxymethyl cellulose (CMC) in a ratio of 1:1 was added to the inoculum, and the infected monolayer was incubated for 48h, at 37ºC in 5% CO2. We followed an immunofluorescence protocol to visualize and quantify the viral particles. Basically, cells were fixed with 4% paraformaldehyde at room temperature (RT), permeabilized with 0.2% Triton-X 100 (Sigma, St. Louis, MO, USA) for 10min, blocked with 1% bovine serum albumin (BSA; Sigma, St. Louis, MO, USA) for 10min, and incubated with a mouse DENV envelope antibody (4G2 antibody, anti-Flavivirus E protein, MAB10216; Merck Darmstadt, Germany) or a mouse SARS-CoV-2 spike antibody (GTX632604; GeneTex, Irvine, CA, USA) for 1h at RT. Afterwards, cells were independently incubated with anti-mouse Alexa 488-conjugated secondary antibody for 1h (Thermo Scientific, Waltham, MA, USA), followed by nuclear staining with 4',6-diamidino-2-phenylindole (DAPI; BioRad, Hercules, CA, USA) for 10min, before analysis. Images of each well were acquired on the IN Cell Analyzer 2000 (Cytiva, Marlborough, MA, USA), using appropriate magnifying objective and the fluorescent focus units (FFU) were counted.

2.3. Testing the effect of drugs without infection

We began by evaluating the effect of the drugs on cell viability, in the absence of infection. Vero, Huh-7 and NCI-H2110 cells were seeded 24h prior to compound addition in 96-well imaging plates, at a density of $2x10^4$/well, and cultured overnight at 37ºC and 5% CO2. We tested six final concentrations (1μM, 5μM, 10μM, 50μM, 100μM and 300μM) of each compound resuspended in DMEM containing 2% FBS. DMSO alone was used as control. The seeded cells in the plates (one for each cell line) had the media replaced with DMEM containing 2% FBS, and each compound was added, for the six tested concentrations. Each concentration had three replicates. After 48h incubation in the presence of the drug, cells were fixed, permeabilized, and stained for nuclear and cell delineation markers with DAPI and HCS CellMask (Thermo Fisher, Waltham, MA, USA) respectively, for 30 min. In the end, images of each well were acquired on the IN Cell Analyzer 2000, using a 10x magnifying objective. Image analysis was performed by using image segmentation and quantification software named Developer Toolbox (GE Healthcare, Chicago, IL, USA) and CellProfiler [21]. DAPI was used to access the number of cells. Three independent experiments were performed, and data were presented as percentage compared with DMSO only control

wells (100%). The half maximal inhibitory concentration (IC50) values in the absence of infection were calculated with Prism software.

2.4. Testing the effect of drugs with viral infection

Then we evaluated the viral inhibition by the different drugs, only in the Vero cells. The procedure was identical to the evaluation of cell viability in the absence of infection, except for the following points: for chlorpromazine, the six final tested concentrations were decreased to 0.1μM, 1μM, 2.5μM, 5μM, 10 μM and 20 μM, given the high impact of this drug in cell viability; 1h after the addition of the drugs, the plates were transferred to the BSL3 facility and infected with SARS-CoV-2 or DENV2 by adding 40 ul of each inoculum to each well, with a final MOI of 1 FFU/cell; after 48h in presence of drugs and viruses, the cells were treated as previously described but they were also fixed and stained for SARS-CoV-2 spike protein or DENV envelope protein (same antibodies mentioned above). The output of infection was measured as the fluorescence of the viral proteins, and the DAPI was used to assess the number of cells. The IC50 values in the presence of infection were determined as previously described.

We then performed infection assays at the IC50 value in the presence of infection for each compound, in the three cells lines Vero, Huh-7 and NCI-H2110 for detailed characterization of the impact of drugs in the infection/endocytosis. The cells were cultured in 24 well plates. The drug treatment and infection were performed as described before. The cells were allowed to grow in the presence of drug and virus for 48h, and we collected supernatant aliquots at three time-points (1h, 24h and 48h post-infection) to have information on the production of infectious viral particles (by FFA as described in section 2.2). We included non-infected and infected in the absence of drugs (addition of DMSO) controls.

3. Results

3.1- The effect of drugs in cell viability (in the absence of infection)

The tested drugs had effect on cells by interfering with their natural endocytosis mechanisms (Figure 1A). We firstly tested the effect of the drugs on cell viability in the various cell lines, in the absence of infection. Drugs were independently added to the three cell lines, and collected the cells after 48h, to be fixed and analysed by DAPI staining (nuclear marker; Figure 1B). This aimed at estimating the interval of drugs concentration to use in subsequent analyses. As can be observed in Figure 1B, and from the comparison of IC50 for cell viability, chlorpromazine had higher impact in cell viability for all cell lines (IC50 values between 4.7-11.8μM) when compared with rosuvastatin (IC50 195.2-480.0μM) and amiloride (IC50 271.6-436.6μM) at the same concentrations. These two last drugs had identical behaviour. Thus, we selected the following intervals of concentrations: 0.1 to 20 μM for chlorpromazine; and 1 to 300 μM for rosuvastatin and amiloride. Comparing the effect of each drug between the three cell lines, chlorpromazine killed more liver cells, rosuvastatin the lung cells, and amiloride the kidney cells.

3.2- The effect of drugs in viral entrance in cells

We next evaluated the potential antiviral activity of the compounds against DENV2 and SARS-CoV-2, in Vero cells. Cells were treated and then independently infected with the two viruses at a MOI of 1. After 48h, cells were fixed and analysed by DAPI staining and immunofluorescence of specific viral proteins (Figure 2A; Supplementary Figure S1). The drugs were tested over the above mentioned range of concentrations, and two IC50 values were calculated (Figure 2B): for cell viability (based on the DAPI marker; red fluorescence); for relative infection (based on the viral protein markers; green fluorescence). Given the fact that we are only infecting Vero cells, and we kept the range of concentrations for rosuvastatin and amiloride, we can compare IC50 values for cell viability in the absence and presence of infection: infection with DENV led to a higher mortality of cells (IC50s of 116.1 μM and 180.9 μM, respectively for both drugs) than SARS-CoV-2 (106.2 and 209.0 μM), but definitely infection by both viruses killed more cells than the non-infection only drugs condition (238.8 and 271.6 μM).

As can be observed in the lateral images of Figure 2B, DENV infects much more cells than SARS-CoV-2, either in controls (in the absence of drug) as in infected cells in the presence of drugs. This is mirrored by the higher separation between IC50-cell viability and IC50-relative infection curves for SARS-CoV-2 than DENV (for this, the effect of chlorpromazine and amiloride was unnoticeable even for high concentrations).

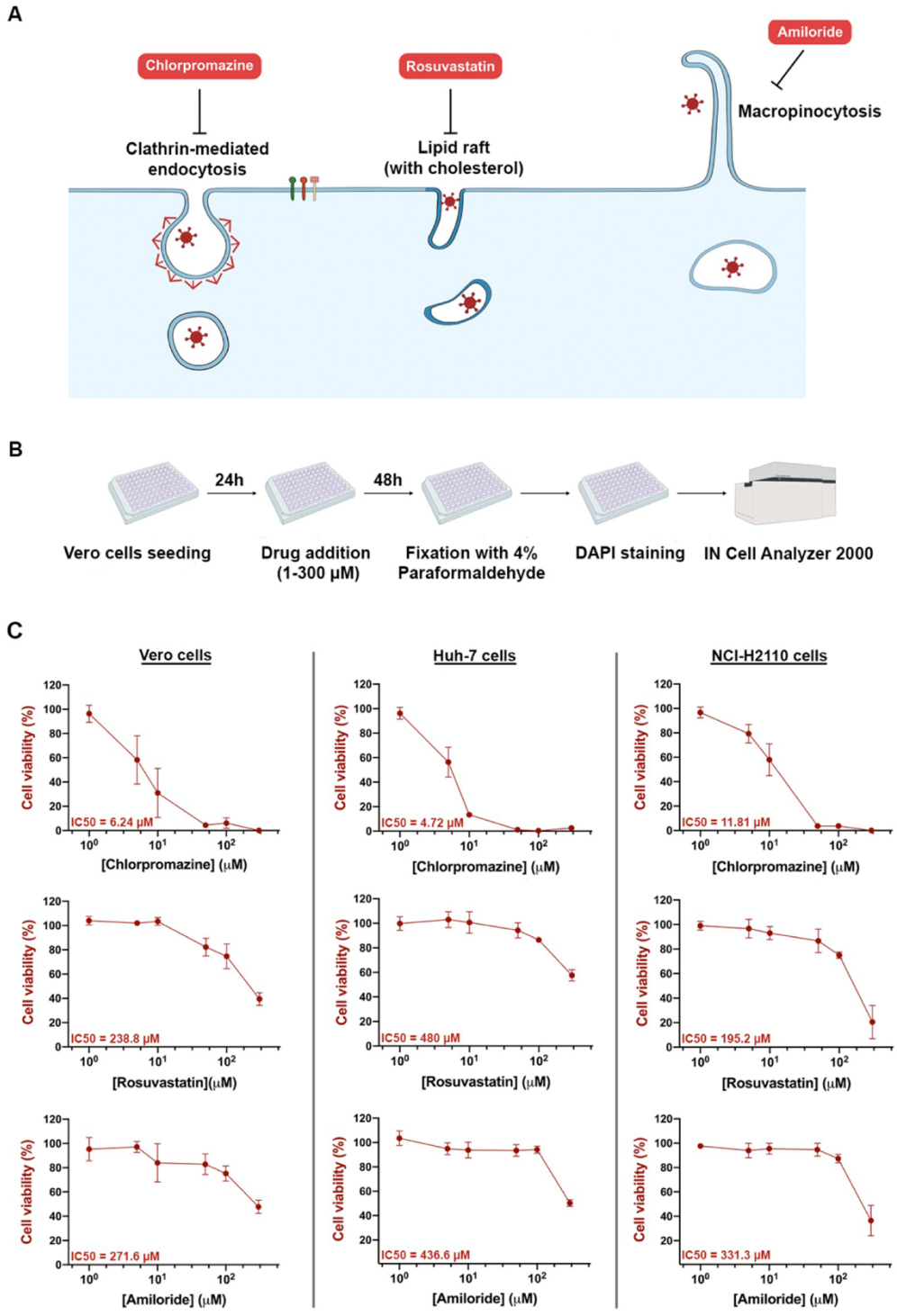


Figure 1- *In vitro* testing of the effect of the chlorpromazine, rosuvastatin and amiloride drugs in cell viability, in the absence of infection. A. Schematic representation of the main effect of each drug in the endocytic pathways: chlorpromazine (serotonin antagonist receptor) inhibiting clathrin-mediated endocytosis; rosuvastatin (statin) involved in depletion of cholesterol in cell membranes; and amiloride (inhibitor of sodium-proton exchange), blocking macropinocytosis. B. Schematic representation of the in vitro test. Cells were seeded in 96 well plates, treated with six concentrations of the three drugs, and incubated for 48 hours.

After fixation of the cells, DAPI staining measured in IN Cell Analyzer 2000 informed on the cell number. C. Plots represent the dose-response curves of the effect of the chlorpromazine, rosuvastatin and amiloride drugs in cell viability for Vero, Huh-7 and NCI-H2110 cell lines, with respective IC50 values indicated. Data are plotted as percentage compared with DMSO only control wells (100%). Values represent mean and standard deviation of three independent experiments.

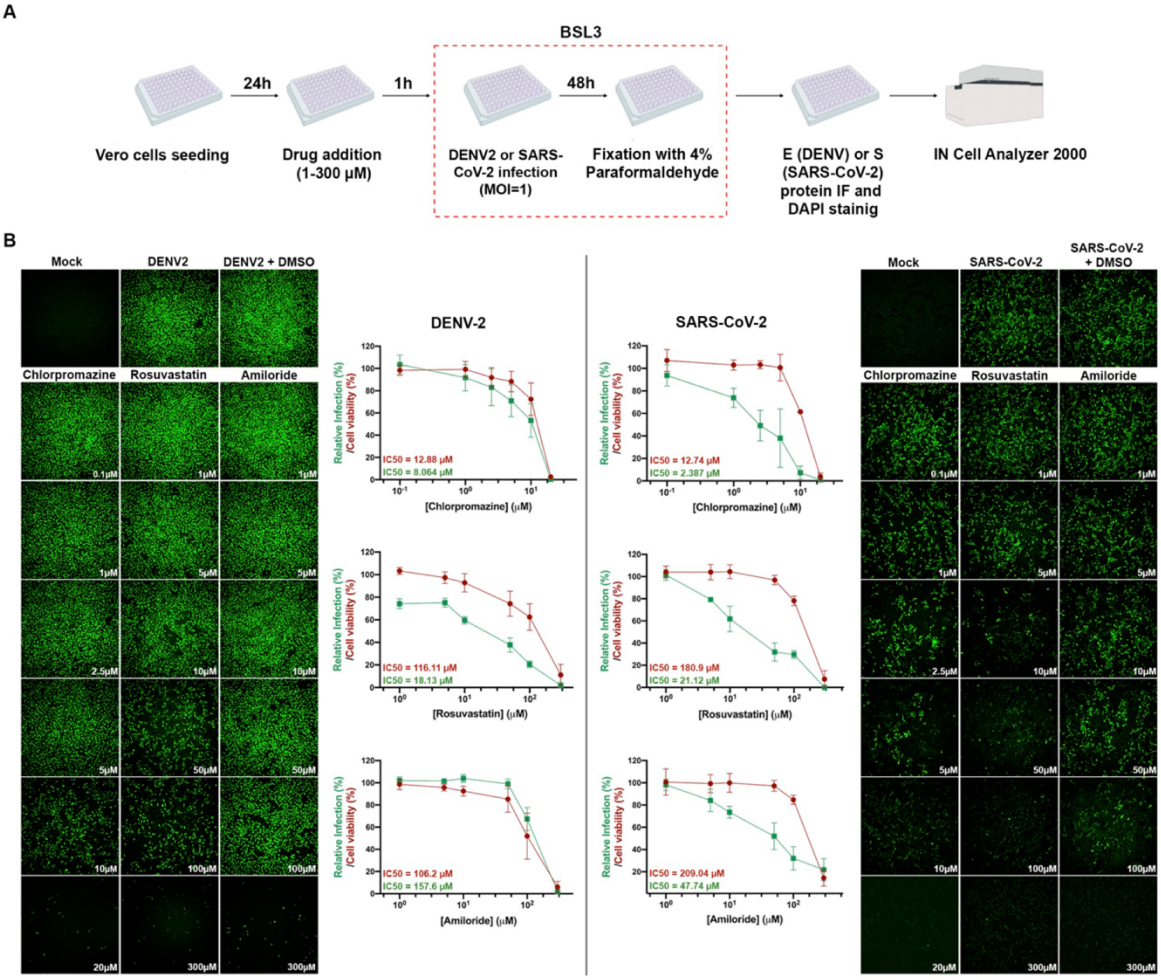


Figure 2- *In vitro* testing of the effect of the chlorpromazine, rosuvastatin and amiloride drugs in cell viability, in the presence of infection. **A.** Schematic representation of the *in vitro* test. Cells were seeded in 96 well plates and treated with six concentrations of the three drugs. One hour later, the cells were infected (in the BSL3) with DENV2 or SARS-CoV-2 at MOI 1, and incubated for 48h. After fixation of the cells, the viral infection rate was evaluated by immunofluorescence (IF) detection of DENV envelope protein or SARS-CoV-2 spike protein in IN Cell Analyzer 2000. DAPI staining informed on the cell viability rate. **B.** Plots represent the dose-response curve for each drug (chlorpromazine, rosuvastatin and amiloride) in the Vero cell line, in terms of cell viability (red lines) and relative infection (green lines), with respective

IC50 values indicated in corresponding colours. Data are plotted as percentage compared with DMSO only control wells (100%). Values represent mean and standard deviation of three independent experiments. The lateral panels consist in the microscope images of the viral protein staining (green) inside cells. The corresponding DAPI-stained cell nuclei images are shown in Supplementary Figure S1.

3.3- The effect of drugs in viral production and release from cells

We next evaluated the viral titer, after treating the three cell lines independently with the three drugs at the respective IC50-relative infection value, and at three time-points post-infection (1h, 24h and 48h post-infection). The viral titer was measured in the supernatants aliquots, reflecting the amount of new virions produced and released to the extracellular space.

For DENV, we can observe (Figure 3, left graphs) that, in the absence of drugs, there was production of new virions and their release from cells at 48h, higher in kidney cells, intermediate in liver cells, and lower by two orders of magnitude in the lung cells. The addition of drugs led to a lower viral titer, especially for chlorpromazine (significant values against the infection without drugs for the Vero and Huh-7 cells).

For SARS-CoV-2 (Figure 3, right graphs), the viral production was restricted to the Vero cells. All the drugs led also to decrease of the viral titer, but now significantly for rosuvastatin. In the liver and lung cells, there seems to be a similar tendency for the drugs to decrease the viral titer, but the viral production is very low for allowing reliable evaluations.

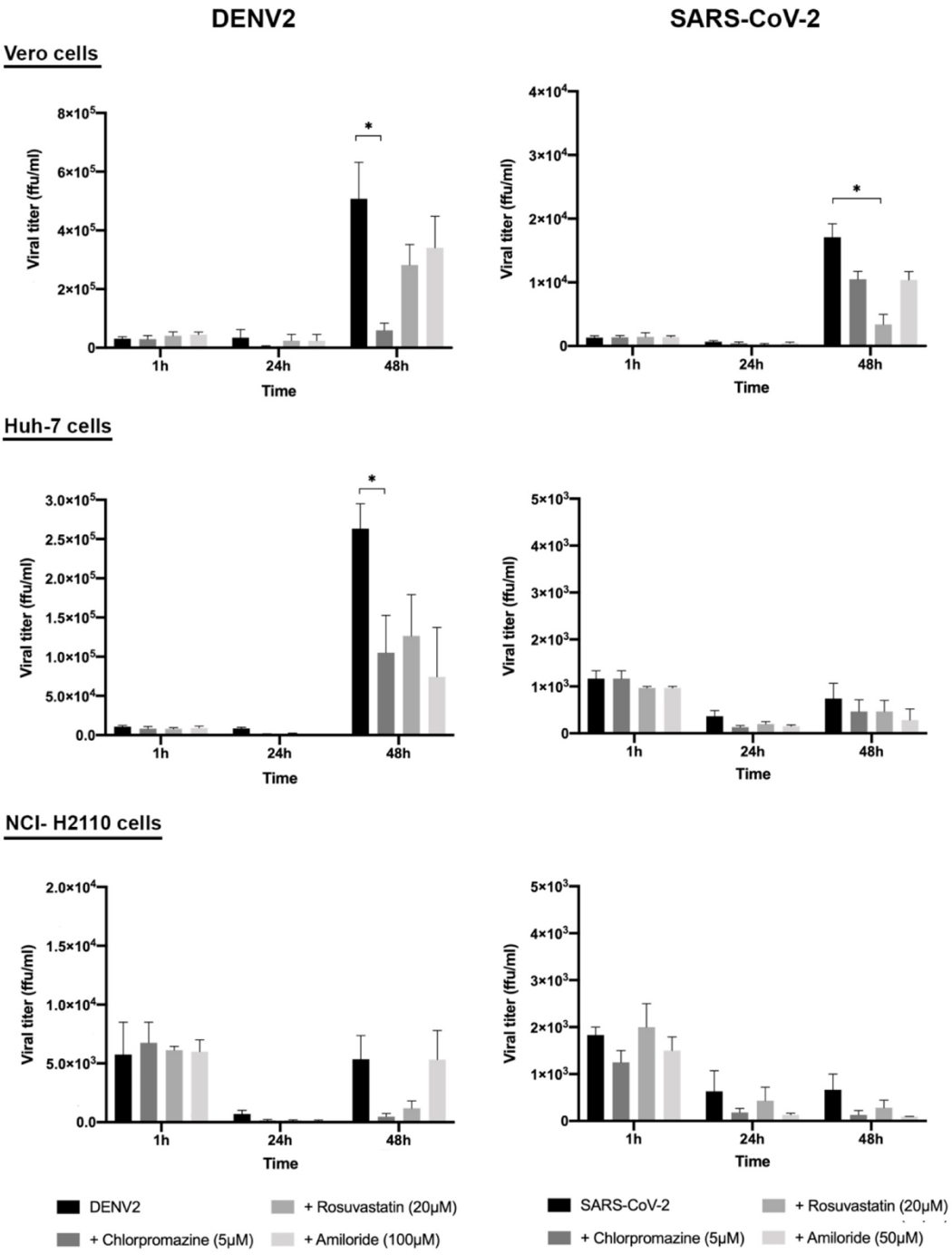


Figure 3- Viral titer measurement after treating the Vero, Huh-7 and NCI-H2110 cell lines independently with the three drugs (chlorpromazine, rosuvastatin and amiloride) at the respective IC50-relative infection value (5µM, 20µM, and 100 or 50µM, respectively). Supernatants aliquots were collected at three time-points post-infection with DENV or SARS-CoV-2 (1h, 24h and 48h post-infection). The controls consisted in the infected cells in the absence of drugs. In the graphs, data represent means ± SD of three independent experiments, and significant Student's t test p-values are indicated (*≤0.05).

4. Conclusions

The use of repurposed drugs saves several years, work and budget to the process of launching a drug for the treatment of patients or for prophylactic protection [22]. Namely, the safety, toxicity and risk assessment tests have already been conducted in human clinical trials for those drugs. We confirmed here, using in vitro assays, that rosuvastatin and amiloride have a low toxicity towards the used cells, with IC50 above 195 μM. Only chlorpromazine showed a higher toxicity, with IC50 between 4 and 12 μM, depending on the cell line.

Globally our results were promising, with the three drugs having potential as antiviral agents against SARS-Cov-2 and DENV. For SARS-CoV-2, all the three compounds were effective in inhibiting virus entry at clearly non-toxic concentrations. It is remarkable that SARS-CoV-2 leads to low production of virions and their release to the extracellular space, conditioning new infection of adjacent cells. Almost only the Vero cells allowed SARS-CoV-2 production, and the reason for this is that these cells lack genes encoding type I interferons, part of the innate immune response against viruses [23]. Thus, we must optimize our in vitro modelling to allow larger production of virions, enabling to ascertain if the observed decrease in viral entrance into cells translates into less virus production. Regarding DENV, the three compounds decreased very significantly the production of new virions, although their impact in viral entrance into cells was surprisingly lower compared to SARS-CoV-2 (except for the LME). Although it needs further investigation, these drugs probably also act in diverse cellular mechanisms besides endocytosis. Interestingly, chlorpromazine, the drug that more significantly affected the viral production in DENV, can be classified as “serotonin receptor antagonist”, one of the four general mechanisms highlighted by an *in silico* analysis performed by us on multi-tissue transcriptomic profiles in dengue fever cohorts [16]. Our independent results reinforce the inclusion of this or related drugs for further testing in the treatment of DENV.

As the three drugs have some effect in both viruses, this may imply that DENV and SARS-CoV-2 are using diverse endocytic mechanisms or that the drugs really affect more than one endocytic mechanism. In the future, we will test combinations two-by-two of these drugs and the three together. The combinations of drugs would potentially be more effective in interfering with the entrance of DENV and SARS-CoV-2 in the cells, although we still have to evaluate the combined toxicity and possible interactions between the drugs. As the DENV results imply the possible involvement of the drugs in other cellular mechanisms besides endocytosis, we intend to follow-

up with the characterisation of the transcriptomic profiles in the infected and drug-treated cells, aiming at characterizing molecularly the global impact of the drugs.

Acknowledgments: The Portuguese Foundation for Science and Technology (FCT) funded this project through the Research4COVID19 projects 109_596696487. i3S is supported by FEDER – Fundo Europeu de Desenvolvimento Regional funds through the COMPETE 2020 – Operational Program for Competitiveness and Internationalization (POCI), Portugal 2020, and by Portuguese funds through FCT/Ministério da Ciência, Tecnologia e Inovação in the framework of the project 'Institute for Research and Innovation in Health Sciences' (POCI-01-0145-FEDER-007274).

References

1. Cossart, P. and A. Helenius, *Endocytosis of viruses and bacteria.* Cold Spring Harb Perspect Biol, 2014. **6**(8): p. a016972.
2. Lin, X.P., J.D. Mintern, and P.A. Gleeson, *Macropinocytosis in Different Cell Types: Similarities and Differences.* Membranes (Basel), 2020. **10**(8).
3. Kennedy, D.A. and A.F. Read, *Why does drug resistance readily evolve but vaccine resistance does not?* Proc Biol Sci, 2017. **284**(1851): p. 20162562.
4. Mazzon, M. and M. Marsh, *Targeting viral entry as a strategy for broad-spectrum antivirals.* F1000Res, 2019. **8**: p. F1000.
5. Ivanov, A.I., *Pharmacological inhibition of endocytic pathways: is it specific enough to be useful?* Methods Mol Biol, 2008. **440**: p. 15-33.
6. Adams, C.E., et al., *Chlorpromazine versus placebo for schizophrenia.* Cochrane Database Syst Rev, 2014(1): p. CD000284.
7. Cortese, F., et al., *Rosuvastatin: Beyond the cholesterol-lowering effect.* Pharmacol Res, 2016. **107**: p. 1-18.
8. Sun, Q. and P. Sever, *Amiloride: A review.* J Renin Angiotensin Aldosterone Syst, 2020. **21**(4): p. 1470320320975893.
9. Debing, Y., D. Jochmans, and J. Neyts, *Intervention strategies for emerging viruses: use of antivirals.* Curr Opin Virol, 2013. **3**(2): p. 217-24.
10. Whitehorn, J., et al., *Lovastatin for the Treatment of Adult Patients With Dengue: A Randomized, Double-Blind, Placebo-Controlled Trial.* Clin Infect Dis, 2016. **62**(4): p. 468-476.
11. Lim, S.C.L., et al., *Efficacy of Ivermectin Treatment on Disease Progression Among Adults With Mild to Moderate COVID-19 and Comorbidities: The I-TECH Randomized Clinical Trial.* JAMA Intern Med, 2022.
12. Horby, P., et al., *Effect of Hydroxychloroquine in Hospitalized Patients with Covid-19.* N Engl J Med, 2020. **383**(21): p. 2030-2040.

13. Cruz-Oliveira, C., et al., *Receptors and routes of dengue virus entry into the host cells.* FEMS Microbiol Rev, 2015. **39**(2): p. 155-70.
14. Saumya, K.U., et al., *Unlike dengue virus, the conserved 14-23 residues in N-terminal region of Zika virus capsid is not involved in lipid interactions.* Biochim Biophys Acta Biomembr, 2020. **1862**(11): p. 183440.
15. Farfan-Morales, C.N., et al., *Anti-flavivirus Properties of Lipid-Lowering Drugs.* Front Physiol, 2021. **12**: p. 749770.
16. Sierra, B., et al., *Multi-Tissue Transcriptomic-Informed In Silico Investigation of Drugs for the Treatment of Dengue Fever Disease.* Viruses, 2021. **13**(8): p. 1540.
17. Clausen, T.M., et al., *SARS-CoV-2 Infection Depends on Cellular Heparan Sulfate and ACE2.* Cell, 2020. **183**(4): p. 1043-1057 e15.
18. Peng, R., et al., *Cell entry by SARS-CoV-2.* Trends Biochem Sci, 2021. **46**(10): p. 848-860.
19. Thépaut, M., et al., *DC/L-SIGN recognition of spike glycoprotein promotes SARS-CoV-2 trans-infection and can be inhibited by a glycomimetic antagonist.* PLoS Pathog, 2021. **17**(5): p. e1009576.
20. Magalhães, A.C., et al., *InfectionCMA: Combining in vitro Infection Assays, Cell Mi-croarrays and Immunocytochemistry for Efficient Biomarker Screening. Lessons from its Application to SARS-CoV-2.* Submitted, 2022.
21. Carpenter, A.E., et al., *CellProfiler: image analysis software for identifying and quantifying cell phenotypes.* Genome Biol, 2006. **7**(10): p. R100.
22. Pushpakom, S., et al., *Drug repurposing: progress, challenges and recommendations.* Nat Rev Drug Discov, 2019. **18**(1): p. 41-58.
23. Desmyter, J., J.L. Melnick, and W.E. Rawls, *Defectiveness of interferon production and of rubella virus interference in a line of African green monkey kidney cells (Vero).* J Virol, 1968. **2**(10): p. 955-61.

IV. Concluding Remarks

The work of this thesis had a broad aim of initiating a niche on translational applications in emerging viruses at the research group Genetic Diversity, i3S. This let to the implementation of all the laboratorial procedures, in BSL3 conditions, for two viruses that were not used as models in the institute. We could have used an approach of infection with lentiviruses containing relevant genes of the viruses under study, as this approach would be easier to implement in BSL2 conditions (Mekkaoui et al. 2021; Tandon et al. 2020). But the *in vitro* modelling with the intact viruses is closer to reality, guaranteeing more robust inferences that compensate the higher complexity of working in BSL3 conditions. In terms of this broad aim, this thesis was fully successful, as we can now efficiently perform *in vitro* modelling for DENV and SARS-CoV-2, in several cell lines representing the different physiology of the main organs affected by these viruses, and further interfere with molecular mechanisms by the addition of drugs. Of notice, the COVID-19 pandemic, although highly disrupting in many aspects (social and professional), served as a unique learning process, providing important insights that most probably would be missed otherwise.

Gaining on the extensive phylogenetic know-how and molecular testing experience of the research group, this work advanced a step further in upgrading to updated POC tests, more compatible with societal demands of faster, easier and cheaper molecular diagnoses. It is always a risk to try to replicate a technique that has been recently published and still being conducted by a single lab, as was the case of the Sherlock method (original publication dated from 2017; (Gootenberg et al. 2017) when this work began. The method had been applied only to blood infected samples, and the COVID-19 pandemic brought challenges of adaptation of the method to respiratory viruses, diagnosed in highly diluted nasopharyngeal samples. Clearly, in our case, the limit of detection for the synthetic positive targets was around 0.1 ng, close to the limit of the detection of the Qubit quantification method. We verified that this method could not detect RNA in the diagnostic samples for SARS-CoV-2. But other authors are also looking for ways to improve the read-out of the reaction that would allow the method to be more sensitive (Fozouni et al. 2021; Liu et al. 2021). Concordantly to these results (Fozouni et al. 2021), we confirmed that the use of two crRNAs for different genes of the same virus, in the same reaction, led to increase of the read-out when compared with one crRNA, for the step 2-based Sherlock method. We intend to test if the tandem use of CRISPR nucleases, as suggested recently (Liu et al. 2021), increases the read-

out in a more significant way, after we produce and purify the Csm6 enzyme. Unfortunately, due to the COVID-19 pandemic limitations, we could not obtain DENV positive samples from collaborators. It is probable that our step 2-based Sherlock implementations would not allow enough sensibility for the DENV diagnostic samples. We still need to redesign a crRNA for DENV1 that is specific for this strain.

Definitely, our results and also attempts by other authors (Fozouni et al. 2021) make us sure that further pursuits on the implementation of this method will focus on avoiding step 1 and improving sensibility of step 2. Despite claims in the literature that RPA is reliable (Li et al. 2018), the fact is that negative results are usually not published, biasing evaluations. The RPA kits are being commercialized only by one company, TwistDx, at a worldwide scale, following their publication of the method in 2006 (Piepenburg et al. 2006). This seems a limited commercial exploration compared with the revolutionising capacity attributed to the technique. And not even the pressure due to COVID-19 pandemic changed this situation. The acquisition of reagents from TwistDx for RPA implied months of waiting for one or two kits in the years 2020 and 2021, limiting extensively our experiments to improve the implementation of RPA.

The instability generated by the COVID-19 pandemic also put extreme pressure on the organization and execution of long experiments in BSL3. The confinements, limitations in the number of personnel authorised in the labs, and imposed isolations due to infection or close contacts (including of the technicians responsible for the scientific platforms), led us to look for solutions allowing to take the most from our experiments. A collaboration with colleagues from our institute, who are experts in preparing material for histological analyses, introduced us to the CMAs (Shidham 2019). We thought it would be an excellent translation application to establish and promote what we called the InfectionCMAs, as efficient tools to investigate the infection kinetics of a pathogen and for associated biomarker screening. We illustrated the potential of this tool by establishing two InfectionCMAs for SARS-CoV-2: one comparing MOIs and times after infection in one cell line (12 observation-points); the other using one MOI but infecting diverse cell lines (18 observation-points). The InfectionCMAs were easy to implement, and despite not using the maximum output allowed by a 5 x 7 mould (35 observation-points; there are larger moulders offering higher output), they led already to substantial gains against a traditional approach: for the first

InfectionCMA, 30 slides versus 180 slides and saving of six times antibodies amounts; for the second InfectionCMA, 30 slides versus 270 slides and saving of nine times antibodies amounts; and for both, only one against 2.5x BSL3 experimental procedures. If the maximum of the 5 x 7 mould was used, the gains would be 30 versus 510 slides and 17 times lower antibodies amounts. Additionally, the InfectionCMA slides can be easily stored for future screening of additional markers, without the need to return to BSL3 to conduct more infection assays. They can also be easily sent to other laboratories, that do not dispose of conditions for viral experiments, for local screening of biomarkers – this is a biological safe tool amenable with easy shipping. In conclusion, the InfectionCMAs allowed us, in a pandemic situation, to easily overcome difficulties raised by the otherwise complex traditional in vitro infection assays, where yield improvements implied increasing the number of cells, viruses, plates, independent infection points and time spent in BSL3.

We used the InfectionCMAs to investigate important biomarkers referred to be used by SARS-CoV-2 to enter the human cells (Murgolo et al. 2021; Peng et al. 2021). We confirmed the significant decrease in the mRNA and protein expressions of ACE2 along the infection course of SARS-CoV-2 (isolate B.1.1.29) in the monkey Vero and the human Huh-7 and Caco-2 cells, as described by others (Glowacka et al. 2010; Zhou et al. 2020). This concurs with claims that ACE2 is the main human receptor for SARS-CoV-2, but we observed the same tendency of NRP1 protein decreased expression along the infection in the three cell types, when the MOI was high (value was not statistically significant because NRP1 has an overall higher expression than ACE2 in most cells and tissues). This result is in agreement with the great reduction on SARS-CoV-2 infection in Caco-2 cells, after suppression of NRP1 expression by short hairpin RNA (Daly et al. 2020). Manipulation of endocytosis mechanisms for DENV and SARS-CoV-2 infection of human cells is a potential treatment strategy.

On the transferability of knowledge for treatment applications, we began by following the recent approach of performing first *in silico* analysis on big data (Loging et al. 2007), in order to highlight a few candidate drugs to be further tested *in vitro*. We generated our own transcriptomic data, to enrich the molecular information for multi-tissues affected by DENV infection. This information can provide insights into drugs that would act in the various organs affected in dengue disease. With the collaboration of our Cuban colleagues, we obtained liver, spleen and encephalon tissues from deceased individuals due to dengue disease and

controls (mainly trauma) and obtained the transcriptome profile at our institute. However, degradation affected the liver and encephalon tissues, leading us to exclude those transcriptomic profiles, and to end up with transcriptomic data for blood (published; (Kwissa et al. 2014; Nascimento et al. 2009), liver (published; (Zanini et al. 2018)) and spleen (our data). We identified heterogeneity between tissues in the molecular pathways affected by DENV: in the spleen, downregulation of immune components and signalling pathways related to the response to angiotensin, and upregulation of insulin and cholesterol metabolic pathways; in the liver, downregulation of cell cycle pathways is noticeable; in the blood, downregulation in the immune system and response to pathogens, and upregulation in cell cycle and repair mechanisms.

We then inputted the top differentially expressed genes for the various tissues on the CMap mining tool (Lamb et al. 2006; Subramanian et al. 2017), and used relevant databases (Inxight: Drugs, PubChem, Drugbank, FDA, EMA and ClinicalTrials) to classify the highlighted drugs in a comprehensive way. The fact that the tissue transcriptomic profiles were dissimilar could imply that different drugs would need to be used for treatment of all the main affected organs. Interestingly, the CMap results highlighted drugs sharing four mechanisms of actions for all the tissues: “NF-kB pathway inhibitor”, “ATPase inhibitor”, “Adrenergic receptor antagonist” and “Serotonin receptor antagonist”. We interpreted this result as reflecting the high connectivity between molecular networks in the body and the multi-effects of drugs. Reassuringly, some of these candidate drugs have been pin-pointedly described in the literature (Barrows et al. 2016; Cheng et al. 2015; Dai et al. 2012; Ko et al. 2007; Mazzon et al. 2019; Pollard et al. 2020; Smith et al. 2014) to have an impact against DENV or other flaviviruses. Our work advances in providing an integrative and comprehensive framework supporting further functional tests of these four molecular mechanisms in various tissue models in Dengue disease. These functional tests must be pursued in a near future, as the validation of these repurposed drugs in Dengue treatment can be highly valuable for a faster battle against this neglected tropical disease that is rapidly spreading across the world.

We also wanted to launch the implementation of the laboratorial procedures for *in vitro* tests of drugs in our viral models. Again, given the COVID-19 pressure felt during this thesis, we decided to not pursue with the testing on drugs from our Paper 3 on DENV only, but to build up on the results from Paper 2, and test drugs

affecting various endocytosis mechanisms allowing entrance of DENV and SARS-CoV-2 in human cells. Even so, chlorpromazine, one of the drugs widely used to interfere with endocytosis (Ivanov 2008), and that we ended up using, can be classified as "serotonin receptor antagonist", one of the four general mechanisms highlighted by the *in silico* analysis on the multi-tissue transcriptomic profiles in dengue fever cohorts. We tested this drug and other two drugs (rosuvastatin and amiloride) *in vitro*, with DENV and SARS-CoV-2.

We have now established the *in vitro* tests of drugs in our viral models, in BSL3 conditions. We calculated the range of concentrations for each drug, after confirming their impact in cell viability. In general, the drugs had low toxicity, but chlorpromazine concentrations should be around 15 times lower than rosuvastatin and amiloride. DENV2 was more efficient in infecting all cell lines than the alpha variant of SARS-CoV-2, and correspondingly, the IC50-relative infection values were higher for DENV2 than SARS-CoV-2. Interestingly, the "serotonin receptor antagonist" chlorpromazine drug was the one that affected more significantly the viral production in DENV. Our independent results, from *in silico* and *in vitro* tests, support the inclusion of this or related drugs for further tests in the treatment of DENV and other viruses. But definitely, our results indicate a decrease in viral production for the three drugs, suggesting that DENV and SARS-CoV-2 are using diverse endocytic mechanisms or that the drugs really affect more than one endocytic mechanism.

We will improve these preliminary insights by testing combinations two-by-two and three of these drugs and assessing the combined toxicity and possible interactions between the drugs. The characterisation of the transcriptome profiles of our *in vitro* drug assays can provide essential insights into the molecular mechanisms used by virus to enter cells.

References

Acosta EG, Castilla V AND Damonte EB. 2009. Alternative infectious entry pathways for dengue virus serotypes into mammalian cells. Cell Microbiol, 11(10): 1533-1549.

Adnan N, Khandker SS, Haq A, Chaity MA, Khalek A, Nazim AQ, Kaitsuka T, Tomizawa K, Mie M, Kobatake E, Ahmed S, Ali NAA, Khondoker MU, Haque M AND Jamiruddin MR. 2021. Detection of SARS-CoV-2 by antigen ELISA test is highly swayed by viral load and sample storage condition. Expert Rev Anti Infect Ther: 1-9.

Almassian DR, Cockrell LM AND Nelson WM. 2013. Portable nucleic acid thermocyclers. Chem Soc Rev, 42(22): 8769-8798.

Altulea D, Maassen S, Baranov MV AND van den Bogaart G. 2021. What makes (hydroxy)chloroquine ineffective against COVID-19: insights from cell biology. J Mol Cell Biol, 13(3): 175-184.

Amemiya T, Gromiha MM, Horimoto K AND Fukui K. 2019. Drug repositioning for dengue haemorrhagic fever by integrating multiple omics analyses. Sci Rep, 9(1): 523.

Andersen KG, Rambaut A, Lipkin WI, Holmes EC AND Garry RF. 2020. The proximal origin of SARS-CoV-2. Nat Med, 26(4): 450-452.

Baldanti F, Ganguly NK, Wang G, Möckel M, O'Neill LA, Renz H, dos Santos Ferreira CE, Tateda K AND Van Der Pol B. 2022. Choice of SARS-CoV-2 diagnostic test: challenges and key considerations for the future. Crit Rev Clin Lab Sci, in press.

Baltimore D. 1971. Expression of animal virus genomes. Bacteriol Rev, 35(3): 235-241.

Barrows NJ, Campos RK, Powell ST, Prasanth KR, Schott-Lerner G, Soto-Acosta R, Galarza-Muñoz G, McGrath EL, Urrabaz-Garza R, Gao J, Wu P, Menon R, Saade G, Fernandez-Salas I, Rossi SL, Vasilakis N, Routh A, Bradrick SS AND Garcia-Blanco MA. 2016. A Screen of FDA-Approved Drugs for Inhibitors of Zika Virus Infection. Cell Host Microbe, 20(2): 259-270.

Bayati A, Kumar R, Francis V AND McPherson PS. 2021. SARS-CoV-2 infects cells after viral entry via clathrin-mediated endocytosis. J Biol Chem, 296: 100306.

Berman JJ. 2019. Chapter 7 - Viruses. In *Taxonomic Guide to Infectious Diseases (Second Edition)*, edited by J.J. Berman: Academic Press, pp. 263-319.

Bhatt S, Gething PW, Brady OJ, Messina JP, Farlow AW, Moyes CL, Drake JM, Brownstein JS, Hoen AG, Sankoh O, Myers MF, George DB, Jaenisch T, Wint GR, Simmons CP, Scott TW, Farrar JJ AND Hay SI. 2013. The global distribution and burden of dengue. Nature, 496(7446): 504-507.

Binnicker MJ AND Kraft CS. 2020. Challenges and Controversies to Testing for COVID-19. J Clin Microbiol, 58(11): e01695-01620.

Blanchard E, Belouzard S, Goueslain L, Wakita T, Dubuisson J, Wychowski C AND Rouillé Y. 2006. Hepatitis C virus entry depends on clathrin-mediated endocytosis. J Virol, 80(14): 6964-6972.

Blanco-Melo D, Nilsson-Payant BE, Liu WC, Uhl S, Hoagland D, Møller R, Jordan TX, Oishi K, Panis M, Sachs D, Wang TT, Schwartz RE, Lim JK, Albrecht RA AND tenOever BR. 2020. Imbalanced Host Response to SARS-CoV-2 Drives Development of COVID-19. Cell, 181(5): 1036-1045.

Blanpain C, Libert F, Vassart G AND Parmentier M. 2002. CCR5 and HIV infection. Recept Channels, 8(1): 19-31.

Booth A, Reed AB, Ponzo S, Yassaee A, Aral M, Plans D, Labrique A AND Mohan D. 2021. Population risk factors for severe disease and mortality in COVID-19: A global systematic review and meta-analysis. PLoS One, 16(3): e0247461.

Boras B, Jones RM, Anson BJ, Arenson D, Aschenbrenner L, Bakowski MA, Beutler N, Binder J, Chen E, Eng H, Hammond H, Hammond J, Haupt RE, Hoffman R, Kadar EP, Kania R, Kimoto E, Kirkpatrick MG, Lanyon L, Lendy EK, Lillis JR, Logue J, Luthra SA, Ma C, Mason SW, McGrath ME, Noell S, Obach RS, MN OB, O'Connor R, Ogilvie K, Owen D, Pettersson M, Reese MR, Rogers TF, Rosales R, Rossulek MI, Sathish JG, Shirai N, Steppan C, Ticehurst M, Updyke LW, Weston S, Zhu Y, White KM, García-Sastre A, Wang J, Chatterjee AK, Mesecar AD, Frieman MB, Anderson AS AND Allerton C. 2021. Preclinical characterization of an intravenous coronavirus 3CL

protease inhibitor for the potential treatment of COVID19. Nat Commun, 12(1): 6055.

Bour S, Geleziunas R AND Wainberg MA. 1995. The human immunodeficiency virus type 1 (HIV-1) CD4 receptor and its central role in promotion of HIV-1 infection. Microbiol Rev, 59(1): 63-93.

Bowers JR, Readler JM, Sharma P AND Excoffon K. 2017. Poliovirus Receptor: More than a simple viral receptor. Virus Res, 242: 1-6.

Brady OJ, Gething PW, Bhatt S, Messina JP, Brownstein JS, Hoen AG, Moyes CL, Farlow AW, Scott TW AND Hay SI. 2012. Refining the global spatial limits of dengue virus transmission by evidence-based consensus. PLoS Negl Trop Dis, 6(8): e1760.

Burrell CJ, Howard CR AND Murphy FA. 2017. Chapter 3 - Virion Structure and Composition. In *Fenner and White's Medical Virology (Fifth Edition)*, edited by C.J. Burrell, C.R. Howard andF.A. Murphy. London: Academic Press, pp. 27-37.

Burrell CJ, Howard CR AND Murphy FA. 2017. Chapter 4 - Virus Replication. In *Fenner and White's Medical Virology (Fifth Edition)*, edited by C.J. Burrell, C.R. Howard andF.A. Murphy. London: Academic Press, pp. 39-55.

Buss LF, Prete CA, Jr., Abrahim CMM, Mendrone A, Jr., Salomon T, de Almeida-Neto C, França RFO, Belotti MC, Carvalho M, Costa AG, Crispim MAE, Ferreira SC, Fraiji NA, Gurzenda S, Whittaker C, Kamaura LT, Takecian PL, da Silva Peixoto P, Oikawa MK, Nishiya AS, Rocha V, Salles NA, de Souza Santos AA, da Silva MA, Custer B, Parag KV, Barral-Netto M, Kraemer MUG, Pereira RHM, Pybus OG, Busch MP, Castro MC, Dye C, Nascimento VH, Faria NR AND Sabino EC. 2021. Three-quarters attack rate of SARS-CoV-2 in the Brazilian Amazon during a largely unmitigated epidemic. Science, 371(6526): 288-292.

Cann AJ. 2008. Replication of Viruses. In *Encyclopedia of Virology (Third Edition)*, edited by B.W.J. Mahy andM.H.V. Van Regenmortel. Oxford: Academic Press, pp. 406-412.

Challen R, Brooks-Pollock E, Read JM, Dyson L, Tsaneva-Atanasova K AND Danon L. 2021. Risk of mortality in patients infected with SARS-CoV-2 variant of concern 202012/1: matched cohort study. Bmj, 372: n579.

Chan JF, Yuan S, Kok KH, To KK, Chu H, Yang J, Xing F, Liu J, Yip CC, Poon RW, Tsoi HW, Lo SK, Chan KH, Poon VK, Chan WM, Ip JD, Cai JP, Cheng VC, Chen H, Hui CK AND Yuen KY. 2020. A familial cluster of pneumonia associated with the 2019 novel coronavirus indicating person-to-person transmission: a study of a family cluster. Lancet, 395(10223): 514-523.

Chan-Yeung M AND Xu RH. 2003. SARS: epidemiology. Respirology, 8 Suppl(Suppl 1): S9-14.

Cheang YZN, Ting HRD, Koh HQV AND Alonso S. 2021. In vitro and in vivo efficacy of Metformin against dengue. Antiviral Res, 195: 105186.

Chen R, Lan Z, Ye J, Pang L, Liu Y, Wu W, Qin X, Guo Y AND Zhang P. 2021. Cytokine Storm: The Primary Determinant for the Pathophysiological Evolution of COVID-19 Deterioration. Front Immunol, 12: 589095.

Chen Y, Maguire T, Hileman RE, Fromm JR, Esko JD, Linhardt RJ AND Marks RM. 1997. Dengue virus infectivity depends on envelope protein binding to target cell heparan sulfate. Nat Med, 3(8): 866-871.

Chen Y, Liu Q AND Guo D. 2020. Emerging coronaviruses: Genome structure, replication, and pathogenesis. J Med Virol, 92(4): 418-423.

Chen Y, Li N, Lourenço J, Wang L, Cazelles B, Dong L, Li B, Liu Y, Jit M, Bosse NI, Abbott S, Velayudhan R, Wilder-Smith A, Tian H, Brady OJ, Procter SR, Wong KLM, Hellewell J, Davies NG, Jarvis CI, McCarthy CV, Medley G, Meakin SR, Rosello A, Finch E, Lowe R, Pearson CAB, Clifford S, Quilty BJ, Flasche S, Gibbs HP, Chapman LAC, Atkins KE, Hodgson D, Barnard RC, Russell TW, Klepac P, Jafari Y, Eggo RM, Mee P, Quaife M, Endo A, Funk S, Hué S, Kucharski AJ, Edmunds WJ, O'Reilly K, Pung R, Villabona-Arenas CJ, Gimma A, Abbas K, Prem K, Knight GM, Sun FY, Waites W, Munday JD, Koltai M, Sandmann FG AND Tully DC. 2022. Measuring the effects of COVID-19-related disruption on dengue transmission in southeast Asia and Latin America: a statistical modelling study. Lancet Infect Dis, S1473-3099(22): 00025-00021

Chen YC, Wang SY AND King CC. 1999. Bacterial lipopolysaccharide inhibits dengue virus infection of primary human monocytes/macrophages by blockade of virus entry via a CD14-dependent mechanism. J Virol, 73(4): 2650-2657.

Chen YJ, Liu X AND Tsai B. 2019. SV40 Hijacks Cellular Transport, Membrane Penetration, and Disassembly Machineries to Promote Infection. Viruses, 11(10): 917.

Cheng YL, Lin YS, Chen CL, Wan SW, Ou YD, Yu CY, Tsai TT, Tseng PC AND Lin CF. 2015. Dengue Virus Infection Causes the Activation of Distinct NF-κB Pathways for Inducible Nitric Oxide Synthase and TNF-α Expression in RAW264.7 Cells. Mediators Inflamm, 2015: 274025.

Cherian S, Potdar V, Jadhav S, Yadav P, Gupta N, Das M, Rakshit P, Singh S, Abraham P, Panda S AND Team N. 2021. SARS-CoV-2 Spike Mutations, L452R, T478K, E484Q and P681R, in the Second Wave of COVID-19 in Maharashtra, India. Microorganisms, 9(7): 1542.

Chia PY, Htun HL, Ling WP, Leo YS, Yeo TW AND Lye DCB. 2018. Hyperlipidemia, statin use and dengue severity. Sci Rep, 8(1): 17147.

Cobián Güemes AG, Youle M, Cantú VA, Felts B, Nulton J AND Rohwer F. 2016. Viruses as Winners in the Game of Life. Annu Rev Virol, 3(1): 197-214.

Cohen C, Kleynhans J, von Gottberg A, McMorrow ML, Wolter N, Bhiman JN, Moyes J, du Plessis M, Carrim M, Buys A, Martinson NA, Kahn K, Tollman S, Lebina L, Wafawanaka F, du Toit JD, Gómez-Olivé FX, Dawood FS, Mkhencele T, Sun K, Viboud C, Tempia S, Bhiman JN, Buys A, Carrim M, Cohen C, de Gouveia L, du Plessis M, du Toit J, Gómez-Olivé FX, Kahn K, Kgasago KP, Kleynhans J, Kotane R, Lebina L, Martinson NA, McMorrow ML, Moloantoa T, Moyes J, Tempia S, Tollman S, von Gottberg A, Wafawanaka F AND Wolter N. 2022. SARS-CoV-2 incidence, transmission, and reinfection in a rural and an urban setting: results of the PHIRST-C cohort study, South Africa, 2020-2021. Lancet Infect Dis, in press.

Cossart P AND Helenius A. 2014. Endocytosis of viruses and bacteria. Cold Spring Harb Perspect Biol, 6(8): a016972.

Cruz-Oliveira C, Freire JM, Conceição TM, Higa LM, Castanho MA AND Da Poian AT. 2015. Receptors and routes of dengue virus entry into the host cells. FEMS Microbiol Rev, 39(2): 155-170.

Daecke J, Fackler OT, Dittmar MT AND Kräusslich HG. 2005. Involvement of clathrin-mediated endocytosis in human immunodeficiency virus type 1 entry. J Virol, 79(3): 1581-1594.

Dai JP, Li WZ, Zhao XF, Wang GF, Yang JC, Zhang L, Chen XX, Xu YX AND Li KS. 2012. A drug screening method based on the autophagy pathway and studies of the mechanism of evodiamine against influenza A virus. PLoS One, 7(8): e42706.

Daly JL, Simonetti B, Klein K, Chen KE, Williamson MK, Antón-Plágaro C, Shoemark DK, Simón-Gracia L, Bauer M, Hollandi R, Greber UF, Horvath P, Sessions RB, Helenius A, Hiscox JA, Teesalu T, Matthews DA, Davidson AD, Collins BM, Cullen PJ AND Yamauchi Y. 2020. Neuropilin-1 is a host factor for SARS-CoV-2 infection. Science, 370(6518): 861-865.

Das AS AND Zou WQ. 2016. Prions: Beyond a Single Protein. Clin Microbiol Rev, 29(3): 633-658.

Davies NG, Jarvis CI, Edmunds WJ, Jewell NP, Diaz-Ordaz K AND Keogh RH. 2021. Increased mortality in community-tested cases of SARS-CoV-2 lineage B.1.1.7. Nature, 593(7858): 270-274.

den Boon JA, Diaz A AND Ahlquist P. 2010. Cytoplasmic viral replication complexes. Cell host & microbe, 8(1): 77-85.

Diamond M AND Pierson T. 2015. Molecular Insight into Dengue Virus Pathogenesis and Its Implications for Disease Control. Cell, 162(3): 488-492.

Dimitrov DS. 2004. Virus entry: molecular mechanisms and biomedical applications. Nat Rev Microbiol, 2(2): 109-122.

Dong E, Du H AND Gardner L. 2020. An interactive web-based dashboard to track COVID-19 in real time. Lancet Infect Dis, 20(5): 533-534.

Dou D, Revol R, Östbye H, Wang H AND Daniels R. 2018. Influenza A Virus Cell Entry, Replication, Virion Assembly and Movement. Front Immunol, 9: 1581.

Drożdżal S, Rosik J, Lechowicz K, Machaj F, Szostak B, Przybyciński J, Lorzadeh S, Kotfis K, Ghavami S AND Łos MJ. 2021. An update on drugs with therapeutic potential for SARS-CoV-2 (COVID-19) treatment. Drug Resist Updat, 59: 100794.

Durbin AP, Vargas MJ, Wanionek K, Hammond SN, Gordon A, Rocha C, Balmaseda A AND Harris E. 2008. Phenotyping of peripheral blood mononuclear cells during acute dengue illness demonstrates infection and increased activation of monocytes in severe cases compared to classic dengue fever. Virology, 376(2): 429-435.

European Medicines Agency, EMA. *Treatments authorised in the European Union (EU) to treat COVID-19, following evaluation by the European Medicines Agency (EMA)* [accessed on March 2022]. Available from https://www.ema.europa.eu/en/human-regulatory/overview/public-health-threats/coronavirus-disease-covid-19/treatments-vaccines/treatments-covid-19/covid-19-treatments-authorised.

Eng H, Dantonio AL, Kadar EP, Obach RS, Di L, Lin J, Patel NC, Boras B, Walker GS, Novak JJ, Kimoto E, Singh RSP AND Kalgutkar AS. 2022. Disposition of PF-07321332 (Nirmatrelvir), an Orally Bioavailable Inhibitor of SARS-CoV-2 3CL Protease, across Animals and Humans. Drug Metab Dispos, in press.

Espy MJ, Uhl JR, Sloan LM, Buckwalter SP, Jones MF, Vetter EA, Yao JD, Wengenack NL, Rosenblatt JE, Cockerill FR, 3rd AND Smith TF. 2006. Real-time PCR in clinical microbiology: applications for routine laboratory testing. Clin Microbiol Rev, 19(1): 165-256.

Farfan-Morales CN, Cordero-Rivera CD, Osuna-Ramos JF, Monroy-Muñoz IE, De Jesús-González LA, Muñoz-Medina JE, Hurtado-Monzón AM, Reyes-Ruiz JM AND del Ángel RM. 2021. The antiviral effect of metformin on zika and dengue virus infection. Sci Rep, 11(1): 8743.

Faria NR, Mellan TA, Whittaker C, Claro IM, Candido DDS, Mishra S, Crispim MAE, Sales FCS, Hawryluk I, McCrone JT, Hulswit RJG, Franco LAM, Ramundo MS, de Jesus JG, Andrade PS, Coletti TM, Ferreira GM, Silva CAM, Manuli ER, Pereira RHM, Peixoto PS, Kraemer MUG, Gaburo N, Jr., Camilo CDC, Hoeltgebaum H, Souza WM, Rocha EC, de Souza LM, de Pinho MC, Araujo LJT, Malta FSV, de Lima AB, Silva JDP, Zauli DAG, Ferreira ACS, Schnekenberg RP, Laydon DJ, Walker PGT, Schlüter HM, Dos Santos ALP, Vidal MS, Del Caro VS, Filho RMF, Dos Santos HM, Aguiar RS, Proença-Modena JL, Nelson B, Hay JA, Monod M, Miscouridou X, Coupland H, Sonabend R, Vollmer M, Gandy A, Prete CA, Jr., Nascimento VH, Suchard MA, Bowden TA, Pond SLK, Wu CH, Ratmann O, Ferguson NM, Dye C, Loman NJ, Lemey P, Rambaut A, Fraiji NA, Carvalho M, Pybus OG, Flaxman S, Bhatt S AND Sabino EC. 2021.

Genomics and epidemiology of the P.1 SARS-CoV-2 lineage in Manaus, Brazil. Science, 372(6544): 815-821.

FDA. *First FDA-approved vaccine for the prevention of dengue disease in endemic regions*, 1 May 2019 [accessed on March 2022]. Available from https://www.fda.gov/news-events/press-announcements/first-fda-approved-vaccine-prevention-dengue-disease-endemic-regions.

FDA. *Coronavirus (COVID-19) Update: FDA Authorizes New Long-Acting Monoclonal Antibodies for Pre-exposure Prevention of COVID-19 in Certain Individuals*, 8 December 2021 [accessed on March 2022]. Available from https://www.fda.gov/news-events/press-announcements/coronavirus-covid-19-update-fda-authorizes-new-long-acting-monoclonal-antibodies-pre-exposure?utm_medium=email&utm_source=govdelivery.

Ferreira IATM, Kemp SA, Datir R, Saito A, Meng B, Rakshit P, Takaori-Kondo A, Kosugi Y, Uriu K, Kimura I, Shirakawa K, Abdullahi A, Agarwal A, Ozono S, Tokunaga K, Sato K, Gupta RK, CITIID-NIHR BioResource COVID-19 Collaboration IS-C-GC AND Consortium TGtPJ. 2021. SARS-CoV-2 B.1.617 Mutations L452R and E484Q Are Not Synergistic for Antibody Evasion. J Infect Dis, 224(6): 989-994.

Finkel Y, Gluck A, Nachshon A, Winkler R, Fisher T, Rozman B, Mizrahi O, Lubelsky Y, Zuckerman B, Slobodin B, Yahalom-Ronen Y, Tamir H, Ulitsky I, Israely T, Paran N, Schwartz M AND Stern-Ginossar N. 2021. SARS-CoV-2 uses a multipronged strategy to impede host protein synthesis. Nature, 594(7862): 240-245.

Flint J, Racaniello V, Rall G, Hatziioannou T AND Skalka A. 2020. *Principles of Virology, 5th Edition*. 2 vols. Vol. 1. ISBN 978-1-683-67358-3

Fozouni P, Son S, Díaz de León Derby M, Knott GJ, Gray CN, D'Ambrosio MV, Zhao C, Switz NA, Kumar GR, Stephens SI, Boehm D, Tsou CL, Shu J, Bhuiya A, Armstrong M, Harris AR, Chen PY, Osterloh JM, Meyer-Franke A, Joehnk B, Walcott K, Sil A, Langelier C, Pollard KS, Crawford ED, Puschnik AS, Phelps M, Kistler A, DeRisi JL, Doudna JA, Fletcher DA AND Ott M. 2021. Amplification-free detection of SARS-CoV-2 with CRISPR-Cas13a and mobile phone microscopy. Cell, 184(2): 323-333 e329.

Fozouni P, Son S, Díaz de León Derby M, Knott GJ, Gray CN, D'Ambrosio MV, Zhao C, Switz NA, Kumar GR, Stephens SI, Boehm D, Tsou CL, Shu J, Bhuiya A, Armstrong

M, Harris AR, Chen PY, Osterloh JM, Meyer-Franke A, Joehnk B, Walcott K, Sil A, Langelier C, Pollard KS, Crawford ED, Puschnik AS, Phelps M, Kistler A, DeRisi JL, Doudna JA, Fletcher DA AND Ott M. 2021. Amplification-free detection of SARS-CoV-2 with CRISPR-Cas13a and mobile phone microscopy. Cell, 184(2): 323-333.e329.

Gainor EM, Harris E AND LaBeaud AD. 2022. Uncovering the Burden of Dengue in Africa: Considerations on Magnitude, Misdiagnosis, and Ancestry. Viruses, 14(2): 233.

Germi R, Crance J-M, Garin D, Guimet J, Lortat-Jacob H, Ruigrok RWH, Zarski J-P AND Drouet E. 2002. Heparan Sulfate-Mediated Binding of Infectious Dengue Virus Type 2 and Yellow Fever Virus. Virology, 292(1): 162-168.

Ghosh S, Dellibovi-Ragheb TA, Kerviel A, Pak E, Qiu Q, Fisher M, Takvorian PM, Bleck C, Hsu VW, Fehr AR, Perlman S, Achar SR, Straus MR, Whittaker GR, de Haan CAM, Kehrl J, Altan-Bonnet G AND Altan-Bonnet N. 2020. β-Coronaviruses Use Lysosomes for Egress Instead of the Biosynthetic Secretory Pathway. Cell, 183(6): 1520-1535.

Glowacka I, Bertram S, Herzog P, Pfefferle S, Steffen I, Muench MO, Simmons G, Hofmann H, Kuri T, Weber F, Eichler J, Drosten C AND Pöhlmann S. 2010. Differential downregulation of ACE2 by the spike proteins of severe acute respiratory syndrome coronavirus and human coronavirus NL63. J Virol, 84(2): 1198-1205.

Goldsmith CS AND Miller SE. 2009. Modern uses of electron microscopy for detection of viruses. Clin Microbiol Rev, 22(4): 552-563.

Gootenberg JS, Abudayyeh OO, Lee JW, Essletzbichler P, Dy AJ, Joung J, Verdine V, Donghia N, Daringer NM, Freije CA, Myhrvold C, Bhattacharyya RP, Livny J, Regev A, Koonin EV, Hung DT, Sabeti PC, Collins JJ AND Zhang F. 2017. Nucleic acid detection with CRISPR-Cas13a/C2c2. Science, 356(6336): 438-442.

Gorbalenya AE, Krupovic M, Mushegian A, Kropinski AM, Siddell SG, Varsani A, Adams MJ, Davison AJ, Dutilh BE, Harrach B, Harrison RL, Junglen S, King AMQ, Knowles NJ, Lefkowitz EJ, Nibert ML, Rubino L, Sabanadzovic S, Sanfaçon H, Simmonds P, Walker PJ, Zerbini FM, Kuhn JH AND International Committee on

Taxonomy of Viruses Executive C. 2020. The new scope of virus taxonomy: partitioning the virosphere into 15 hierarchical ranks. Nat Microbiol, 5(5): 668-674.

Gordon DE, Hiatt J, Bouhaddou M, Rezelj VV, Ulferts S, Braberg H, Jureka AS, Obernier K, Guo JZ, Batra J, Kaake RM, Weckstein AR, Owens TW, Gupta M, Pourmal S, Titus EW, Cakir M, Soucheray M, McGregor M, Cakir Z, Jang G, O'Meara MJ, Tummino TA, Zhang Z, Foussard H, Rojc A, Zhou Y, Kuchenov D, Hüttenhain R, Xu J, Eckhardt M, Swaney DL, Fabius JM, Ummadi M, Tutuncuoglu B, Rathore U, Modak M, Haas P, Haas KM, Naing ZZC, Pulido EH, Shi Y, Barrio-Hernandez I, Memon D, Petsalaki E, Dunham A, Marrero MC, Burke D, Koh C, Vallet T, Silvas JA, Azumaya CM, Billesbølle C, Brilot AF, Campbell MG, Diallo A, Dickinson MS, Diwanji D, Herrera N, Hoppe N, Kratochvil HT, Liu Y, Merz GE, Moritz M, Nguyen HC, Nowotny C, Puchades C, Rizo AN, Schulze-Gahmen U, Smith AM, Sun M, Young ID, Zhao J, Asarnow D, Biel J, Bowen A, Braxton JR, Chen J, Chio CM, Chio US, Deshpande I, Doan L, Faust B, Flores S, Jin M, Kim K, Lam VL, Li F, Li J, Li YL, Li Y, Liu X, Lo M, Lopez KE, Melo AA, Moss FR, 3rd, Nguyen P, Paulino J, Pawar KI, Peters JK, Pospiech TH, Jr., Safari M, Sangwan S, Schaefer K, Thomas PV, Thwin AC, Trenker R, Tse E, Tsui TKM, Wang F, Whitis N, Yu Z, Zhang K, Zhang Y, Zhou F, Saltzberg D, Hodder AJ, Shun-Shion AS, Williams DM, White KM, Rosales R, Kehrer T, Miorin L, Moreno E, Patel AH, Rihn S, Khalid MM, Vallejo-Gracia A, Fozouni P, Simoneau CR, Roth TL, Wu D, Karim MA, Ghoussaini M, Dunham I, Berardi F, Weigang S, Chazal M, Park J, Logue J, McGrath M, Weston S, Haupt R, Hastie CJ, Elliott M, Brown F, Burness KA, Reid E, Dorward M, Johnson C, Wilkinson SG, Geyer A, Giesel DM, Baillie C, Raggett S, Leech H, Toth R, Goodman N, Keough KC, Lind AL, Klesh RJ, Hemphill KR, Carlson-Stevermer J, Oki J, Holden K, Maures T, Pollard KS, Sali A, Agard DA, Cheng Y, Fraser JS, Frost A, Jura N, Kortemme T, Manglik A, Southworth DR, Stroud RM, Alessi DR, Davies P, Frieman MB, Ideker T, Abate C, Jouvenet N, Kochs G, Shoichet B, Ott M, Palmarini M, Shokat KM, García-Sastre A, Rassen JA, Grosse R, Rosenberg OS, Verba KA, Basler CF, Vignuzzi M, Peden AA, Beltrao P AND Krogan NJ. 2020. Comparative host-coronavirus protein interaction networks reveal pan-viral disease mechanisms. Science, 370(6521): eabe9403.

Gottlieb RL, Vaca CE, Paredes R, Mera J, Webb BJ, Perez G, Oguchi G, Ryan P, Nielsen BU, Brown M, Hidalgo A, Sachdeva Y, Mittal S, Osiyemi O, Skarbinski J, Juneja K, Hyland RH, Osinusi A, Chen S, Camus G, Abdelghany M, Davies S, Behenna-Renton N, Duff F, Marty FM, Katz MJ, Ginde AA, Brown SM, Schiffer JT AND Hill JA. 2021.

Early Remdesivir to Prevent Progression to Severe Covid-19 in Outpatients. N Engl J Med, 386(4): 305-315.

Guan W-j, Ni Z-y, Hu Y, Liang W-h, Ou C-q, He J-x, Liu L, Shan H, Lei C-l, Hui DSC, Du B, Li L-j, Zeng G, Yuen K-Y, Chen R-c, Tang C-l, Wang T, Chen P-y, Xiang J, Li S-y, Wang J-l, Liang Z-j, Peng Y-x, Wei L, Liu Y, Hu Y-h, Peng P, Wang J-m, Liu J-y, Chen Z, Li G, Zheng Z-j, Qiu S-q, Luo J, Ye C-j, Zhu S-y AND Zhong N-s. 2020. Clinical Characteristics of Coronavirus Disease 2019 in China. N Engl J Med, 382(18): 1708-1720.

Gubler DJ. 2011. Dengue, Urbanization and Globalization: The Unholy Trinity of the 21(st) Century. Trop Med Health, 39(4 Suppl): 3-11.

Gupta A, Gonzalez-Rojas Y, Juarez E, Crespo Casal M, Moya J, Falci DR, Sarkis E, Solis J, Zheng H, Scott N, Cathcart AL, Hebner CM, Sager J, Mogalian E, Tipple C, Peppercorn A, Alexander E, Pang PS, Free A, Brinson C, Aldinger M AND Shapiro AE. 2021. Early Treatment for Covid-19 with SARS-CoV-2 Neutralizing Antibody Sotrovimab. N Engl J Med, 385(21): 1941-1950.

Guzman MG, Alvarez M AND Halstead SB. 2013. Secondary infection as a risk factor for dengue hemorrhagic fever/dengue shock syndrome: an historical perspective and role of antibody-dependent enhancement of infection. Arch Virol, 158(7): 1445-1459.

Guzman MG, Gubler DJ, Izquierdo A, Martinez E AND Halstead SB. 2016. Dengue infection. Nat Rev Dis Primers, 2: 16055.

Halstead SB, Nimmannitya S AND Cohen SN. 1970. Observations related to pathogenesis of dengue hemorrhagic fever. IV. Relation of disease severity to antibody response and virus recovered. Yale J Biol Med, 42(5): 311-328.

Harrison AG, Lin T AND Wang P. 2020. Mechanisms of SARS-CoV-2 Transmission and Pathogenesis. Trends Immunol, 41(12): 1100-1115.

Hirabara SM, Serdan TDA, Gorjao R, Masi LN, Pithon-Curi TC, Covas DT, Curi R AND Durigon EL. 2021. SARS-COV-2 Variants: Differences and Potential of Immune Evasion. Front Cell Infect Microbiol, 11: 781429.

Hoffmann M, Kleine-Weber H AND Pöhlmann S. 2020. A Multibasic Cleavage Site in the Spike Protein of SARS-CoV-2 Is Essential for Infection of Human Lung Cells. Molecular Cell, 78(4): 779-784 e775.

Hoffmann M, Kleine-Weber H, Schroeder S, Krüger N, Herrler T, Erichsen S, Schiergens TS, Herrler G, Wu NH, Nitsche A, Müller MA, Drosten C AND Pöhlmann S. 2020. SARS-CoV-2 Cell Entry Depends on ACE2 and TMPRSS2 and Is Blocked by a Clinically Proven Protease Inhibitor. Cell, 181(2): 271-280 e278.

Holland PM, Abramson RD, Watson R AND Gelfand DH. 1991. Detection of specific polymerase chain reaction product by utilizing the 5'----3' exonuclease activity of Thermus aquaticus DNA polymerase. Proc Natl Acad Sci U S A, 88(16): 7276-7280.

Horby P, Lim WS, Emberson JR, Mafham M, Bell JL, Linsell L, Staplin N, Brightling C, Ustianowski A, Elmahi E, Prudon B, Green C, Felton T, Chadwick D, Rege K, Fegan C, Chappell LC, Faust SN, Jaki T, Jeffery K, Montgomery A, Rowan K, Juszczak E, Baillie JK, Haynes R AND Landray MJ. 2021. Dexamethasone in Hospitalized Patients with Covid-19. N Engl J Med, 384(8): 693-704.

Humphrey JM, Cleton NB, Reusken CB, Glesby MJ, Koopmans MP AND Abu-Raddad LJ. 2016. Dengue in the Middle East and North Africa: A Systematic Review. PLoS Negl Trop Dis, 10(12): e0005194.

Hwang Y-C, Lu R-M, Su S-C, Chiang P-Y, Ko S-H, Ke F-Y, Liang K-H, Hsieh T-Y AND Wu H-C. 2022. Monoclonal antibodies for COVID-19 therapy and SARS-CoV-2 detection. J Biomed Sci, 29(1): 1.

Ivanov AI. 2008. Pharmacological inhibition of endocytic pathways: is it specific enough to be useful? Methods Mol Biol, 440: 15-33.

Jayk Bernal A, Gomes da Silva MM, Musungaie DB, Kovalchuk E, Gonzalez A, Delos Reyes V, Martín-Quirós A, Caraco Y, Williams-Diaz A, Brown ML, Du J, Pedley A, Assaid C, Strizki J, Grobler JA, Shamsuddin HH, Tipping R, Wan H, Paschke A, Butterton JR, Johnson MG AND De Anda C. 2021. Molnupiravir for Oral Treatment of Covid-19 in Nonhospitalized Patients. N Engl J Med, 386(6): 509-520.

Jessie K, Fong MY, Devi S, Lam SK AND Wong KT. 2004. Localization of dengue virus in naturally infected human tissues, by immunohistochemistry and in situ hybridization. J Infect Dis, 189(8): 1411-1418.

Jindadamrongwech S, Thepparit C AND Smith DR. 2004. Identification of GRP 78 (BiP) as a liver cell expressed receptor element for dengue virus serotype 2. Arch Virol, 149(5): 915-927.

Kaminski MM, Abudayyeh OO, Gootenberg JS, Zhang F AND Collins JJ. 2021. CRISPR-based diagnostics. Nat Biomed Eng, 5(7): 643-656.

Kaptein SJF, Goethals O, Kiemel D, Marchand A, Kesteleyn B, Bonfanti JF, Bardiot D, Stoops B, Jonckers THM, Dallmeier K, Geluykens P, Thys K, Crabbe M, Chatel-Chaix L, Münster M, Querat G, Touret F, de Lamballerie X, Raboisson P, Simmen K, Chaltin P, Bartenschlager R, Van Loock M AND Neyts J. 2021. Publisher Correction: A pan-serotype dengue virus inhibitor targeting the NS3-NS4B interaction. Nature, 599(7883): E2.

Kellner MJ, Koob JG, Gootenberg JS, Abudayyeh OO AND Zhang F. 2019. SHERLOCK: nucleic acid detection with CRISPR nucleases. Nat Protoc, 14(10): 2986-3012.

Khan AG, Pickl-Herk A, Gajdzik L, Marlovits TC, Fuchs R AND Blaas D. 2010. Human rhinovirus 14 enters rhabdomyosarcoma cells expressing icam-1 by a clathrin-, caveolin-, and flotillin-independent pathway. J Virol, 84(8): 3984-3992.

Kim D, Lee JY, Yang JS, Kim JW, Kim VN AND Chang H. 2020. The Architecture of SARS-CoV-2 Transcriptome. Cell, 181(4): 914-921.e910.

Klein S, Cortese M, Winter SL, Wachsmuth-Melm M, Neufeldt CJ, Cerikan B, Stanifer ML, Boulant S, Bartenschlager R AND Chlanda P. 2020. SARS-CoV-2 structure and replication characterized by in situ cryo-electron tomography. Nat Commun, 11(1): 5885.

Ko HC, Wang YH, Liou KT, Chen CM, Chen CH, Wang WY, Chang S, Hou YC, Chen KT, Chen CF AND Shen YC. 2007. Anti-inflammatory effects and mechanisms of the ethanol extract of Evodia rutaecarpa and its bioactive components on neutrophils and microglial cells. Eur J Pharmacol, 555(2-3): 211-217.

Kokic G, Hillen HS, Tegunov D, Dienemann C, Seitz F, Schmitzova J, Farnung L, Siewert A, Höbartner C AND Cramer P. 2021. Mechanism of SARS-CoV-2 polymerase stalling by remdesivir. Nat Commun, 12(1): 279.

Korber B, Fischer WM, Gnanakaran S, Yoon H, Theiler J, Abfalterer W, Hengartner N, Giorgi EE, Bhattacharya T, Foley B, Hastie KM, Parker MD, Partridge DG, Evans CM, Freeman TM, de Silva TI, McDanal C, Perez LG, Tang H, Moon-Walker A, Whelan SP, LaBranche CC, Saphire EO AND Montefiori DC. 2020. Tracking Changes in SARS-CoV-2 Spike: Evidence that D614G Increases Infectivity of the COVID-19 Virus. Cell, 182(4): 812-827.

Kraemer MU, Sinka ME, Duda KA, Mylne AQ, Shearer FM, Barker CM, Moore CG, Carvalho RG, Coelho GE, Van Bortel W, Hendrickx G, Schaffner F, Elyazar IR, Teng HJ, Brady OJ, Messina JP, Pigott DM, Scott TW, Smith DL, Wint GR, Golding N AND Hay SI. 2015. The global distribution of the arbovirus vectors Aedes aegypti and Ae. albopictus. Elife, 4: e08347.

Kraemer MUG, Reiner RC, Brady OJ, Messina JP, Gilbert M, Pigott DM, Yi D, Johnson K, Earl L, Marczak LB, Shirude S, Davis Weaver N, Bisanzio D, Perkins TA, Lai S, Lu X, Jones P, Coelho GE, Carvalho RG, Van Bortel W, Marsboom C, Hendrickx G, Schaffner F, Moore CG, Nax HH, Bengtsson L, Wetter E, Tatem AJ, Brownstein JS, Smith DL, Lambrechts L, Cauchemez S, Linard C, Faria NR, Pybus OG, Scott TW, Liu Q, Yu H, Wint GRW, Hay SI AND Golding N. 2019. Past and future spread of the arbovirus vectors Aedes aegypti and Aedes albopictus. Nat Microbiol, 4(5): 854-863.

Krzyzaniak MA, Zumstein MT, Gerez JA, Picotti P AND Helenius A. 2013. Host cell entry of respiratory syncytial virus involves macropinocytosis followed by proteolytic activation of the F protein. PLoS Pathog, 9(4): e1003309.

Kunz S. 2009. Receptor binding and cell entry of Old World arenaviruses reveal novel aspects of virus-host interaction. Virology, 387(2): 245-249.

Kwissa M, Nakaya HI, Onlamoon N, Wrammert J, Villinger F, Perng GC, Yoksan S, Pattanapanyasat K, Chokephaibulkit K, Ahmed R AND Pulendran B. 2014. Dengue virus infection induces expansion of a CD14(+)CD16(+) monocyte population that stimulates plasmablast differentiation. Cell Host Microbe, 16(1): 115-127.

Kyriazopoulou E, Huet T, Cavalli G, Gori A, Kyprianou M, Pickkers P, Eugen-Olsen J, Clerici M, Veas F, Chatellier G, Kaplanski G, Netea MG, Pontali E, Gattorno M, Cauchois R, Kooistra E, Kox M, Bandera A, Beaussier H, Mangioni D, Dagna L, van der Meer JWM, Giamarellos-Bourboulis EJ, Hayem G, Kyriazopoulou E, Huet T, Cavalli

G, Gori A, Kyprianou M, Pickkers P, Eugen-Olsen J, Clerici M, Veas F, Chatellier G, Kaplanski G, Netea MG, Pontali E, Gattorno M, Cauchois R, Kooistra E, Kox M, Bandera A, Beaussier H, Mangioni D, Dagna L, van der Meer JWM, Giamarellos-Bourboulis EJ, Hayem G, Volpi S, Sormani MP, Signori A, Bozzi G, Minoia F, Aliberti S, Grasselli G, Alagna L, Lombardi A, Ungaro R, Agostoni C, Blasi F, Costantino G, Fracanzani AL, Montano N, Peyvandi F, Sottocorno M, Muscatello A, Filocamo G, Papadopoulos A, Mouktaroudi M, Karakike E, Saridaki M, Gkavogianni T, Katrini K, Vechlidis N, Avgoustou C, Chalvatzis S, Marantos T, Damoulari C, Damoraki G, Ktena S, Tsilika M, Koufargyris P, Karageorgos A, Droggiti D-I, Koliakou A, Poulakou G, Tsiakos K, Myrodia D-M, Gravvani A, Trontzas IP, Syrigos K, Kalomenidis I, Kranidioti E, Panagopoulos P, Petrakis V, Metallidis S, Loli G, Tsachouridou O, Dalekos GN, Gatselis N, Stefos A, Georgiadou S, Lygoura V, Milionis H, Kosmidou M, Papanikolaou IC, Akinosoglou K, Giannitsioti E, Chrysos G, Mavroudis P, Sidiropoulou C, Adamis G, Fragkou A, Rapti A, Alexiou Z, Symbardi S, Masgala A, Kostaki K, Kostis E, Samarkos M, Bakakos P, Tzavara V, Dimakou K, Tzatzagou G, Chini M, Kotsis V, Tsoukalas G, Bliziotis I, Doumas M, Argyraki A, Kainis I, Fantoni M, Cingolani A, Angheben A, Cardellino CS, Castelli F, Serino FS, Nicastri E, Ippolito G, Bassetti M AND Selmi C. 2021. Effect of anakinra on mortality in patients with COVID-19: a systematic review and patient-level meta-analysis. Lancet Rheumatol, 3(10): e690-e697.

Lamb J, Crawford ED, Peck D, Modell JW, Blat IC, Wrobel MJ, Lerner J, Brunet JP, Subramanian A, Ross KN, Reich M, Hieronymus H, Wei G, Armstrong SA, Haggarty SJ, Clemons PA, Wei R, Carr SA, Lander ES AND Golub TR. 2006. The Connectivity Map: using gene-expression signatures to connect small molecules, genes, and disease. Science, 313(5795): 1929-1935.

Lauer SA, Grantz KH, Bi Q, Jones FK, Zheng Q, Meredith HR, Azman AS, Reich NG AND Lessler J. 2020. The Incubation Period of Coronavirus Disease 2019 (COVID-19) From Publicly Reported Confirmed Cases: Estimation and Application. Ann Intern Med, 172(9): 577-582.

Le BL, Andreoletti G, Oskotsky T, Vallejo-Gracia A, Rosales R, Yu K, Kosti I, Leon KE, Bunis DG, Li C, Kumar GR, White KM, García-Sastre A, Ott M AND Sirota M. 2021. Transcriptomics-based drug repositioning pipeline identifies therapeutic candidates for COVID-19. Sci Rep, 11(1): 12310.

Lee S, Lee SO, Lee JE, Kim K-H, Lee SH, Hwang S, Kim S-W, Chang H-H, Kim Y, Bae S, Kim AS AND Kwon KT. 2022. Regdanvimab in patients with mild-to-moderate SARS-CoV-2 infection: A propensity score–matched retrospective cohort study. Int Immunopharmacol, 106: 108570.

Lee SY, Song MY, Kim D, Park C, Park DK, Kim DG, Yoo JS AND Kim YH. 2019. A Proteotranscriptomic-Based Computational Drug-Repositioning Method for Alzheimer's Disease. Front Pharmacol, 10: 1653.

Leela SL, Srisawat C, Sreekanth GP, Noisakran S, Yenchitsomanus P-t AND Limjindaporn T. 2016. Drug repurposing of minocycline against dengue virus infection. Biochem Biophys Res Commun, 478(1): 410-416.

Li J, Macdonald J AND von Stetten F. 2018. Review: a comprehensive summary of a decade development of the recombinase polymerase amplification. Analyst, 144(1): 31-67.

Li M, Zhang D, Li C, Zheng Z, Fu M, Ni F, Liu Y, Du T, Wang H, Griffin GE, Zhang M AND Hu Q. 2020. Characterization of Zika Virus Endocytic Pathways in Human Glioblastoma Cells. Front Microbiol, 11: 242.

Lim SCL, Hor CP, Tay KH, Mat Jelani A, Tan WH, Ker HB, Chow TS, Zaid M, Cheah WK, Lim HH, Khalid KE, Cheng JT, Mohd Unit H, An N, Nasruddin AB, Low LL, Khoo SWR, Loh JH, Zaidan NZ, Ab Wahab S, Song LH, Koh HM, King TL, Lai NM, Chidambaram SK, Peariasamy KM AND Group I-TS. 2022. Efficacy of Ivermectin Treatment on Disease Progression Among Adults With Mild to Moderate COVID-19 and Comorbidities: The I-TECH Randomized Clinical Trial. JAMA Intern Med, in press.

Liu TY, Knott GJ, Smock DCJ, Desmarais JJ, Son S, Bhuiya A, Jakhanwal S, Prywes N, Agrawal S, Díaz de León Derby M, Switz NA, Armstrong M, Harris AR, Charles EJ, Thornton BW, Fozouni P, Shu J, Stephens SI, Kumar GR, Zhao C, Mok A, Iavarone AT, Escajeda AM, McIntosh R, Kim S, Dugan EJ, Pollard KS, Tan MX, Ott M, Fletcher DA, Lareau LF, Hsu PD, Savage DF AND Doudna JA. 2021. Accelerated RNA detection using tandem CRISPR nucleases. Nat Chem Biol, 17(9): 982-988.

Loging W, Harland L AND Williams-Jones B. 2007. High-throughput electronic biology: mining information for drug discovery. Nat Rev Drug Discov, 6(3): 220-230.

Loo YM, McTamney PM, Arends RH, Abram ME, Aksyuk AA, Diallo S, Flores DJ, Kelly EJ, Ren K, Roque R, Rosenthal K, Streicher K, Tuffy KM, Bond NJ, Cornwell O, Bouquet J, Cheng LI, Dunyak J, Huang Y, Rosenbaum AI, Pilla Reddy V, Andersen H, Carnahan RH, Crowe JE, Jr., Kuehne AI, Herbert AS, Dye JM, Bright H, Kallewaard NL, Pangalos MN AND Esser MT. 2022. The SARS-CoV-2 monoclonal antibody combination, AZD7442, is protective in nonhuman primates and has an extended half-life in humans. Sci Transl Med, 14(635): eabl8124.

Louten J. 2016. Chapter 4 - Virus Replication. In *Essential Human Virology*: Elsevier Inc., pp. 49-70.

Lozach PY, Burleigh L, Staropoli I, Navarro-Sanchez E, Harriague J, Virelizier JL, Rey FA, Desprès P, Arenzana-Seisdedos F AND Amara A. 2005. Dendritic cell-specific intercellular adhesion molecule 3-grabbing non-integrin (DC-SIGN)-mediated enhancement of dengue virus infection is independent of DC-SIGN internalization signals. J Biol Chem, 280(25): 23698-23708.

Lu R, Zhao X, Li J, Niu P, Yang B, Wu H, Wang W, Song H, Huang B, Zhu N, Bi Y, Ma X, Zhan F, Wang L, Hu T, Zhou H, Hu Z, Zhou W, Zhao L, Chen J, Meng Y, Wang J, Lin Y, Yuan J, Xie Z, Ma J, Liu WJ, Wang D, Xu W, Holmes EC, Gao GF, Wu G, Chen W, Shi W AND Tan W. 2020. Genomic characterisation and epidemiology of 2019 novel coronavirus: implications for virus origins and receptor binding. Lancet, 395(10224): 565-574.

Lu X, Bambrick H, Pongsumpun P, Dhewantara PW, Toan DTT AND Hu W. 2021. Dengue outbreaks in the COVID-19 era: Alarm raised for Asia. PLoS Negl Trop Dis, 15(10): e0009778.

Ma Q, Liu J, Liu Q, Kang L, Liu R, Jing W, Wu Y AND Liu M. 2021. Global Percentage of Asymptomatic SARS-CoV-2 Infections Among the Tested Population and Individuals With Confirmed COVID-19 Diagnosis: A Systematic Review and Meta-analysis. JAMA Netw Open, 4(12): e2137257-e2137257.

Maginnis MS. 2018. Virus-Receptor Interactions: The Key to Cellular Invasion. J Mol Biol, 430(17): 2590-2611.

Malathi VG AND Renuka Devi P. 2019. ssDNA viruses: key players in global virome. Virusdisease, 30(1): 3-12.

Manoff SB, Sausser M, Falk Russell A, Martin J, Radley D, Hyatt D, Roberts CC, Lickliter J, Krishnarajah J, Bett A, Dubey S, Finn T AND Coller BA. 2019. Immunogenicity and safety of an investigational tetravalent recombinant subunit vaccine for dengue: results of a Phase I randomized clinical trial in flavivirus-naïve adults. Hum Vaccin Immunother, 15(9): 2195-2204.

Martinez-Gutierrez M, Correa-Londoño LA, Castellanos JE, Gallego-Gómez JC AND Osorio JE. 2014. Lovastatin Delays Infection and Increases Survival Rates in AG129 Mice Infected with Dengue Virus Serotype 2. PLoS One, 9(2): e87412.

Martínez-Gutierrez M, Castellanos JE AND Gallego-Gómez JC. 2011. Statins reduce dengue virus production via decreased virion assembly. Intervirology, 54(4): 202-216.

Mayer SV, Tesh RB AND Vasilakis N. 2017. The emergence of arthropod-borne viral diseases: A global prospective on dengue, chikungunya and zika fevers. Acta tropica, 166: 155-163.

Mazzon M, Ortega-Prieto AM, Imrie D, Luft C, Hess L, Czieso S, Grove J, Skelton JK, Farleigh L, Bugert JJ, Wright E, Temperton N, Angell R, Oxenford S, Jacobs M, Ketteler R, Dorner M AND Marsh M. 2019. Identification of Broad-Spectrum Antiviral Compounds by Targeting Viral Entry. Viruses, 11(2): 176.

Mekkaoui L, Bentley EM, Ferrari M, Lamb K, Ward K, Karattil R, Akbar Z, Bughda R, Sillibourne J, Onuoha S, Mattiuzzo G, Takeuchi Y AND Pule M. 2021. Optimised Method for the Production and Titration of Lentiviral Vectors Pseudotyped with the SARS-CoV-2 Spike. Bio Protoc, 11(16): e4194.

Mercer J AND Helenius A. 2008. Vaccinia virus uses macropinocytosis and apoptotic mimicry to enter host cells. Science, 320(5875): 531-535.

Mercer J AND Helenius A. 2009. Virus entry by macropinocytosis. Nat Cell Biol, 11(5): 510-520.

Mercer J, Schelhaas M AND Helenius A. 2010. Virus entry by endocytosis. Annu Rev Biochem, 79: 803-833.

Mesev EV, LeDesma RA AND Ploss A. 2019. Decoding type I and III interferon signalling during viral infection. Nat Microbiol, 4(6): 914-924.

Miller JL, de Wet BJ, Martinez-Pomares L, Radcliffe CM, Dwek RA, Rudd PM AND Gordon S. 2008. The mannose receptor mediates dengue virus infection of macrophages. PLoS Pathog, 4(2): e17.

Mlcochova P, Kemp SA, Dhar MS, Papa G, Meng B, Ferreira I, Datir R, Collier DA, Albecka A, Singh S, Pandey R, Brown J, Zhou J, Goonawardane N, Mishra S, Whittaker C, Mellan T, Marwal R, Datta M, Sengupta S, Ponnusamy K, Radhakrishnan VS, Abdullahi A, Charles O, Chattopadhyay P, Devi P, Caputo D, Peacock T, Wattal C, Goel N, Satwik A, Vaishya R, Agarwal M, Mavousian A, Lee JH, Bassi J, Silacci-Fegni C, Saliba C, Pinto D, Irie T, Yoshida I, Hamilton WL, Sato K, Bhatt S, Flaxman S, James LC, Corti D, Piccoli L, Barclay WS, Rakshit P, Agrawal A AND Gupta RK. 2021. SARS-CoV-2 B.1.617.2 Delta variant replication and immune evasion. Nature, 599(7883): 114-119.

Mühlemann B, Jones TC, Damgaard PB, Allentoft ME, Shevnina I, Logvin A, Usmanova E, Panyushkina IP, Boldgiv B, Bazartseren T, Tashbaeva K, Merz V, Lau N, Smrčka V, Voyakin D, Kitov E, Epimakhov A, Pokutta D, Vicze M, Price TD, Moiseyev V, Hansen AJ, Orlando L, Rasmussen S, Sikora M, Vinner L, Osterhaus A, Smith DJ, Glebe D, Fouchier RAM, Drosten C, Sjögren KG, Kristiansen K AND Willerslev E. 2018. Ancient hepatitis B viruses from the Bronze Age to the Medieval period. Nature, 557(7705): 418-423.

Mukherjee S, Sirohi D, Dowd KA, Chen Z, Diamond MS, Kuhn RJ AND Pierson TC. 2016. Enhancing dengue virus maturation using a stable furin over-expressing cell line. Virology, 497: 33-40.

Murgolo N, Therien AG, Howell B, Klein D, Koeplinger K, Lieberman LA, Adam GC, Flynn J, McKenna P, Swaminathan G, Hazuda DJ AND Olsen DB. 2021. SARS-CoV-2 tropism, entry, replication, and propagation: Considerations for drug discovery and development. PLoS Pathog, 17(2): e1009225.

Murphy BR AND Whitehead SS. 2011. Immune response to dengue virus and prospects for a vaccine. Annu Rev Immunol, 29: 587-619.

Nanaware N, Banerjee A, Mullick Bagchi S, Bagchi P AND Mukherjee A. 2021. Dengue Virus Infection: A Tale of Viral Exploitations and Host Responses. Viruses, 13(10): 1967.

Nanbo A, Imai M, Watanabe S, Noda T, Takahashi K, Neumann G, Halfmann P AND Kawaoka Y. 2010. Ebolavirus is internalized into host cells via macropinocytosis in a viral glycoprotein-dependent manner. PLoS Pathog, 6(9): e1001121.

Nascimento EJ, Braga-Neto U, Calzavara-Silva CE, Gomes AL, Abath FG, Brito CA, Cordeiro MT, Silva AM, Magalhães C, Andrade R, Gil LH AND Marques ET, Jr. 2009. Gene expression profiling during early acute febrile stage of dengue infection can predict the disease outcome. PLoS One, 4(11): e7892.

Nguyen M AND Haenni AL. 2003. Expression strategies of ambisense viruses. Virus Res, 93(2): 141-150.

National Library of Medicine (U.S.), NLM. *Study of a Dengue Vaccine (V180) in Healthy Adults (V180-001)*, 15 January 2019, Identifier: NCT01477580 [accessed on March 2022]. Available from https://clinicaltrials.gov/ct2/show/NCT01477580.

National Library of Medicine (U.S.), NLM. *Efficacy, Safety and Immunogenicity of Takeda's Tetravalent Dengue Vaccine (TDV) in Healthy Children (TIDES)*, 18 August 2021, Identifier: NCT02747927 [accessed on March 2022]. Available from https://clinicaltrials.gov/ct2/show/NCT02747927.

National Library of Medicine (U.S.), NLM. *Metformin in Dengue With Obesity (MeDO)*, 12 October 2021, Identifier: NCT04377451 [accessed on March 2022]. Available from https://www.clinicaltrials.gov/ct2/show/NCT04377451.

National Library of Medicine (U.S.), NLM. *A Study of JNJ-64281802 in Participants With Confirmed Dengue Fever*, 23 March 2022, Identifier: NCT04906980 [accessed on March 2022]. Available from https://www.clinicaltrials.gov/ct2/show/NCT04906980.

Nomura R, Kiyota A, Suzaki E, Kataoka K, Ohe Y, Miyamoto K, Senda T AND Fujimoto T. 2004. Human coronavirus 229E binds to CD13 in rafts and enters the cell through caveolae. J Virol, 78(16): 8701-8708.

Olive M-M, Baldet T, Devillers J, Fite J, Paty M-C, Paupy C, Quénel P, Quillery E, Raude J, Stahl J-P, Thiann-Bo-Morel M AND Roiz D. 2020. The COVID-19 pandemic should not jeopardize dengue control. PLoS Negl Trop Dis, 14(9): e0008716.

Oliveira BB, Veigas B AND Baptista PV. 2021. Isothermal Amplification of Nucleic Acids: The Race for the Next “Gold Standard”. Front Sens, 2: 752600.

Osorio JE, Wallace D AND Stinchcomb DT. 2016. A recombinant, chimeric tetravalent dengue vaccine candidate based on a dengue virus serotype 2 backbone. Expert Rev Vaccines, 15(4): 497-508.

Osterman A, Badell I, Basara E, Stern M, Kriesel F, Eletreby M, Öztan GN, Huber M, Autenrieth H, Knabe R, Späth PM, Muenchhoff M, Graf A, Krebs S, Blum H, Durner J, Czibere L, Dächert C, Kaderali L, Baldauf H-M AND Keppler OT. 2022. Impaired detection of omicron by SARS-CoV-2 rapid antigen tests. Med Microbiol Immunol, in press.

Osuna-Ramos JF, Reyes-Ruiz JM AND Del Ángel RM. 2018. The Role of Host Cholesterol During Flavivirus Infection. Front Cell Infect Microbiol, 8: 388.

Pasdeloup D, Blondel D, Isidro AL AND Rixon FJ. 2009. Herpesvirus capsid association with the nuclear pore complex and viral DNA release involve the nucleoporin CAN/Nup214 and the capsid protein pUL25. J Virol, 83(13): 6610-6623.

Payne S. 2017. Chapter 1 - Introduction to Animal Viruses. In *Viruses*, edited by S. Payne: Academic Press, pp. 1-11.

Payne S. 2017. Chapter 3 - Virus Interactions With the Cell. In *Viruses*, edited by S. Payne: Academic Press, pp. 23-35.

Peacock TP, Goldhill DH, Zhou J, Baillon L, Frise R, Swann OC, Kugathasan R, Penn R, Brown JC, Sanchez-David RY, Braga L, Williamson MK, Hassard JA, Staller E, Hanley B, Osborn M, Giacca M, Davidson AD, Matthews DA AND Barclay WS. 2021. The furin cleavage site in the SARS-CoV-2 spike protein is required for transmission in ferrets. Nat Microbiol, 6(7): 899-909.

Pelkmans L. 2005. Secrets of caveolae- and lipid raft-mediated endocytosis revealed by mammalian viruses. Biochim Biophys Acta, 1746(3): 295-304.

Peng R, Wu LA, Wang Q, Qi J AND Gao GF. 2021. Cell entry by SARS-CoV-2. Trends Biochem Sci, 46(10): 848-860.

Piccini LE, Castilla V AND Damonte EB. 2015. Dengue-3 Virus Entry into Vero Cells: Role of Clathrin-Mediated Endocytosis in the Outcome of Infection. PLoS One, 10(10): e0140824.

Piepenburg O, Williams CH, Stemple DL AND Armes NA. 2006. DNA detection using recombination proteins. PLoS Biol, 4(7): e204.

Plante JA, Liu Y, Liu J, Xia H, Johnson BA, Lokugamage KG, Zhang X, Muruato AE, Zou J, Fontes-Garfias CR, Mirchandani D, Scharton D, Bilello JP, Ku Z, An Z, Kalveram B, Freiberg AN, Menachery VD, Xie X, Plante KS, Weaver SC AND Shi PY. 2021. Spike mutation D614G alters SARS-CoV-2 fitness. Nature, 592(7852): 116-121.

Pollard BS, JC BL AND Pollard JR. 2020. Classical Drug Digitoxin Inhibits Influenza Cytokine Storm, With Implications for Covid-19 Therapy. In Vivo, 34(6): 3723-3730.

Poltronieri P, Sun B AND Mallardo M. 2015. RNA Viruses: RNA Roles in Pathogenesis, Coreplication and Viral Load. Curr Genomics, 16(5): 327-335.

Porta M. 2008. *A Dictionary of Epidemiology* 5ed: Oxford University Press. Original edition, 2008. ISBN 9780195314496

Praena B, Bello-Morales R AND López-Guerrero JA. 2020. Hsv-1 Endocytic Entry into a Human Oligodendrocytic Cell Line is Mediated by Clathrin and Dynamin but Not Caveolin. Viruses, 12(7): 734.

Priyamvada L AND Satheshkumar PS. 2021. Variola and Monkeypox Viruses (Poxviridae). In *Encyclopedia of Virology (Fourth Edition)*, edited by D.H. Bamford andM. Zuckerman. Oxford: Academic Press, pp. 868-874.

Pushpakom S, Iorio F, Eyers PA, Escott KJ, Hopper S, Wells A, Doig A, Guilliams T, Latimer J, McNamee C, Norris A, Sanseau P, Cavalla D AND Pirmohamed M. 2019. Drug repurposing: progress, challenges and recommendations. Nat Rev Drug Discov, 18(1): 41-58.

Qin C, Zhou L, Hu Z, Zhang S, Yang S, Tao Y, Xie C, Ma K, Shang K, Wang W AND Tian DS. 2020. Dysregulation of Immune Response in Patients With Coronavirus 2019 (COVID-19) in Wuhan, China. Clin Infect Dis, 71(15): 762-768.

Rajapakse S, Rodrigo C AND Rajapakse A. 2012. Treatment of dengue fever. Infect Drug Resist, 5: 103-112.

Ramos-Castañeda J, Barreto Dos Santos F, Martínez-Vega R, Galvão de Araujo JM, Joint G AND Sarti E. 2017. Dengue in Latin America: Systematic Review of Molecular Epidemiological Trends. PLoS Negl Trop Dis, 11(1): e0005224.

Rampersad S AND Tennant P. 2018. Chapter 3 - Replication and Expression Strategies of Viruses. In *Viruses*: Elsevier Inc., pp. 55-82.

Ravindran MS, Bagchi P, Cunningham CN AND Tsai B. 2016. Opportunistic intruders: how viruses orchestrate ER functions to infect cells. Nat Rev Microbiol, 14(7): 407-420.

Razonable RR, Pawlowski C, O'Horo JC, Arndt LL, Arndt R, Bierle DM, Borgen MD, Hanson SN, Hedin MC, Lenehan P, Puranik A, Seville MT, Speicher LL, Tulledge-Scheitel SM, Venkatakrishnan AJ, Wilker CG, Badley AD AND Ganesh R. 2021. Casirivimab-Imdevimab treatment is associated with reduced rates of hospitalization among high-risk patients with mild to moderate coronavirus disease-19. eClinicalMedicine, 40: 101102.

Reyes-Del Valle J, Chávez-Salinas S, Medina F AND Del Angel RM. 2005. Heat shock protein 90 and heat shock protein 70 are components of dengue virus receptor complex in human cells. J Virol, 79(8): 4557-4567.

Rhoads D, Peaper DR, She RC, Nolte FS, Wojewoda CM, Anderson NW AND Pritt BS. 2020. College of American Pathologists (CAP) Microbiology Committee Perspective: Caution Must Be Used in Interpreting the Cycle Threshold (Ct) Value. Clin Infect Dis, 72(10): e685-e686.

Richards AL, Soares-Martins JA, Riddell GT AND Jackson WT. 2014. Generation of unique poliovirus RNA replication organelles. mBio, 5(2): e00833.

Ripa I, Andreu S, López-Guerrero JA AND Bello-Morales R. 2021. Membrane Rafts: Portals for Viral Entry. Front Microbiol, 12: 631274.

Riva L, Yuan S, Yin X, Martin-Sancho L, Matsunaga N, Pache L, Burgstaller-Muehlbacher S, De Jesus PD, Teriete P, Hull MV, Chang MW, Chan JF-W, Cao J, Poon VK-M, Herbert KM, Cheng K, Nguyen T-TH, Rubanov A, Pu Y, Nguyen C, Choi A, Rathnasinghe R, Schotsaert M, Miorin L, Dejosez M, Zwaka TP, Sit K-Y, Martinez-Sobrido L, Liu W-C, White KM, Chapman ME, Lendy EK, Glynne RJ, Albrecht R, Ruppin E, Mesecar AD, Johnson JR, Benner C, Sun R, Schultz PG, Su AI, García-Sastre A,

Chatterjee AK, Yuen K-Y AND Chanda SK. 2020. Discovery of SARS-CoV-2 antiviral drugs through large-scale compound repurposing. Nature, 586(7827): 113-119.

Rodenhuis-Zybert IA, Wilschut J AND Smit JM. 2010. Dengue virus life cycle: viral and host factors modulating infectivity. Cell Mol Life Sci, 67(16): 2773-2786.

Rosa RB, Dantas WM, do Nascimento JCF, da Silva MV, de Oliveira RN AND Pena LJ. 2021. In Vitro and In Vivo Models for Studying SARS-CoV-2, the Etiological Agent Responsible for COVID-19 Pandemic. Viruses, 13(3): 379.

Rosas IO, Bräu N, Waters M, Go RC, Hunter BD, Bhagani S, Skiest D, Aziz MS, Cooper N, Douglas IS, Savic S, Youngstein T, Del Sorbo L, Cubillo Gracian A, De La Zerda DJ, Ustianowski A, Bao M, Dimonaco S, Graham E, Matharu B, Spotswood H, Tsai L AND Malhotra A. 2021. Tocilizumab in Hospitalized Patients with Severe Covid-19 Pneumonia. N Engl J Med, 384(16): 1503-1516.

Ryu W-S. 2017. Chapter 17 - Retroviruses. In *Molecular Virology of Human Pathogenic Viruses*, edited by W.-S. Ryu. Boston: Academic Press, pp. 227-246.

Salazar DE AND Gormley G. 2017. Chapter 41 - Modern Drug Discovery and Development. In *Clinical and Translational Science (Second Edition)*, edited by D. Robertson andG.H. Williams: Academic Press, pp. 719-743.

Salazar G, Zhang N, Fu T-M AND An Z. 2017. Antibody therapies for the prevention and treatment of viral infections. npj Vaccines, 2(1): 19.

Salvagno GL, Henry BM, Pighi L, De Nitto S, Montagnana M AND Lippi G. 2022. SARS-CoV-2 Omicron infection is associated with high nasopharyngeal viral load. J Infect, in press.

Sankaran N. 2018. On the historical significance of Beijerinck and his contagium vivum fluidum for modern virology. Hist Philos Life Sci, 40(3): 41.

Saravolatz LD, Depcinski S AND Sharma M. 2022. Molnupiravir and Nirmatrelvir-Ritonavir: Oral COVID Antiviral Drugs. Clin Infect Dis, in press.

Schubert K, Karousis ED, Jomaa A, Scaiola A, Echeverria B, Gurzeler L-A, Leibundgut M, Thiel V, Mühlemann O AND Ban N. 2020. SARS-CoV-2 Nsp1 binds the ribosomal mRNA channel to inhibit translation. Nat Struct Mol Biol, 27(10): 959-966.

Scudellari M. 2021. How the coronavirus infects cells - and why Delta is so dangerous. Nature, 595(7869): 640-644.

Shi R, Hou L, Wei L AND Liu J. 2021. Involvement of adaptor proteins in clathrin-mediated endocytosis of virus entry. Microb Pathog, 161(Pt A): 105278.

Shidham VB. 2019. CellBlockistry: Chemistry and art of cell-block making - A detailed review of various historical options with recent advances. Cytojournal, 16: 12.

Shrotri M, Swinnen T, Kampmann B AND Parker EPK. 2021. An interactive website tracking COVID-19 vaccine development. Lancet Glob Health, 9(5): e590-e592.

Shukla D AND Spear PG. 2001. Herpesviruses and heparan sulfate: an intimate relationship in aid of viral entry. J Clin Invest, 108(4): 503-510.

Shukla R, Ramasamy V, Shanmugam RK, Ahuja R AND Khanna N. 2020. Antibody-Dependent Enhancement: A Challenge for Developing a Safe Dengue Vaccine. Front Cell Infect Microbiol, 10: 572681.

Silva S, Magalhães JJF AND Pena L. 2021. Simultaneous Circulation of DENV, CHIKV, ZIKV and SARS-CoV-2 in Brazil: an Inconvenient Truth. One Health, 12: 100205.

Smith JL, Stein DA, Shum D, Fischer MA, Radu C, Bhinder B, Djaballah H, Nelson JA, Früh K AND Hirsch AJ. 2014. Inhibition of dengue virus replication by a class of small-molecule compounds that antagonize dopamine receptor d4 and downstream mitogen-activated protein kinase signaling. J Virol, 88(10): 5533-5542.

Soleimani Zakeri NS, Pashazadeh S AND MotieGhader H. 2021. Drug Repurposing for Alzheimer's Disease Based on Protein-Protein Interaction Network. Biomed Res Int, 2021: 1280237.

Spoden G, Freitag K, Husmann M, Boller K, Sapp M, Lambert C AND Florin L. 2008. Clathrin- and caveolin-independent entry of human papillomavirus type 16--involvement of tetraspanin-enriched microdomains (TEMs). PLoS One, 3(10): e3313.

Sridhar S, Luedtke A, Langevin E, Zhu M, Bonaparte M, Machabert T, Savarino S, Zambrano B, Moureau A, Khromava A, Moodie Z, Westling T, Mascareñas C, Frago

C, Cortés M, Chansinghakul D, Noriega F, Bouckenooghe A, Chen J, Ng SP, Gilbert PB, Gurunathan S AND DiazGranados CA. 2018. Effect of Dengue Serostatus on Dengue Vaccine Safety and Efficacy. N Engl J Med, 379(4): 327-340.

Stass R, Ng WM, Kim YC AND Huiskonen JT. 2019. Chapter Two - Structures of enveloped virions determined by cryogenic electron microscopy and tomography. In *Adv Virus Res*, edited by F.A. Rey: Academic Press, pp. 35-71.

Strauss JH AND Strauss EG. 2008. CHAPTER 1 - Overview of Viruses and Virus Infection. In *Viruses and Human Disease (Second Edition)*, edited by J.H. Strauss andE.G. Strauss. London: Academic Press, pp. 1-33.

Subramanian A, Narayan R, Corsello SM, Peck DD, Natoli TE, Lu X, Gould J, Davis JF, Tubelli AA, Asiedu JK, Lahr DL, Hirschman JE, Liu Z, Donahue M, Julian B, Khan M, Wadden D, Smith IC, Lam D, Liberzon A, Toder C, Bagul M, Orzechowski M, Enache OM, Piccioni F, Johnson SA, Lyons NJ, Berger AH, Shamji AF, Brooks AN, Vrcic A, Flynn C, Rosains J, Takeda DY, Hu R, Davison D, Lamb J, Ardlie K, Hogstrom L, Greenside P, Gray NS, Clemons PA, Silver S, Wu X, Zhao WN, Read-Button W, Wu X, Haggarty SJ, Ronco LV, Boehm JS, Schreiber SL, Doench JG, Bittker JA, Root DE, Wong B AND Golub TR. 2017. A Next Generation Connectivity Map: L1000 Platform and the First 1,000,000 Profiles. Cell, 171(6): 1437-1452 e1417.

Suksanpaisan L, Susantad T AND Smith DR. 2009. Characterization of dengue virus entry into HepG2 cells. J Biomed Sci, 16(1): 17.

Szymański P, Markowicz M AND Mikiciuk-Olasik E. 2012. Adaptation of high-throughput screening in drug discovery-toxicological screening tests. Int J Mol Sci, 13(1): 427-452.

Tanaka T, Asano T, Okui T, Kuraoka S, Singh SA, Aikawa M AND Aikawa E. 2021. Computational Screening Strategy for Drug Repurposing Identified Niclosamide as Inhibitor of Vascular Calcification. Front Cardiovasc Med, 8: 826529.

Tandon R, Mitra D, Sharma P, McCandless MG, Stray SJ, Bates JT AND Marshall GD. 2020. Effective screening of SARS-CoV-2 neutralizing antibodies in patient serum using lentivirus particles pseudotyped with SARS-CoV-2 spike glycoprotein. Sci Rep, 10(1): 19076.

Tao YJ AND Ye Q. 2010. RNA Virus Replication Complexes. PLoS Pathog, 6(7): e1000943.

Tassaneetrithep B, Burgess TH, Granelli-Piperno A, Trumpfheller C, Finke J, Sun W, Eller MA, Pattanapanyasat K, Sarasombath S, Birx DL, Steinman RM, Schlesinger S AND Marovich MA. 2003. DC-SIGN (CD209) mediates dengue virus infection of human dendritic cells. J Exp Med, 197(7): 823-829.

Tegally H, Wilkinson E, Giovanetti M, Iranzadeh A, Fonseca V, Giandhari J, Doolabh D, Pillay S, San EJ, Msomi N, Mlisana K, von Gottberg A, Walaza S, Allam M, Ismail A, Mohale T, Glass AJ, Engelbrecht S, Van Zyl G, Preiser W, Petruccione F, Sigal A, Hardie D, Marais G, Hsiao NY, Korsman S, Davies MA, Tyers L, Mudau I, York D, Maslo C, Goedhals D, Abrahams S, Laguda-Akingba O, Alisoltani-Dehkordi A, Godzik A, Wibmer CK, Sewell BT, Lourenço J, Alcantara LCJ, Kosakovsky Pond SL, Weaver S, Martin D, Lessells RJ, Bhiman JN, Williamson C AND de Oliveira T. 2021. Detection of a SARS-CoV-2 variant of concern in South Africa. Nature, 592(7854): 438-443.

Thepparit C AND Smith DR. 2004. Serotype-specific entry of dengue virus into liver cells: identification of the 37-kilodalton/67-kilodalton high-affinity laminin receptor as a dengue virus serotype 1 receptor. J Virol, 78(22): 12647-12656.

Thoms M, Buschauer R, Ameismeier M, Koepke L, Denk T, Hirschenberger M, Kratzat H, Hayn M, Mackens-Kiani T, Cheng J, Straub JH, Stürzel CM, Fröhlich T, Berninghausen O, Becker T, Kirchhoff F, Sparrer KMJ AND Beckmann R. 2020. Structural basis for translational shutdown and immune evasion by the Nsp1 protein of SARS-CoV-2. Science, 369(6508): 1249-1255.

Tugizov SM, Herrera R AND Palefsky JM. 2013. Epstein-Barr virus transcytosis through polarized oral epithelial cells. J Virol, 87(14): 8179-8194.

Uva P, Bosco MC, Eva A, Conte M, Garaventa A, Amoroso L AND Cangelosi D. 2021. Connectivity Map Analysis Indicates PI3K/Akt/mTOR Inhibitors as Potential Anti-Hypoxia Drugs in Neuroblastoma. Cancers, 13(11): 2809.

van der Schaar HM, Rust MJ, Chen C, van der Ende-Metselaar H, Wilschut J, Zhuang X AND Smit JM. 2008. Dissecting the cell entry pathway of dengue virus by single-particle tracking in living cells. PLoS Pathog, 4(12): e1000244.

VanBlargan LA, Errico JM, Halfmann PJ, Zost SJ, Crowe JE, Purcell LA, Kawaoka Y, Corti D, Fremont DH AND Diamond MS. 2022. An infectious SARS-CoV-2 B.1.1.529 Omicron virus escapes neutralization by therapeutic monoclonal antibodies. Nat Med, 28(3): 490-495.

Vashist SK. 2017. Point-of-Care Diagnostics: Recent Advances and Trends. Biosensors (Basel), 7(4): 62.

Vasilakis N, Cardosa J, Hanley KA, Holmes EC AND Weaver SC. 2011. Fever from the forest: prospects for the continued emergence of sylvatic dengue virus and its impact on public health. Nat Rev Microbiol, 9(7): 532-541.

Vengoji R, Atri P, Macha MA, Seshacharyulu P, Perumal N, Mallya K, Liu Y, Smith LM, Rachagani S, Mahapatra S, Ponnusamy MP, Jain M, Batra SK AND Shonka N. 2021. Differential gene expression-based connectivity mapping identified novel drug candidate and improved Temozolomide efficacy for Glioblastoma. J Exp Clin Cancer Res, 40(1): 335.

Verma DK, Gupta D AND Lal SK. 2018. Host Lipid Rafts Play a Major Role in Binding and Endocytosis of Influenza A Virus. Viruses, 10(11): 650.

Viana R, Moyo S, Amoako DG, Tegally H, Scheepers C, Althaus CL, Anyaneji UJ, Bester PA, Boni MF, Chand M, Choga WT, Colquhoun R, Davids M, Deforche K, Doolabh D, du Plessis L, Engelbrecht S, Everatt J, Giandhari J, Giovanetti M, Hardie D, Hill V, Hsiao N-Y, Iranzadeh A, Ismail A, Joseph C, Joseph R, Koopile L, Kosakovsky Pond SL, Kraemer MUG, Kuate-Lere L, Laguda-Akingba O, Lesetedi-Mafoko O, Lessells RJ, Lockman S, Lucaci AG, Maharaj A, Mahlangu B, Maponga T, Mahlakwane K, Makatini Z, Marais G, Maruapula D, Masupu K, Matshaba M, Mayaphi S, Mbhele N, Mbulawa MB, Mendes A, Mlisana K, Mnguni A, Mohale T, Moir M, Moruisi K, Mosepele M, Motsatsi G, Motswaledi MS, Mphoyakgosi T, Msomi N, Mwangi PN, Naidoo Y, Ntuli N, Nyaga M, Olubayo L, Pillay S, Radibe B, Ramphal Y, Ramphal U, San JE, Scott L, Shapiro R, Singh L, Smith-Lawrence P, Stevens W, Strydom A, Subramoney K, Tebeila N, Tshiabuila D, Tsui J, van Wyk S, Weaver S, Wibmer CK, Wilkinson E, Wolter N, Zarebski AE, Zuze B, Goedhals D, Preiser W, Treurnicht F, Venter M, Williamson C, Pybus OG, Bhiman J, Glass A, Martin DP, Rambaut A, Gaseitsiwe S, von Gottberg A AND de Oliveira T. 2022. Rapid epidemic expansion of the SARS-CoV-2 Omicron variant in southern Africa. Nature, 603(7902): 679-686.

Volz E, Hill V, McCrone JT, Price A, Jorgensen D, O'Toole Á, Southgate J, Johnson R, Jackson B, Nascimento FF, Rey SM, Nicholls SM, Colquhoun RM, da Silva Filipe A, Shepherd J, Pascall DJ, Shah R, Jesudason N, Li K, Jarrett R, Pacchiarini N, Bull M, Geidelberg L, Siveroni I, Goodfellow I, Loman NJ, Pybus OG, Robertson DL, Thomson EC, Rambaut A AND Connor TR. 2021. Evaluating the Effects of SARS-CoV-2 Spike Mutation D614G on Transmissibility and Pathogenicity. Cell, 184(1): 64-75.

Volz E, Mishra S, Chand M, Barrett JC, Johnson R, Geidelberg L, Hinsley WR, Laydon DJ, Dabrera G, O'Toole Á, Amato R, Ragonnet-Cronin M, Harrison I, Jackson B, Ariani CV, Boyd O, Loman NJ, McCrone JT, Gonçalves S, Jorgensen D, Myers R, Hill V, Jackson DK, Gaythorpe K, Groves N, Sillitoe J, Kwiatkowski DP, Flaxman S, Ratmann O, Bhatt S, Hopkins S, Gandy A, Rambaut A AND Ferguson NM. 2021. Assessing transmissibility of SARS-CoV-2 lineage B.1.1.7 in England. Nature, 593(7858): 266-269.

Walsh D AND Mohr I. 2011. Viral subversion of the host protein synthesis machinery. Nat Rev Microbiol, 9(12): 860-875.

Wan J, Zhang Z, Tian S, Huang S, Jin H, Liu X AND Zhang W. 2022. Single cell study of cellular diversity and mutual communication in chronic heart failure and drug repositioning. Genomics, 114(3): 110322.

Whitehorn J, Nguyen CVV, Khanh LP, Kien DTH, Quyen NTH, Tran NTT, Hang NT, Truong NT, Hue Tai LT, Cam Huong NT, Nhon VT, Van Tram T, Farrar J, Wolbers M, Simmons CP AND Wills B. 2016. Lovastatin for the Treatment of Adult Patients With Dengue: A Randomized, Double-Blind, Placebo-Controlled Trial. Clin Infect Dis, 62(4): 468-476.

WHO. *Dengue and severe dengue - Fact sheets*, 10 January 2022 [accessed on February 2022]. Available from https://www.who.int/news-room/fact-sheets/detail/dengue-and-severe-dengue.

Wilder-Smith A, Quam M, Sessions O, Rocklov J, Liu-Helmersson J, Franco L AND Khan K. 2014. The 2012 dengue outbreak in Madeira: exploring the origins. Euro Surveill, 19(8): 20718.

Wilder-Smith A, Flasche S AND Smith PG. 2019. Vaccine-attributable severe dengue in the Philippines. Lancet, 394(10215): 2151-2152.

Wilder-Smith A, Ooi EE, Horstick O AND Wills B. 2019. Dengue. Lancet, 393(10169): 350-363.

Wu F, Zhao S, Yu B, Chen YM, Wang W, Song ZG, Hu Y, Tao ZW, Tian JH, Pei YY, Yuan ML, Zhang YL, Dai FH, Liu Y, Wang QM, Zheng JJ, Xu L, Holmes EC AND Zhang YZ. 2020. A new coronavirus associated with human respiratory disease in China. Nature, 579(7798): 265-269.

Wu SJ, Grouard-Vogel G, Sun W, Mascola JR, Brachtel E, Putvatana R, Louder MK, Filgueira L, Marovich MA, Wong HK, Blauvelt A, Murphy GS, Robb ML, Innes BL, Birx DL, Hayes CG AND Frankel SS. 2000. Human skin Langerhans cells are targets of dengue virus infection. Nat Med, 6(7): 816-820.

Wu Y AND Zhao S. 2021. Furin cleavage sites naturally occur in coronaviruses. Stem Cell Res, 50: 102115.

Xiong Y, Liu Y, Cao L, Wang D, Guo M, Jiang A, Guo D, Hu W, Yang J, Tang Z, Wu H, Lin Y, Zhang M, Zhang Q, Shi M, Liu Y, Zhou Y, Lan K AND Chen Y. 2020. Transcriptomic characteristics of bronchoalveolar lavage fluid and peripheral blood mononuclear cells in COVID-19 patients. Emerg Microbes Infect, 9(1): 761-770.

Xu H-T, Colby-Germinario SP, Hassounah SA, Fogarty C, Osman N, Palanisamy N, Han Y, Oliveira M, Quan Y AND Wainberg MA. 2017. Evaluation of Sofosbuvir (β-D-2′-deoxy-2′-α-fluoro-2′-β-C-methyluridine) as an inhibitor of Dengue virus replication. Sci Rep, 7(1): 6345.

Yang C, Zhang H, Chen M, Wang S, Qian R, Zhang L, Huang X, Wang J, Liu Z, Qin W, Wang C, Hang H AND Wang H. 2022. A survey of optimal strategy for signature-based drug repositioning and an application to liver cancer. Elife, 11: e71880.

Zaki AM, van Boheemen S, Bestebroer TM, Osterhaus AD AND Fouchier RA. 2012. Isolation of a novel coronavirus from a man with pneumonia in Saudi Arabia. N Engl J Med, 367(19): 1814-1820.

Zanini F, Pu SY, Bekerman E, Einav S AND Quake SR. 2018. Single-cell transcriptional dynamics of flavivirus infection. Elife, 7: e32942.

Zhang K, Miorin L, Makio T, Dehghan I, Gao S, Xie Y, Zhong H, Esparza M, Kehrer T, Kumar A, Hobman TC, Ptak C, Gao B, Minna JD, Chen Z, García-Sastre A, Ren Y,

Wozniak RW AND Fontoura BMA. 2021. Nsp1 protein of SARS-CoV-2 disrupts the mRNA export machinery to inhibit host gene expression. Sci Adv, 7(6): eabe7386.

Zhang L, Cui Z, Li Q, Wang B, Yu Y, Wu J, Nie J, Ding R, Wang H, Zhang Y, Liu S, Chen Z, He Y, Su X, Xu W, Huang W AND Wang Y. 2021. Ten emerging SARS-CoV-2 spike variants exhibit variable infectivity, animal tropism, and antibody neutralization. Commun Biol, 4(1): 1196.

Zhao Y, Chen F, Li Q, Wang L AND Fan C. 2015. Isothermal Amplification of Nucleic Acids. Chem Rev, 115(22): 12491-12545.

Zhou P, Yang XL, Wang XG, Hu B, Zhang L, Zhang W, Si HR, Zhu Y, Li B, Huang CL, Chen HD, Chen J, Luo Y, Guo H, Jiang RD, Liu MQ, Chen Y, Shen XR, Wang X, Zheng XS, Zhao K, Chen QJ, Deng F, Liu LL, Yan B, Zhan FX, Wang YY, Xiao GF AND Shi ZL. 2020. A pneumonia outbreak associated with a new coronavirus of probable bat origin. Nature, 579(7798): 270-273.

Zhu L, Wang N AND Wang X. 2021. Virion Assembly: From Small Picornaviruses (Picornaviridae) to Large Herpesviruses (Herpesviridae). In *Encyclopedia of Virology (Fourth Edition)*, edited by D.H. Bamford andM. Zuckerman. Oxford: Academic Press, pp. 480-487.

Zybert IA, van der Ende-Metselaar H, Wilschut J AND Smit JM. 2008. Functional importance of dengue virus maturation: infectious properties of immature virions. J Gen Virol, 89(Pt 12): 3047-3051.

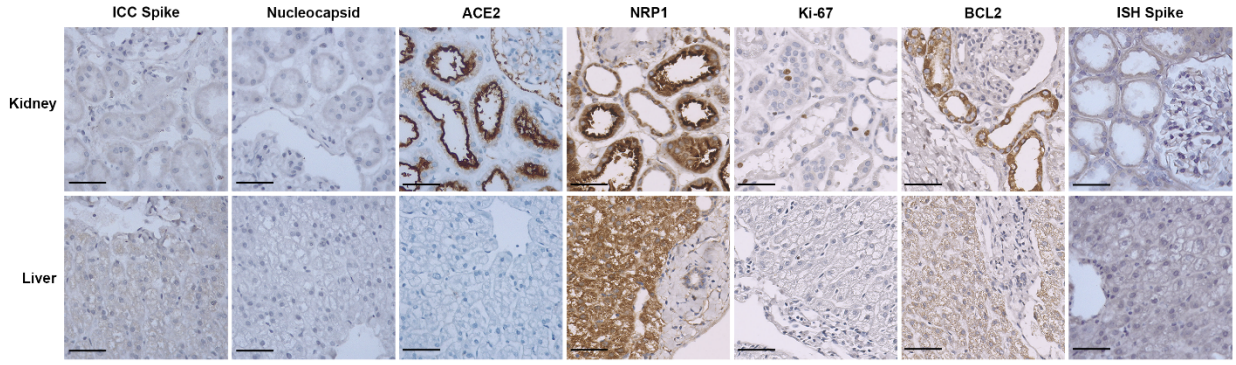
Appendices

Appendix A - Supplementary information from paper II

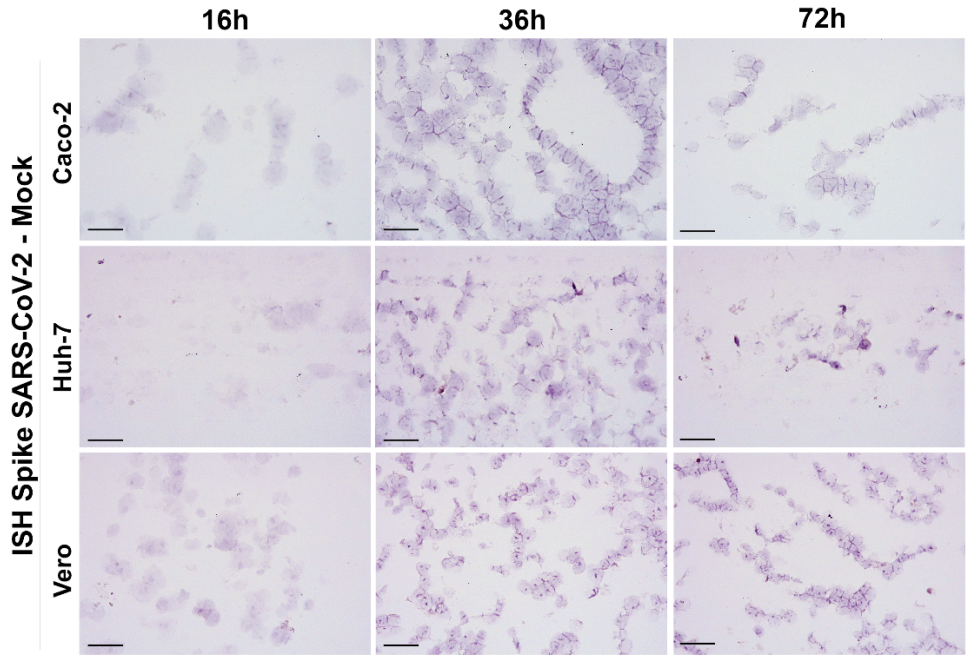
InfectionCMA: a Cell MicroArray Approach for Efficient Biomarker Screening in *in vitro* Infection Assays

Ana C. Magalhães [1,2,3], Sara Ricardo [1,2,4], Ana C. Moreira [1,3,5], Mariana Nunes [1,2,3], Margarida Tavares [6,7,8], Ricardo J. Pinto [1,2,3], Maria Salomé Gomes [1,3,5] and Luisa Pereira [1,2,*]

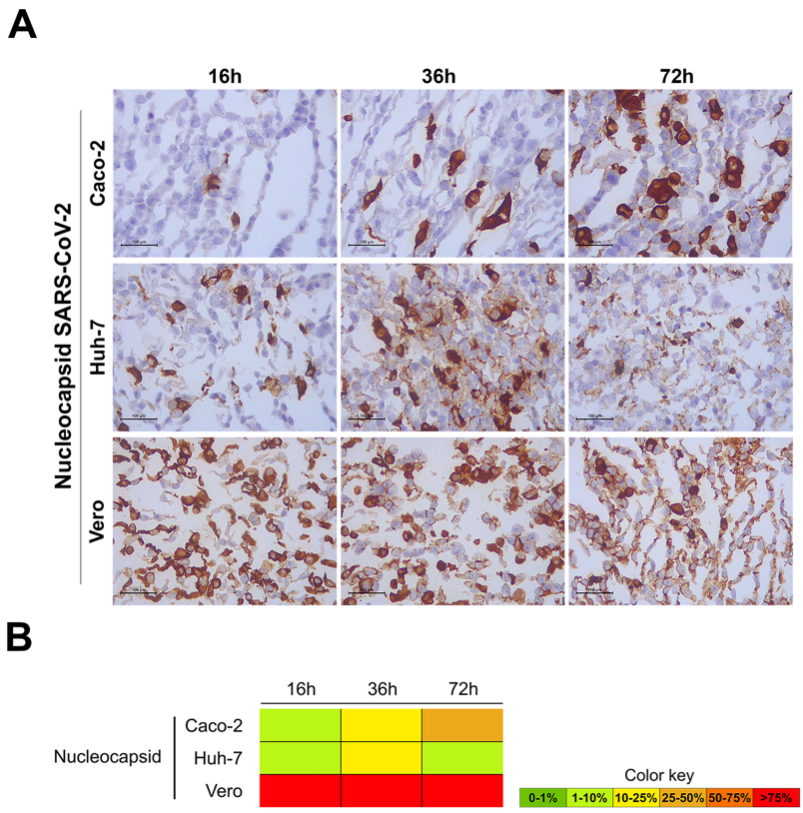
Supplementary Material:



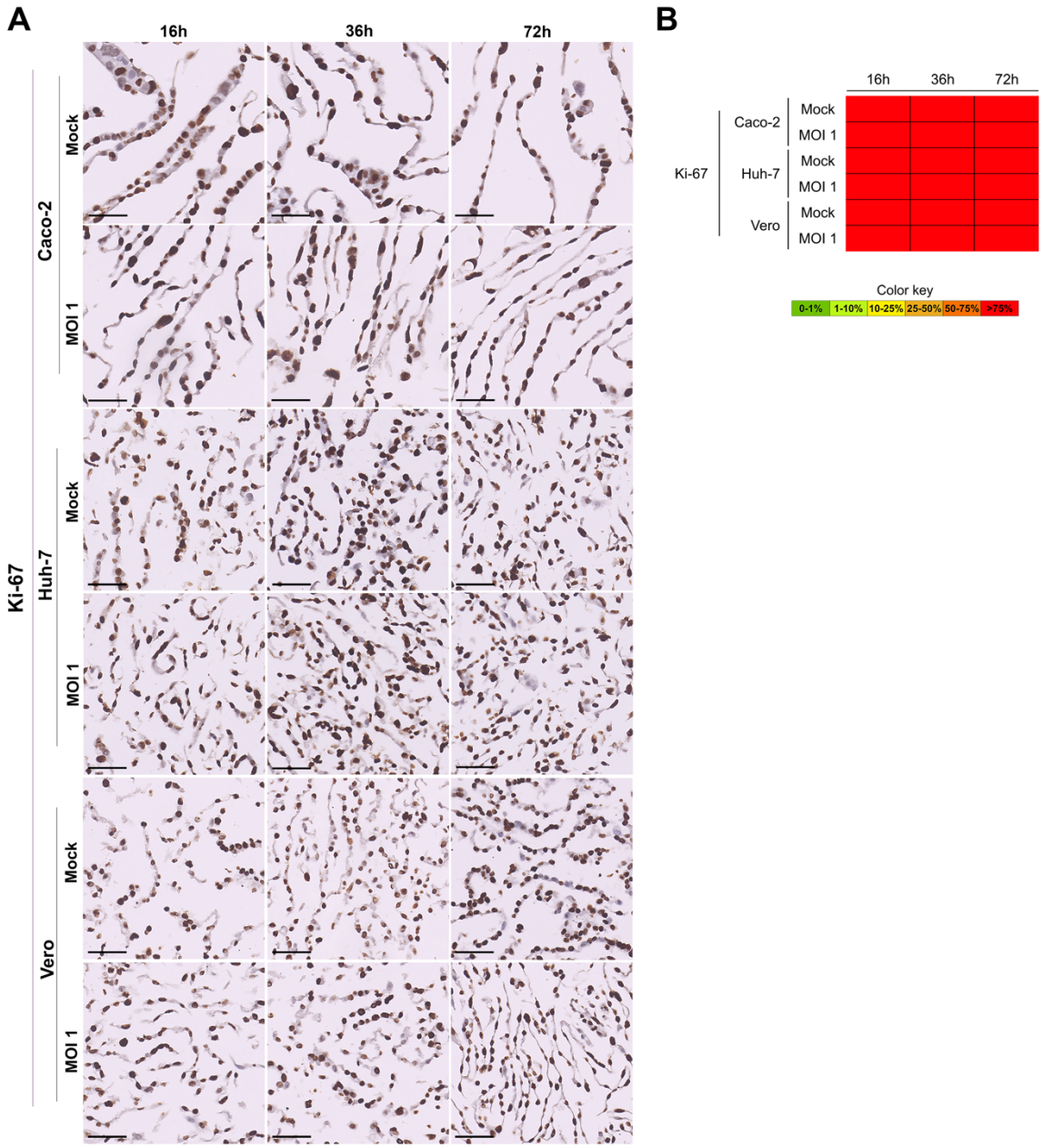
Supplementary Figure S1- ICC for the spike, nucleocapsid, ACE2, NRP1, Ki-67 and BCL2, and ISH for the spike, in the tumour tissue cores of kidney and liver. Scale bar 50µm.



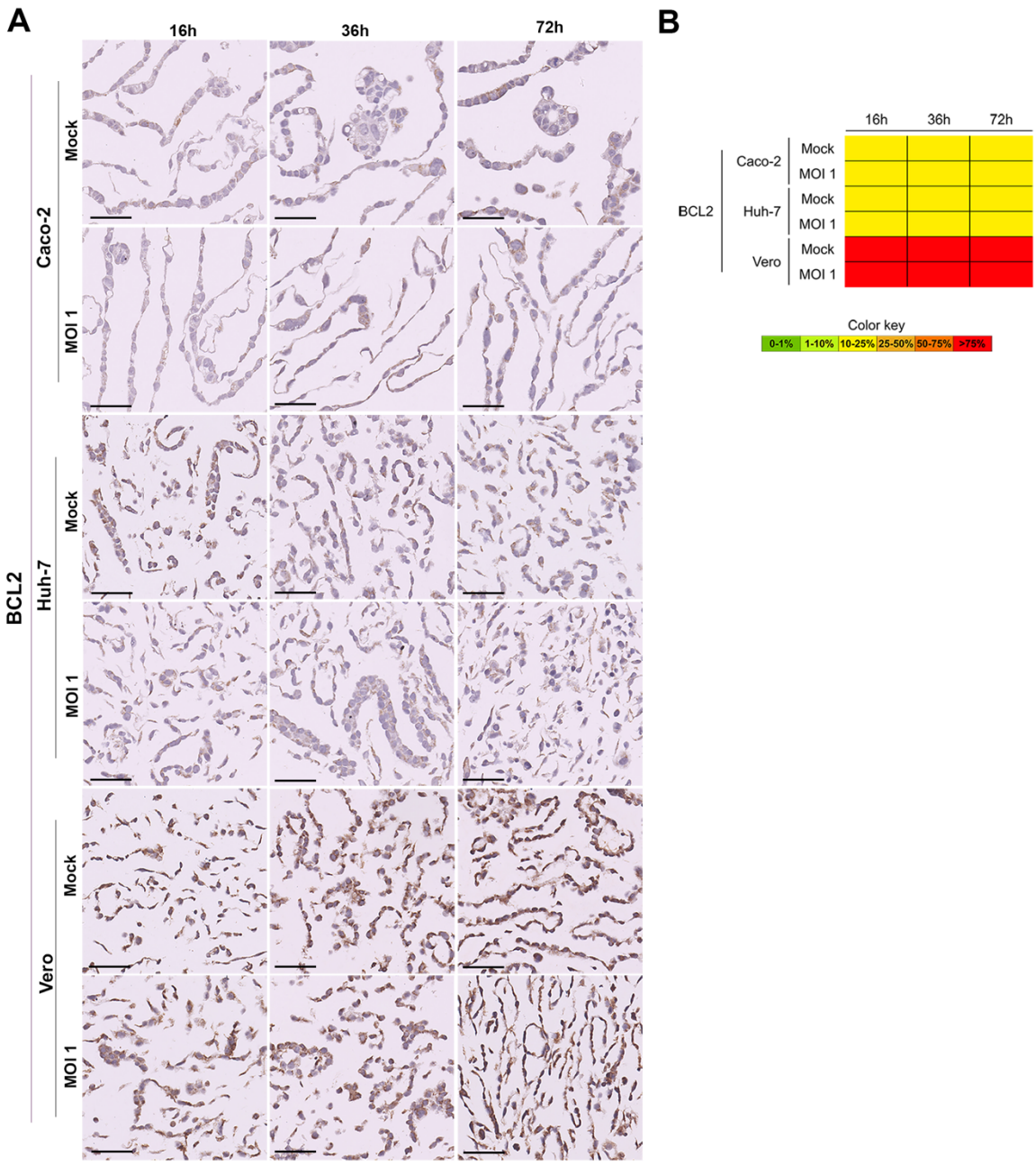
Supplementary Figure S2- Controls for the characterization of SARS-CoV-2 spike mRNA expression in the human (Caco-2 and Huh-7) and Vero cell lines, at different time-points, by ISH. Microscopic images with 100µm scale bar.



Supplementary Figure S3- Characterization of SARS-CoV-2 nucleocapsid expression in the human (Caco-2 and Huh-7) and Vero cell lines, at different time-points after infection with MOI 1, by ICC (A- light microscopic images with 100µm scale bar; B- heat map).



Supplementary Figure S4- Characterization of Ki-67 expression in the human (Caco-2 and Huh-7) and Vero cell lines, at different time-points after infection with MOI 1, by ICC (A- light microscopic images with 50µm scale bar; B- heat map).



Supplementary Figure S5- Characterization of BCL-2 expression in the human (Caco-2 and Huh-7) and Vero cell lines, at different time-points after infection with MOI 1, by ICC (A- light microscopic images with 50µm scale bar; B- heat map).

Appendix B - Supplementary information from paper III

Multi-Tissue Transcriptomic-Informed In Silico Investigation of Drugs for the Treatment of Dengue Fever Disease

Beatriz Sierra [1], Ana Cristina Magalhães [2,3,4], Daniel Soares [2,3], Bruno Cavadas [2,3], Ana B. Perez [1], Mayling Alvarez [1], Eglis Aguirre [1], Claudia Bracho [1], Luisa Pereira [2,3,*] and Maria G. Guzman [1]

Supplementary file

Table S1- Additional information on the individuals from whom samples were collected for transcriptomics.

Group	ID number	Date of symptom onset	Date of death	Age	Gender	Results of dengue RT-PCR (2018) and dengue nested RT-PCR (2014) n tissues	Province	Clinical classification
Cases	37478	26 July 2018	31 July 2018	71	F	DENV-2 in spleen and liver	Camagüey	DSS
	39539	24 July 2018	28 July 2018	49	F	DENV-2 in spleen and liver	Camagüey	DSS
	39538	22 July 2018	30 July 2018	59	M	DENV-2 in liver	Camagüey	DSS
	900	7 October 2014	13 October 2014	66	F	DENV-2 in liver	Habana	DSS
	875	21 October 2014	26 October 2014	48	M	DENV-2 in liver	Habana	DSS
Controls	F1	NA	July 2018	32	M	Negative	Habana	NA
	F2	NA	July 2018	24	F	Negative	Habana	NA
	F4	NA	July 2018	47	M	Negative	Habana	NA

DWWS – dengue with warning signs.

NA- not applicable.

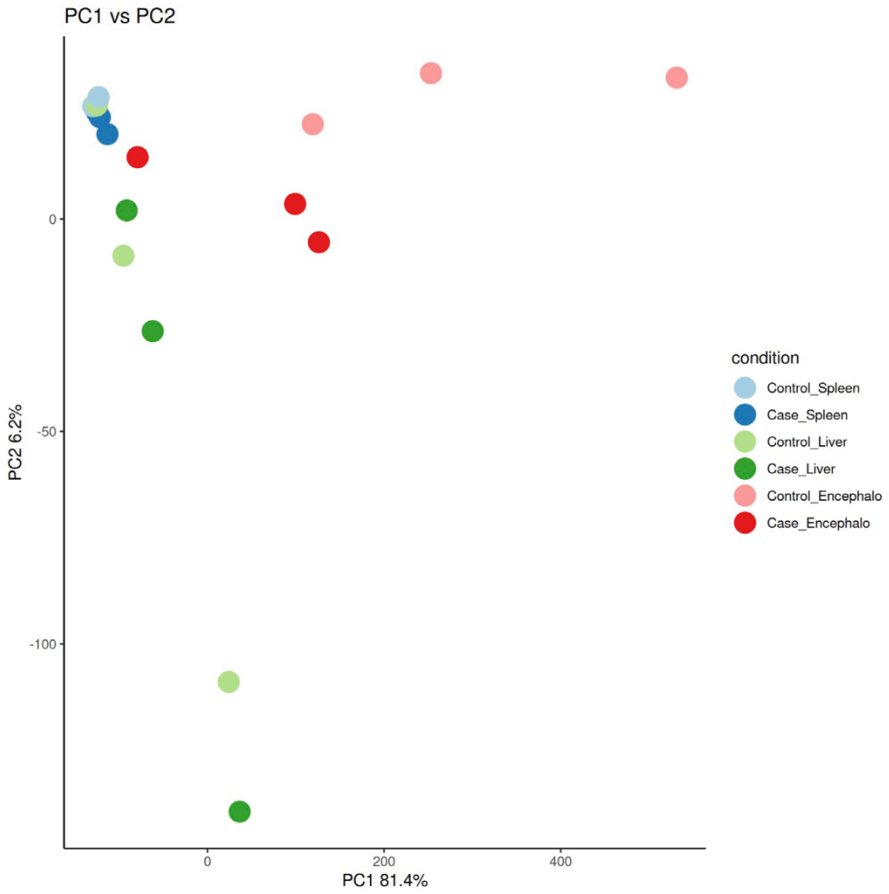


Figure S1- PCA plot (PC1 explaining 81.4% of variation vs. PC2 explaining 6.2% of variation) of the human transcriptomic profile of the spleen, liver and encephalon tissues.

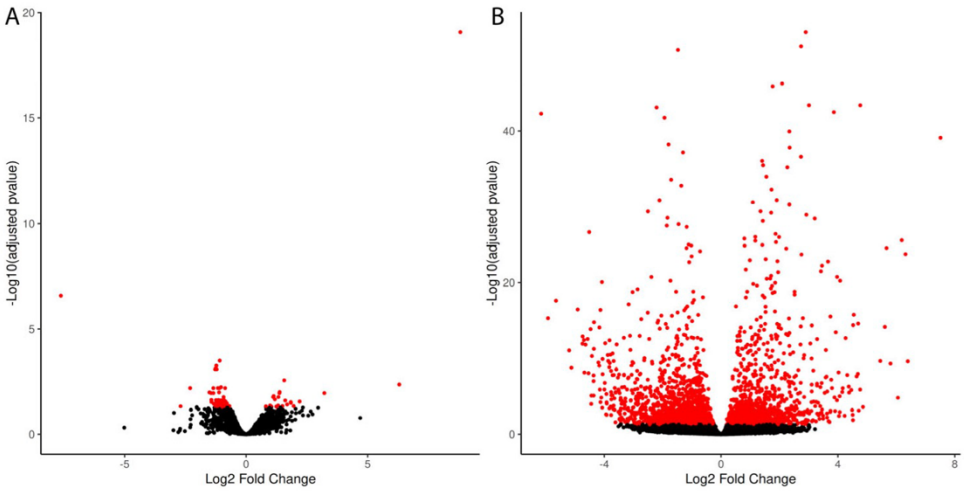


Figure S2- Volcano plots for the gene differential expression in the (A) spleen and (B) liver cell datasets. The points represented on red are the statistically significant genes. The negative side of the graph refers to downregulated genes in patients when compared to controls; the positive side of the graph refers to upregulated genes in patients when compared to controls.

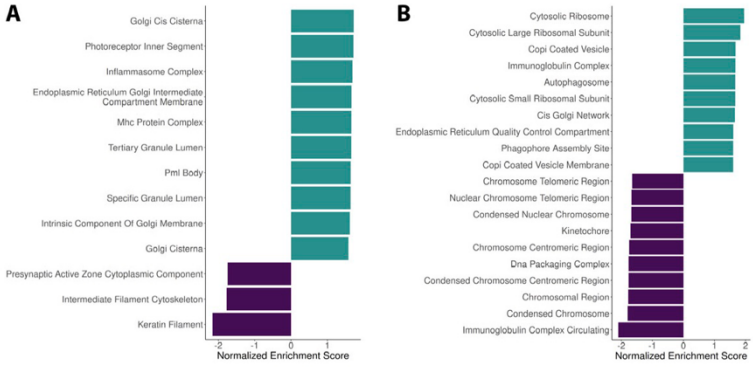


Figure S3- Top 20 Gene Ontology Cellular Component (GO-CC) pathways in the (A) Spleen and (B) Liver cells (cut-off value; nominal p-value < 0.05 and FDR < 0.25). Positive NES (in purple) show upregulated pathways in the infected individuals versus controls, while negative NES values (in green) mean downregulated pathways in the infected individuals versus controls.

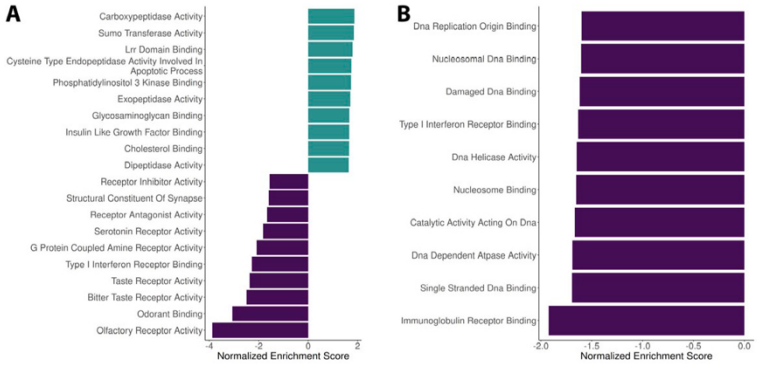


Figure S4- Top 20 Gene Ontology Molecular Function (GO-MF) pathways in the (A) Spleen and (B) Liver cells (cut-off value; nominal p-value < 0.05 and FDR < 0.25). Positive NES (in purple) show upregulated pathways in the infected individuals versus controls, while negative NES values (in green) mean downregulated pathways in the infected individuals versus controls.

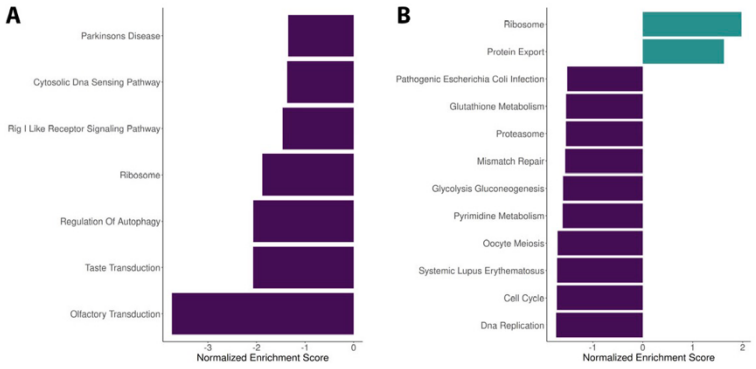


Figure S5- Top 20 significantly enriched KEGG pathways in the (A) Spleen and (B) Liver cells (cut-off value; nominal p-value < 0.05 and FDR < 0.25). Positive NES (in purple) show upregulated pathways in the infected individuals versus controls, while negative NES values (in green) mean downregulated pathways in the infected individuals versus controls.

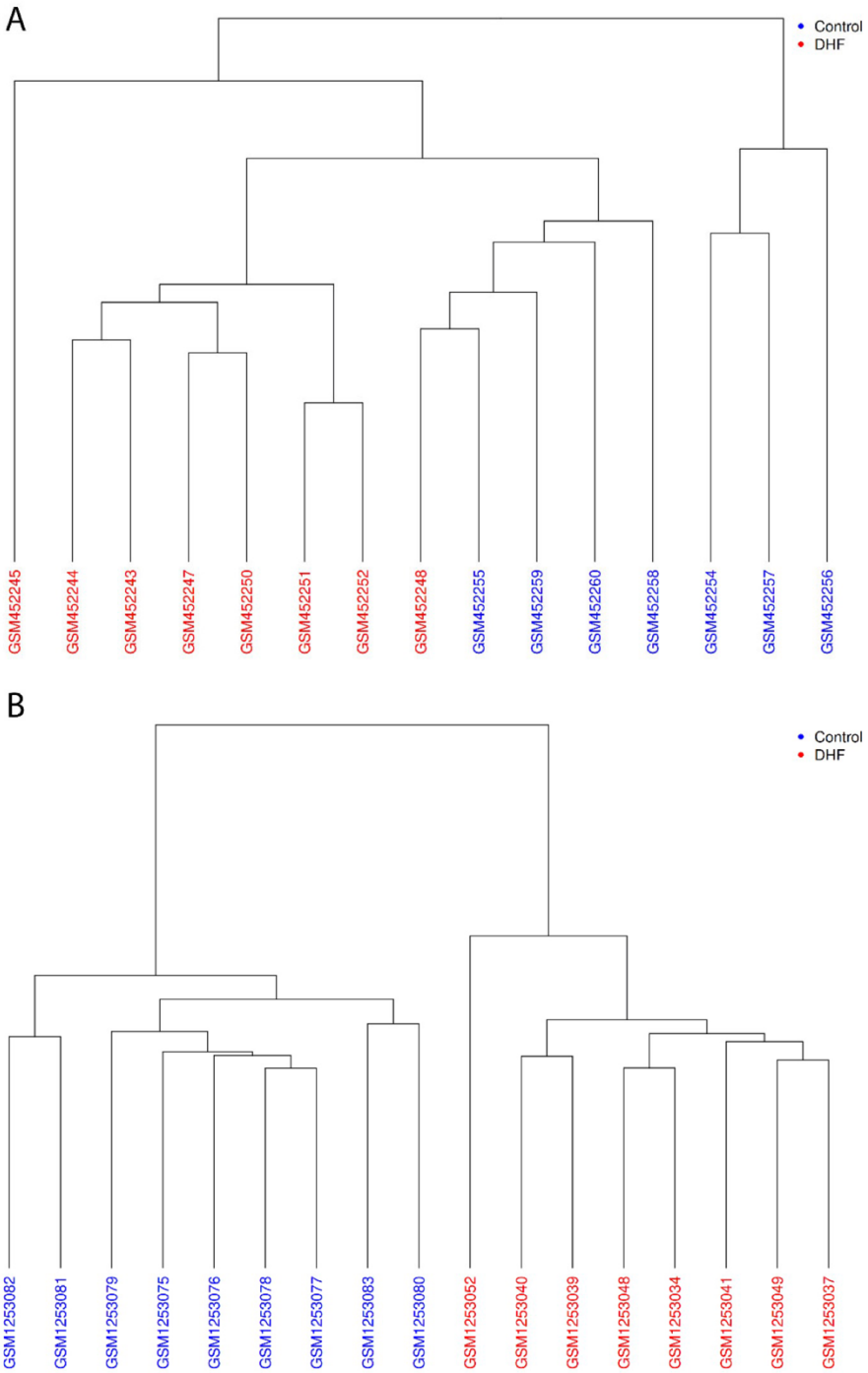


Figure S6- Dendrograms for the gene expression profiles in the two blood datasets: (A) GSE18090 and (B) GSE51808. The red points indicate the infected dengue haemorrhagic fever individuals (DHF), while the blue points indicate control samples.

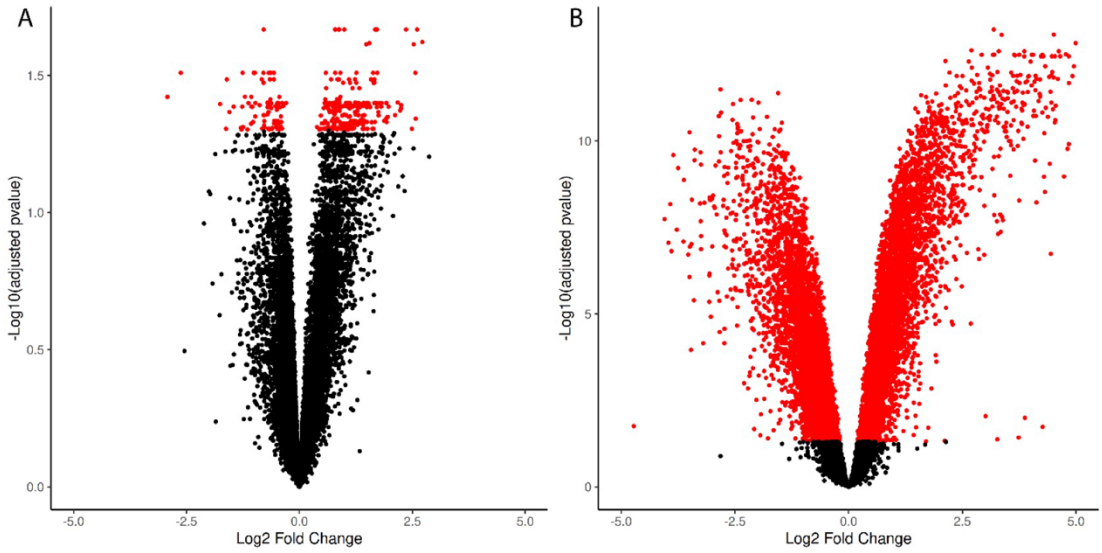


Figure S7- Volcano plots for the gene differential expression in the two blood datasets: (A) GSE18090 and (B) GSE51808. The points represented in red are the statistically significant genes. The negative side of the graph refers to downregulated genes in patients when compared to controls; the positive side of the graph refers to upregulated genes in patients when compared to controls.

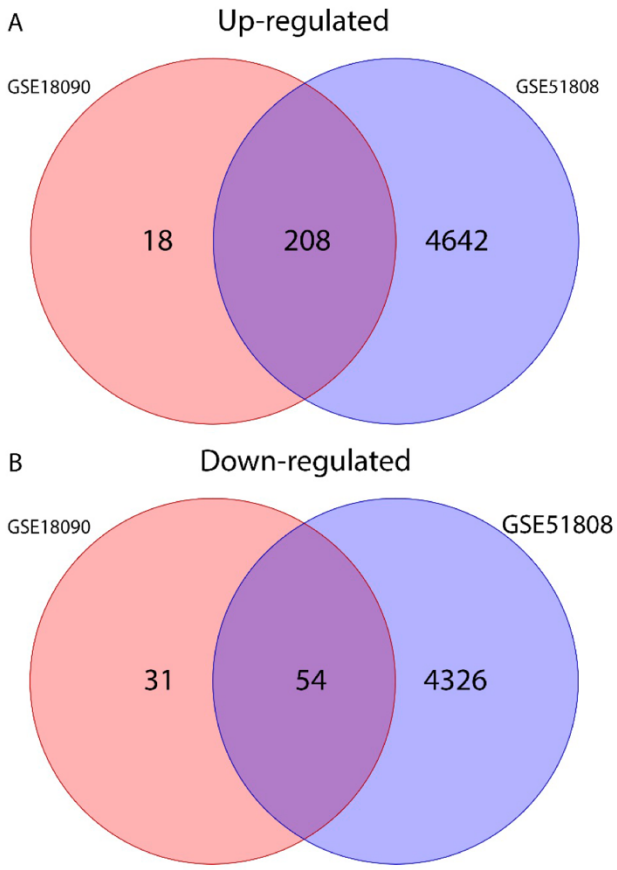


Figure S8- Venn diagrams of the upregulated (A) and downregulated (B) genes in the two blood datasets.

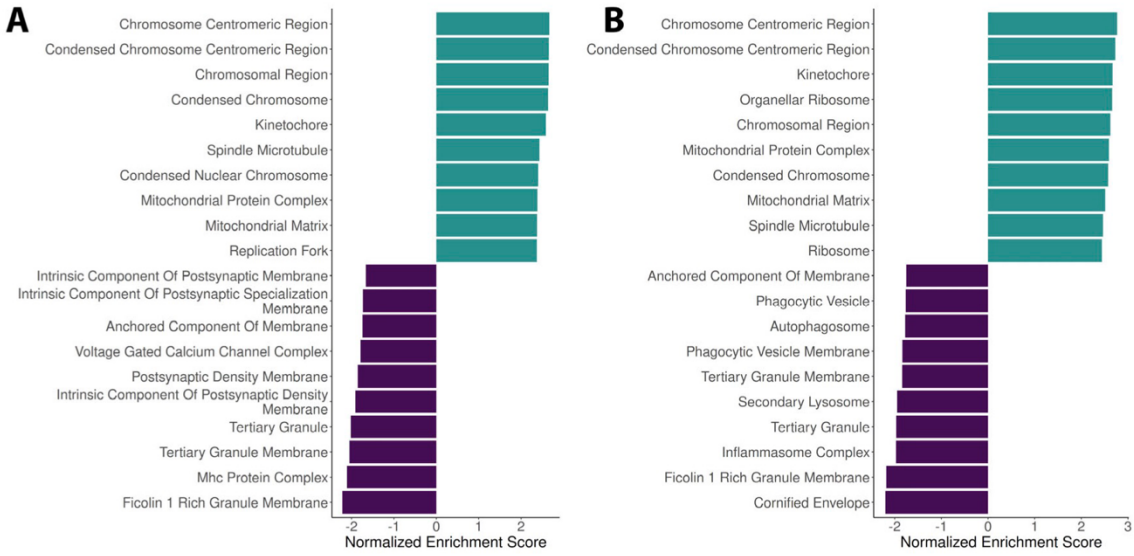


Figure S9- Top 20 Gene Ontology Cellular Component (GO-CC) pathways in the (A) GSE18090 and (B) GSE51808 (cut-off value; nominal p-value < 0.05 and FDR < 0.25). Positive NES (in purple) show upregulated pathways in the infected individuals versus controls, while negative NES values (in green) mean downregulated pathways in the infected individuals versus controls.

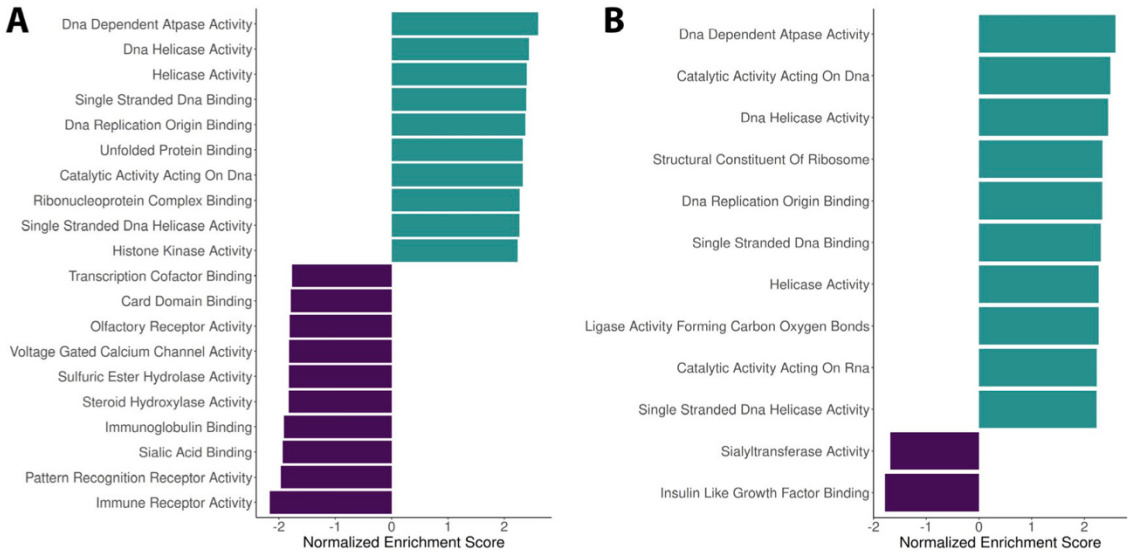


Figure S10- Top 20 Gene Ontology Molecular Function (GO-MF) pathways in the (A) GSE18090 and (B) GSE51808 (cut-off value; nominal p-value < 0.05 and FDR < 0.25). Positive NES (in purple) show upregulated pathways in the infected individuals versus controls, while negative NES values (in green) mean downregulated pathways in the infected individuals versus controls.

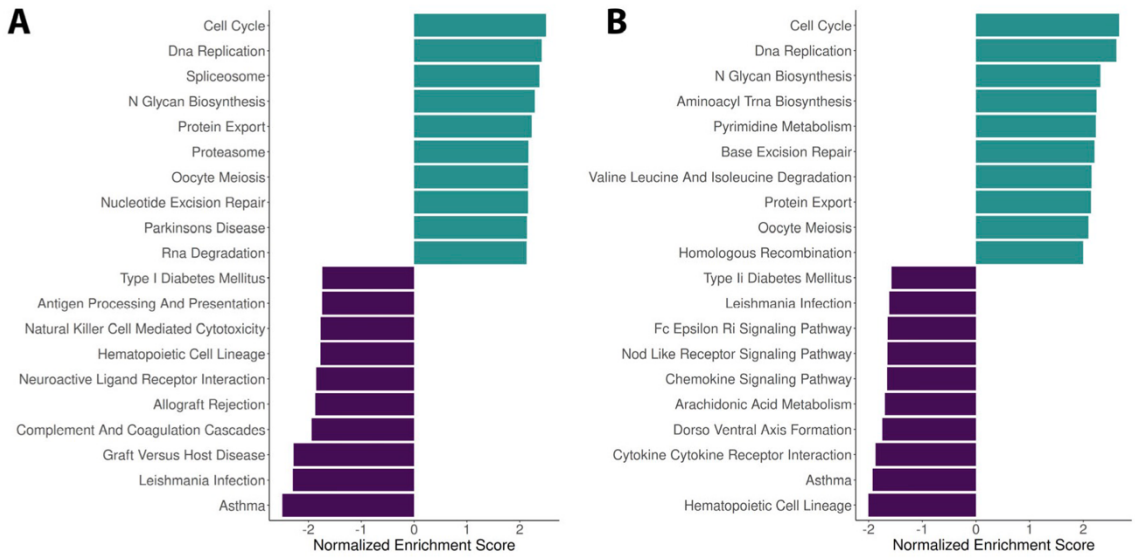
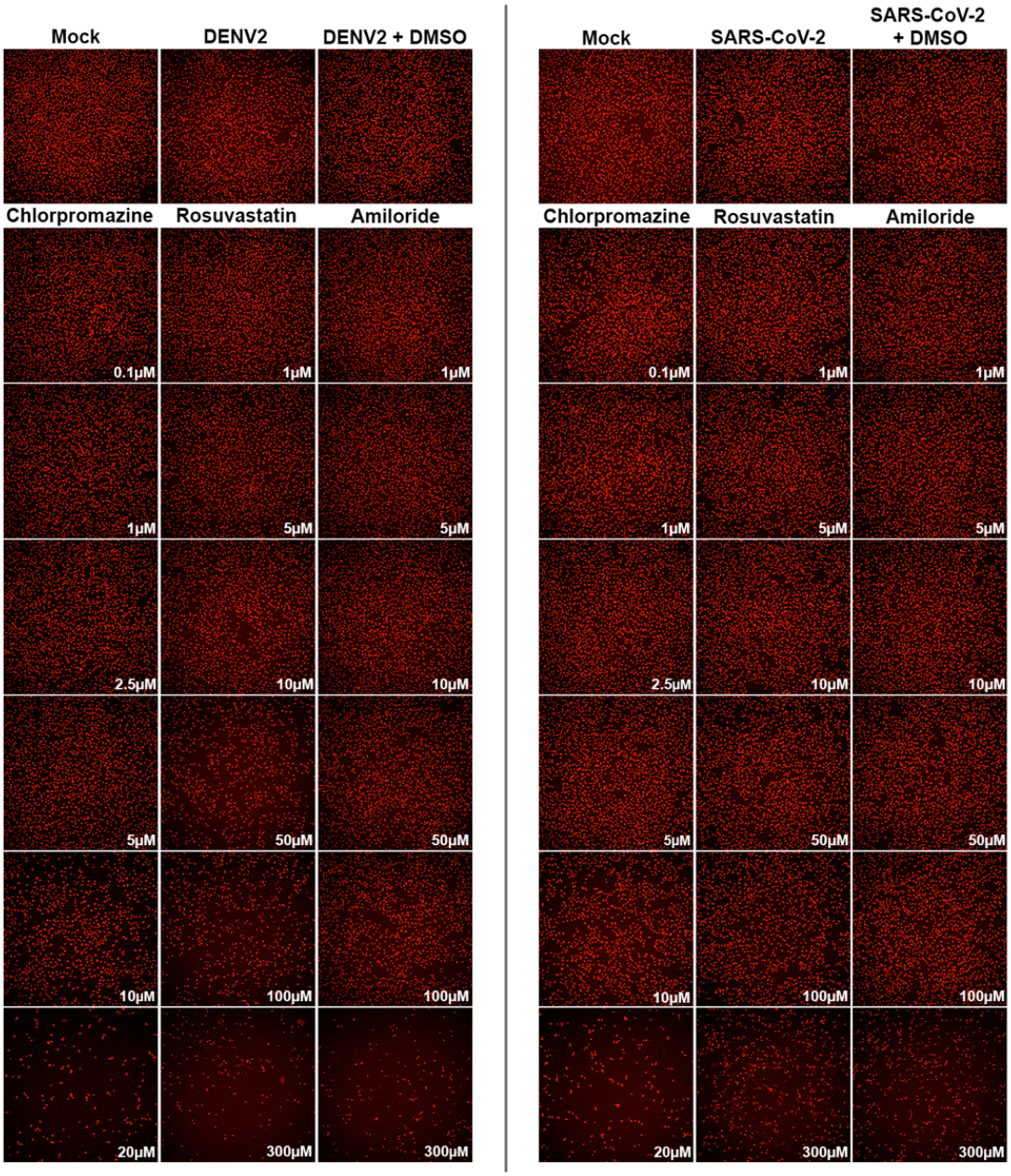


Figure S11- Top 20 significantly enriched KEGG pathways in the (A) GSE18090 and (B) GSE51808 (cut-off value; nominal p-value < 0.05 and FDR < 0.25). Positive NES (in purple) show upregulated pathways in the infected individuals versus controls, while negative NES values (in green) mean downregulated pathways in the infected individuals versus controls.

Appendix C - Supplementary information from paper IV

Endocytic pathways as pharmacological targets for DENV and SARS-CoV-2 infection

Ana C. Magalhaes[1,2,3], Ana C. Moreira[1,2,4], Maria S. Gomes[1,2,4], Luisa Pereira[1,3]



Supplementary Figure S1- Microscope images for the evaluation of cell viability rate by immunofluorescence detection (in the IN Cell Analyzer 2000) of the DAPI staining (red), when performing the *in vitro* testing of the effect of the chlorpromazine, rosuvastatin and amiloride drugs in the presence of infection with DENV2 (left panel) and SARS-CoV-2 (right panel).